

Flow Investigation of Two Phase Flow in Bubble Column Using Particle Image Velocimetry and Image Processing

Tushar A. Pol

A Dissertation Submitted to
Indian Institute of Technology Hyderabad
In Partial Fulfilment of the Requirements for
The Degree of Master of Technology



भारतीय प्रौद्योगिकी संस्थान हैदराबाद
Indian Institute of Technology Hyderabad

Department of Chemical Engineering

June, 2016

Declaration

I declare that this written submission represents my ideas in my own words, and where others' ideas or words have been included, I have adequately cited and referenced the original sources. I also declare that I have adhered to all principles of academic honesty and integrity and have not misrepresented or fabricated or falsified any idea/data/fact/source in my submission. I understand that any violation of the above will be a cause for disciplinary action by the Institute and can also evoke penal action from the sources that have thus not been properly cited, or from whom proper permission has not been taken when needed.

P. Tushar

Tushar A. Pol

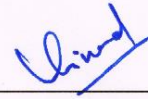
Roll No. - CH14MTECH11016

Approval Sheet

This thesis entitled “**Flow Investigation of Two Phase Flow in Bubble Column Using Particle Image Velocimetry and Image Processing**” by Tushar A. Pol is approved for the degree of Master of Technology from IIT Hyderabad.



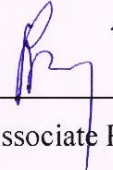
Dr. Narasimha Mangadoddy; Assistant Professor
Adviser



Dr. Vinod Janardhanan; Associate Professor
Examiner



Dr. Saptarshi Majumdar; Assistant Professor
Examiner



Dr. Raja Banerjee; Associate Professor
Chairman

Acknowledgements

It is a humbling experience to acknowledge those people who have, mostly out of kindness, helped along the journey of my M.Tech. study. I am indebted to so many for encouragement and support.

I express my gratitude to my supervisor Dr. Narasimha Mangadoddy for his motivation, enthusiasm, immense knowledge, excellent guidance and support throughout my M.Tech. project. His guidance helped me in all the time of research and writing of this thesis. I could not have imagined having a better advisor and mentor for my M.Tech. study.

I would like to thank my thesis committee members Dr. Raja Banerjee, Dr. Vinod Janardhanan and Dr. Saptarshi Majumdar for their encouragement, intuitive comments, and valuable suggestions. I would also like to express my thanks to Director Uday B. Desai.

I would like to show my deep appreciation to my lab mates Balraju Vadlakonda and Teja Reddy Vakamalla for their co-operation and help. To my friend and roommate Sabbani Manohar, thank you for listening, offering me advice, and supporting me through this entire process. I would also like to thank my friend Rakesh Kale for helping me in performing experiments, image processing coding and also for challenging my thinking by his interesting question, assumptions and view from multiple perspectives.

I would like to express my greatest gratitude to my parents, and my siblings for their encouragement and support throughout my life. My sincere thanks to all the people who helped and supported me during the course of this M.Tech. program at Indian Institute of Technology, Hyderabad.

Dedicated to

My Inspiring Parents and Sisters

Abstract

Bubble size distribution, gas hold up, planar liquid flow field, bubble rise velocity, residence time distribution of bubbles are the key parameters for bubble column design and performance evaluation. Flow visualization and gas-liquid two phase interactions in bubble column can be examined using particle image velocimetry (PIV) as well as image processing techniques.

In this work, we present use of flow visualisation and measurement techniques such as PIV and image processing for determining the bubble size distribution (BSD), gas hold-up, planar liquid flow field, bubble rise velocity, residence time distribution of bubbles, trajectories followed by bubble for different surfactant concentration addition, and other parameters in a needle and nozzle sparger of different design in rectangular bubble column for understanding the column hydrodynamics. Particle image velocimetry is widely used technique for investigating the fluid flow in a whole plane, which is non-intrusive where flow-marker or tracer particles are added into the flow and their behaviour is observed. Image processing technique is an effective and appropriate method for the assessment of BSD, bubble rise velocity, residence time distribution of bubbles, bubble trajectory and indirect approximation of gas hold-up up. A 700 x 200 x 57 mm single/multiple needle rectangular bubble column operating a wide range of superficial velocities is used for the investigation.

The effect of bubble break-up and coalescence is observed through the change in BSD for different superficial gas velocity. BSD curves are broad for heterogeneous phase as compared to the homogeneous. Magnitude of liquid velocity and vorticity around the bubbles were assessed for different gas flow rate conditions. Comparison of gas hold-ups is made between the amounts of gas hold up calculated by measurement of clear and dispersed liquid height as well as by measuring volume of each and every bubble throughout the column and adding it up. Also effect of surfactant addition on bubble rise velocity and trajectories followed by bubble is observed. Addition of surfactants increases time spend by bubble in a rectangle column.

Keywords: PIV; Image processing; BSD; Gas hold-up; Bubble breakup and coalescence; Shadowgraph, HSVC, Bubble rise velocity, RTD of bubbles.

Nomenclature

d_e	Equivalent diameter
H_C	Clear liquid height
H_D	Dispersed liquid height
U_T	Terminal velocity
V_F	Fluid velocity
ρ_a	Apparent density of bubbles
ρ_F	Fluid Density
μ	Viscosity
ρ_P	Particle Density
ρ_s	Average slurry density
ρ_w	Water density
V	Volume
ΔP	Pressure difference between two measurement points
ε_g	Gas holdup

Abbreviations

2D	Two Dimensional
3D	Three Dimensional
BSD	Bubble Size Distribution
CCD	Charged Coupled Device
CMOS	Complementary metal-oxide semiconductor
HSVC	High speed video camera
L2F	Laser two focus
LDA	Laser Doppler Anemometry
LIF	Laser induced fluorescence
MIBC	Methyl isobutyl carbinol
PIV	Particle Image Velocimetry
ROI	Region of interest
RTD	Residence time distribution

List of tables

Table 2.1	Earlier experimental work on rectangular bubble column (air-water) characterization. ...	12
Table 3.1	Specification of the 2-D PIV system used.....	20
Table 3.2	Comparison between small and large tracer particles used in PIV experiment.....	23
Table 4.1	Experimental conditions.....	38
Table 5.1	Experimental conditions.....	49
Table 6.1	Experimental conditions.....	56

List of figures

Figure 1.1	Sketch of a bubble column reactor.....	1
Figure 2.1	Flow regimes in a vertical bubble columns	6
Figure 2.2	Bubble columns for laboratory use	7
Figure 2.3	Schematic of the gas holdup behaviour for different flow regime.....	14
Figure 3.1	Schematic of a bubble column setup.	17
Figure 3.2	Needle sparger schematic used for experiment.....	18
Figure 3.3	Nozzles sparger schematic used for experiment	19
Figure 3.4	Actual photograph of laboratory PIV system used to investigate 2-D bubble column	19
Figure 3.5	PIV optical configuration.....	20
Figure 3.6	Schematic of PIV setup.....	22
Figure 3.7	Steps involved in a generic PIV program	22
Figure 3.8	Relationship between tracer particle motion and flow condition.....	24
Figure 3.9	Maxey–Riley equation with factors affecting the flow.....	25
Figure 3.10	Calibration image after adjustment of ROI and image pre-processing.....	28
Figure 3.11	Selected reference position for calibration.....	29
Figure 3.12	(a) Frame A original positions of particles, (b) Frame B displaced positions of particles	30
Figure 3.13	Velocity vector measurement	30
Figure 3.14	(a) Image at $t = t_0$, (b) Interrogation area at $t = t_0$, (c) Interrogation area at $t = t_0 + \Delta t$, (d) Image at $t = t_0 + \Delta t$, (e) Particle velocity vector, (f) Vector field.....	30
Figure 3.15	Stepwise PIV demonstration for single bubble	31
Figure 3.16	Schematic diagram of shadowgraph technique.....	32
Figure 3.17	Actual lab setup of shadowgraph along with HSVC	33
Figure 3.18	Steps involved in extraction of Dia. And volume information of a bubble	34
Figure 3.19	Image processing to evaluate BSD	35

Figure 3.20 (a) calibrated image, (b) reference frame origin and angle, (c) selected object of interest	36
Figure 3.21 (a) bubble velocity vector, (b) trajectory followed by marked bubble.....	37
Figure 4.1 Time-averaged liquid velocity profiles of (a) 50 L/h, (b) 200 L/h, and (c) 500 L/h.	39
Figure 4.2 Time-averaged horizontal liquid velocity (U m/s) profiles at five positions above the needle for flow (a) 50 L/h, (b) 200 L/h.....	40
Figure 4.3 Time-averaged vertical liquid velocity (V m/s) profiles at five positions above the needle for flow (a) 50 L/h, (b) 200 L/h.....	40
Figure 4.4 Time-averaged resultant liquid velocity (m/s) profiles at five positions above the needle for flow (a) 50 L/h, (b) 200 L/h.....	40
Figure 4.5 Time-averaged (a) horizontal liquid velocity (U m/s), (b) vertical liquid velocity (V m/s) and (c) resultant liquid velocity (m/s) profiles at five positions above the needle for flow 500 L/h...	41
Figure 4.6 Time-averaged resultant liquid velocity profiles for flow (a) 50 L/h, (b) 200 L/h, (c) 500 L/h.....	42
Figure 4.7 Time-averaged vorticity profiles for flow (a) 50 L/h, (b) 200 L/h, (c) 500 L/h.....	42
Figure 4.8 Time-averaged streamline profiles for flow (a) 50 L/h, (b) 200 L/h, (c) 500 L/h.....	43
Figure 4.9 Flow visualization for (a) 50 L/h, (b) 200 L/h, and (c) 500 L/h gas flow rates.....	45
Figure 4.10 Effect of gas flow rate on BSD.....	45
Figure 4.11 Gas holdup as a function of gas flow rates	47
Figure 5.1 Time-averaged resultant liquid velocity profiles of flow (a) 10 L/h, (b) 20 L/h, (c) 30 L/h for 1.5 ml MIBC and 0.5 mm dia.	50
Figure 5.2 Time-averaged vorticity profiles of flow (a) 10 L/h, (b) 20 L/h, (c) 30 L/h for 1.5 ml MIBC	51
Figure 5.3 Time-averaged streamline profiles of flow (a) 10 L/h, (b) 20 L/h, (c) 30 L/h for 1.5 ml MIBC and 0.5 mm dia.....	51
Figure 5.4 Bubble track plots of 10 L/h flow for (a) 0.5 mm dia., (b) 0.7 mm dia., and (c) 0.9 mm dia. nozzle	53
Figure 5.5 Flow visualization of 3 ml MIBC concentration for (a) 10 L/h, (b) 20 L/h, and (c) 30 l/h	53

Figure 5.6 Resultant velocity of bubble for (a) 10 L/h, (b) 20L/h, and (c) 30 L/h	54
Figure 5.7 RTD for (a) 0.5 mm, (b) 0.7 mm, (c) 0.9 mm nozzle dia.....	54
Figure 6.1 Time-averaged (a) resultant liquid velocity profiles, (b) vorticity profiles, (c) streamline profiles for flow 60 L/h for 0.5 mm nozzle dia.	57
Figure 6.2 Flow visualisation of 3 nozzle sparger of 60 L/h flow for (a) w/o MIBC, (b) 0.5 ml MIBC, (c) 3 ml concentration for 0.5 mm dia.....	58

Contents

Declaration	ii
Approval Sheet	iii
Acknowledgements	iv
Abstract	vi
Nomenclature	vii
Abbreviations	viii
List of tables	ix
List of figures	x
1 Introduction	1
1.1 Bubble column background	1
1.2 Key performance parameters of bubble column	2
1.3 PIV and image processing applications on bubble column	3
1.4 Scope of Work	4
1.5 Outline of this thesis	4
2 Literature review	6
2.1 Flow Regime identification and measurement	6
2.2 Bubble size distribution and measurement	11
2.3 Gas holdup and measurement	14
2.4 Bubble rise velocity, RTD, effect surfactant addition	15
3 Experimental Procedure & Methodology	17
3.1 Bubble Column Experimental setup	17
3.2 PIV theory	19
3.2.1 PIV system Components	23
3.3 PIV experimental setup and measurements	26
3.3.1 2-D PIV system calibration	27
3.3.2 PIV analysis	29
3.4 Image processing for BSD measurement	32
3.5 Image processing for RTD, Bubble rise velocity, trajectory	35
4 Single needle source bubble dynamic	38
4.1 Bubble Column flow investigation by PIV	38

4.2	Bubble size distribution by image processing.....	44
4.3	Gas holdup.....	47
5	Single nozzle source bubble dynamics	49
5.1	Bubble Column flow investigation by PIV	49
5.2	Rise velocity , RTD and trajectory of bubble by image processing	52
6	Multiple nozzle source bubble dynamics	56
6.1	Bubble Column flow investigation by PIV	56
6.1	Bubble Column flow visualisation by HSVC	57
7	Conclusion and future work.....	60
7.1	Conclusion.....	60
7.2	Future work.....	61
Appendix A -Flow visualisation with the help of HSVC and shadowgraph		62
Appendix B -PIV flow field profiles.....		71
Appendix C -BSD and gas holdup as bar diagrams for 3.5 mm needle source		99
Appendix D -Bubble track plots for single nozzle source (0.5mm, 0.7mm, 0.9mm diameter) .		103
Appendix E -Tables for time-averaged liquid velocity plots at five positions above the needle for single needle source (3.5 mm diameter) bubble dynamic		105
Appendix F -MATLAB Code for BSD calculation.....		125
References.....		132

Chapter 1

Introduction

1.1 Bubble column background

A bubble column reactor is a multiphase reactor used to make and regulate gas-liquid chemical reactions. It comprises of a vertically-arranged cylindrical column filled with liquid, at the lowest part of which usually gas is introduced as shown in Figure 1.1. In several industrial equipment bubble flows are encountered. Typical gas-liquid contactors mainly includes bubble column reactor, column flotation, evaporators, boilers, and plate column for absorption of gases as well as distillation. Bubble column reactors are extensively used in chemical, metallurgical, biochemical and petrochemical industries.

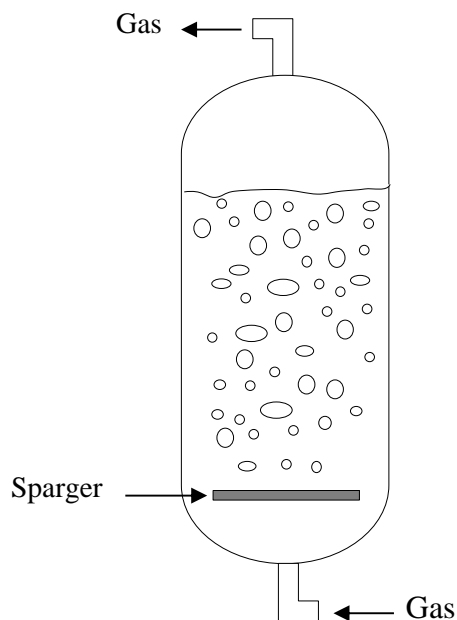


Figure 1.1 Sketch of a bubble column reactor

The gas introduced into the bubble column is in the form of bubbles and used for either a liquid or a liquid–solid flow systems. Whenever solid phase exists these types of reactors are called as slurry bubble column reactors. Bubble column reactors are used mainly in chemical practices

such as hydrogenation, oxidation, alkylation and biological wastewater treatment. They are superior to other reactors when it comes to heat and mass transfer, little upkeep and low operational costs, durability of the catalyst (Urseanu 2000). 2D rectangular bubble columns offer advantage over 3D bubble columns as they allow better control on local hydrodynamics and experimental information is easier to obtain. The investigational study of gas plume hydrodynamics in 3D columns remain more complicated by meandering and turbulent motion of the bubble plume. Where in 2D rectangular bubble columns with large width to depth proportion (around 3-4) avoids swirling and rigorous meandering.

1.2 Key performance parameters of bubble column

Bubble size distribution (BSD), gas hold up, bubble rise velocity, dispersion of the gas phase in different flow regimes are the key parameters for bubble column design and performance evaluation.

a. Bubble size distribution:

The effect of bubble break-up and coalescence is observed through the change in BSD for different superficial gas velocity. BSD curves are broad for heterogeneous phase as compared to the homogeneous flow regimes.

b. Gas Holdup:

Gas holdup and its distribution are the most significant parameter characterizing the hydrodynamics of bubble columns. Gas holdup is the ratio between volume of the gas and total volume of the dispersion in the two or three phase mixture. Gas hold up depends mainly on the superficial gas velocity and given column design conditions. Correct estimation of the gas holdup profiles is essential for determining liquid mixing, flow regime transition, heat and mass transfer rates.

c. Flow regimes:

Flow regimes in the bubble column are mainly distinguished into two types depends on strength of the rising bubble plume. Homogenous flow regime is triggered at lower superficial gas velocities and within this flow regime bubbles are uniformly distributed along column length but at higher gas superficial velocities a highly turbulent flow regime appears which is recognised as heterogeneous flow where bubble break-up and coalescence is observed and various size bubbles travels with different velocities as shown in Figure 2.1.

d. Bubble rise velocity:

Bubbles are almost of uniform shape and size when they rise in the homogeneous flow regime but for heterogeneous flow regime larger bubbles are moulded by coalescence as well as they

break into smaller ones. The amount of gas conveyed by larger bubbles linearly upsurges with gas velocity because larger bubbles have significant higher rise velocity than the small ones.

1.3 PIV and image processing applications on bubble column

In chemical and petroleum practices online measurement of two-phase flow parameters is one of the most important task to do. It plays an important role not only in analysing the effect of the flow configuration on phase element and flow rate measurement but also in the safety of operation and the dependability of everyday courses. The difficulty faced when measuring flow parameters is limited amount of information on boundary of homogeneous to heterogeneous bubbly flow provided by traditional flow measurement techniques. Intrusive and non-intrusive are the main types of techniques used for flow visualization and measurement. Where in intrusive technique physical probes are introduced in the flow which may cause local disturbance at high speed, which includes temperature probes and hot wire anemometer. Second method used for investigating the flow is non-intrusive technique where flow-marker or tracer particles are added into the flow and their behaviour is observed. As very small amount of tracer particles were added in to the flow so which leads to no modification of the flow. E.g. laser two focus (L2F), laser Doppler anemometry (LDA), and particle image velocimetry (PIV) (Raffel et al. 2007), (Adrian 2005).

LDA and other techniques excluding PIV provides point velocity information. In this context particle image velocimetry (PIV) is a more promising technique as it provides whole field statistics and have advantage over LDA as it gives valuable information regarding particle interaction with coherent structure. For modelling of the bubbly flow with good physical deliberation, gas hold-up, BSD and gas - liquid velocities over entire flow domain should be known. Though exceptional image acquisition and analysing approaches are required in order to get all the preferred parameters listed above.

There are numerous ways to find BSD, gas hold-up for bubble column but as like flow visualization and measurement techniques they also classified into two categories intrusive and non-intrusive. Some of the intrusive technique includes capillary suction probes (Laakkonen et al. 2007) , wire-mesh sensors (Prasser, Scholz, and Zippe 2001) and non-intrusive approaches include tomographic techniques, image processing technique (Sadr-Kazemi and Cilliers 1997) . Non-intrusive approaches are able to measure gas hold-up and BSD of the system without affecting the flow. Limitations of the tomographic gears are cost and poor spatial resolution. But whereas photographic techniques have the potential to measure BSD precisely but only when system is transparent and moderate bubble numbers.

1.4 Scope of Work

It has come to be clear that there are still a number of gaps in the understanding of two-phase gas-liquid flows. Advanced experimental techniques such as PIV is a great tool to achieve this. We can use particle image velocimetry to characterize the gas-liquid flow in the bubble column. In PIV, flow is seeded with tracer particles, region of interest (ROI) is illuminated with a thin sheet of laser light and sequential images of illuminated ROI are captured in pair forms with a small time-delay on CCD camera. PIV images are then analysed by splitting into small interrogation areas with the help of cross-correlation technique and the velocity field info found. To get good images for finding BSD and gas holdup by image processing, shadowgraph technique has been widely used and entire experiments supposed to be carried out in a darkroom. Image processing mainly involve edge detection method for bubble diameter, and volume calculations. In the present work we propose to use the particle image velocimetry and image processing techniques for flow investigation of two phase flow (air-water) in a bubble column, measurement gas hold-up and bubble size distribution particularly when bubbles concentration is diluted and bubbles originates from single and multiple sources. The method engaged in the current work uses fluorescent seeding particles and long wave pass filter (550 nm) to avoid the flaring triggered by laser light reflection. The scope of this thesis is

- Flow investigation and measurement of a two phase flow field in rectangular bubble column using PIV and image processing technique
- Estimation of gas-hold up and BSD using shadowgraph based HSVC and dispersed height measurement
- Parametric study of rectangular bubble column design and operating condition and thereby understanding the local hydrodynamics in bubble column
- Effect of superficial gas velocity on dispersion of gas bubbles in a given liquid phase
- Bubble behaviour for different frother concentration such as their trajectories and residence time distribution

1.5 Outline of this thesis

In this chapter 1 both experimental techniques such as PIV and image processing are briefly presented. The remaining of this thesis comprises of four chapters, which are completed in an alike manner. Chapter 2 is concerned with literature review on flow regime identification and measurement, bubble size distribution and measurement, gas holdup and measurement etc.

Chapter 3 deals with experimental Procedure & Methodology adopted which mainly includes bubble column experimental setup, PIV experiments, image processing.

Chapter 4 comprises of flow investigation by PIV, bubble size distribution for different flow rates, effect of gas flow rates on gas holdup for single needle source 2-D bubble column reactor.

Chapter 5 is deals with flow visualisation by HSVC, flow investigation by PIV, bubble rise velocity, RTD and trajectory of bubble by image processing and effect of surfactant addition on above listed parameters for single nozzle source 2-D bubble column reactor. In chapter 6 flow investigation and visualisation techniques such as PIV and HSVC has been used to understand bubble dynamics for multiple nozzle source 2-D bubble column reactor.

In chapter 7 conclusions are drawn and recommendations for further work are given.

Chapter 2

Literature review

2.1 Flow Regime identification and measurement

A small selection of the available research work on particle image velocimetry (Raffel et al. 2007), bubble column and image processing is presented here with brief explanation. Homogeneous (dispersed) and heterogeneous (discrete) are two regimes of operation of a bubble column as shown in Figure 2.1. In homogeneous regime, the bubbles are uniformly distributed all over the column cross section, occurs at low superficial gas velocity, BSD is narrow and little interaction between bubbles. At higher superficial gas velocity heterogeneous bubbly flow starts building up where BSD is broad and bubble coalescence and break-up is more. At higher superficial gas velocity heterogeneous bubbly flow starts building up where BSD is broad and bubble coalescence and break-up is more.

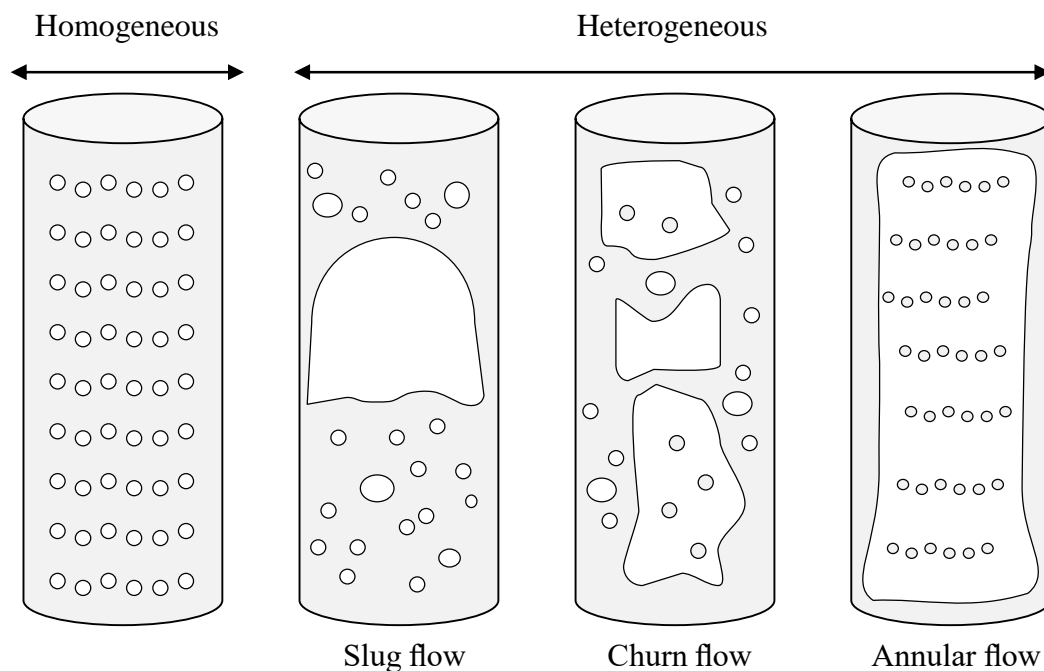


Figure 2.1 Flow regimes in a vertical bubble columns

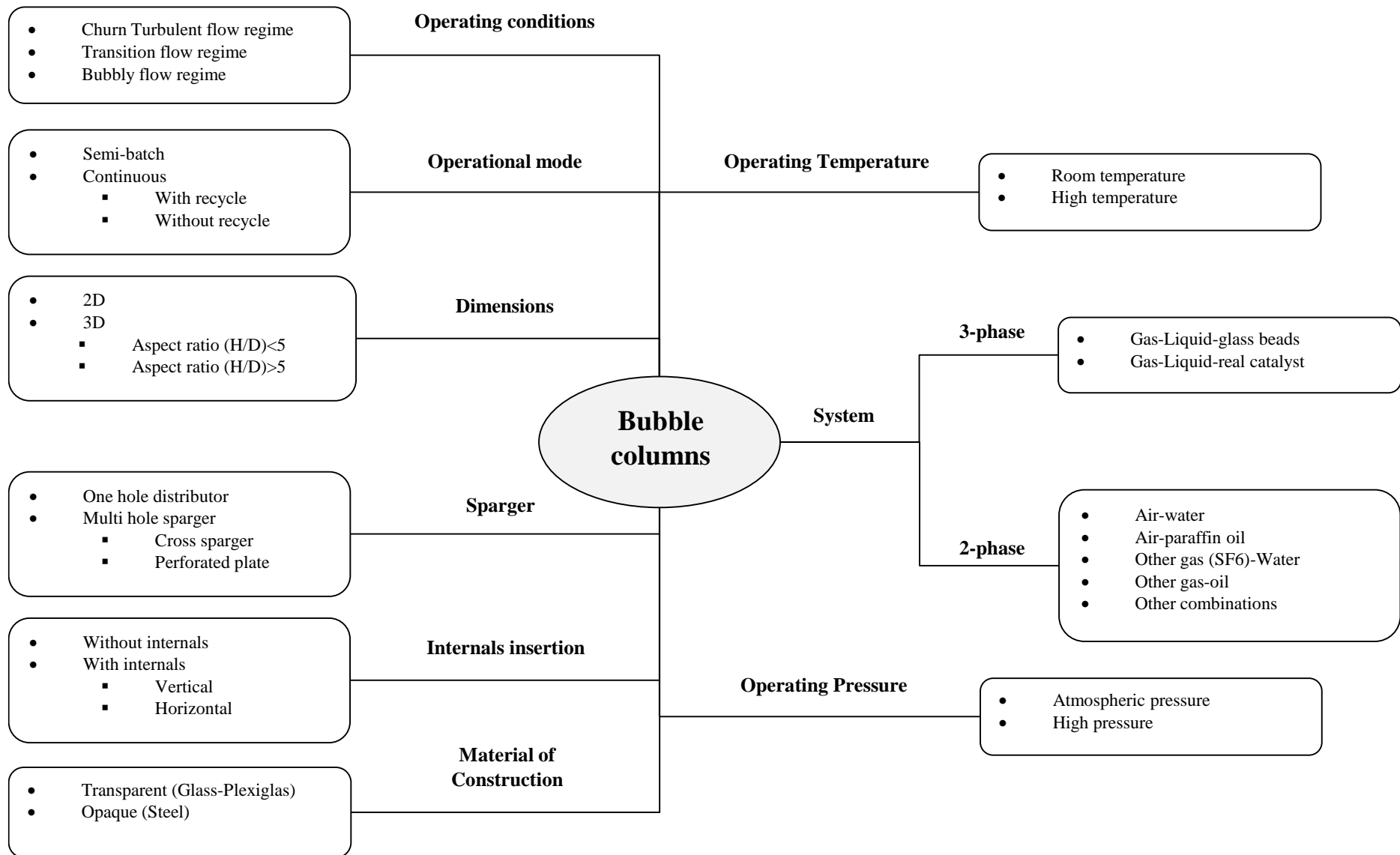


Figure 2.2 Bubble columns for laboratory use

Figure 2.2 shows the design criteria and operating conditions of the bubble columns used for laboratory purpose. The struggle is restricted amount of information provided by traditional flow measurement techniques. Flow measuring techniques used for bubbly flows are mainly classified into two types Intrusive and Non-intrusive.(Bryanston-Cross et al. 2000) (Jensen 2004) These paper mainly deals with several diagnostic techniques used for flow visualization, measurement and their perfection and drawback for given environmental conditions. This paper also talks about their future scope and development .There are mainly two types of techniques used for flow visualization nowadays intrusive and non-intrusive as follows:

- **Intrusive technique**

In Intrusive technique physical probes are introduced in the flow which may cause local disturbance at high speed, these include temperature probes and hot wire anemometer

- **Non-intrusive technique**

Second method for analysing the flow is non-intrusive where flow-marker or tracer particles are added into the flow and their behaviour is witnessed. As tracer particles are added in very small measure the flow behaviour won't change that much. E.g. Laser two focus (L2F), Laser Doppler anemometry (LDA), and particle image velocimetry (PIV).

A brief summary of some of these techniques mentioned below:

- **Laser Two Focus (L2F)**

This is single point method, where velocity of small particle (in micron) in the flow is measured. Two highly focused parallel beams are projected which function as a light barrier. One of the particles conveyed by the flow which passes through the two beams emits two consecutive light signals and the time interval serves as a value in the determination of the particle velocity.

- **Laser Doppler Anemometry (LDA)**

Laser Doppler anemometry (LDA) also known as laser Doppler velocimetry (LDV), consist of two sections namely transmitting and receiving. This method works via interference patterns from an intersecting grid of coherent light and can measure 3 components of velocity at a point. The problem with this technique is when we have to map whole flow field we have to move the interrogating spot from one place to another which is time consuming and unable to give instantaneous flow mapping. Another problems are to get good results we will need proficiency in that field and patience to inspect the obtained results.

- **Particle image velocimetry (PIV)**

Here in particle image velocimetry (PIV) flow is seeded with appropriate tracer particles then flow is illuminated by dual power laser source. The time between two illumination is noted down, and these two illuminations are captured by using CCD camera on two different frames and divided into small areas known as interrogation window. These interrogation windows from both the frames are compared by using cross-correlation analysis where we will get distance between particle positions on the respective interrogation windows. As we know the distance and time then we can get velocity for each interrogation window, so by reconstructing image we will get velocity map for given flow field. This technique is advantageous over LDA if we want flow mapping instead of point measurement but requires more time to get setup ready and costly because use of CCD camera, high powered system.

Numerous experimental works regarding gas–liquid flow in 2D columns have been carried out in the last decades as shown in Table 2.1 (Becker, Sokolichin, and Eigenberger 1995) , (Delnoij, Kuipers, and van Swaaij 1997) , (Buwa and Ranade 2002) , (Buwa and Ranade 2004). Visualisation study by (Delnoij, Kuipers, and van Swaaij 1997) , (Tzeng, Chen, and Fan 1993) , (J. J. J. Chen, Jamialahmadi, and Li 1989) , (R. C. Chen, Reese, and Fan 1994) , (Sarraf 1999) displayed flow structures in bubble column. Over the years many instruments have been used to visualise and characterise bubble column reactors. Simplest technique used for characterizing bubble flow by (Drahoš et al. 1991) , (Letzel et al. 1997) , (Kulkarni and Joshi 2006) , (Buwa and Ranade 2003) via measurement of wall pressure variation. This method is widely used because of its simple gears and high precision. U-tube manometer or pressure transducers can be used to measure the pressure variations between any two locations. With the help of optical fiber probe local void fraction and instantaneous positioning of the plume fronts were measured by (Rensen and Roig 2001). Recently used laser-Doppler anemometer technique provides point velocity information (Becker, Sokolichin, and Eigenberger 1995) , (Becker, De Bie, and Sweeney 1999) , (Mudde, Groen, and Van Den Akker 1997) , (Bhole, Roy, and Joshi 2006) , (Olmos et al. 2003).

The initial studies on bubble column with the use of PIV reported are (T.J. Lin et al. 1996) , (Mudde et al. 1997). Phase discrimination technique have been used to separate bubbles and used tracer particles (R. C. Chen and Fan 1992) , (Bröder and Sommerfeld 2003). In this phase discrimination scheme distinguished bubbles were isolated using technique called masking, mask image consist of marked areas where bubbles are present. Detected bubbles pixel value is fixed to 1 and other region pixel value to 0 so, when image arithmetic operations like image

multiplication is done between original images and masked image only we will get desired phase. In the case of large bubbles which reflects more scattered light than those of tracer particles so detection of tracer particles in the locality of such bubbles is very challenging. Also, the flares caused by intense laser reflection are exist in the flow domain so the determination of bubble shape is very problematic. Which indirectly leads toward low resolution velocity field.

(Tokuhiro et al. 1998) Proposed phase discrimination technique based on shadowgraph imaging to distinguish between bubble and liquid phase. Where they have used two cameras facing towards each other for collecting PIV and shadowgraph data on Single bubble fixed in downward liquid flow but backlight intensity and placing of two cameras is critical for the accomplishment of the experiment. The use of fluorescent seeding particles and appropriate filters on cameras has been very productive scheme to avoid the flaring triggered by laser light reflection (Delnoij et al. 2000).

(Liu et al. 2005) Observed that as fluid viscosity reduces the bubble rising path changes from 1-D to 3-D, also turbulence intensity and Reynolds stress is more intense in liquid of low viscosity and turbulence is also enhanced by the frequency of bubble formation. (Liu and Zheng 2006) confirmed that a bubble is in ellipsoid shape when it is in the high viscosity liquid but gets nearly spherical shape as viscosity of the liquid decreases also magnitude of vorticity behind the bubble for high viscosity liquid is more than low viscosity liquid for same flow rate and bubble size.

(Brady et al. 2006) Homogeneous isotropic turbulence generated by cylindrical grids using PIV is discussed in this paper. As flotation process occurs at high turbulence flow of three phases (Solid, liquid, gas) so their detailed understanding is quite limited. (Schubert 1999) used solid particle heavier than water (As particle mass increases, the Stokes number increases). Similarly (Saffman and Turner 1956) assumed that Stokes number in between 1 or less, while (Abrahamson 1975) assumed that stokes number as infinity, so none of these models are applicable for real flotation conditions. To study how these conditions are affecting collision etc. operations, fluid velocity measured in grid turbulence. (Jambunathan et al. 1995) In this paper authors have proposed improved cross correlation method for analysing images in PIV because there might be chances that velocity gradient presence within interrogation window. Firstly authors have explained conventional cross correlation method and its drawback, here two consecutive frames are divided into interrogation windows and compared.

When high cross correlation value is observed then we can say that particles from first frame are matching with the shifted second frame and Small cross correlation peaks may be observed when individual particle images match with other particle images. Helmholtz velocity theory divides a movement of a flow element into three subsidiary terms namely translation, rotation and element bi-axial shear respectively. (Westerweel 1993) has noticed that, if the examination window is considered as a flow element, then the rigid shift results in parts of frame A and frame B only contributes to cross correlation value, rotation and deformation terms lead to enlargement of the peak (Willert and Gharib 1991).The improved cross correlation method restructures a second image by considering the effects of the three terms in a two-dimensional flow and given algorithm shows to be significantly more accurate for simulated uniform, recirculating and bi-axial shearing flows.

2.2 Bubble size distribution and measurement

In air-liquid two phase flow substantial bubble properties like bubble break-up and coalescence, bubble rise velocity, BSD, gas phase volume fraction controls the mass transfer operation. Bubble size distribution, gas holdup are main topics of recent research on bubble columns(Bouaifi et al. 2001) , (Luo et al. 1999) , (Anabtawi et al. 2003) , (Veera, Kataria, and Joshi 2004).

There are numerous ways to find BSD, gas hold-up for bubble column for instance intrusive techniques like capillary suction probes (Laakkonen et al. 2007) , wire-mesh sensors (Prasser, Scholz, and Zippe 2001) and non-intrusive techniques like tomographic, image processing technique (Sadr-Kazemi and Cilliers 1997) . Mainly non-intrusive technique offers advantage over intrusive in terms of investigation of high gas hold-up and BSD of the system without affecting the flow at higher gas flow rates. Tomographic tools are relatively costly and obtained results are often poor in spatial resolution and photographic techniques have the potential to measure BSD precisely but only employed where system is transparent.

Optical, photographic and acoustical are the widely used and accepted BSD evaluating practices throughout the years.

- **Optical Method**

The optical method is mainly based on either the light-blocking principle or dark-field specular reflection and monitoring the transmitted light intensity. A laser beam is projected into the flow and a photo sensor is engaged to measure the reflected and refracted light coming from a gas bubble or solid particle.

Table 2.1 Earlier experimental work on rectangular bubble column (air-water) characterization.

Author	Column Dimension W×D×H (m)	Measurement Technique	Methods and Findings
Chen et al. (1989)	0.76 × 0.05 × 1.2 & 0.175 × 0.015 × 1.8	Visual observations	Effect of various gas flow rates and H/W ratio on flow structure was studied.
Tzeng et al. (1993)	0.483 × 0.0127 × 1.6	Visual observations	Influence of various gas flow rates and gas injectors on flow structure was studied.
Becker et al. (1994)	0.50 × 0.08 × 2	Laser Doppler anemometry	At fixed superficial gas velocity liquid flow field information compared to simulation results and Plume oscillation frequency found out.
Lin et al. (1996)	0.1016, 0.1524, 0.2032, 0.3048, 0.4826 × 0.0127 × 1.6 & 0.6096 × 0.0064 × 2.29	Particle image velocimetry	For various column widths and superficial gas velocities -flow structures, vortex size, wavelength, and frequency was studied
Delnoij et al. (1997)	0.25×0.02×2	Visual observations	Plume oscillation frequency measurement for different flow rates and H/W ratio
Becker et al. (1999)	0.20×0.05×0.45	Laser Doppler anemometry	Plume oscillation frequency measurement for various superficial gas velocities
Sarrafi et al. (1999)	0.15×0.1×1.5	Visual observations	For perforated plate gas distributor gas velocity leading to the transition in-between homogeneous to heterogeneous regimes a criterion has been developed for the gas velocity.
Rensen and Voig (2001)	0.15×0.15×0.67	Optical fibre probes	Plume oscillation frequency, plume width for different superficial gas velocities
Buwa and Ranade (2002)	0.20×0.05×0.90	Pressure transducer	Plume oscillation frequency at various sparger design and superficial gas velocities
Olmos et al. (2003)	0.4×0.04×1.2	Laser Doppler anemometry	Characterization of flow regime with the help of various signal processing methods on LDA measurements

The bubble size need to be bigger than the wavelength of the light. This method is incessant one, however only applied on small investigation portion of the flow (Meernik 2016) , (Zhang and Sun 2012).

- **Photographic Method**

The photographic imaging system comprises of a HSVC with appropriate lighting. The interrogation areas are larger compared to the optical method, however for not losing resolution interrogation area should be kept smaller. Disadvantage offered by this method is tedious analysis and cameras price. Recent studies on bubble size distribution shows that this method only employed for transparent systems(Sadr-Kazemi and Cilliers 1997) , (Grau and Heiskanen 2002) , (T. J. Lin, Tsuchiya, and Fan 1998) , (Lage and Esp??sito 1999) , (Homayouni et al. 2008).

- **Acoustic Method**

In this method BSD measurement is based on a distribution of sound wave through a multiphase (air-liquid) flow. Signal strength recognized by receiver and speed at which signal travels is strongly affected by bubble motion. These signal are later analysed and BSD is found out on the basis of signal strength. Recent studies(Pandit et al. 1992) , (Wu and Chahine 2010) on bubble size distribution shows that this method offers great advantages over previous techniques such as it does not require transparent system, measurements are easily and rapidly conducted, distinguishes between bubbles and particles, interrogation area and spatial coverage is greater compared to previous techniques.

Overall, non-intrusive approaches are superior over intrusive. Digital image analysis (Rafael C. Gonzalez, Richard E.Woods, and Eddins 2009) have advantages in terms of easier optics arrangement as compared to laser- diffraction methodologies along with the ability of providing the velocity and size statistics of the gas phase. In general, non-intrusive like high-speed video visualisation of the bubble flow combined with digital image processing offers valuable statistics concerning bubble size distribution. Recorded images by HSVC with the help of shadowgraph technique, analysed by the use of commercially available software's such as MATLAB. Digital image processing can employed for estimation of the bubble size distribution and velocity information of rising bubble and also allow bubble tracking.

Unfortunately, the withdrawal of data about bubble size, shape and motion turn out to be further difficult with increment in the gas hold-up as bubbles overlap each other. Latest discoveries on bubble size distributions at immovable locations in the reactors show that bubble sizes are

subjective to significant change at elevated pressure and temperature conditions (Schafer, Merten, and Eigenberger 2002) , (Wilkinson and v. Dierendonck 1990).

2.3 Gas holdup and measurement

The easiest way to define gas holdup (or void fraction) is the amount of volumetric gas fraction. In a bubble column, gas holdup is easily determined by measuring the clear liquid height and dispersed liquid height or pressure change with and without aeration. Gas holdup is one of the major subjects of latest research on bubble columns(Bouaifi et al. 2001) , (Luo et al. 1999) , (Anabtawi et al. 2003) , (Veera, Kataria, and Joshi 2004) .Gas holdup is mainly depend on the amount gas flow rate introduced into the column. The relationship between gas hold up and gas flow rates for specific flow regime is represented in Figure 2.3 .

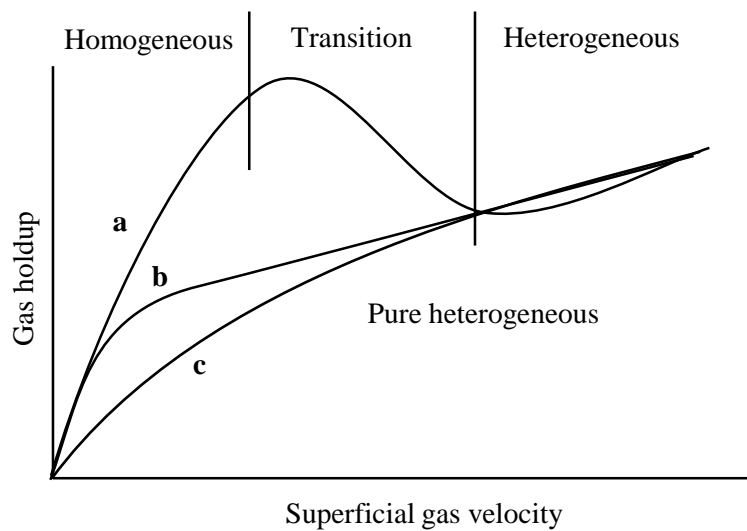


Figure 2.3 Schematic of the gas holdup behaviour for different flow regime.

When homogeneous, transitional, and heterogeneous flow regimes are created, there are two dissimilar associations of gas holdup as a function of gas flow rate; one yields a local maximum gas holdup (curve a) and other one does not (curve b). The reason behind it use of different aeration plate. For curve c continues but nonlinear behaviour is observed. Numerous studies has been done on effect of gas holdup on bubble column hydrodynamics in past decades. The easiest way to calculate gas holdup in bubble column is either by pressure drop measurement (Hikita et al. 1980) using pressure transducers (Kumar et al. 2012), water manometer (Xia, Yang, and Wang 2011), (Moshtari, Babakhani, and Moghaddas 2009).

If we consider ρ_s as average slurry density, ρ_w as water density and ρ_a as apparent density of bubbles between two measurement locations. Then gas hold is measured using following formula,

For water manometer,

$$\varepsilon_g = \frac{\rho_s - \rho_w \left(1 - \frac{h}{L}\right)}{\rho_s - \rho_a}$$

For differential pressure transmitters,

$$\varepsilon_g = \frac{\rho_s - \rho_w \left(\frac{\Delta P}{\rho_w g L}\right)}{\rho_s - \rho_a}$$

Using electrical tomography (Sharifi and Young 2013),(Jin et al. 2007),(Fransolet et al. 2005) optical fiber probe (Li et al. 2012),etc. also employed for finding gas holdup in bubble column reactor. Image processing techniques can be used for transparent and dilute systems to find out gas hold up. Here in this technique whole reactor is divided into number of interrogation areas and individual interrogation areas their images were taken. These obtained images then stored and processed to find out diameter and equivalent volume information of each and every bubble. So, obtained bubble volume is added up together to get volume of gas present in the reactor.

2.4 Bubble rise velocity, RTD, effect surfactant addition

The Motion study of a single bubble rising in still liquid is valuable to comprehend and describe gas-liquid bubbly flows. As it is known, buoyancy and drag forces regulates the bubble's rise velocity in a liquid column. Interactions between forces occur due to surface tension, viscosity, inertia and buoyancy produce a several effects which are often proved by dissimilar bubble shapes and trajectories(Talaia 2007) .If we consider a train of rising bubbles in still liquid then its rise velocity can be determined by single bubble plus the velocity defect affected by the wakes (Marks 2014). In bubble columns, the slip velocity between phases can be expressed in terms of a single bubble terminal velocity and the gas volume fraction (Shah et al. 1982).

In water treatment operations, a bubble column employed to transfer ozone from a gaseous to a liquid phase. The key factor affecting the efficiency of these reactors is the contact time with microorganisms, oxidizable compounds, and ozone(Le Sauze et al. 1992). The residence time distribution (RTD) of a bubble is defined as the amount of time spend inside the reactor. An understanding of residence-time distribution of bubbles and their effects on column reactor

performance is one of the requirements. Time spend by particular bubble inside reactor is depend up on the surface area of a bubble. Some of the bubbles may escape immediately while others spent so much time depend up on the size of the bubble. What is vital in the study of bubble column is not average residence time of the bubbles but rather the residence time of each bubble.

Surfactants are the materials which made up of molecules which consist both polar and non-polar parts. The main advantage of surfactants is they reduce surface and interfacial tension by accumulating at the interface of immiscible fluids. These types of materials can have a significant effect upon the gas-liquid hydrodynamics, specifically on the bubble size and gas hold-up. If an effect of surfactant addition is compared between surfactant free water and surfactant added water then it is found that surfactant added water have an increase in number of bubble. In surfactant added water bubbles tend to become smaller with decreasing surface tension of water. Therefore, surfactant presence upsurges the gas hold-up(Asari and Hormozi 2013).

Chapter 3

Experimental procedure & methodology

3.1 Bubble Column Experimental setup

To investigate the two phase flow in a bubble column, a test rig with 700 (Height) x 200 (Width) x 57 (Depth) mm convectional acrylic glass bubble column is designed and commissioned at IIT Hyderabad. A single needle sparger was used. Leintz (3 HP) compressor having free air delivery of 0.003331948997 cumecs (cubic meter per second) was used to force air through the sparger.

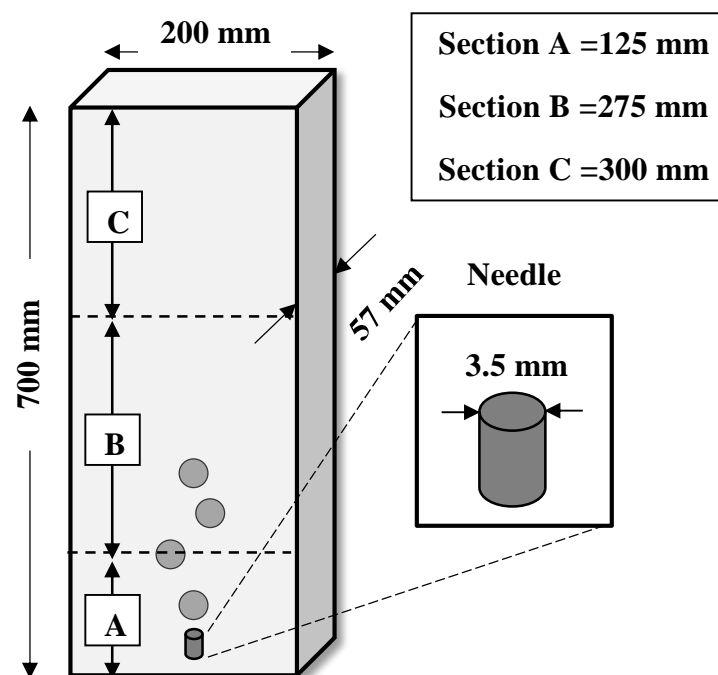


Figure 3.1 Schematic of a bubble column setup.

Variable area rota meters having range of 10L/h to 30 L/h and 60 L/h 600 L/h were used to measure the gas flow rate. H/W (liquid height to column width) ratio of 2 maintained with a clear liquid height of 400 mm in the column with the use of tap water. It has been reported in recent literature on 2-D bubble column that different values of H/W result in the existence/nonexistence of unsteady structures and generation of them. In this manner, when H/W=1 bubble plume does not oscillate, establishing a simply still bubble jet that either rises vertically or moves horizontally, forming a lone liquid circulation cell (Borchers et al. 1999) ,

(Delnoij, Kuipers, and van Swaaij 1997). For $H/W = 2$ the staggered vortices mode of circulation prevailed and the development of unsteady structures has been reported (Delnoij, Kuipers, and van Swaaij 1997) , (Elena Díaz, Montes, and Galán 2006). In addition, as the H/W increased to 2, the number of unsteady vortices increases to 3 .Therefore, the aspect ratio has been proven to be a very important experimental variable when studying non stationary structures.

Figure 3.1 shows the representation of the experimental setup of bubble column. Figure 3.2 show needle sparger schematic having 3.5 mm single central diameter were used to perform experiment in rectangular bubble column. Similarly, Figure 3.3 shows the nozzles sparger schematic having nozzle diameters of 0.5, 0.7, and 0.9 mm with pitch between the nozzles around 30mm. While using 5 point nozzle sparger central, extreme left and right nozzles were kept open and others in closed position because of even gas distribution through nozzles.

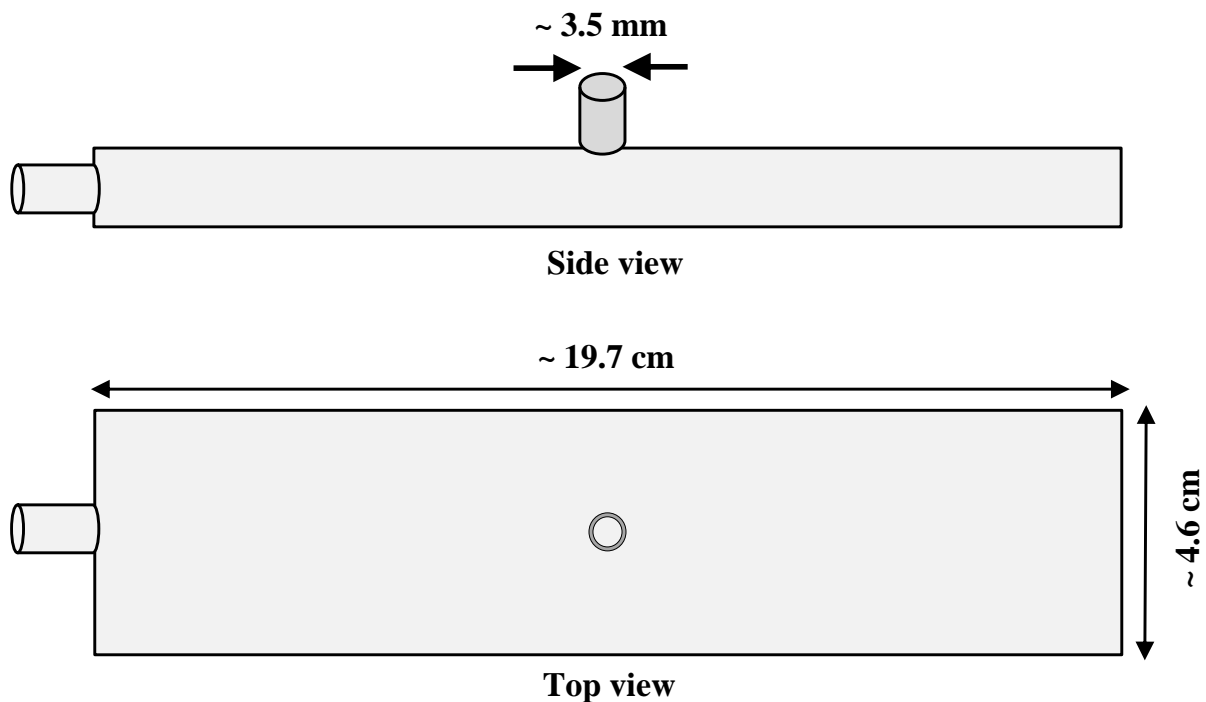


Figure 3.2 Needle sparger schematic used for experiment

Different gas flow rates of 50 L/h, 100 L/h, 150 L/h, 200 L/h, 300 L/h, 400 L/h, and 500 L/h were used to perform the experiment.

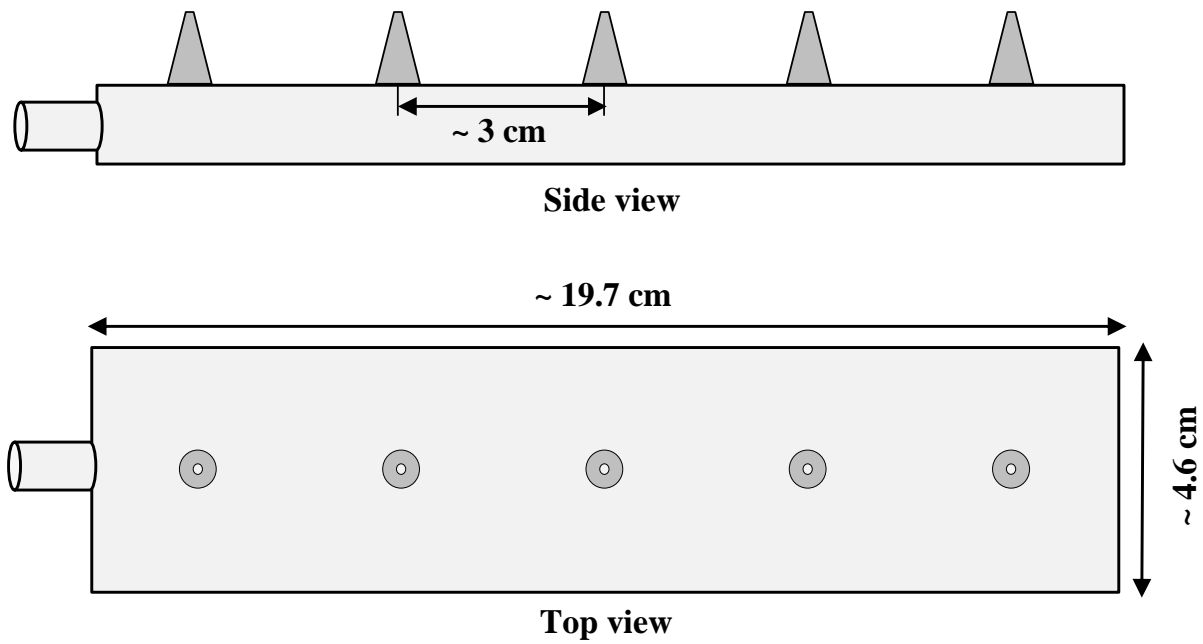


Figure 3.3 Nozzles sparger schematic used for experiment

3.2 PIV theory

In order to observe fluid flow behaviour addition of the tracer particles is not new, it has been used over ages .The first person to try this in more systematic manner to study the flow was Ludwig Prandtl (1875-1953), a German scientist , in the early 20th century.

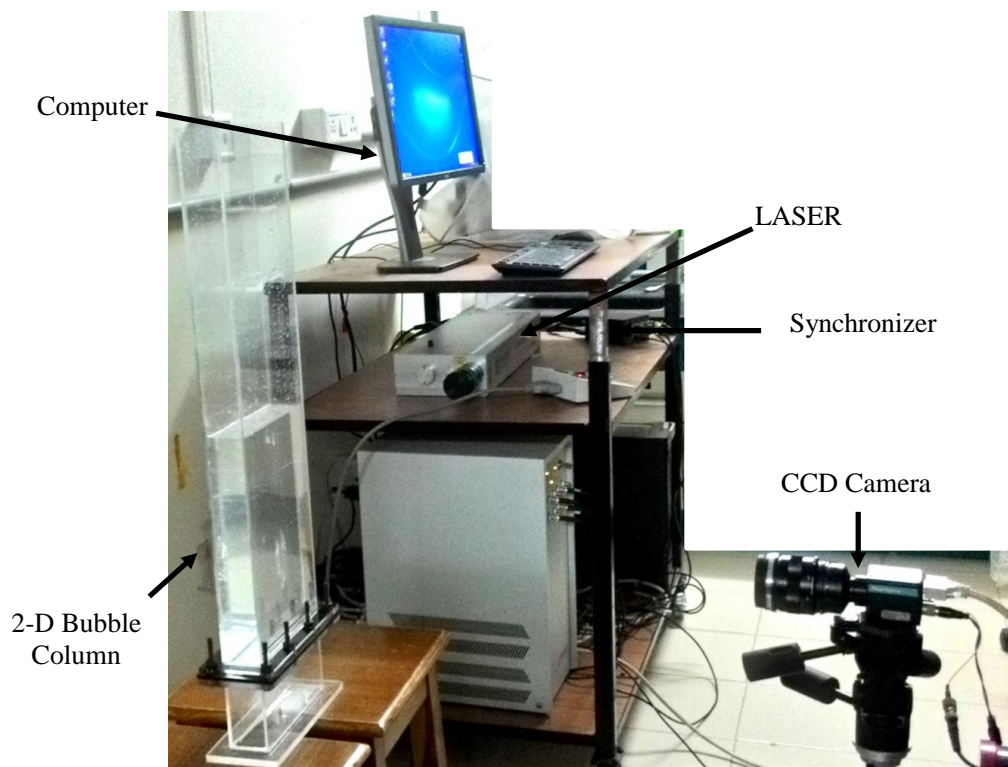


Figure 3.4 Actual photograph of laboratory PIV system used to investigate 2-D bubble column

Roots of PIV can be found in Laser speckle velocimetry, a practice that numerous groups initiated investigating with in the late 1970s. In the early 1980s it was observed that it was beneficial to reduce the particle concentration where distinct particles can be detected. The actual laboratory 2-D PIV system used to measure bubble column flow component shown in Figure 3.4.

Table 3.1 summarizes the specification of the 2-D PIV system used, which was composed of a double-pulse laser, laser-sheet optics arrangement, a CCD camera, a synchronizer, and a computer for image processing.

Table 3.1 Specification of the 2-D PIV system used

Model	Nano L 135-15 PIV
Laser	Nd:YAG double pulse
Output (maximum)	400 mJ/pulse
Wave length	532 nm
Pulse interval	50 μ m
Pulse duration	4 ns
CCD camera used	FlowSense4M (Model 9080C0913)
CCD camera resolution	2048 \times 2048 pixels

Laser has some unique properties such as availability of large amount of light (from 20 mJ to 400 mJ) in short time (\sim 5ns), monochromatic and parallel which make it ideal candidate for PIV application. To convert a laser beam into a thin plane laser sheet for PIV applications is one of the challenging task to do. Figure 3.5 shows PIV optical arrangement for producing sheet of laser light. The essential elements for producing laser sheet are Nd: YAG double pulsed laser, mirror, dichroic filter, spherical lens and cylindrical lens.

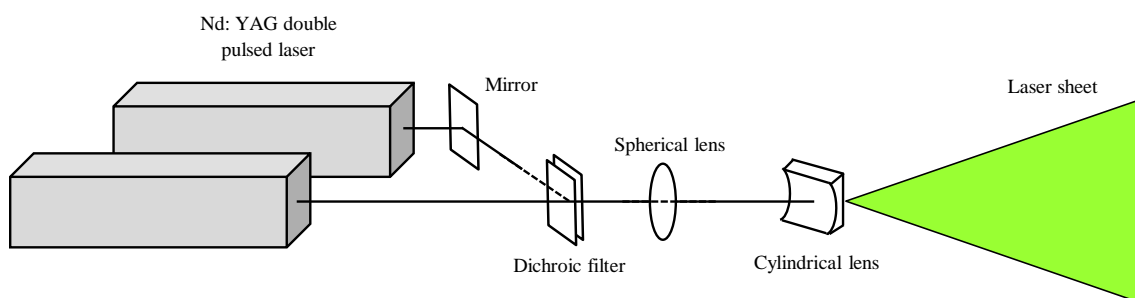


Figure 3.5 PIV optical configuration

While using laser like argon-ion laser which is have small diameter then only one cylindrical lens can be enough to produce laser sheet of required shape. But for other light sources such as Nd: YAG lasers, an arrangement of various lenses is typically required to create tinny light sheets. In this case atleast one more lens is requires to focus laser light to an appropriate thickness.

PIV optical configuration to produce this sheet of laser consist of several movable lenses and use the identical principle which is stated below:

- Spreading operation comprise of adjustment of the sheet width and evolution of the width and which can be achieved by using cylindrical lenses
- Focusing operation involves the evolution of the sheet thickness and can be achieved by using spherical lenses.

Dichroic filter transmit only certain wavelengths of light, reflecting the rest of the wavelength range coming from either mirror or laser source directly. The main advantage using dichronic filter is they do not absorb this unwanted energy through process and so do not become practically as hot as the equivalent conventional filter. Spherical lenses generally does not permit light sheet height and thickness coming from diachronic filters independently. Cylindrical lenses converge or expand light coming from spherical lens in only one dimension.

As we know it the cylindrical lens produce laser into plane while the spherical lens transforms the plane into thin sheet. This is important issue because 2- D PIV does not measure flow properties normal to the laser sheet and it can be eliminated by preserving laser sheet to 2- D laser sheet.

The schematic of a PIV setup and involved components arrangement is shown in Figure 3.6. Following steps are followed when performing PIV experiments

- Flow is seeded with the help tracer particles
- Region of interest (ROI) is illuminated by using thin sheet of laser light
- Consecutive images of illuminated ROI are taken in pair forms with a small time-difference
- PIV images then analysed by splitting into small examination regions with the help of autocorrelation or cross-correlation method and the velocity field information found

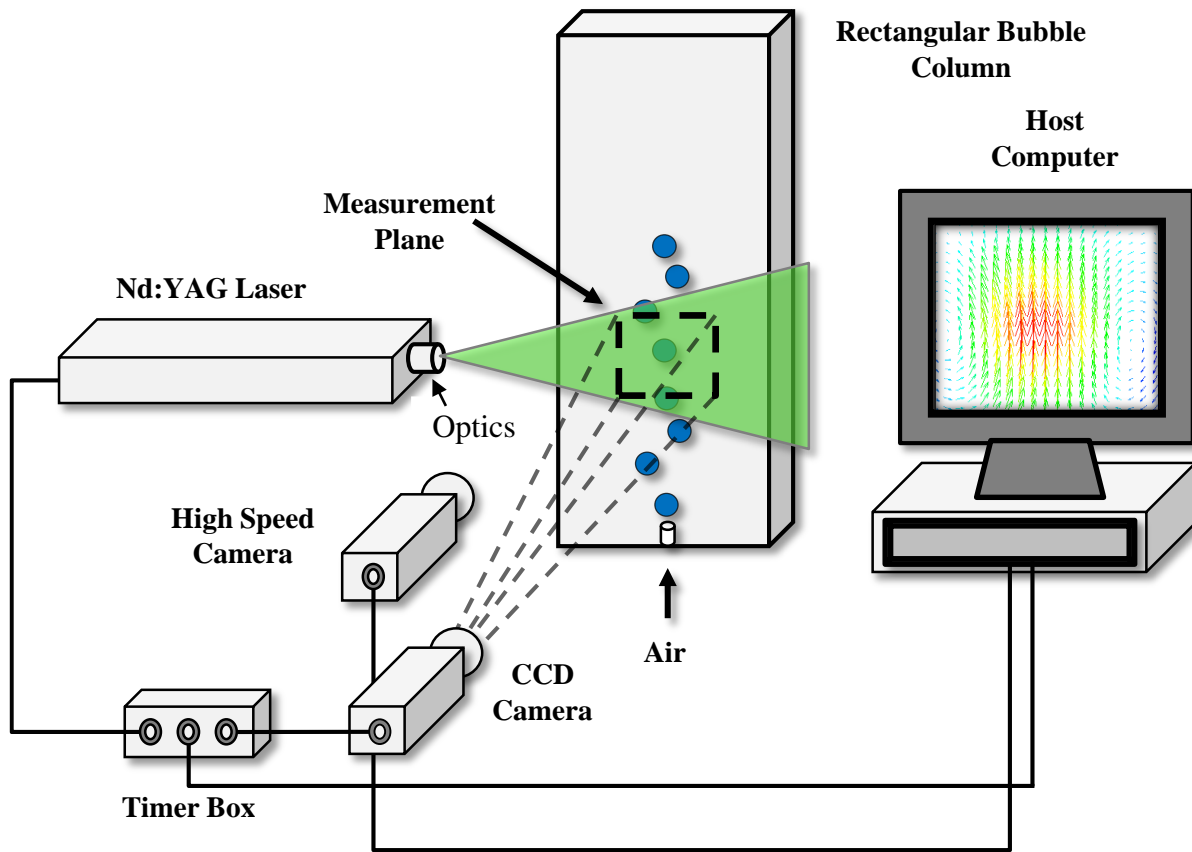


Figure 3.6 Schematic of PIV setup

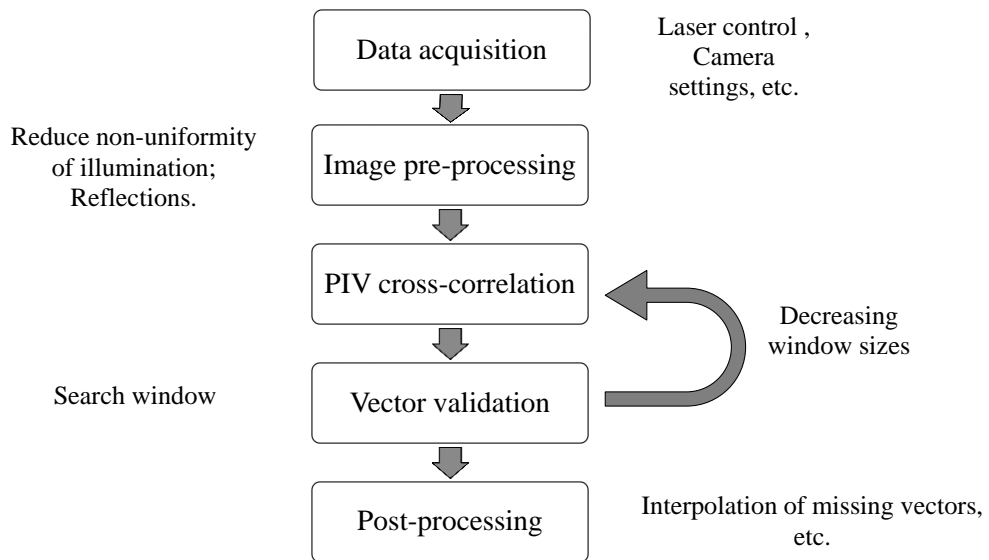


Figure 3.7 Steps involved in a generic PIV program

Figure 3.7 shows the steps involved in a generic PIV program followed. In data acquisition step high quality images acquired to do so PIV system components are arranged and set in appropriate manner. Acquired images then pre-processed to eliminate unwanted distortion or reflection and to enhance some image feature. Pre-processed images then further investigated

for velocity information by using cross-correlation methods. Insufficient particle image pairs, gradients may produce spurious vectors which can be eliminated by reducing integration window size. Finally post processing involves interpolation of missing vectors.

3.2.1 PIV system Components

- **Tracer particles**

The tracer particles usage in PIV experiments is an inherently critical factor (Melling 1997). The tracer particle must match the fluid properties which is under investigation or else they won't follow the flow reasonably adequate required for the PIV investigation to be considered precise. If we choose small tracer particles then they might follow the flow exactly and their step response is good but problem persist when we take light scattering effect into the account as they have bad light scattering effect. Similarly if we choose large tracer particles for PIV experiments then they have bad step response and won't follow flow motion but their light scattering effect is good as shown in Table 3.2.

- **Criteria for choosing tracer particles:**

Table 3.2 Comparison between small and large tracer particles used in PIV experiment

	Follow the flow	Light scattering	Step response
Small particles	Good	Bad	Good
Large particles	Bad	Good	Bad

- ✓ Non-toxic, Non-corrosive , Non-volatile, chemically inert
- ✓ Should follow the fluid motion
- ✓ Should be distributed homogeneously
- ✓ Uniform displacement within interrogation region

- **Types of tracer particles used for different flow**

- ✓ **For gas flow:**

- TiO₂, Al₂O₃, glass, olive oil, corn oil
 - Usually particle diameter of 1-5 μm is a good compromise

- ✓ **For liquid flow:**

- TiO₂, Al₂O₃, polymer, polystyrene, micro sphere H₂ bubble
 - Usually particle diameter of 10-20 μm is a good compromise

- **Reason why particle may not follow flow**

- ✓ Specific Forces (Electrostatic, Magnetic).
- ✓ Particle Inertia.
- ✓ Particles near boundary (Gradients).
- ✓ Random thermal vibration of particle (Brownian motion).
- ✓ Sedimentation

In stokes regime or low Reynolds number (small particles) inertia property can be neglected and terminal velocity (highest velocity attained by particle as it falls and where drag force + buoyancy force = gravity force) equation will become,

$$U_T = \frac{(\rho_P - \rho_F)4r_P^2 g}{18\mu}$$

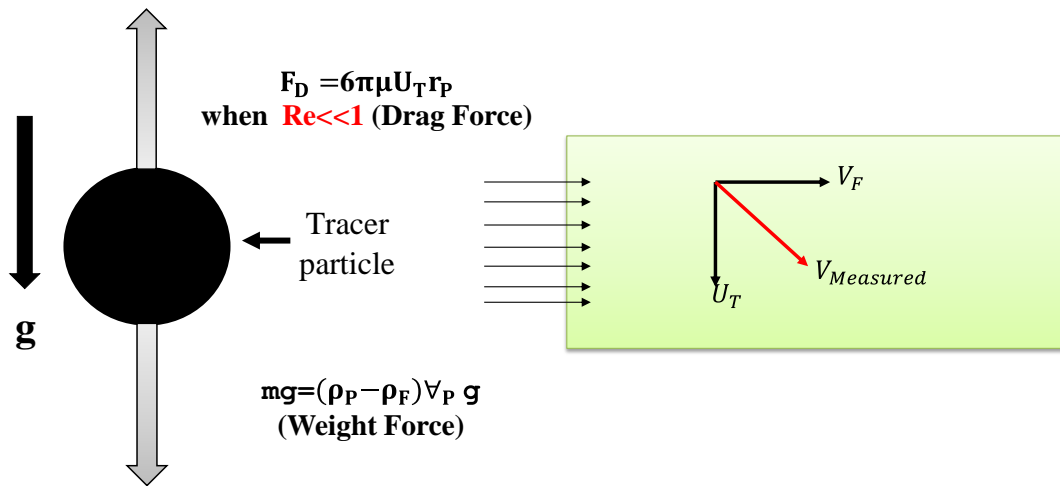


Figure 3.8 Relationship between tracer particle motion and flow condition

In above equation buoyancy force can be neglected as density difference between tracer particle and fluid is negligible. So until unless $U_T \ll V_F$ no problem with the tracer particles but when $U_T \geq V_F$ need to work more as shown in Figure 3.8 . Here V_F stand for velocity of the fluid in which tracer particles are added. For spherical particle having Reynolds number $Re > 1$ Maxey–Riley equation used to tack the motion as shown in Figure 3.9.

- **Camera used**

For performing PIV study on the required flow, two exposures of laser light are essential on the camera from the flow. Initially, because of camera incapability to capture multiple frames at great speed, both exposures were used to capture on single frame.

- **Helium-Neon(633nm)**
 - ✓ Continuous wave laser
 - ✓ Cheap but not very powerful
- **Argon-Ion(488,514nm)**
 - ✓ Continuous wave laser
 - ✓ Can be very powerful
- **LEDs**
 - ✓ Short pulse
 - ✓ Available in various colours
- **White Light**
 - ✓ Xe flash lamp
 - ✓ Short pulse
 - ✓ Overheat problem
- **Nd:YAG (Neodymium-doped yttrium aluminium garnet; Nd:Y₃Al₅O₁₂) laser (1064,532,355,266nm)**
 - ✓ Short laser pulses(~5ns)
 - ✓ Monochromatic and parallel
 - ✓ Lots of photon in short amount of time
 - ✓ 532nm good range for safety reasons and can be seen by naked eyes
 - ✓ Heavily used in PIV

- **Synchronizer**

The synchronizer which is controlled by computer perform as an external activator for both the camera(s) and the laser source. The main job done by synchronizer is command timing of each and every frame of the CCD camera conjunction with the laser source firing within precision of 1 nanosecond. Information of this timing is precarious as it is required to determine the velocity of the fluid in the PIV investigation.

3.3 PIV experimental setup and measurements

Figure 3.6 represents a schematic illustration of the PIV system. PIV was applied to estimate two velocity-field components over a plane analogous to the x and y-axes. The PIV system used, consist of FlowSense 4M CCD (model 9080C0913) camera with 2048 x 2048 pixels resolution and Dantec Dynamics double-pulsed Nd:YAG (neodymium-doped yttrium aluminium garnet; Nd:Y₃Al₅O₁₂) laser of 532 nm wavelength. Specified flow field was seeded using Rhodamine B-Particle having density of 1050 kg/m³ and a mean diameter of 9.84 μm.

With the help of homogenizer tracer particles were distributed homogeneously over whole column.

A laser induced fluorescence (LIF) technique was applied to capture the images of both bubbles and tracer particles simultaneously. To ensure that CCD camera records only the red scattered light by fluorescent particles not green light scattered by bubbles a long wave pass filter (550 nm) mounted in front of the CCD camera. To get good resolution PIV images, column has been divided into three sections namely section A, B, C as shown in Fig.8. The statistics of PIV velocity field were performed using Dynamic Studio (Version: 3.41.38.0).

3.3.1 2-D PIV system calibration

Once PIV system components are put together, following few operational aspects has to be examined before going for actual experiments: optimisation of the image, calibration of an imaging system in the presence of normal directional laser sheet. Utmost important aspect among them is calibration of an imaging system. Calibration of an imaging system governs the precision of velocity measurements, so careful calibration has to be done in order to get accurate results. Quality of measurement is affected by the quality if the image acquired. It is possible to improve recorded images further with help of image pre-processing, but it always better to have best acquired image possible in the original recordings. There are several factors which may cause bad acquisition of desired images such as uneven laser pulse energies, imbalanced light intensity, low particle concentration, uneven background, laser flaring and poor visibility of particles. These parameters can be reduced by varying the laser energy, particle concentration and exposure time delay.

The camera obtains images in pixel dimensions. These pixel dimensions required to be transformed into a metric dimension for the velocity calculation to be meaningful. In order to get velocity information in terms of metric units, the flow coordinated scheme has been established manually along the measurement plane while doing PIV experiments. An important step that determines the success of PIV is the calibration of the camera and laser sheet of plane. This means finding the origin, positioning of the x-y plane and defining the scale within the precision needed by the experimental conditions. For good positional correctness fixed object of known dimensions or calibration plate has been used. Placement of this plate has to be on the flow measurement plane which we want to determine by using PIV. For 2-D PIV systems a ruler is introduced on the laser plane to decide the scale factor of an acquired image. When using a ruler, we must be able to get two accurate positions that are a known distance separately



Figure 3.10 Calibration image after adjustment of ROI and image pre-processing

on a computer screen. Ruler calibration could have significant variation in the scale factor contained. The reason behind this is ruler lines edges are smeared over some pixels and it makes difficult to find exact location of the marking. If several z-planes needs to be measured then calibration plate should be accurately movable alongside z-plane. These are the few steps followed while doing the calibration of a 2-D PIV imaging system:

1. Ruler is introduced on the laser plane and the camera is then introduced in perfectly normal direction to the plane of laser sheet by adjusting it then few images were acquired for calibration as shown in Figure 3.10.
2. Acquired images then pre-processed to obtain improved images of good visibility of ruler scale
3. Finally two accurate positions that are a known distance (metric dimensions) are marked on the images as shown in Figure 3.11 and their real life distance (usually mm) is compared with pixel distance and scale factor obtained.

As from Figure 3.11 known distance was 60mm then number of the pixels present in between those measuring points measured which were around 1000 pixels. So now 60mm is equal to 1000 pixels that means 1mm is equivalent to 16.67 pixels.

The precision of the calculated scale factor is proportional with the distance between reference marks A and B. A large distance will give a better precision.

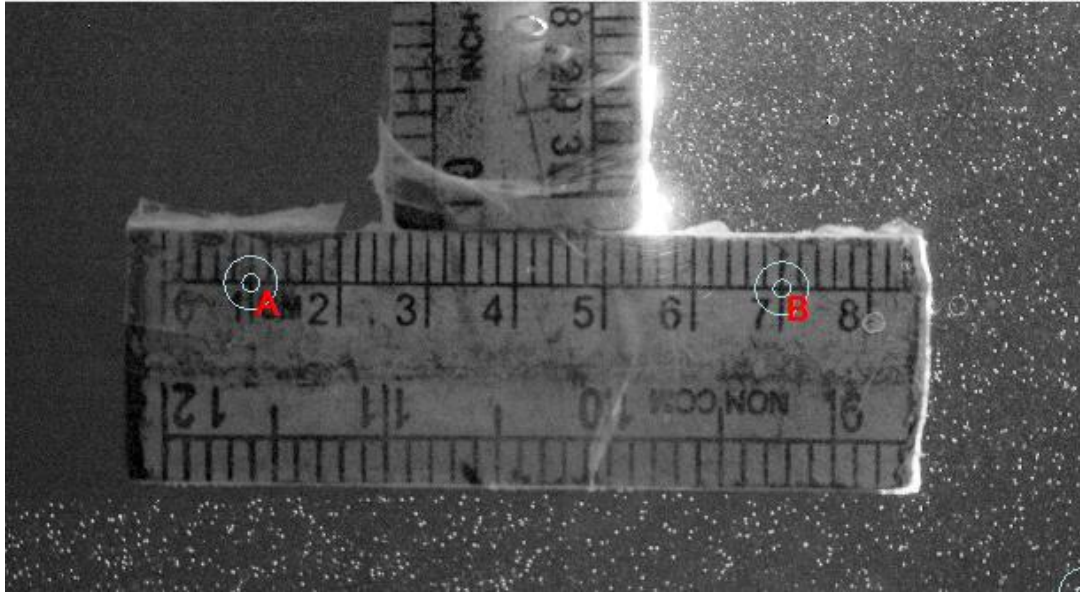


Figure 3.11 Selected reference position for calibration

3.3.2PIV analysis

It is very difficult to find same particles in both frames because all the particles look alike. So instead of finding single particle in both frames PIV uses statistical approach such as cross-correlation to find out displacement of group of particles. Both the frames are divided into smaller interrogation regions Figure 3.12 (a) and Figure 3.12 (b). The group of particles for given interrogation area creates unique fingerprint that can be searched into both frames. Cross-correlation technique has been used to calculate particle displacement over time Δt as shown in Figure 3.13 for each and every window and thus the velocity.

Let's consider Frame A is original position of group of particles Figure 3.12 (a) captured at $t = t_0$ while Frame B is displaced position of group of same particles Figure 3.12 (b) at $t = t_0 + \Delta t$ time. Frame B is then scanned in defined search area and relative correlation value is determined. Correlation value will be maximum when unique fingerprint is found on frame B of that original interrogation window. The horizontal (X) and vertical (Y) displacement of particles are determined by the offset of interrogation window. Since we know time interval between two frames which is Δt and displacement (ΔX and ΔY) which is used to determine velocity vector Figure 3.13 by using simple formula $(\Delta X \text{ or } \Delta Y) / \Delta t$.

Now it is possible to estimate a displacement vector for each and every real PIV image interrogation window with assistance of signal processing by cross-correlation techniques mentioned above.

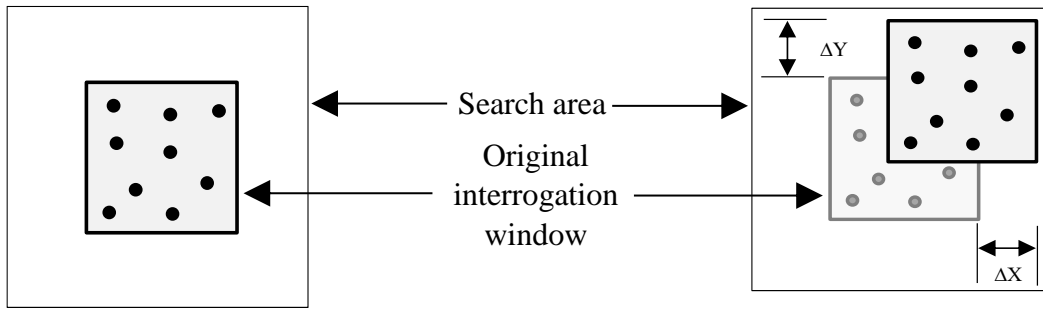


Figure 3.12 (a) Frame A original positions of particles, (b) Frame B displaced positions of particles

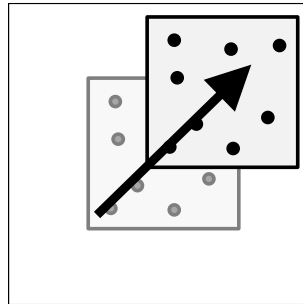


Figure 3.13 Velocity vector measurement

Velocity vector field (Figure 3.14(f)) for entire frame (Figure 3.14 (a), (Figure 3.14 (d))) has been calculated with the help of cross-correlation method.

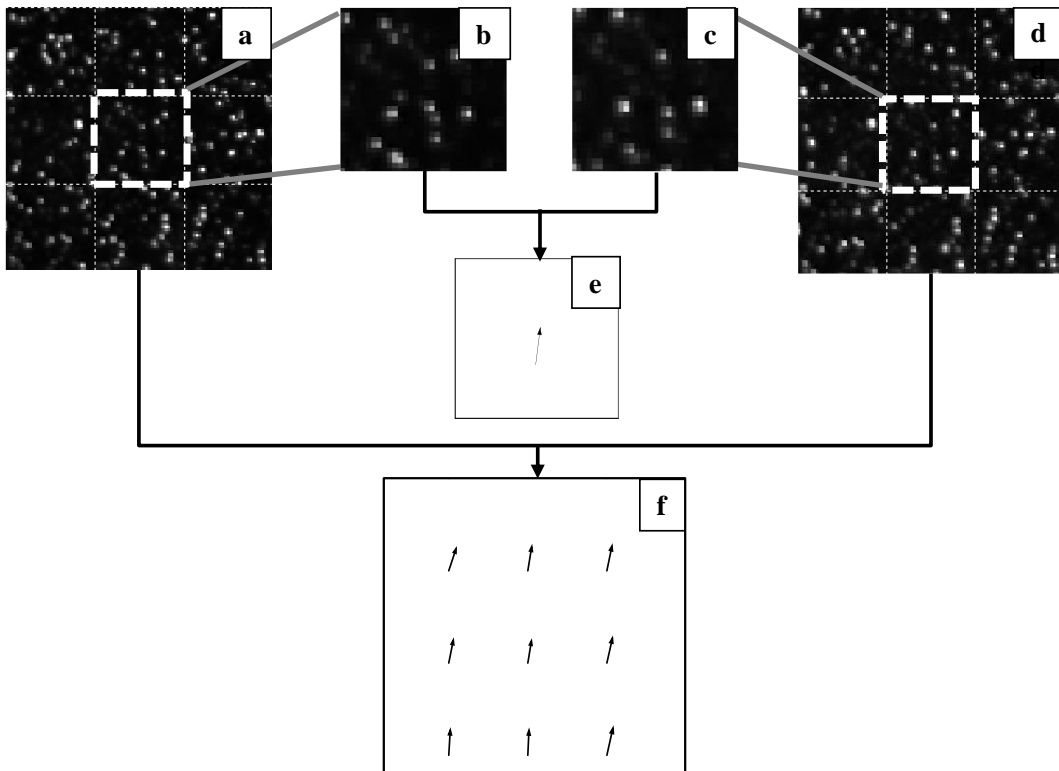


Figure 3.14 (a) Image at $t = t_0$, (b) Interrogation area at $t = t_0$, (c) Interrogation area at $t = t_0 + \Delta t$, (d) Image at $t = t_0 + \Delta t$, (e) Particle velocity vector, (f) Vector field

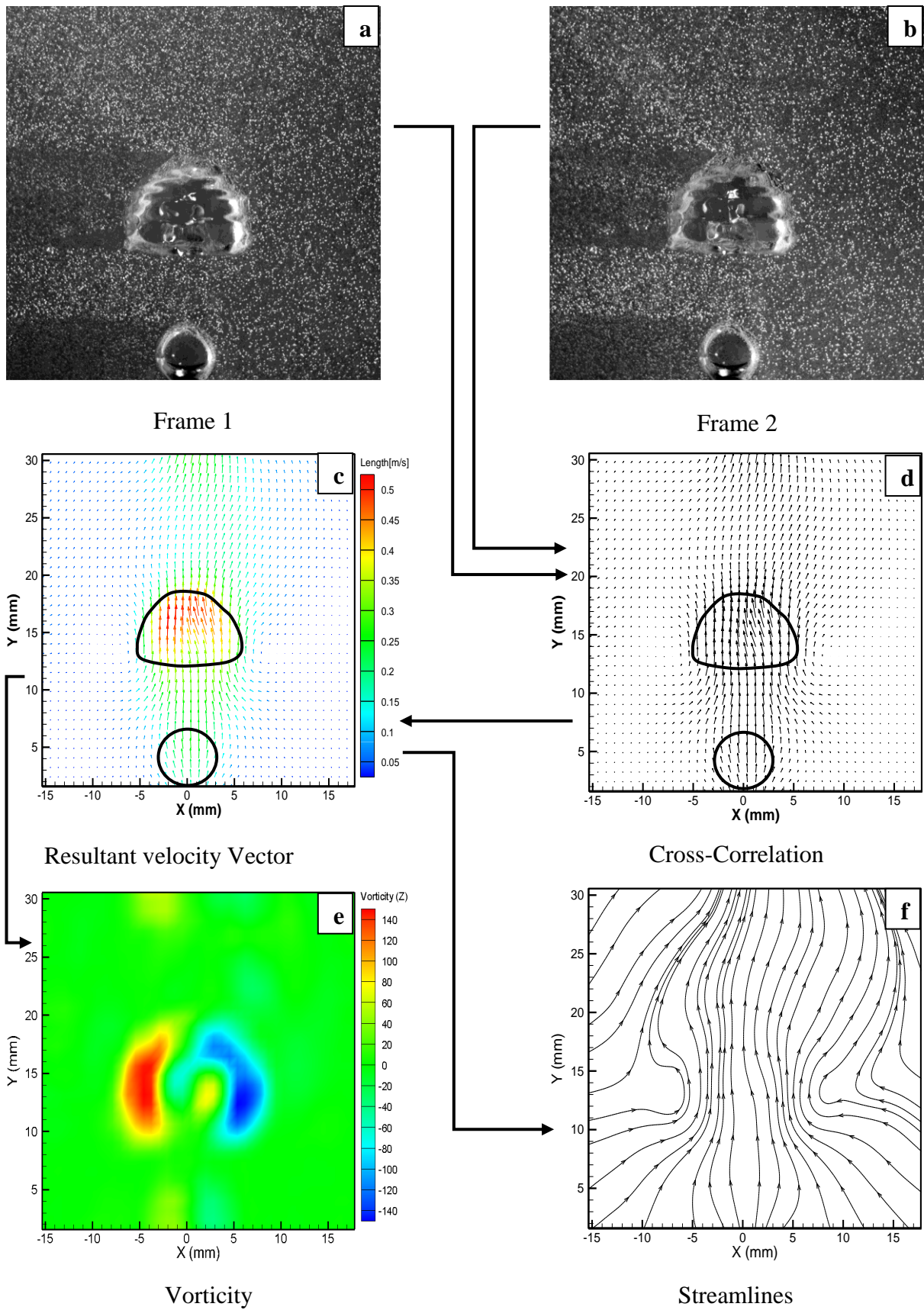


Figure 3.15 Stepwise PIV demonstration for single bubble

Figure 3.15 represents stepwise PIV demonstration for single bubble rising in liquid water. PIV images Figure 3.15 (a) & Figure 3.15 (b) has been processed to get velocity field information (Figure 3.15 (c)), vorticity value around rising bubble (Figure 3.15 (e)) and streamlines pattern (Figure 3.15 (f)).

3.4 Image processing for BSD measurement

To avoid interferences from the light outside the entire experiments were carried out in a darkroom. The shadowgraph technique has been used to get much more precise evidence on the bubble shape and size than front lighting photography. To calculate BSD obtained shadowgraph images were analysed by MATLAB (academic Version: 2015b).

- **Shadowgraph technique**

Shadowgraph technique has been used extensively used in experimental fluid mechanics

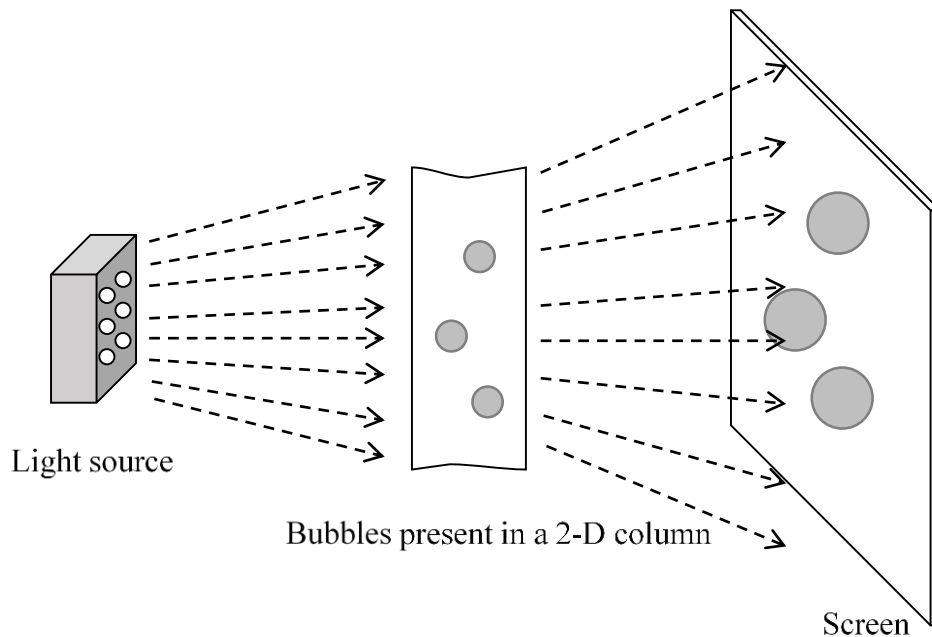


Figure 3.16 Schematic diagram of shadowgraph technique

Shadowgraph technique simplest and oldest techniques works based on the refraction of light in an inhomogeneous surroundings. The simplest shadowgraph setup consist of only a bright light, an object (bubbles) and a suitable screen or camera on which the shadowgraph images are required/acquired. Figure 3.16 shows a schematic of the shadowgraph technique.

The shadowgraph technique produces patterns with uneven greyscale level for non-uniform refractive index field (in present case bubbles), which is a function of the fluid density.

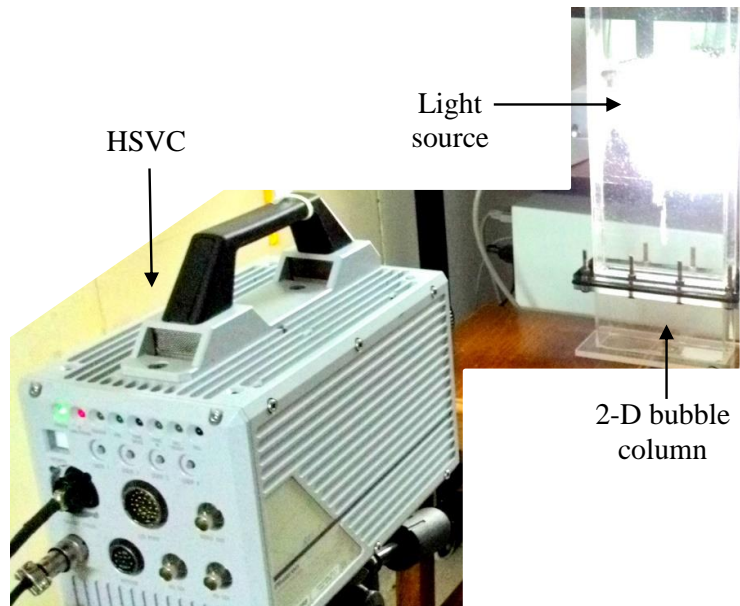


Figure 3.17 Actual lab setup of shadowgraph along with HSVC

Therefore, it is possible to find the correlation between the light intensity of the shadowgraph image and the varying refractive index of the field. Figure 3.17 shows actual lab setup of shadowgraph technique along with HSVC.

Manual image processing is still extensively used technique for evaluating various parameters and properties of observed objects. The image processing technique used to calculate BSD from image is described in the following steps:

1. Read image file
2. Image calibration provides a pixel-to-real-distance conversion factor (i.e. the calibration factor, pixels/cm), that allows image scaling to metric units. To do so we gave length of already measured object in metric dimension (i.e. mm)

Six points $P_1, P_2, P_3, P_4, P_5, P_6$ were carefully chosen on the surface edges of bubbles to obtain parameters a, b, c, d, e and f in the ellipse equation

$$ax^2 + bxy + cy^2 + dx + ex + f = 0 \quad \dots (1)$$

3. These are the following steps involved in from selecting points to ellipse fitting
 - I. Let $P_1=(x_1, y_1), P_2=(x_2, y_2) \dots \dots P_6=(x_6, y_6)$ were selected points
 - II. Now, all the selected points must satisfy the ellipse equation

$$ax_1^2 + bx_1y_1 + cy_1^2 + dx_1 + ex_1 + f = 0$$

$$ax_2^2 + bx_2y_2 + cy_2^2 + dx_2 + ex_2 + f = 0 \dots\dots$$

$$ax_6^2 + bx_6y_6 + cy_6^2 + dx_6 + ex_6 + f = 0$$

III. Since , all the points lies on same ellipse that means above equation (1) must have common solution

IV. Coefficient a , b , c , d , e , f of equation (1) found using Gaussian elimination as follows

$$\begin{bmatrix} x_1^2 & x_1y_1 & y_1^2 & x_1 & x_1 & 1 \\ x_2^2 & x_2y_2 & y_2^2 & x_2 & x_2 & 1 \\ x_3^2 & x_3y_3 & y_3^2 & x_3 & x_3 & 1 \\ \cdot & \cdot & \cdot & \cdot & \cdot & \cdot \\ x_6^2 & x_6y_6 & y_6^2 & x_6 & x_6 & 1 \end{bmatrix} \begin{bmatrix} a \\ b \\ c \\ d \\ e \\ f \end{bmatrix} = 0$$

V. Now, after getting final equation with known coefficient, ellipse fitting has been done by method developed by (Hal and Flusser 1998) and the analysis yielded the major and minor axes, orientation angle.

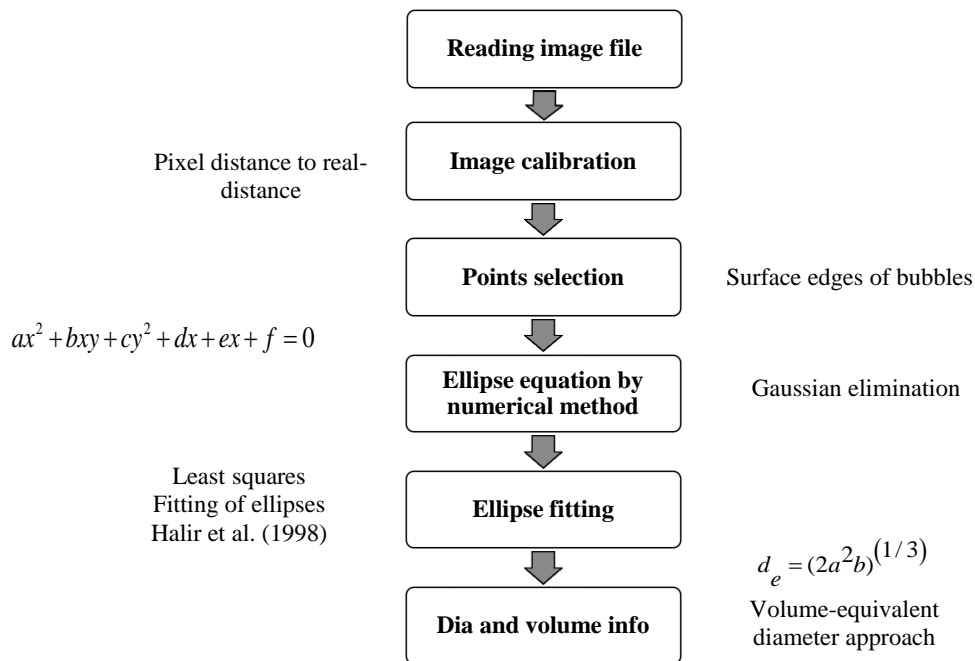


Figure 3.18 Steps involved in extraction of Dia. And volume information of a bubble

The volume-equivalent diameter approach was used to calculate the bubble diameter. It was assumed that the bubble depth was equal to the major axis, so the bubble volume equation might be expressed as follows i.e. an oblate spheroid $V=(4\pi/3)a^2b$. Thus, the volume-equivalent diameter is expressed as $d_e=(2a^2b)^{(1/3)}$.

This process mainly involve reading of an image file, image calibration, point selection, ellipse equation by numerical method, ellipse fitting, diameter, and volume information as shown in Figure 3.18.

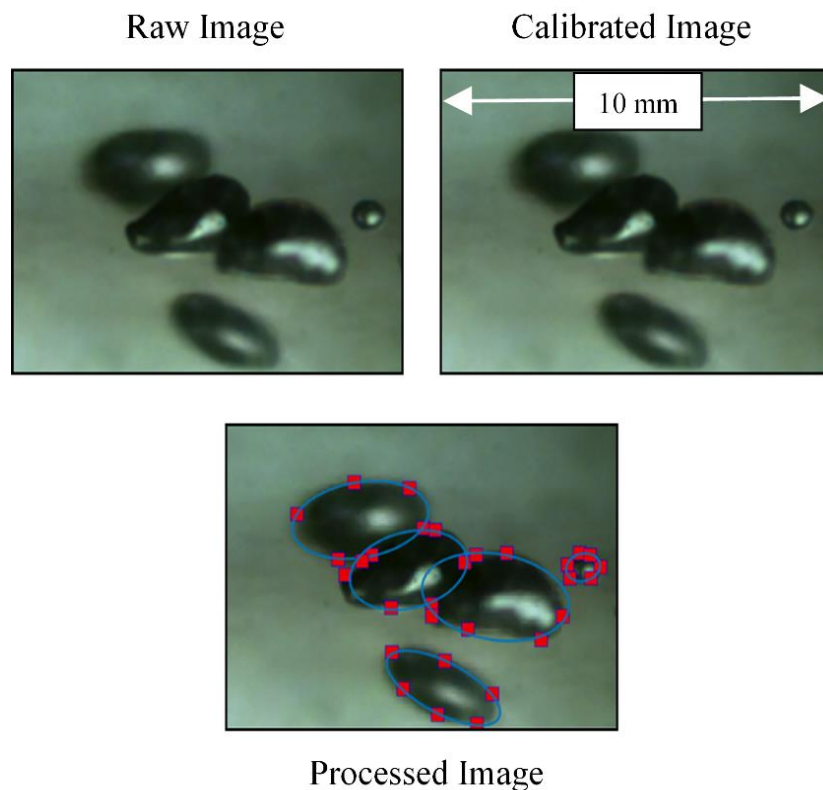


Figure 3.19 Image processing to evaluate BSD

Figure 3.19 shows raw, calibrated and processed image of actual air-liquid system. Diameter and volume information of each and every bubble is stored to find out BSD and gas hold up. This technique has an advantages in terms of direct use of processing person knowledge and have disadvantage in terms of time required for processing and possibility of high error rate because an inaccurate boundaries selection.

3.5 Image processing for RTD, Bubble rise velocity, trajectory

The shadowgraph method has been used to get video of more exact indication on the bubble shape and size than front lighting photography. These video files with 1000 fps (frames per second) were used to calculate rise velocity and, RTD and trajectories followed by the

particular bubble in different flow conditions. The reason behind taking video of 1000 fps is for easy estimation of time from frame number. All these tasks has been done by using open source video analysis and modelling software (Tracker 4.92).

Following are the key steps followed while calculation of the above listed parameters:

1. Importing the video file
2. Video calibration that allows scaling from pixel to metric units
3. Setting the reference frame origin and angle.
4. Selecting objects of interest with mouse
5. Tracking an object by marking its position on every frame
6. Storing distances and time between two consecutive frames and getting velocity and RTD information.

Figure 3.20 represents above steps in pictorial manner. Where Figure 3.20 (a) represents calibrated image, Figure 3.20 (b) represents reference frame origin and angle, Figure 3.20 (c) represents selected object of interest with mouse, Figure 3.21 (a) represents tracked object velocity vector plots and Figure 3.21 (b) represents trajectory followed by bubble.

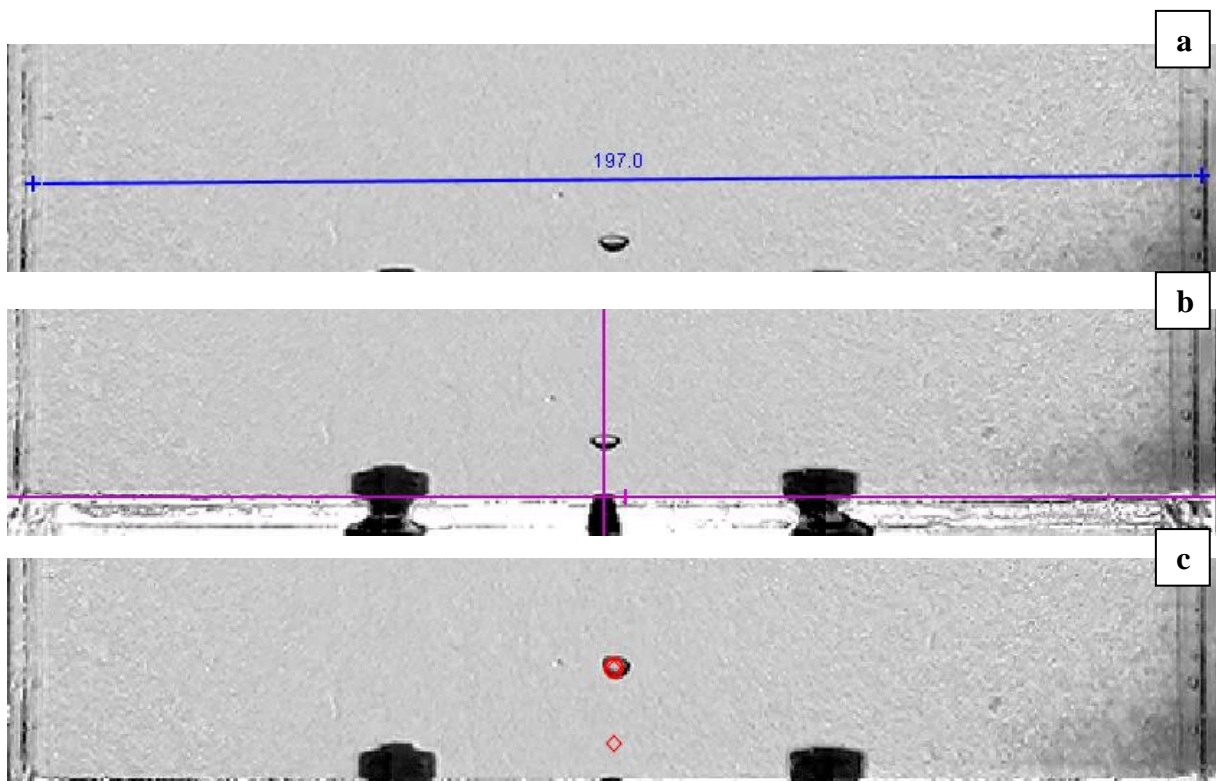


Figure 3.20 (a) calibrated image, (b) reference frame origin and angle, (c) selected object of interest

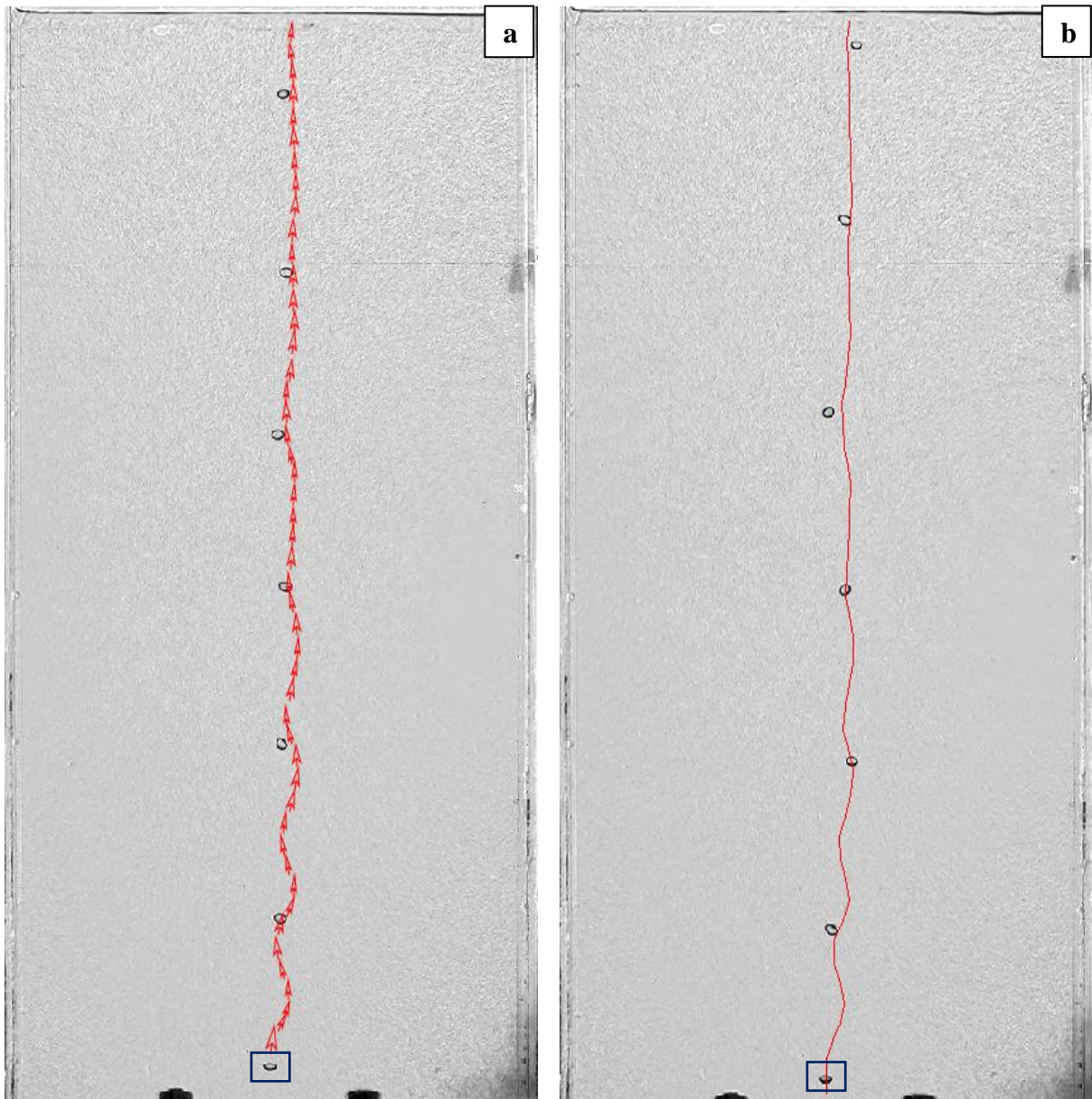


Figure 3.21 (a) bubble velocity vector, (b) trajectory followed by marked bubble

Chapter 4

Single needle source bubble dynamics

4.1 Bubble Column flow investigation by PIV

This chapter comprises of flow investigation of single needle sparger source bubble dynamics in air-liquid rectangular bubble column by PIV, image processing and flow visualisation with help of HSV. PIV has been used to calculate liquid flow field affected by rising bubble plume for three different gas flow rates. BSD and gas hold up has been evaluated using image processing technique described in previous section.

Table 4.1 Experimental conditions

Parameter	Value
Density of water	$\rho = 1000 \text{ kg/m}^3$
Initial water height	H=400 mm
Atmospheric pressure	101 kPa
Temperature of environment	22-25 °C
Density of gas (air)	1.25 kg/m ³
Gas flow rate	50 , 100 , 150 , 200 , 300 , 400 , and 500 L/h
Sparger	Needle sparger of 3.5 mm dia.

Experimental outcomes were scrutinised for the three different gas flow rates i.e. low gas-flow rates, medium gas flow rates and high gas flow rates for H/W ratio of 2. For the measurement of the liquid phase velocity with PIV it is presumed that the tracer particles follows exactly the liquid phase motion. Table 4.1 specifies various conditions used for the experiment. The time averaged liquid phase velocity field acquired from PIV measurements along liquid height (H/W=2) for different flow configuration of 50 L/h, 200 L/h, 500 L/h and section 2 is depicted in Figure 4.1 shows that the liquid is being dragged by bubbles upward towards column centre and moves downwards near the walls of the column. Total five horizontal positions were measure along height of the column namely H/W=0.1,0.25,0.50,1.0 and 1.5. The results from Figure 4.2 and Figure 4.5(a) shows that horizontal velocity components varies in range of negative to positive because of clockwise and anticlockwise circulation of liquid near around

the bubble plume. From Figure 4.2 (a) it has been observed that from left wall of the column towards centre of the column horizontal liquid velocity component (U m/s) is declining and then rising for curve $H/W = 1.5$ but for the curve $H/W = 0.50$ from left of the column wall towards centre horizontal velocity component is rising and then declining in other half towards right of the column. This is mainly because half of the measuring points of $H/W = 1.5$ lies in left half of the column and the top of anticlockwise circulation of liquid caused by bubble plume. Similarly for $H/W = 0.50$ curve half of the measuring points lies in left half of the column and the bottom of anticlockwise circulation of liquid caused by bubble plume. It has been observed that gas holdup increases as gas flow rates increases.

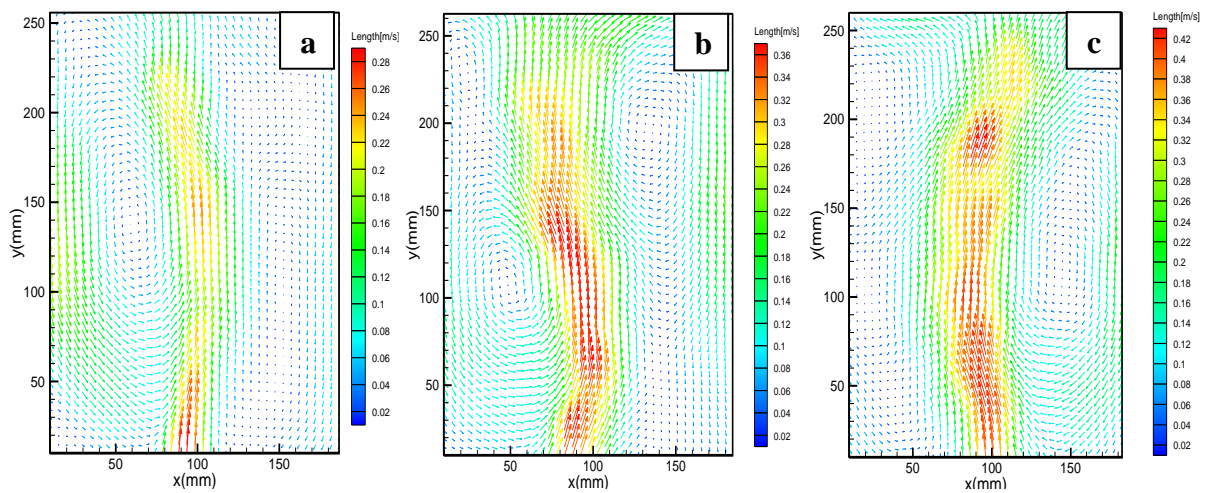


Figure 4.1 Time-averaged liquid velocity profiles of (a) 50 L/h, (b) 200 L/h, and (c) 500 L/h.

Figure 4.3 and Figure 4.5 (b) shows reasonable agreement that strong flow at the centre and low flow near the wall of the rectangular bubble column. At the centre of the column value of vertical velocity for different flow configurations 50 L/h, 200 L/h and 500 L/h are higher compared to region towards wall of the column. Figure 4.3 and Figure 4.5(b) strongly support the statement made above as towards wall vertical velocity values are negative and positive at the centre. It is also observed that at increased H/W ratio of liquid the distribution of vertical velocity along width of the column gets broad.

Resultant velocity plots from Figure 4.4 and Figure 4.5 (c) shows reasonable agreement to previous literature work on rectangular bubble column ((Besbes et al. 2015) ,(Liu et al. 2005) and (Rodrigo and Sanchez 2015)). Figure 4.6 shows the time-averaged resultant liquid velocity profiles induced by bubbles. The liquid field affected by bubbles gets wider when gas flow is increased from 50L/h to 500L/h.

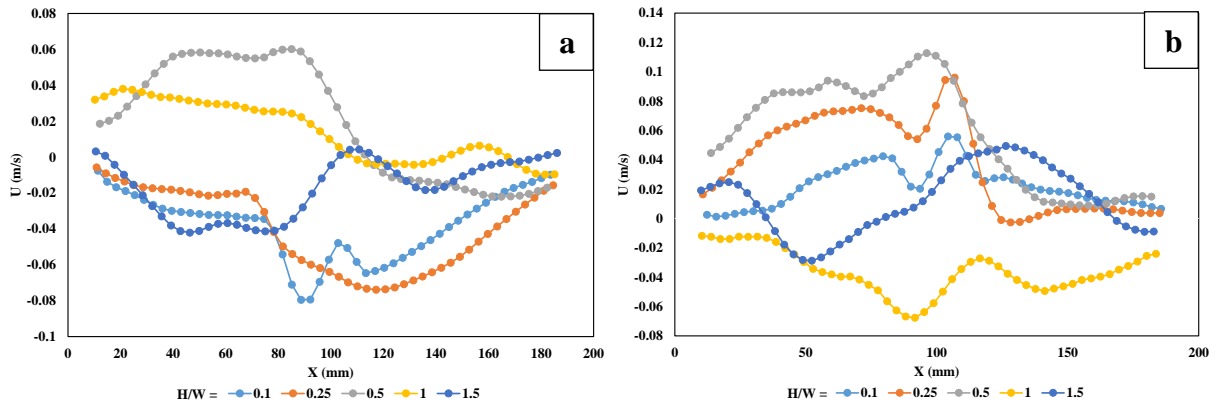


Figure 4.2 Time-averaged horizontal liquid velocity (U m/s) profiles at five positions above the needle for flow (a) 50 L/h, (b) 200 L/h

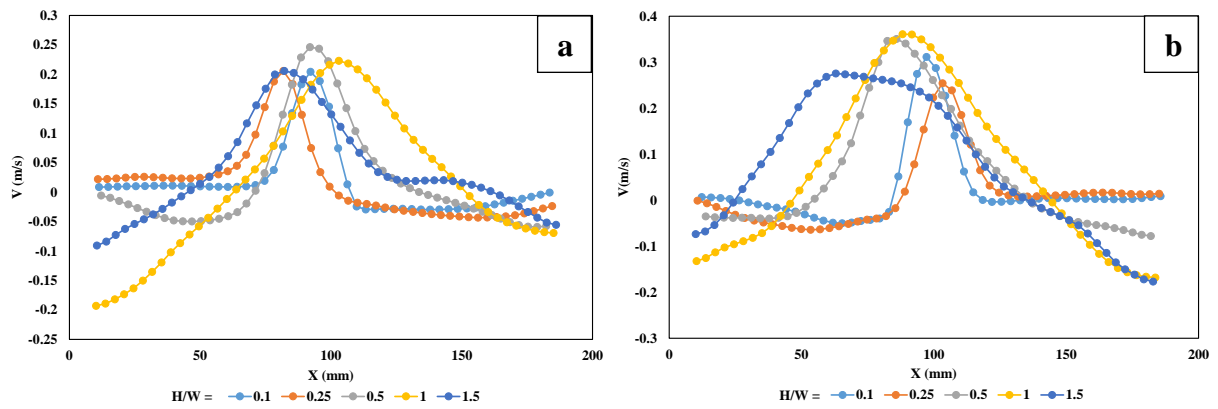


Figure 4.3 Time-averaged vertical liquid velocity (V m/s) profiles at five positions above the needle for flow (a) 50 L/h, (b) 200 L/h.

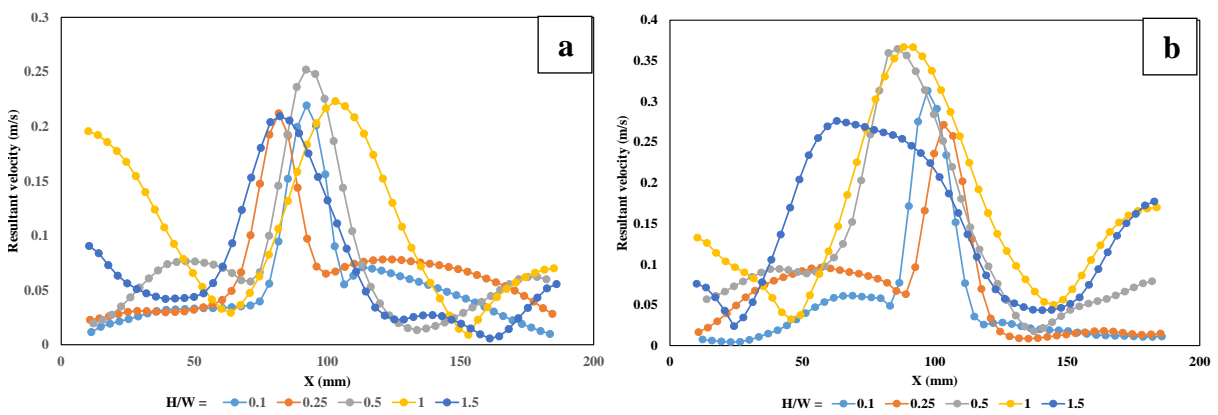


Figure 4.4 Time-averaged resultant liquid velocity (m/s) profiles at five positions above the needle for flow (a) 50 L/h, (b) 200 L/h.

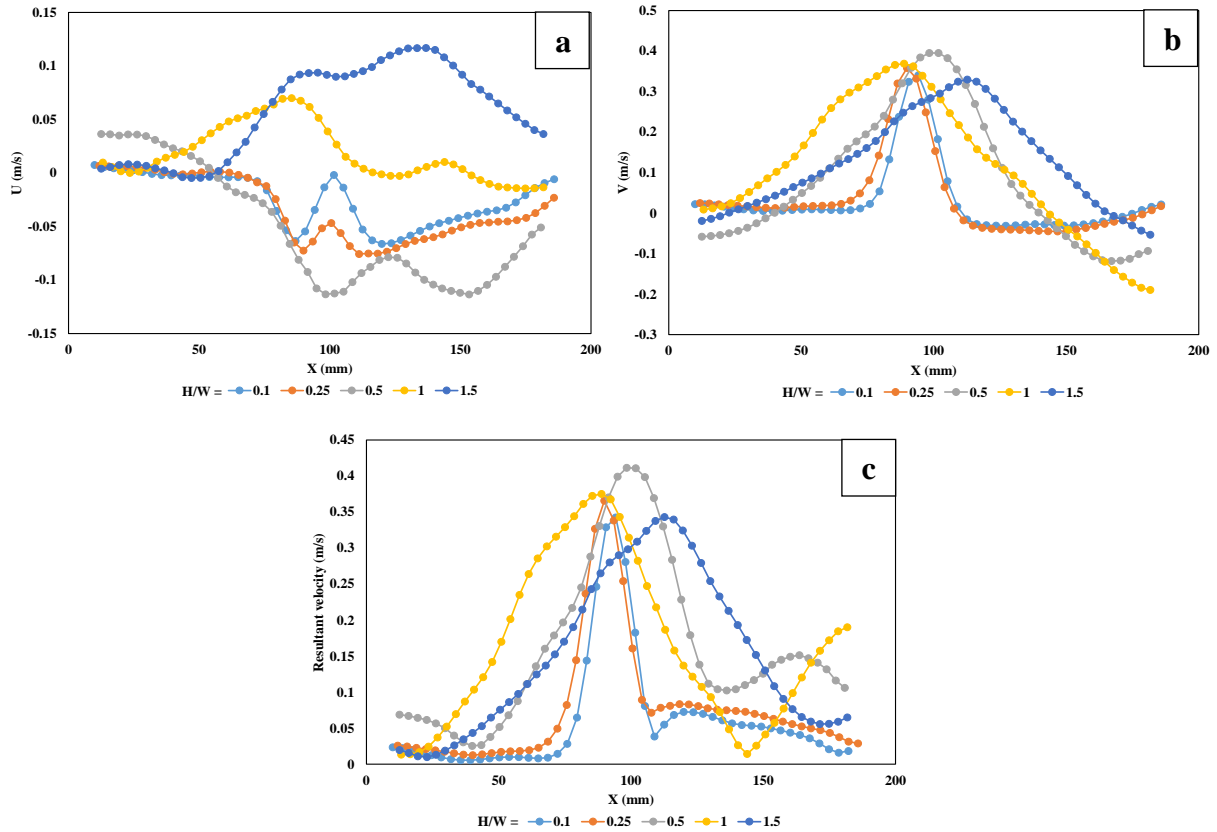


Figure 4.5 Time-averaged (a) horizontal liquid velocity (U m/s), (b) vertical liquid velocity (V m/s) and (c) resultant liquid velocity (m/s) profiles at five positions above the needle for flow 500 L/h

Figure 4.7 illustrates the time-averaged vorticity contours. The liquid field affected by bubbles gets wider when gas flow is increased from 50L/h to 500L/h. From the centre of the column to left vorticity climbs to maximum positive value, then reduces lower value to near the wall. Similarly from the centre of the column to right vorticity climbs to maximum negative value, then reduces to lower value near the wall. Positive vorticity represents shows anti-clockwise rotation of liquid phase while negative vorticity value denotes clockwise rotational motion. There is no vorticity along the middle of the rising bubble path. Figure 4.8 displays the whole field time-averaged streamlines during different gas flow rates which mainly indicates that the ascending flow accelerates along the bubble plume. The flow pattern in the rectangular bubble column considered in the current study varies from homogeneous to heterogeneous according to the gas flow rates. From Figure 4.6 it is witnessed that there are two large circulation flow regions of liquid near the bubble plume (at the right and the left side of the bubble plume).

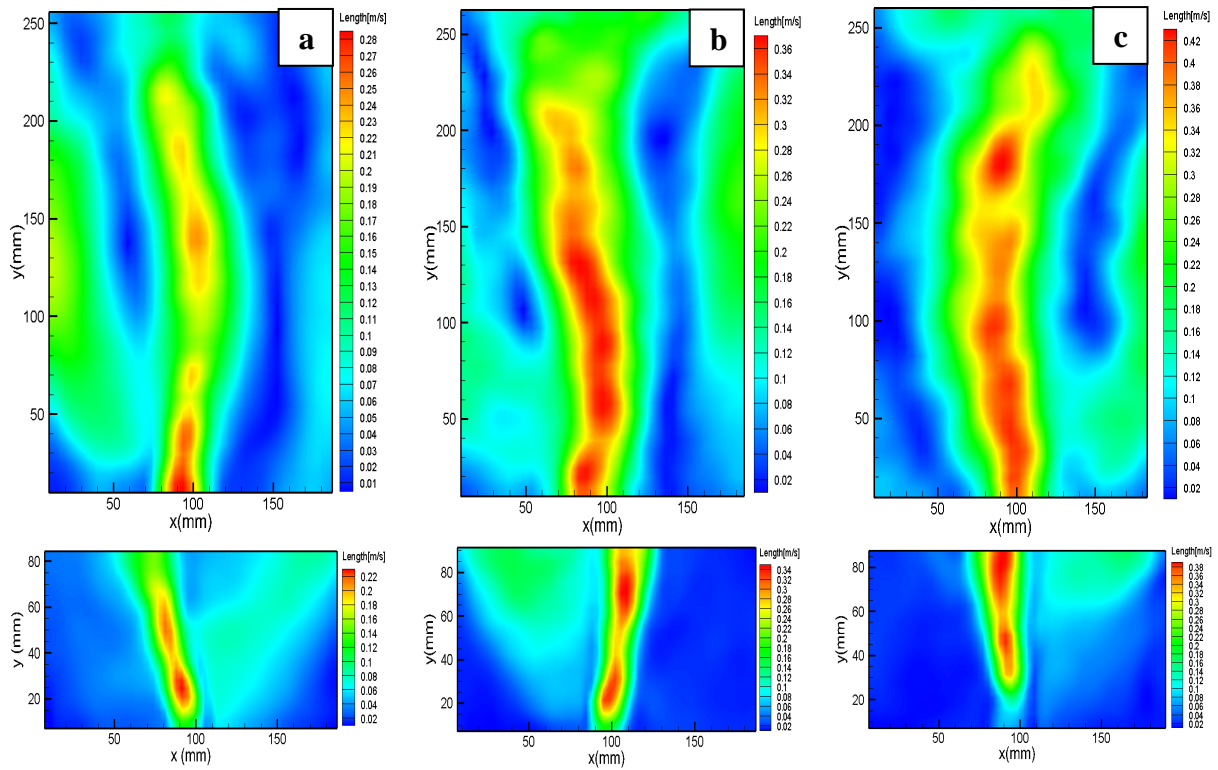


Figure 4.6 Time-averaged resultant liquid velocity profiles for flow (a) 50 L/h, (b) 200 L/h, (c) 500 L/h

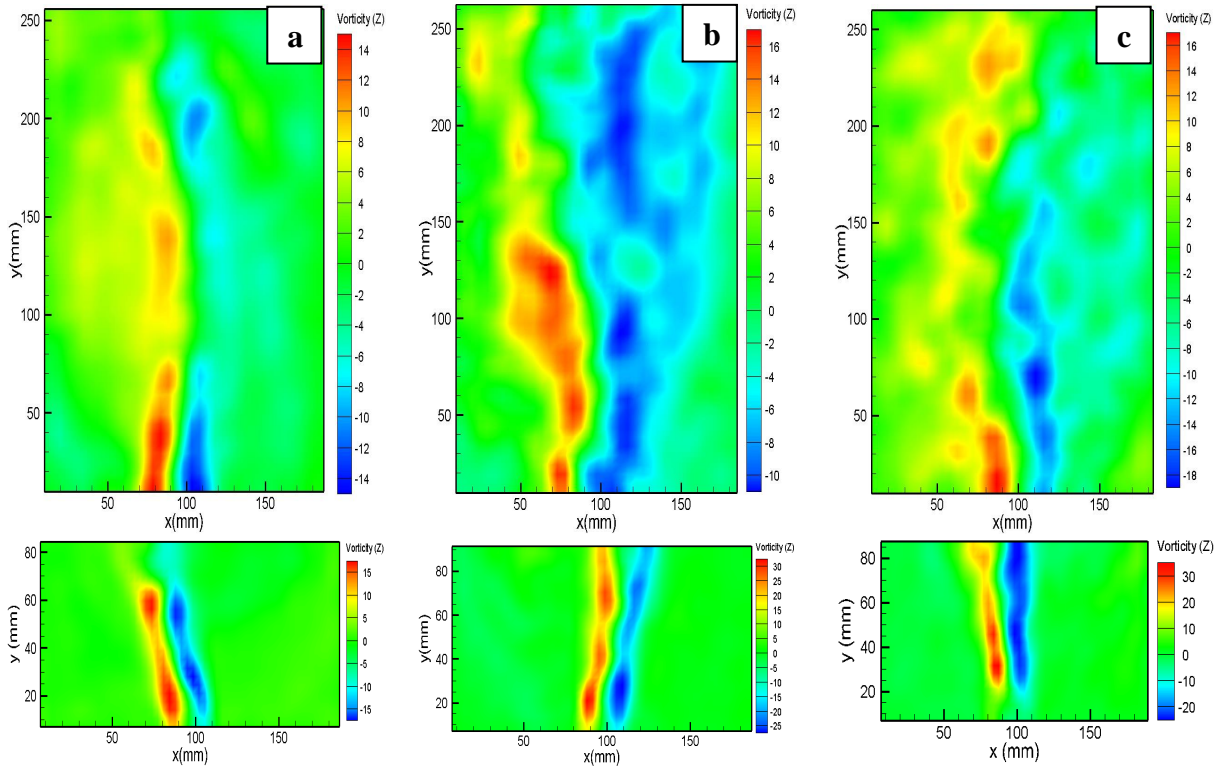


Figure 4.7 Time-averaged vorticity profiles for flow (a) 50 L/h, (b) 200 L/h, (c) 500 L/h

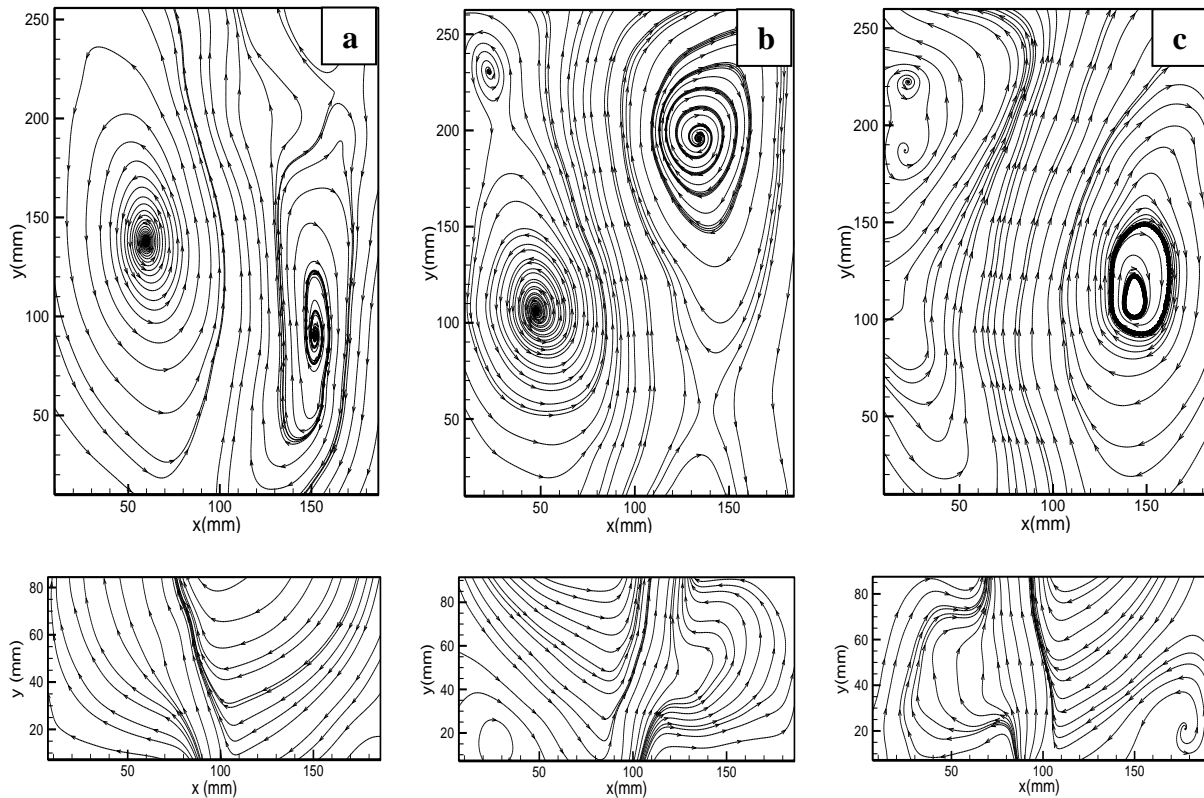


Figure 4.8 Time-averaged streamline profiles for flow (a) 50 L/h, (b) 200 L/h, (c) 500 L/h

The local liquid flow pattern around the bubble plume depends on the gas flow rate. It is recognized that as the gas flow rate increases, the magnitude of velocity increases and the active area of the bubble plume (the width of the flow) expands in the horizontal course. Inside the bubble plume and near the free surface, the velocity of the two-phase flow is higher while it is slower in other regions. Hence, high speed two-phase flow is maintained and further accelerated along the vertical axis, and which yields large entrainment flow in the lower section. This is due to the effect of the buoyancy of bubbles. Hence, the formation of this high speed flow is considered as a main influence to boost a strong surface flow. If a vertically rising liquid is employed to boost the surface flow instead of the bubble plume, the high speed upward flow is not preserved near the free surface due to the turbulent momentum dissipation and the deficiency of the buoyancy inside the jet, and in this situation the power efficiency is significantly less due to the dissipation of momentum under the free surface.

From Figure 4.8 it can be concluded that the spacing of the streamlines turn out to be smallest at the free surface. Additionally, near the free surface, the liquid flow in the x- direction is preserved over long distances. Hence, the extreme velocity in the x- direction is observed to be nearby the free surface. This means that the x-velocity is fastest on the free surface as there is

no shear stress acting on the free surface. This is also one of the cause why such a wide and thin surface flow is induced by the bubble plume. The velocity of the liquid is high inside the bubble plume, in the water layer but low in other regions. The liquid velocity is negative near the wall suggesting liquid recirculation which is representative of the heterogeneous flow regime. It shows that the liquid velocities in both x and y directions vary rapidly in the centre where bubbles travel, but insignificantly near the wall. The liquid velocities in x-direction are generally insignificant in comparison with y-direction. The velocity profile in the y-direction has three extreme values with the highest up-flowing velocity in the centre and two down-flowing velocities near the wall. When the frequency of bubble formation increases, both the up-flowing velocities and the down-flowing velocities increase, but the width of the humps remains the same, which suggests the still liquid regions are not affected by bubble formation frequency.

The time averaged rising liquid velocity in the column core is due to the zigzag motion of the bubbles and the larger upward liquid velocity in the locality of bubbles than the descending liquid flow between bubble streams. The typical example of the liquid spiral motion is observed in Figure 4.6 where liquid first flows diagonally downward toward the lower-left corner and turns toward the lower-right corner (at the middle of the figure) and finally turns back again toward the lower-left corner (at the top of the figure). When the gas velocity is further increased, the local breakup of the spiral motion becomes more significant and eventually breaks down the global central bubble stream spiral flow pattern. A slugging flow will then be experienced in a small diameter column but a fully turbulent flow will occur in a large one.

4.2 Bubble size distribution by image processing

Figure 4.10 represents bubble size distribution plots for different gas flow rates. It has been observed that for 50 L/h gas flow rate corresponding curve is narrow compared to other curves of any higher gas flow rates. For higher gas flow rates BSD curves gets broad, which indicates that there is significant bubble breakup and coalescence for higher gas flow rates compared to lower gas flow rate. Surface energy increases with decreasing bubble size. Hence bubbles tend to coalesce as long as the gain in surface energy is not compensated by increased drag and inertial forces causing bubble breakage. From a gas flow rate 100 to 400 L/h (Figure 4.10) coalescence and break-up of bubbles start to play a role. When the superficial gas velocity is low, bubbles disperse uniformly in the bubble column and no bubble collisions occurs. The bubble size is small and uniform, resulting in uniform bubble rise velocities. As the superficial

gas velocity increases, the meandering motion of the bubble plume changes to a circulation pattern.

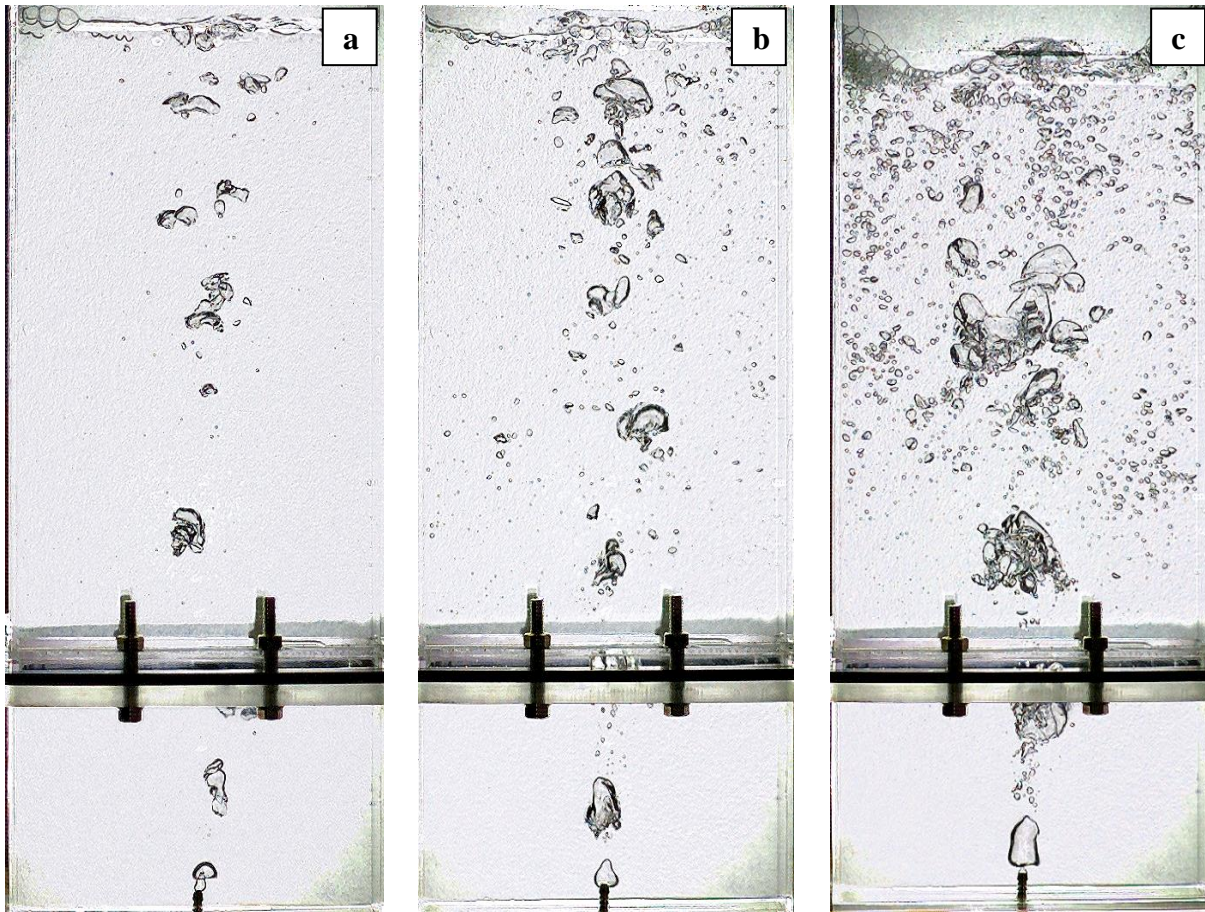


Figure 4.9 Flow visualization for (a) 50 L/h, (b) 200 L/h, and (c) 500 L/h gas flow rates

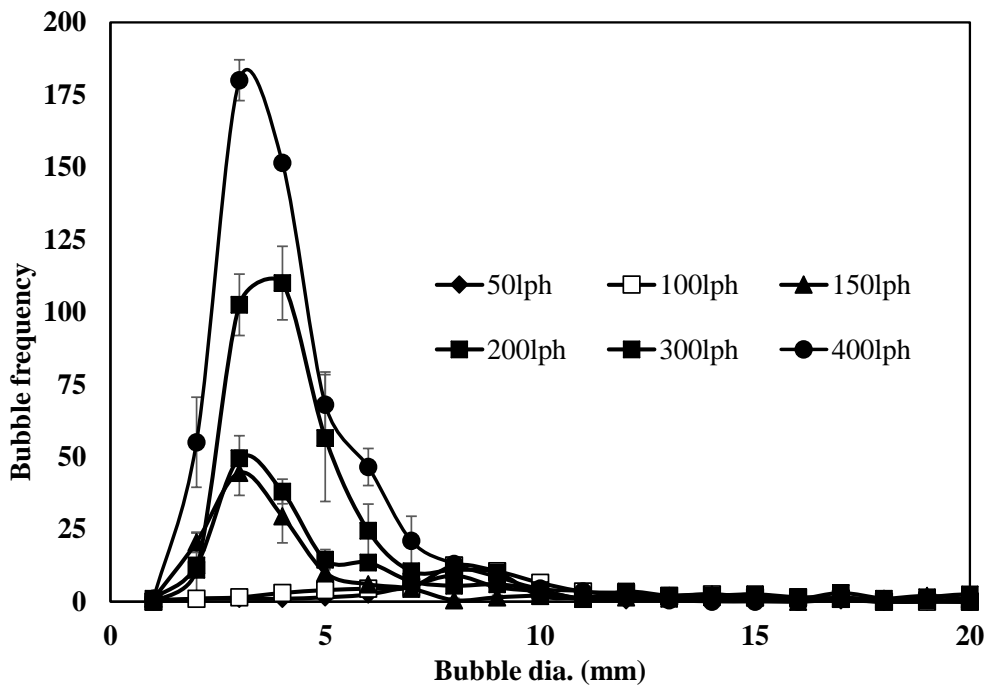


Figure 4.10 Effect of gas flow rate on BSD

Images have been taken by high speed video camera to view the interfacial structure of the two-phase flows investigated in this study and are presented in Figure 4.9.

A plume is a dynamic region within the bubble column, where the bubbles rise with a higher velocity. Bubbles in this dynamic region are larger due to coalescence of bubbles as seen from Figure 4.9. Most of the bubbles rise in the middle of the column and few move downwards at the wall region due to liquid circulation. The presence of large scale fluctuations, bubble coalescence and breakup make it difficult to characterize the amount of turbulence generated by bubbles of a typical size. In ideally-separated bubble flow or at low gas flow rates (Figure 4.9 (a)), the bubbles do not interact with each other directly or indirectly. The bubbles thus behave like single bubbles. In interacting bubble flow i.e. at increased gas flow rates (Figure 4.9 (b)), bubble number density becomes so large that the bubbles begin to interact with each other directly or indirectly due to collisions or the effects of wakes caused by other bubbles. With a further increase in bubble number density or gas flow rates (Figure 4.9 (c)), the bubbles tend to coalesce to form so-called cap bubbles, and the flow changes to churn turbulent bubble flow. The flow contains cap bubbles formed in this way and also smaller bubbles; it is highly agitated due to the interactions between bubble motions and turbulent flow.

The large bubbles occasionally form clustering of bubbles, as shown in Figure 4.9 (c), and they behave like a single gas slug. After a certain travel, they sometimes coalesce to form a gas slug and sometimes, they separate into individual bubbles. This flow regime is thus a transition from bubble flow to slug or churn flow. The rate of bubble coalescence is higher for higher gas flow rates. Another important finding that can be observed from Figure 4.9 is that the more number of large bubbles are present near the column centre than near the wall. The small bubbles are present throughout the column cross section. However, the small bubbles account for less volume fraction of the gas compared to large ones. The non-uniform distribution of bubbles along the cross section should be viewed with reference to the lift force. For the larger bubbles the lift coefficient is negative (forcing towards smaller liquid velocity gradient) while the lift coefficient for small bubbles is positive (forcing towards higher liquid velocity gradient).

The fact that large bubbles are concentrated towards the centre indicates the presence of lateral force acting on the bubbles. This finding has experimental backing from other researchers as well ((Kantarci, Borak, and Ulgen 2005) and (Tzeng, Chen, and Fan 1993)). The experimental investigation by (Tomiyama 2002) provide the proof of negative lift coefficient for large bubbles. At higher the superficial gas velocity, the mean bubble velocity decreases slightly along the column height which may be due to the spreading of the bubble plume over the cross sectional area.

4.3 Gas holdup

Bubble behaviour in a swarm will be influenced by degree of bubble interaction. As a measure of interaction it is common to use gas hold-up((Letzel et al. 1999) and (Krishna and Ellenberger 1996)). From Figure 4.11 it has been observed that gas holdup increases as gas flow rates increases. Most published studies have shown that increasing the superficial gas velocity leads to increase in the gas holdup (Hyndman, Larachi, and Guy 1997; Krishna et al. 1997). Gas holdup curves from liquid height measurements are cross validated against image processing technique. Both the findings are similar for two different measurement techniques.

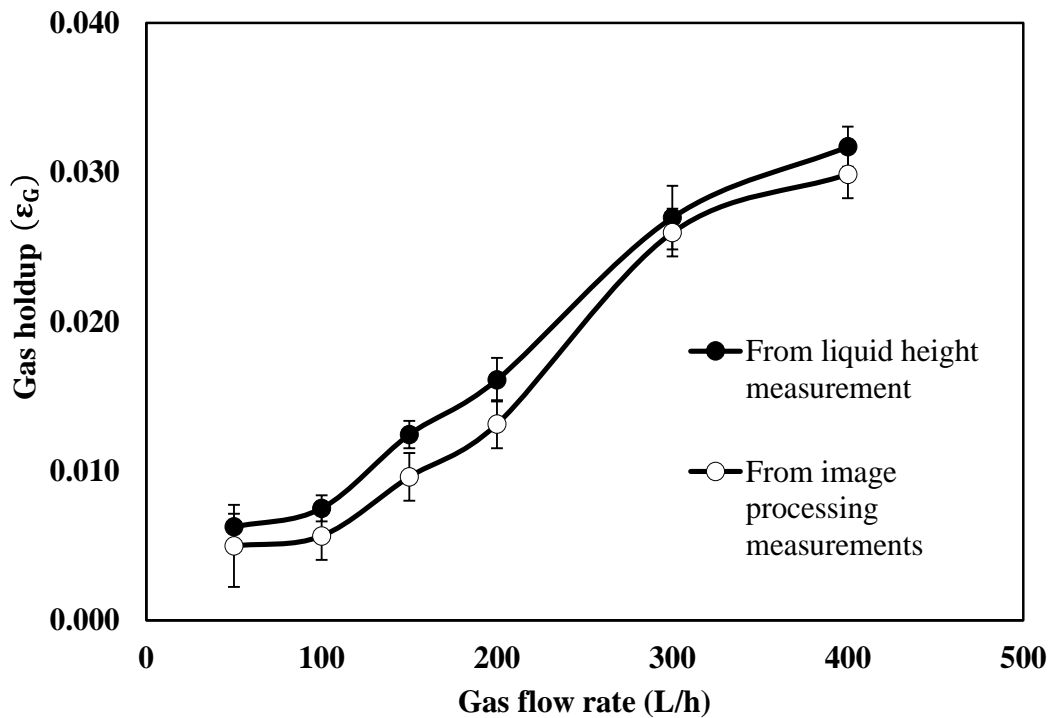


Figure 4.11 Gas holdup as a function of gas flow rates

First techniques used to calculate gas holdup is height measurement where clear liquid height (H_C) and dispersed liquid height (H_D) i.e. $(H_D - H_C)/H_D$ and second one is from volume measurement from BSD data by using $V_g / (V_g + V_l)$. To get volume of gas phase i.e. V_g each and every bubbles volume obtained from image processing measurement were added and volume occupied by liquid (V_l) is obtained by using $H_C * W * D$, where W is width of the column i.e. 200mm and D is depth which is 57mm.

It has been observed that value of gas holdup from Figure 4.11 for ideally-separated to interacting bubble flow is 0.1 and value of gas holdup for interacting bubble flow to churn turbulent bubble flow. It observed that the time averaged liquid velocity and gas hold-up are

not uniform over the column cross section in heterogeneous regime. Bubble coalescence increases due to a wider range of bubble rise velocities, caused by a wider bubble size distribution with increasing superficial gas velocity. Whereas bubble breakup is increased because of larger bubbles results into increase in turbulence.

It is observed from the Figure 4.6 that two large circulation flow regions of liquid near the bubble plume i.e. to the left and right of the bubble plume. The velocity profile in the vertical direction has three extreme values with the highest up-flowing velocity in the centre and two down-flowing velocities near the wall. As moving from lower to higher gas flow rates BSD curves gets broad (Figure 4.10), which shows that there is substantial bubble breakup and coalescence for higher gas flow rates compared to lower one (Figure 4.9).

Chapter 5

Single nozzle source bubble dynamics

5.1 Bubble Column flow investigation by PIV

This chapter focuses on the measurements of bubble properties influenced by surfactant addition in a rectangular bubble column for single source nozzle. For the understanding of high void fraction flows in bubble columns, quantitative information on bubble size, bubble velocity is of crucial importance. PIV and image processing has been used to calculate liquid flow field, bubble rise velocity, trajectories followed by bubble and RTD for bubble.

Table 5.1 Experimental conditions

Parameter	Value
Density of water	$\rho = 1000 \text{ kg/m}^3$
Initial water height	H=400 mm
Atmospheric pressure	101 kPa
Temperature of environment	22-25 °C
Density of gas (air)	1.25 kg/m ³
Gas flow rate	10,20 , and 30 L/h
Surfactant concentration(MIBC)	0.5,1.5and 3 ml
Sparger	Central nozzle sparger of 0.5,0.7,0.9 mm dia.

Experimental results were examined for various gas flow rates and nozzle diameter. For the measurement of the liquid phase velocity with PIV it is presumed that the tracer particles follows exactly the liquid phase motion. Table 5.1 specifies various conditions used for the experiment.

The time averaged liquid phase velocity field acquired from PIV measurements along liquid height (H/W=2) for different gas flow rates of 10 L/h, 20 L/h, 50 L/h and surfactant concentration of 1.5 ml MIBC is depicted in Figure 5.1. To get good resolution CCD images column has been investigated at three different positions. The time interval (Δt) between the first and second images is 135 ms. Bubbles perform differently in different liquid systems. The

liquid field affected by bubbles gets wider when gas flow is increased from 10L/h to 30L/h as depicted in Figure 5.1, which illustrates time average resultant liquid flow field.

Figure 5.2 displays time average vorticity profiles for gas flow rates of 10 L/h, 20 L/h and 30

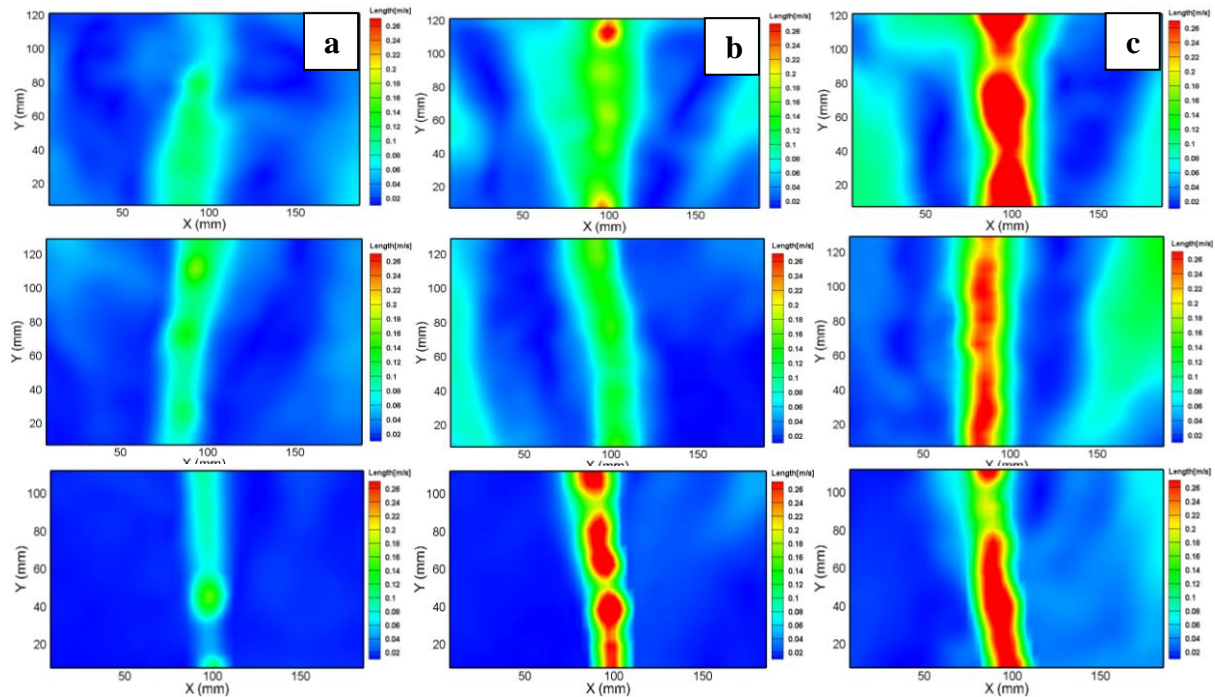


Figure 5.1 Time-averaged resultant liquid velocity profiles of flow (a) 10 L/h, (b) 20 L/h, (c) 30 L/h for 1.5 ml MIBC and 0.5 mm dia.

L/h for 1.5 ml MIBC concentration. From the centre of the column towards left vorticity climbs to maximum positive value, then reduces to the lowest value near wall. Similarly from the centre of the column towards right vorticity climbs to maximum negative value, then reduces to the lowest near wall shown Figure 5.2. The reason behind this is when bubble moves upward area affected by bubble towards its left moves in anticlockwise manner so we will get positive vorticity value and similarly towards left of the bubble we will get negative value because of clockwise circulations of the liquid.

Without considering the negative and positive signs, vorticity is nearly symmetric against the central axis with the highest value on both sides of the axis while no vorticity along the centre of the rising bubble trajectory. Figure 5.3 shows the whole field time-averaged streamlines during different gas flow rates which mainly indicates that the ascending flow accelerates along the bubble plume.

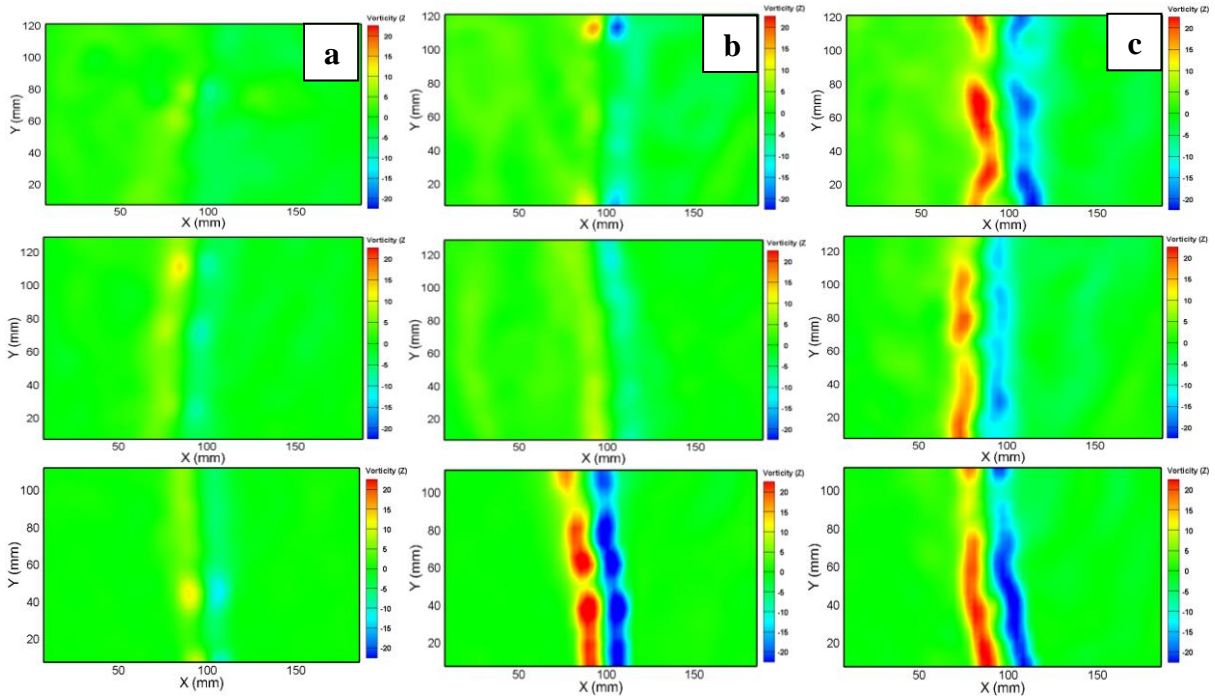


Figure 5.2 Time-averaged vorticity profiles of flow (a) 10 L/h, (b) 20 L/h, (c) 30 L/h for 1.5 ml MIBC

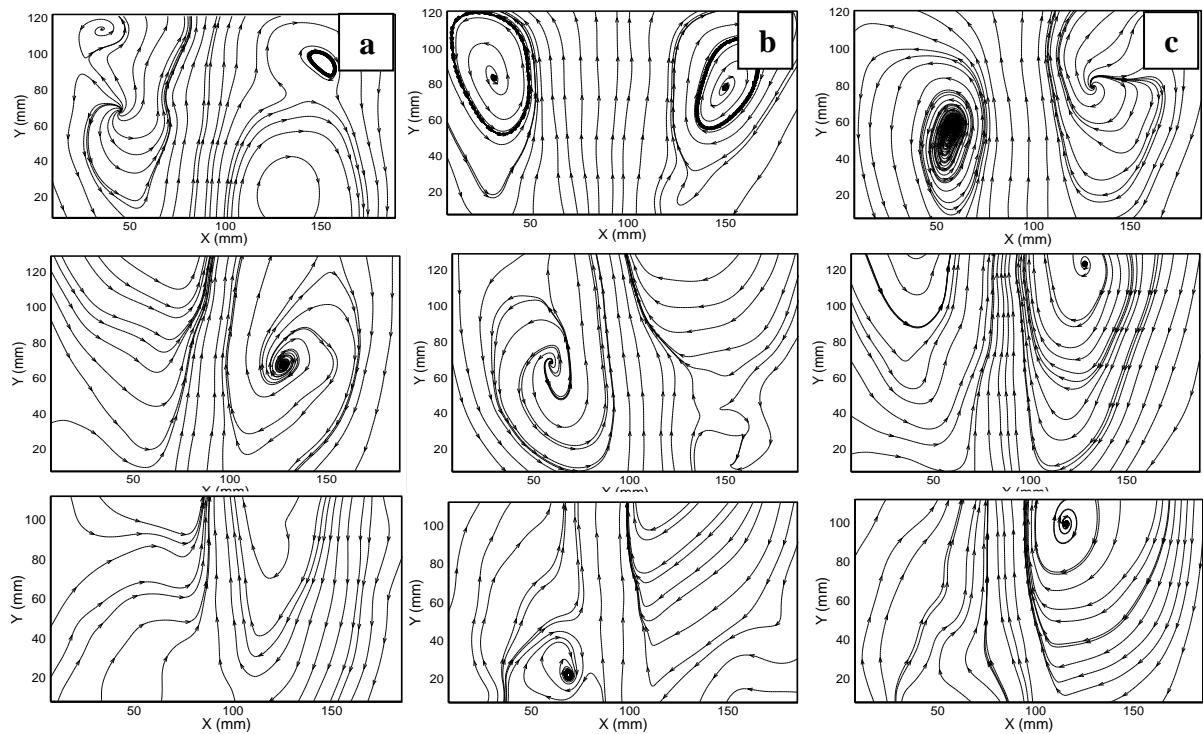


Figure 5.3 Time-averaged streamline profiles of flow (a) 10 L/h, (b) 20 L/h, (c) 30 L/h for 1.5 ml MIBC and 0.5 mm dia.

5.2 Rise velocity , RTD and trajectory of bubble by image processing

Bubble motion and bubble interfacial dynamics govern the performance of the bubble column reactors, the understanding of the bubble motion and interfacial dynamics are important to effective operation of the bubble column reactors. It is known fact that when surfactant accumulates on a bubble surface, the bubbles tend to spherical and eventually slowdown. As bubbles rose through the stagnant liquid in a chain, both the shape and the trajectory of rising bubbles are observed to change in liquid of different surfactant concentration. Their shapes and movement are also captured by the digital camera.

Figure 5.4 depicts the tracked bubble trajectories for different gas superficial velocities, surfactant and diameter. It is seen from Figure 5.4 that for lower gas flow rates bubble moves upward along centre of the column but when increased in flow rate bubble trajectories followed by bubble changes from linear to zigzag way and moves away from centre of the column. Effect of surfactant addition is also observed in similar ways. As observed above, bubbles rise in different trajectories with dissimilar shapes. The diversity of bubbles' motion is expected to induce different liquid flow structures and bubble wakes. Rising bubbles push the liquid ahead while the liquid behind them is sucked into bubble wakes. It has been witnessed from Figure 5.5 that, as the frequency of bubble formation increases or flow rate increases, the distance between adjacent bubbles shortens. Due to the surface tension forces at the nozzle tip inhibiting bubble detachment, the time required for bubbles to detach increases and the frequency of bubble formation decreases on the generator with a smaller pore size.

From Figure 5.6 it is seen that addition of surfactant reduces the resultant velocity of rising bubble. The reason behind this is reduction of surface area. Addition surfactant results into smaller bubble size so reduction in buoyancy force acting on bubble and indirectly affecting the bubble rise velocity. The effect of nozzle diameter also comes into picture when dealing with bubble velocity as bubble size is depend upon the nozzle diameter we are using .For larger nozzle diameter bubble formed is also bigger as compared to smaller nozzle diameter. Larger the bubble the greater the buoyancy force acting on it. From Figure 5.7 it is seen that increase in the nozzle diameter (indirectly increasing the bubble size) results into higher velocities attained by bubble. In the region close to the injection point there is a steep gradient in bubble velocity radially, and the motion of the bubbles is strongly affected by the gas injection velocity and mode of injection. In the fully-developed flow region, the mean bubble velocity is affected only through buoyancy, the axial bubble velocity decreases more rapidly as liquid begins to flow radially outwards from the plume.

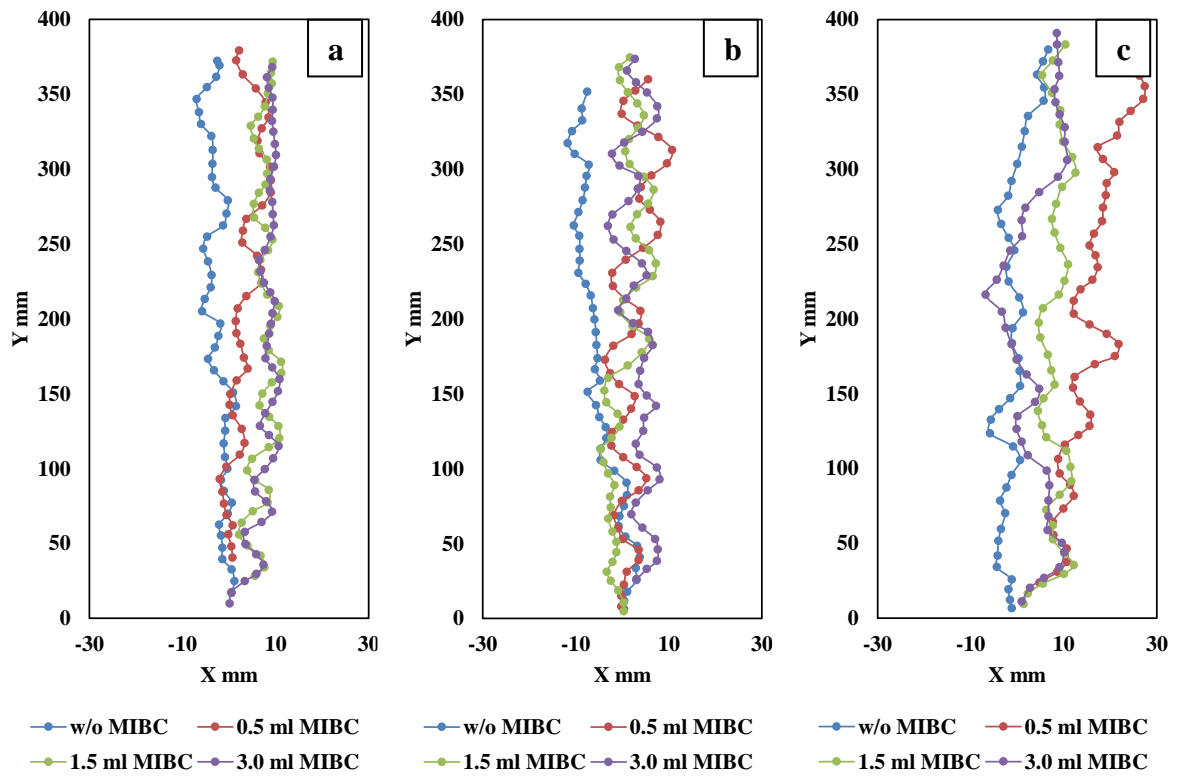


Figure 5.4 Bubble track plots of 10 L/h flow for (a) 0.5 mm dia., (b) 0.7 mm dia., and (c) 0.9 mm dia. nozzle

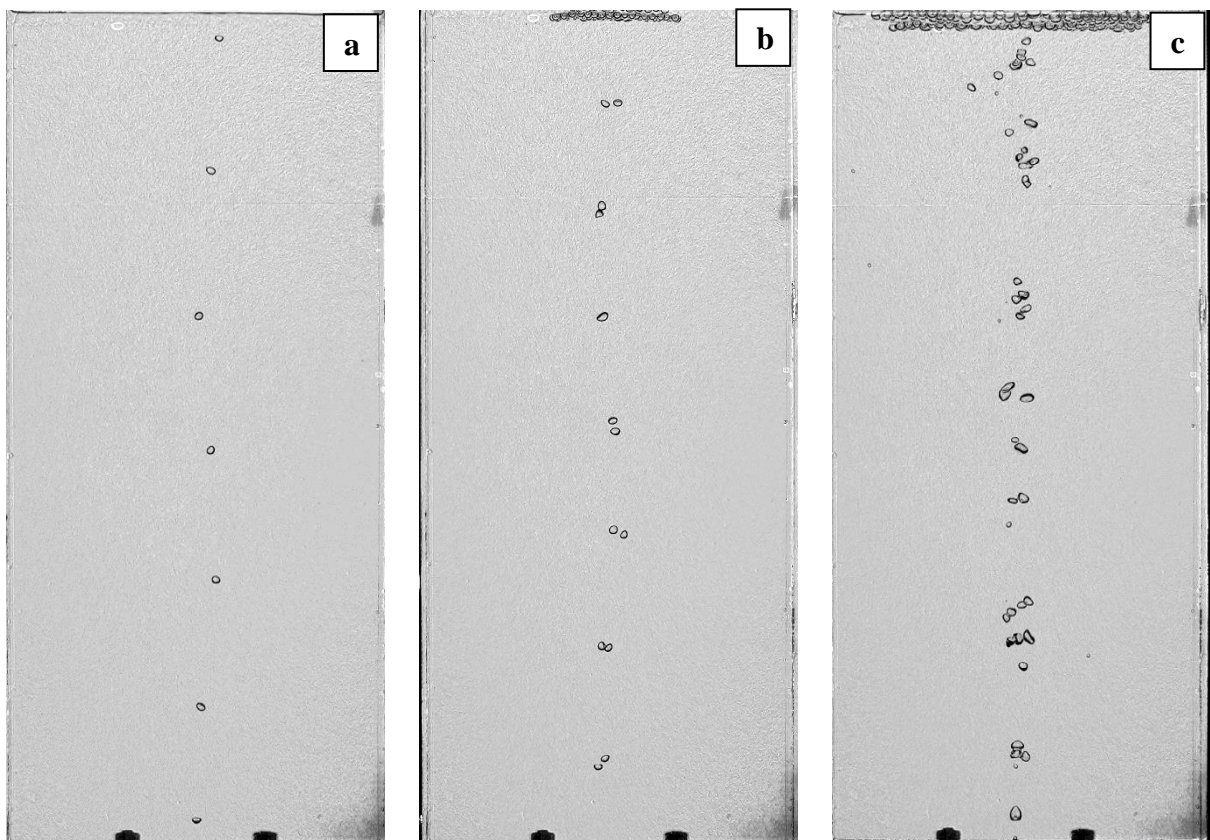


Figure 5.5 Flow visualization of 3 ml MIBC concentration for (a) 10 L/h, (b) 20 L/h, and (c) 30 L/h

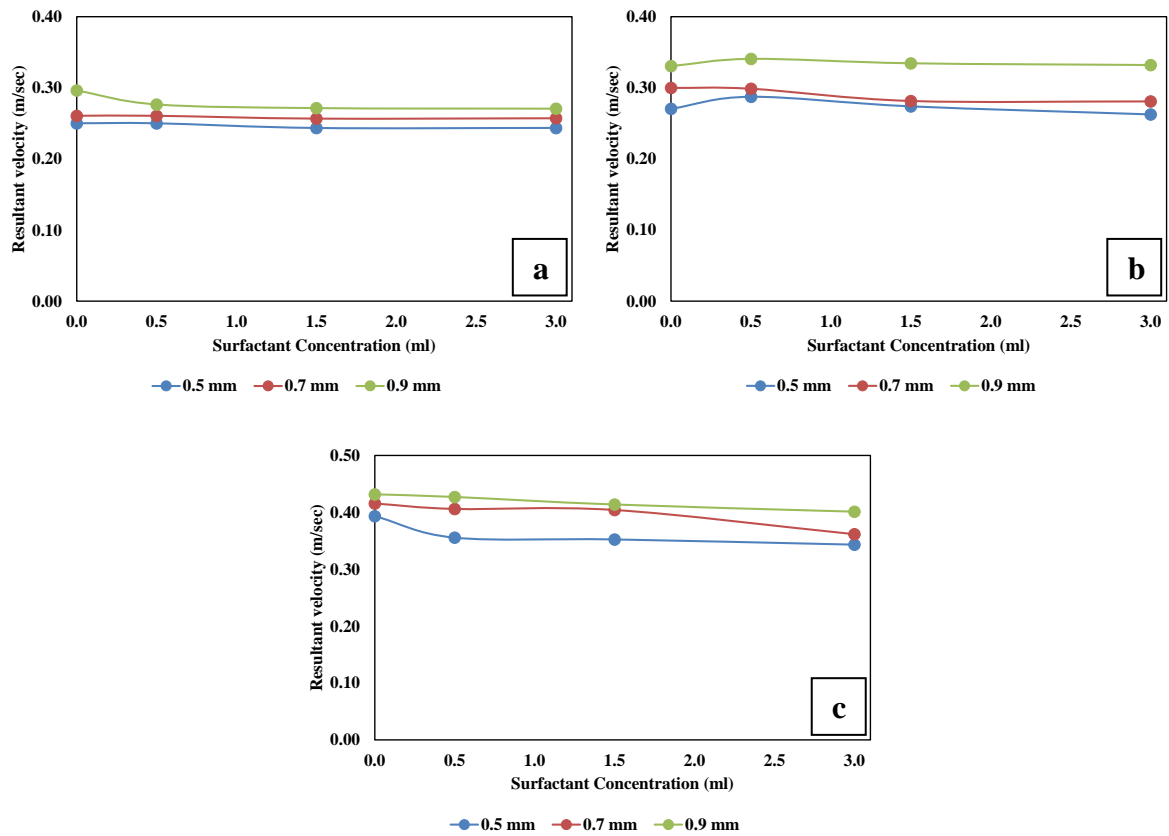


Figure 5.6 Resultant velocity of bubble for (a) 10 L/h, (b) 20L/h, and (c) 30 L/h

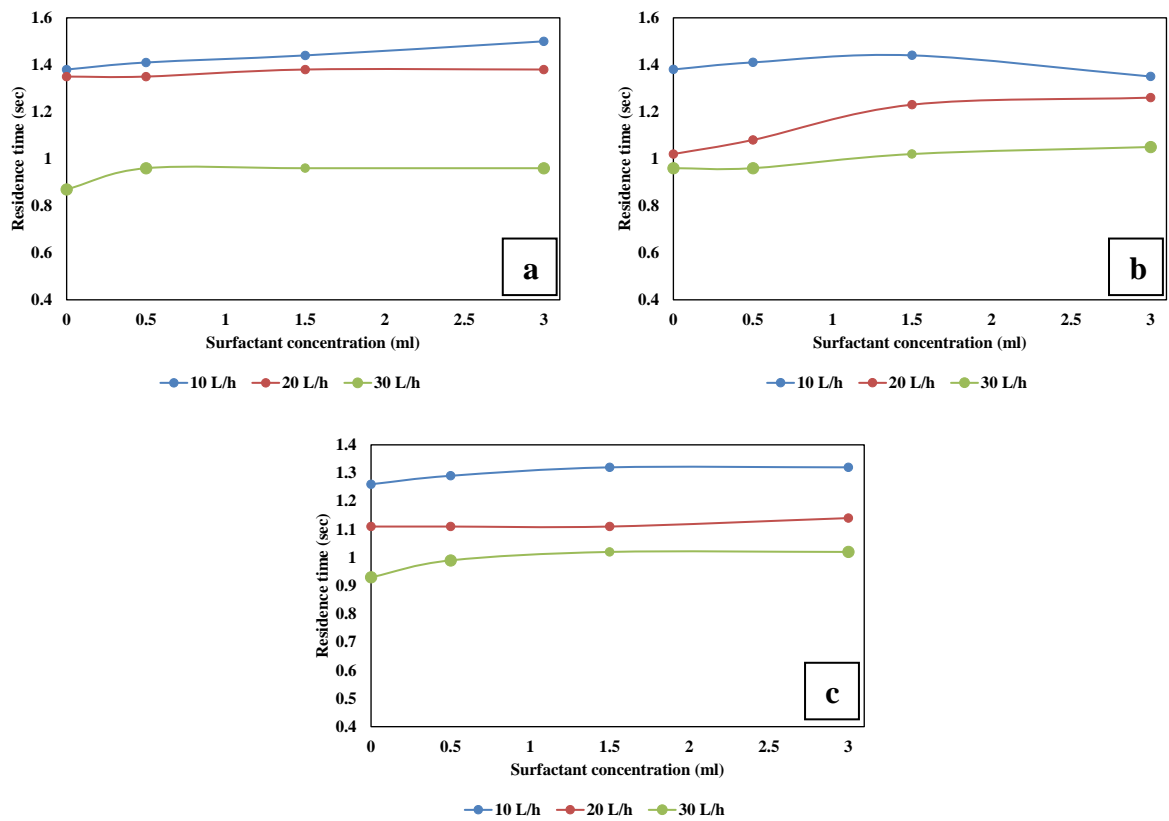


Figure 5.7 RTD for (a) 0.5 mm, (b) 0.7 mm, (c) 0.9 mm nozzle dia.

From Figure 5.7 it has been observed that residence time distribution of bubble increases with the increasing in the surfactant concentration. The reason behind this is addition of surfactant reduces the size of bubble so bubble rise velocity and time spend by bubble increases as it takes time for bubble to escape from the still liquid. Which will indirectly lead to more gas hold up attained by bubble column under this condition. In case of addition of surfactant the surface-area-to-volume ratio also increases as larger bubble breaks into smaller ones which will lead to more gas holdup value. Gas hold vales are also depend up on gas superficial velocity we are using. Increase in the gas superficial velocity reduces the RTD of bubbles.

The results show that liquid flow field (Figure 5.1) is influenced by rising bubble plume and its effect on liquid flow field velocity gets broad as we move up. Bubble rise velocity (Figure 5.6) is affected by size of bubble, surfactant concentration present, gas flow rates, etc. RTD (Figure 5.7) for smaller bubbles is more compared to larger ones and bubble rise velocity is more for larger bubbles. Similarly for lower gas flow rates RTD is less compared to higher gas flow rates.

Chapter 6

Multiple nozzle source bubble dynamics

6.1 Bubble Column flow investigation by PIV

In this chapter, the flow field investigation of a three-point nozzle source bubble sparger has been examined using PIV along with high speed video camera. Experiments were performed for different nozzle diameter and for surfactant concentration.

Table 6.1 Experimental conditions

Parameter	Value
Density of water	$\rho = 1000 \text{ kg/m}^3$
Initial water height	H=400 mm
Atmospheric pressure	101 kPa
Temperature of environment	22-25 °C
Density of gas (air)	1.25 kg/m ³
Gas flow rate	60 L/h
Surfactant concentration(MIBC)	0.5,1.5and 3 ml
Sparger	Three point nozzle sparger of 0.5,0.7,0.9 mm dia.

Experimental results are examined for fixed gas flow rate of 60 L/h and different nozzle diameter of 0.5 mm, 0.7 mm and 0.9 mm using PIV and HSV in various surfactant concentration. Table 6.1 stipulates various conditions used for the experiment. The time averaged liquid phase velocity field acquired from PIV measurements along liquid height (H/W=2) for flow configuration 60 L/h and for different nozzle diameter.

Figure 6.1 displays the time-averaged resultant liquid velocity profiles, vorticity and streamline profiles for fixed gas flow rate of 60 L/h. The time-averaged vorticity (Figure 6.1 (b)) contours clearly show two regions of intense vorticity on either side of the flow centre. For central nozzle, from the nozzle centre towards the left wall, the vorticity begins with zero, ascends to the highest positive value, then reduces to zero again near the bubble stream coming from extreme left nozzle. On the right half side, the opposite trend is observed. For the left nozzle,

from the centre of the left nozzle to the left wall, the vorticity begins with zero, ascends to the highest positive value, then reduces to zero again. On the right half side, the opposite trend is observed up to central nozzle bubble stream. And for the right nozzle, from the centre of the right nozzle to the right of the wall, the vorticity begins with zero, ascends to the highest negative value, then reduces to zero again near the wall. On the left half side, the opposite trend is observed up to central nozzle bubble stream. Positive vorticity indicates counter-clockwise rotation of fluid elements and negative value represents clock-wise rotation.

Without considering the negative and positive signs, vorticity is nearly symmetric against the

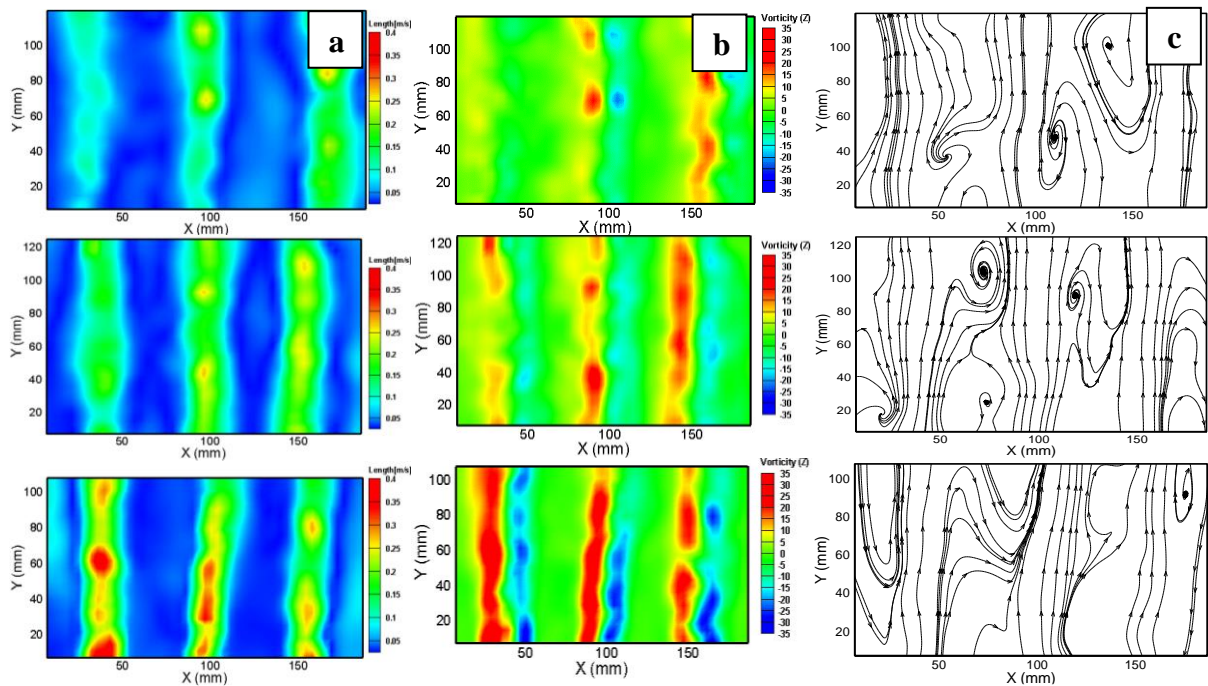


Figure 6.1 Time-averaged (a) resultant liquid velocity profiles, (b) vorticity profiles, (c) streamline profiles for flow 60 L/h for 0.5 mm nozzle dia.

centre of the nozzle with the highest value on both sides of the axis while no vorticity along the centre of the rising bubble trajectory. Streamlines from Figure 6.1 (c) shows the direction in which a massless fluid component transportable at any point in time.

6.1 Bubble Column flow visualisation by HSVC

The demarcation criteria of the flow regimes may vary with design or operating variables such as column size, type of distributor, and liquid properties. From Figure 6.2 it is seen that addition of surfactant results into transformation of irregular shape bubbles to elliptical bubbles.

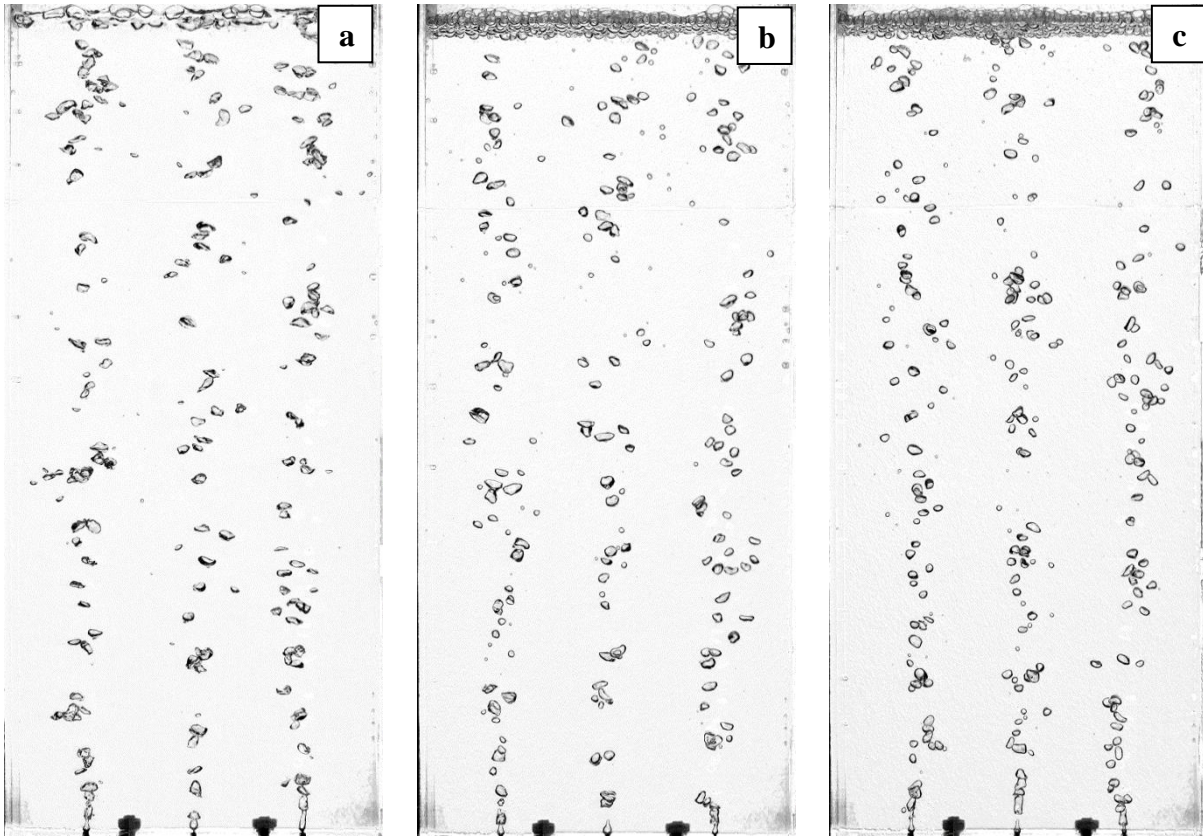


Figure 6.2 Flow visualisation of 3 nozzle sparger of 60 L/h flow for (a) w/o MIBC, (b) 0.5 ml MIBC, (c) 3 ml concentration for 0.5 mm dia.

Addition of surfactant reduces the bubble size and increases number of bubble present in the reactor so the surface to volume ratio increase and amount of gas holdup for fixed flow rates also increases. It has been observed that addition of surfactant results into reduction in velocity of rising bubble of same gas superficial velocity. It seems that a little surfactant addition is able to prevent coalescence but more addition is required to establish the surface tension gradients required to counter the dynamic forces causing the bubble to become oblate. The same observation is reported by (Finch, Nasset, and Acuña 2008) for single bubble generation.

In terms of bubble interactions, the evidence points to faster rising bubbles speeding up slower moving ones (Figure 6.2) and slower moving bubbles retarding faster moving ones (Figure 6.2). That faster rising large bubbles draw up smaller bubbles in their wake is well known as observed by (Lee, Luo, and Fan 1999) ,(De Vries 2001). The smaller bubbles accumulate close to the side walls and are dragged down by the down-flow of the liquid. The flow visualization and the PIV results show that the liquid rises upward with the rising bubbles near bubble source location and flows downward between these bubbles streams in this dispersed bubble regime.

In the region close to the column wall, a descending liquid flow can always be found due to the lack of bubble motion.

The outcomes from experiments shows that time-averaged vorticity contours (Figure 6.1(b)) have two regions of intense vorticity on either side of the flow centre of the nozzle. Addition of surfactant consequences into alteration of asymmetrical shape bubbles to elliptical bubbles (Figure 6.2). It is observed that little surfactant addition is able to avoid coalescence but more addition is required to bubble become oblate. In the region close to the column wall, a downward liquid flow (Figure 6.1(a)) can be found all the time due to the lack of bubble motion.

Chapter 7

Conclusion and future work

7.1 Conclusion

In the present work, bubble properties such as bubble size distribution, gas hold-up, liquid flow field, etc. in a needle sparger rectangular bubble column has been investigated for understanding of bubble column hydrodynamics. The effect of different superficial gas velocities on the above listed parameters has been investigated experimentally. Optical diagnostic techniques such as particle image velocimetry are used for measurement of instantaneous liquid velocity, average liquid velocity, and vorticity. Bubble size distribution, gas holdup, bubble rise velocity, residence time distribution of bubbles and trajectories followed by bubble for different surfactant concentration addition has been investigated by using image processing technique. This study presents improvement of image processing technique used for evaluating BSD in bubble columns.

The following key conclusions are made from this work.

1. The liquid flow field around bubble plume is influenced by the gas flow rate. It is observed that with the increment in the gas flow rates, the amount of velocity upsurges and the active area of the bubble plume enlarges along the column width.
2. Most of the bubbles rise in the centre of the column but because of liquid circulations some moves downwards the near wall region.
3. It is noted that the value of vorticity grows in positive manner from centre of the column to wall region towards left and grows in negative manner from centre to wall region towards right. Which proves that anti-clockwise liquid circulations in the left half of the column and clockwise in the right half of the column.
4. Bubble size distribution curves gets broader and broader with increment of the corresponding gas flow rates. Which indicates that there is significant bubble breakup for higher gas flow rates.
5. The value of gas holdup increases with the increment in the gas flow rates.
6. Addition of surfactants increases time spend by bubble in a rectangle column

7. Addition of surfactant also increase surface to volume ration of bubbles
8. Bubble shape changes from irregular to elliptical after addition of surfactant
9. RTD of larger bubbles is less compared to smaller ones

7.2 Future work

On the basis of the concussions are drawn, some future work consideration are presented in the following

1. Improvement of current image processing algorithm to detect and measure irregular shape bubbles
2. Validation with computational fluid dynamics (CFD) models
3. Further improvement in flow visualisation and measurement with help of pressure transducers and tomographic technique

Appendix A

Flow visualisation with the help of HSVC and shadowgraph

1) For single needle source(3.5 mm diameter) bubble dynamic

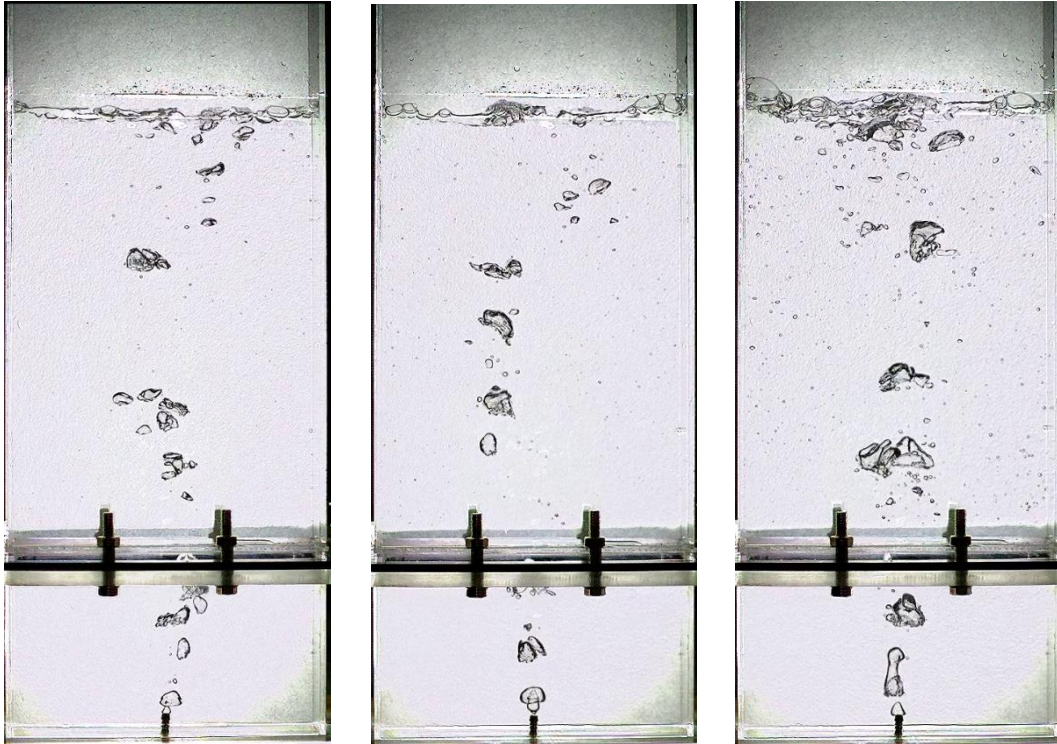


Figure 1 For flow gas rate (a) 50L/h, (b) 100L/h and (c) 150L/h

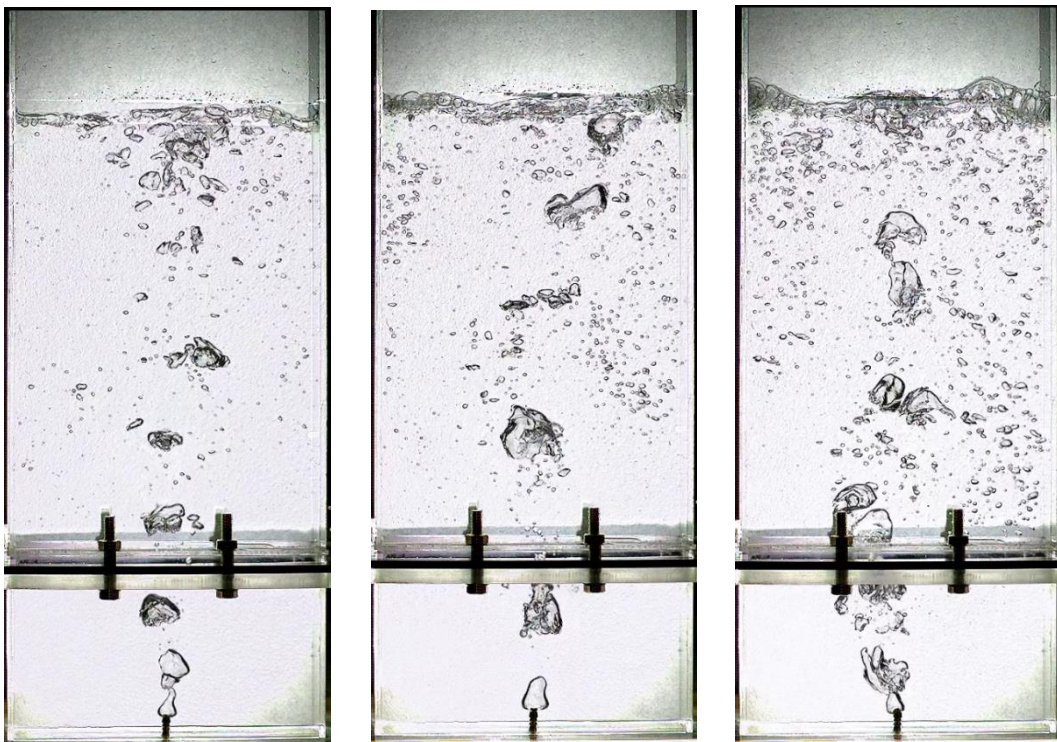


Figure 2 For flow gas rate (a) 200L/h, (b) 300L/h and (c) 400L/h

2) For Single nozzle source (0.5mm,0.7mm,0.9mm diameter)bubble dynamics



Figure 3 For flow gas rate (a) 10L/h, (b) 20L/h and (c) 30L/h for 0.5 mm diameter nozzle w/o MIBC

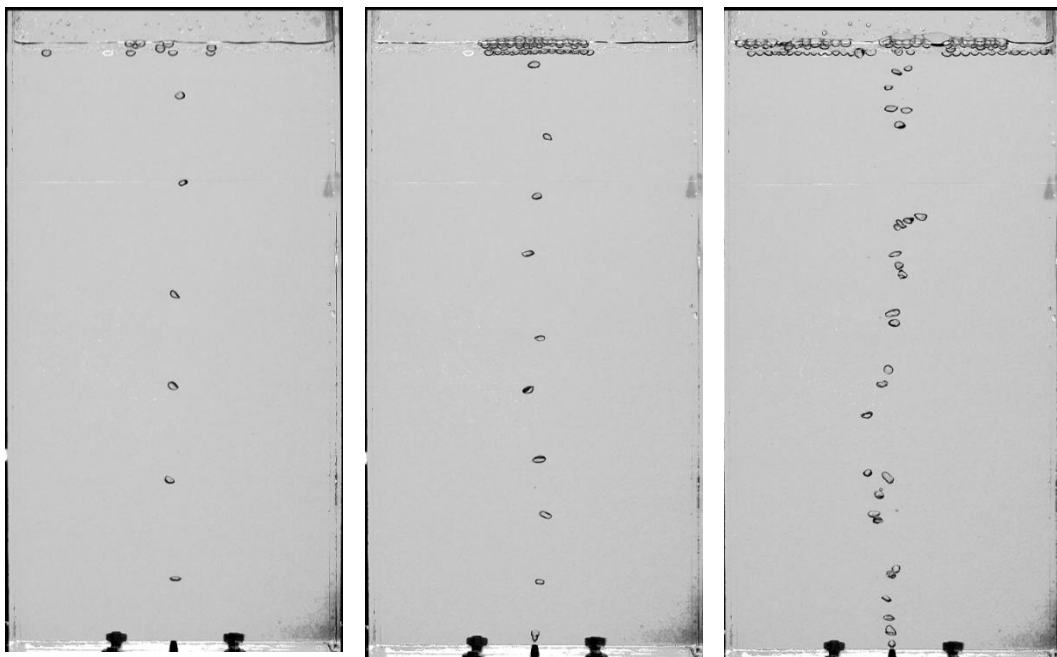


Figure 4 For flow gas rate (a) 10L/h, (b) 20L/h and (c) 30L/h for 0.5 mm diameter nozzle with 0.5 ml MIBC

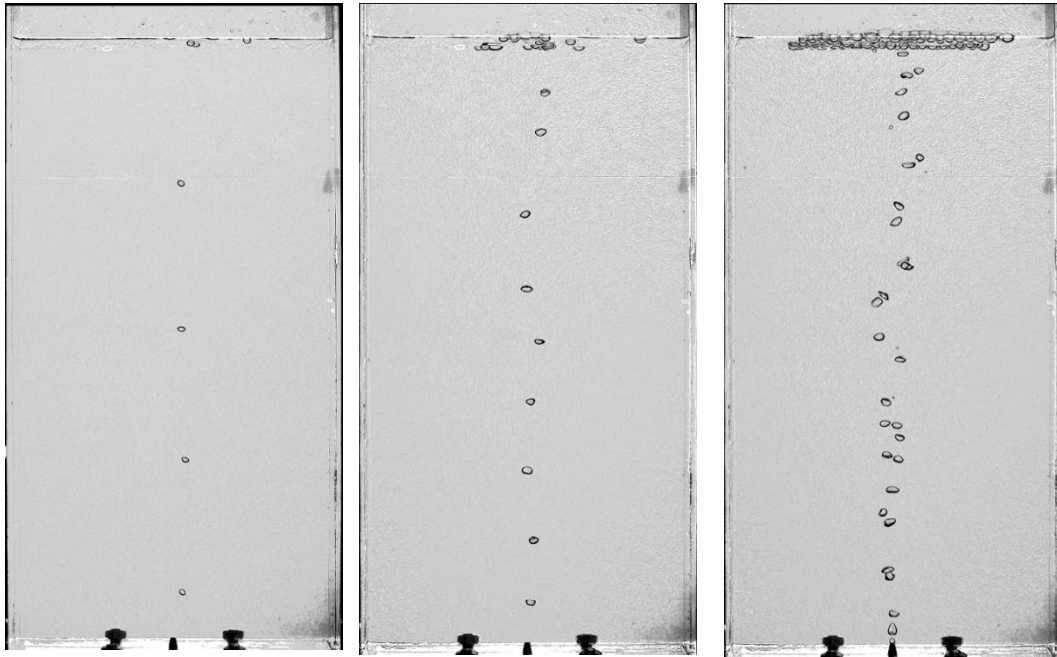


Figure 5 For flow gas rate (a) 10L/h, (b) 20L/h and (c) 30L/h for 0.5 mm diameter nozzle with 1.5 ml MIBC

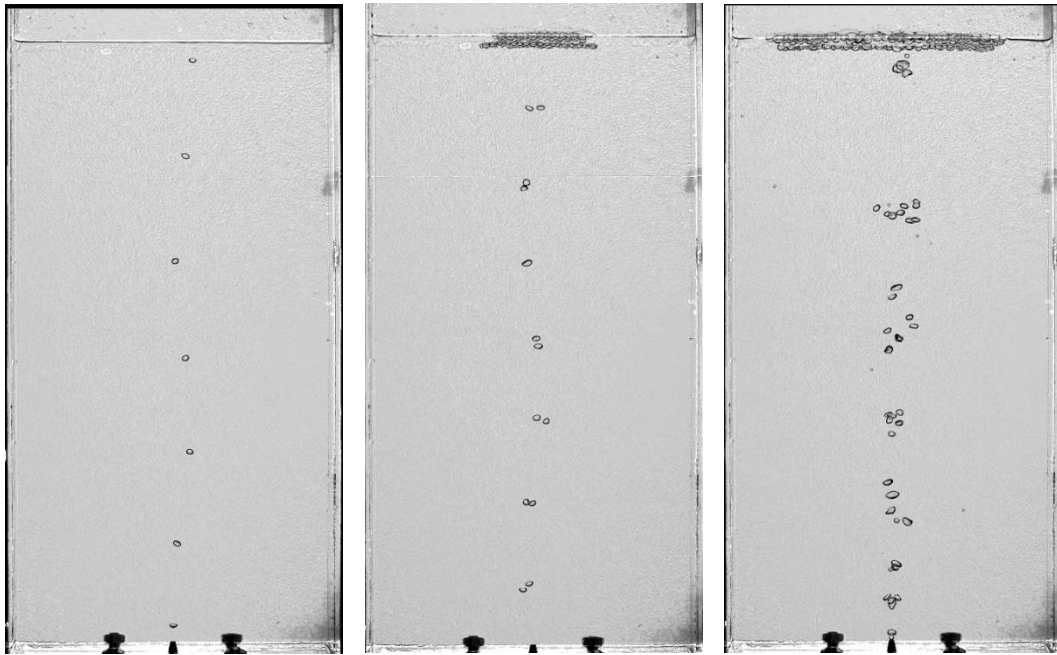


Figure 6 For flow gas rate (a) 10L/h, (b) 20L/h and (c) 30L/h for 0.5 mm diameter nozzle with 3 ml MIBC



Figure 7 For flow gas rate (a) 10L/h, (b) 20L/h and (c) 30L/h for 0.7 mm diameter nozzle w/o MIBC

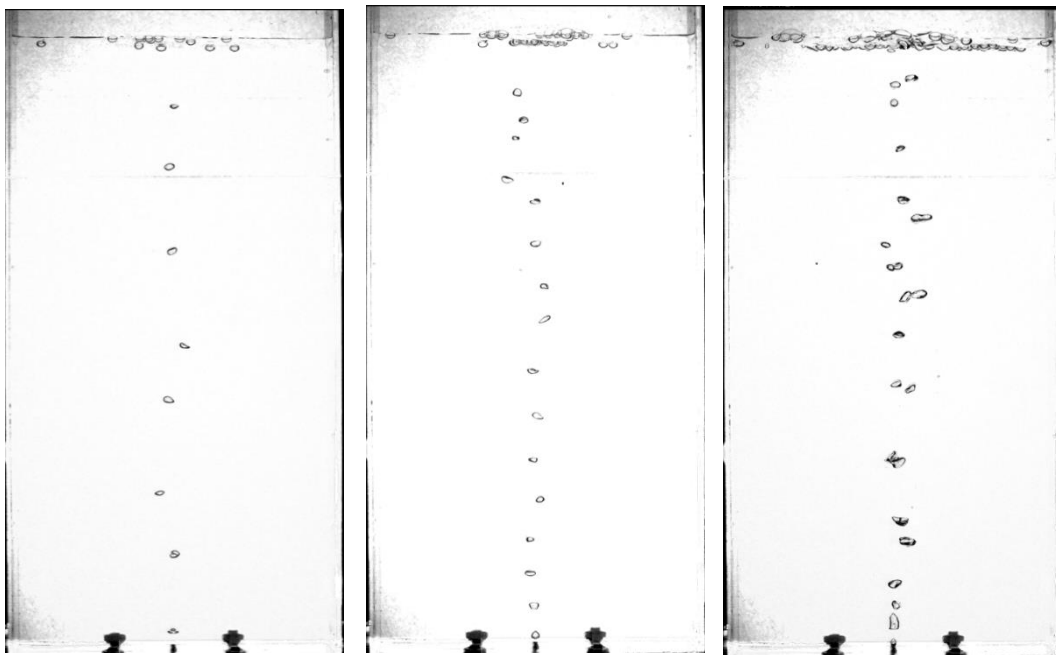


Figure 8 For flow gas rate (a) 10L/h, (b) 20L/h and (c) 30L/h for 0.7 mm diameter nozzle with 0.5 ml MIBC

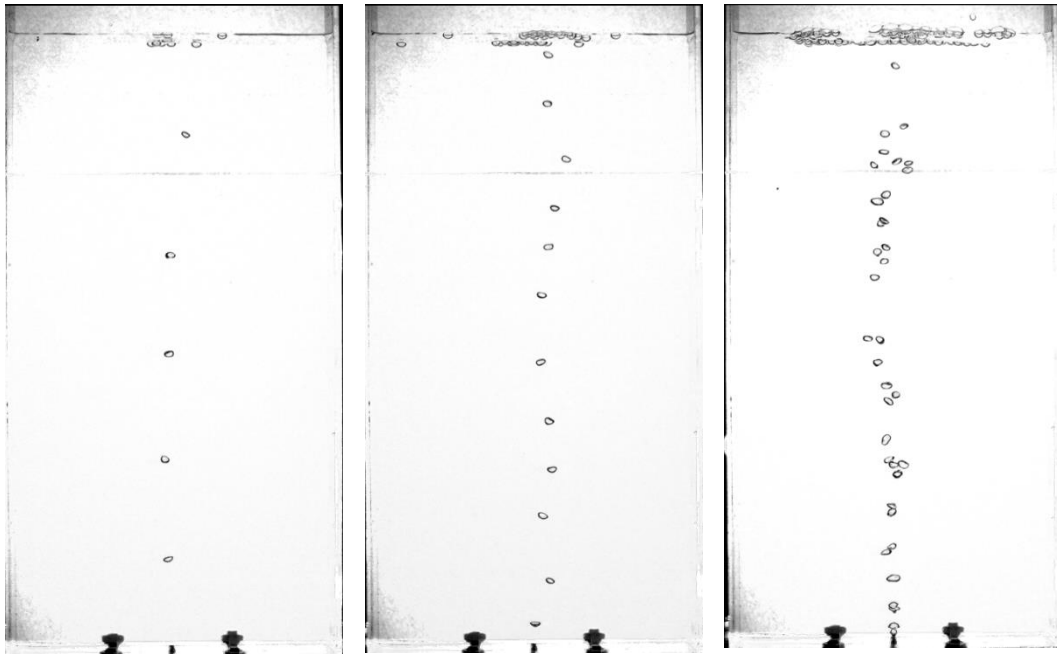


Figure 9 For flow gas rate (a) 10L/h, (b) 20L/h and (c) 30L/h for 0.7 mm diameter nozzle with 1.5 ml MIBC

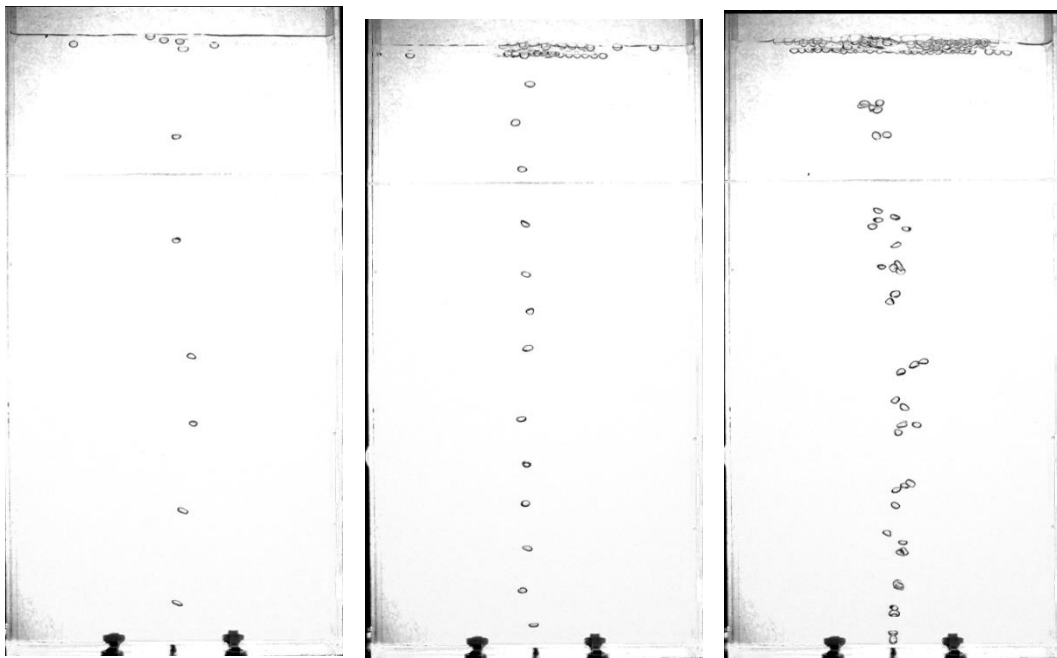


Figure 10 For flow gas rate (a) 10L/h, (b) 20L/h and (c) 30L/h for 0.7 mm diameter nozzle with 3ml MIBC



Figure 11 For flow gas rate (a) 10L/h, (b) 20L/h and (c) 30L/h for 0.9 mm diameter nozzle w/o MIBC

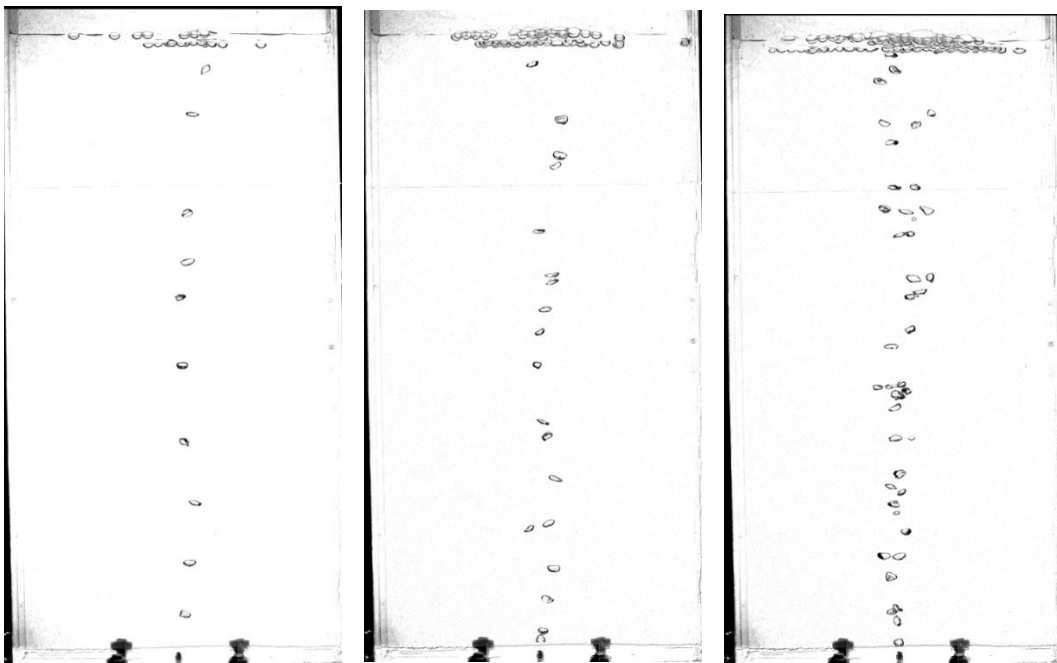


Figure 12 For flow gas rate (a) 10L/h, (b) 20L/h and (c) 30L/h for 0.9 mm diameter nozzle with 0.5 ml MIBC

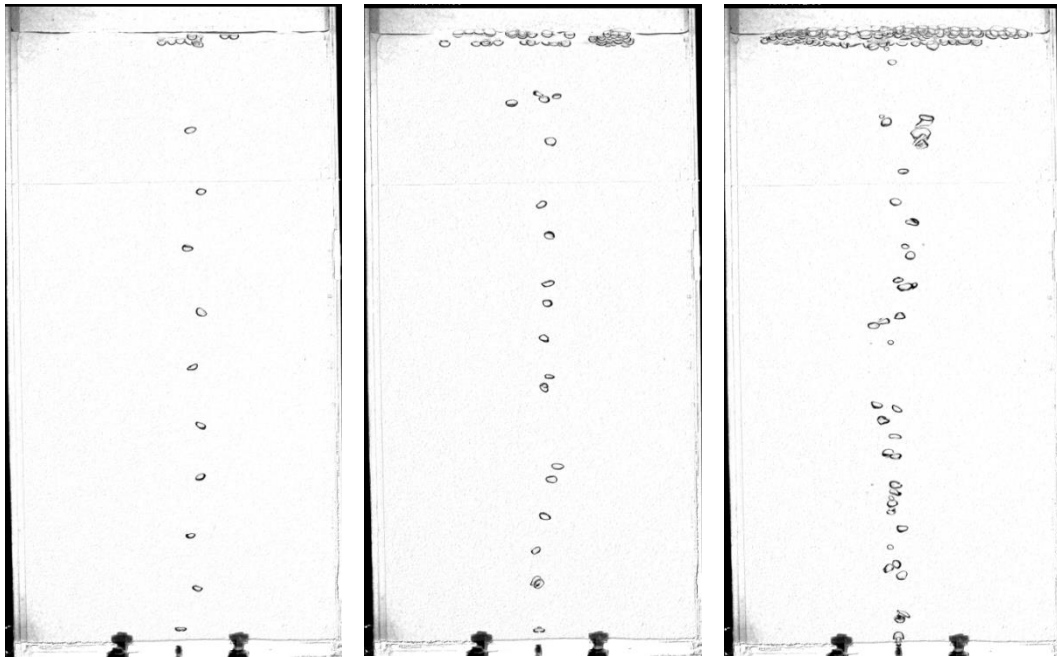


Figure 13 For flow gas rate (a) 10L/h, (b) 20L/h and (c) 30L/h for 0.9 mm diameter nozzle with 1.5 ml MIBC

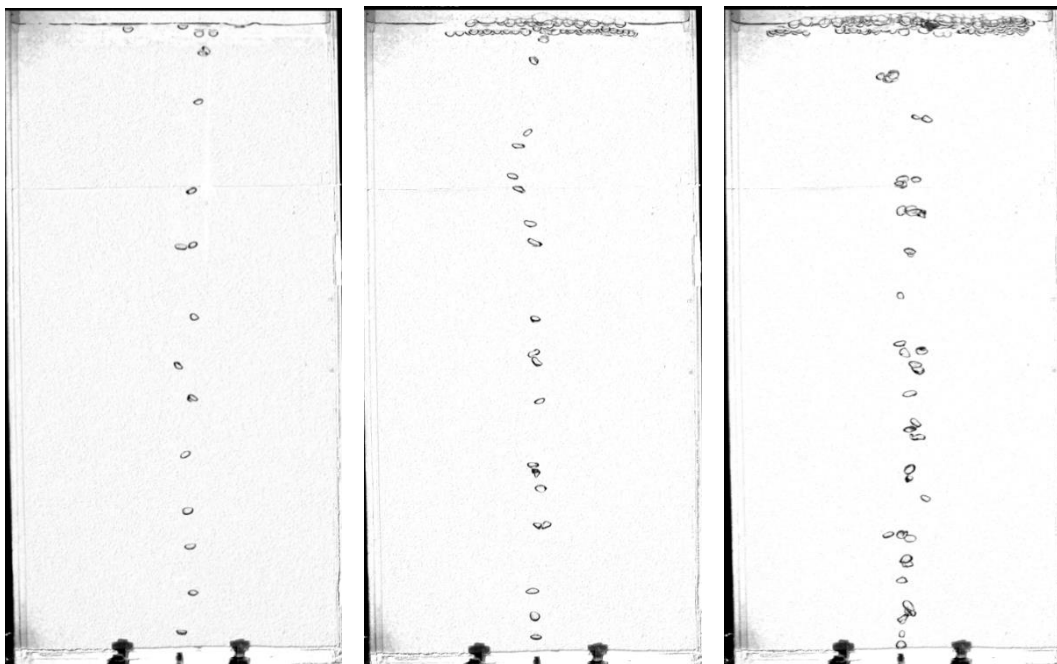


Figure 14 For flow gas rate (a) 10L/h, (b) 20L/h and (c) 30L/h for 0.9 mm diameter nozzle with 3 ml MIBC

3) For Multiple nozzle source (0.5mm,0.7mm,0.9mm diameter)bubble dynamics

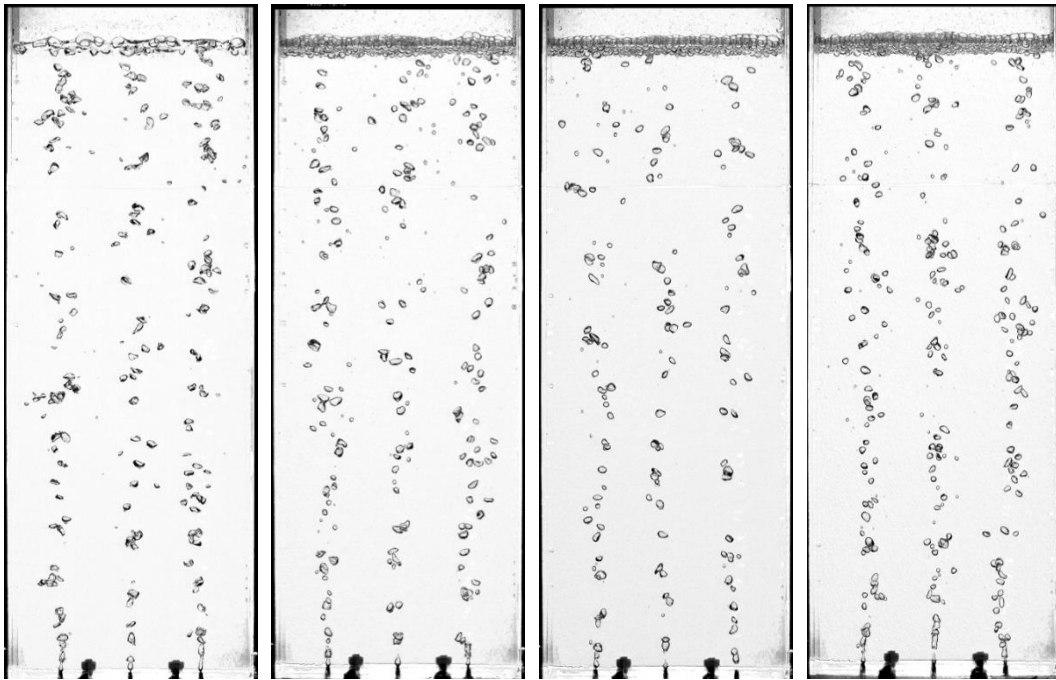


Figure 15 For flow gas rate of 60L/h and 0.5 mm diameter multiple nozzle with (a)w/o,(b)0.5 ml,(c)1.5 ml and (d) 3 ml MIBC

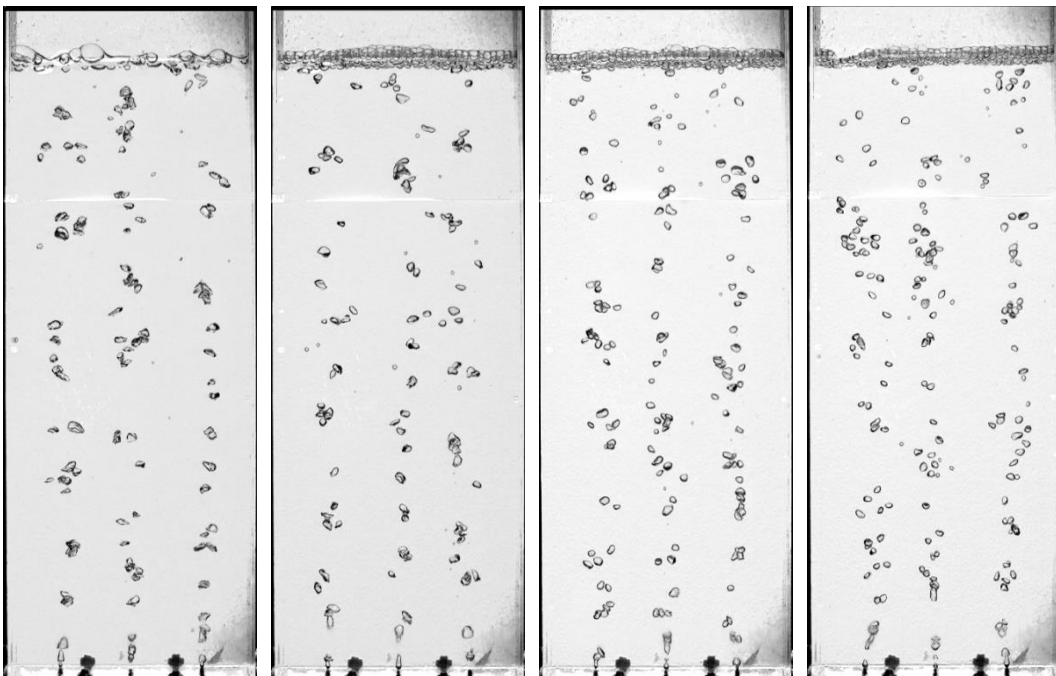


Figure 16 For flow gas rate of 60L/h and 0.7 mm diameter multiple nozzle with (a)w/o,(b)0.5 ml,(c)1.5 ml and (d) 3 ml MIBC

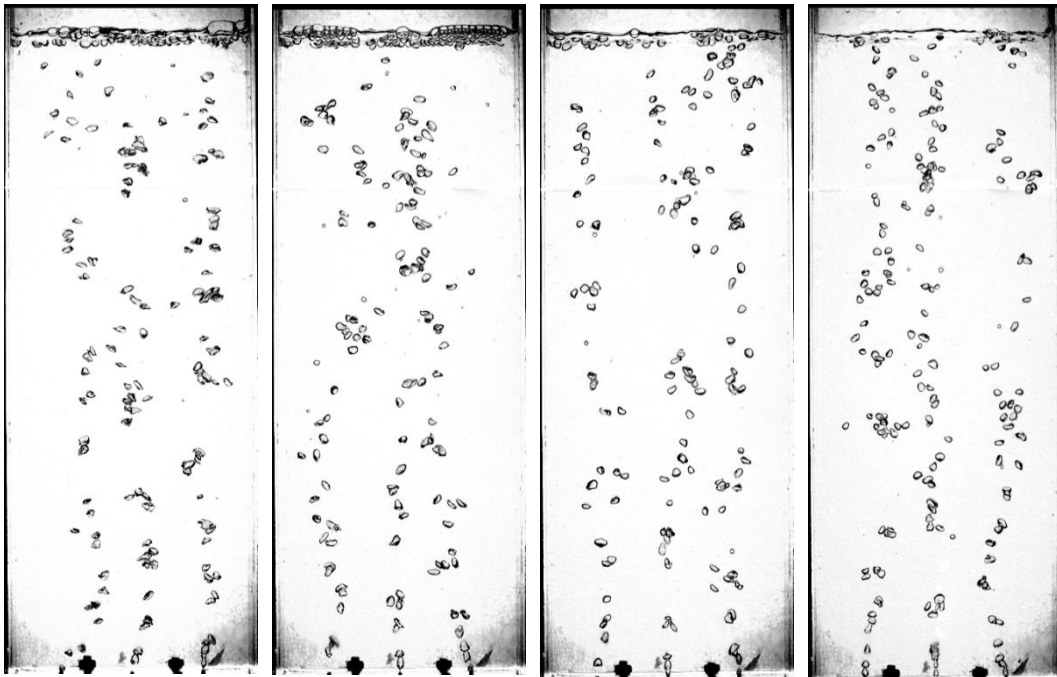


Figure 17 For flow gas rate of 60L/h and 0.9 mm diameter multiple nozzle with (a)w/o,(b)0.5 ml,(c)1.5 ml and (d) 3 ml MIBC

Appendix B

PIV flow field profiles

1) For single needle source(3.5 mm diameter) bubble dynamic

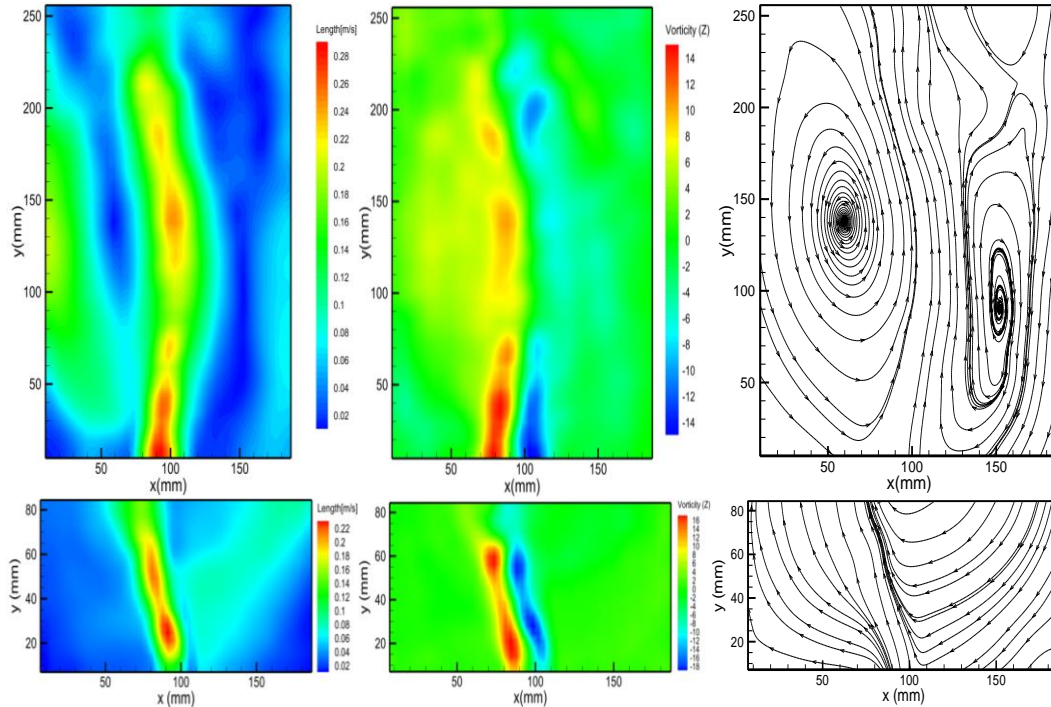


Figure 18 Time-averaged (a) resultant liquid velocity profiles, (b) vorticity profiles, (c) streamline profiles for flow 50 L/h for 3.5 mm needle diameter.

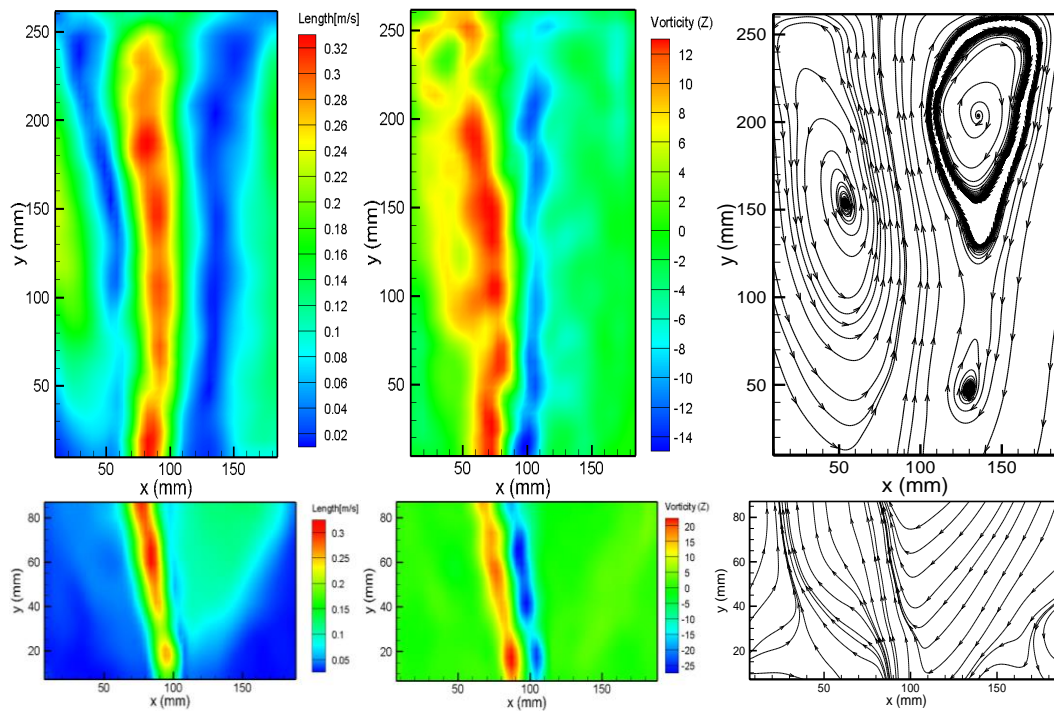


Figure 19 Time-averaged (a) resultant liquid velocity profiles, (b) vorticity profiles, (c) streamline profiles for flow 100 L/h for 3.5 mm needle diameter.

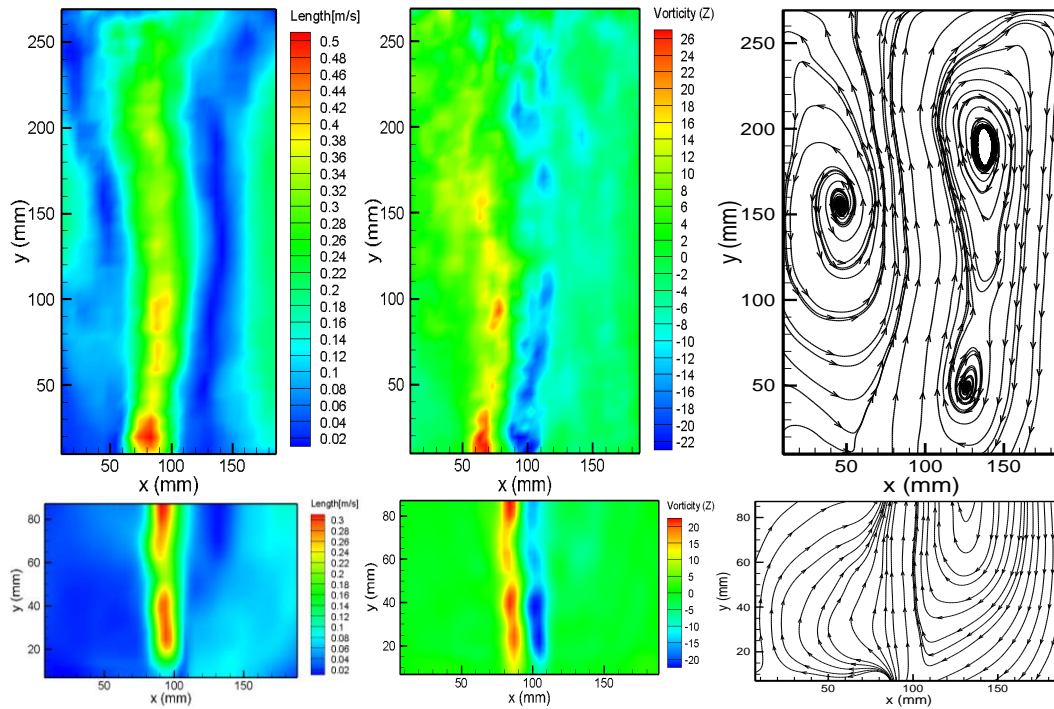


Figure 20 Time-averaged (a) resultant liquid velocity profiles, (b) vorticity profiles, (c) streamline profiles for flow 150 L/h for 3.5 mm needle diameter.

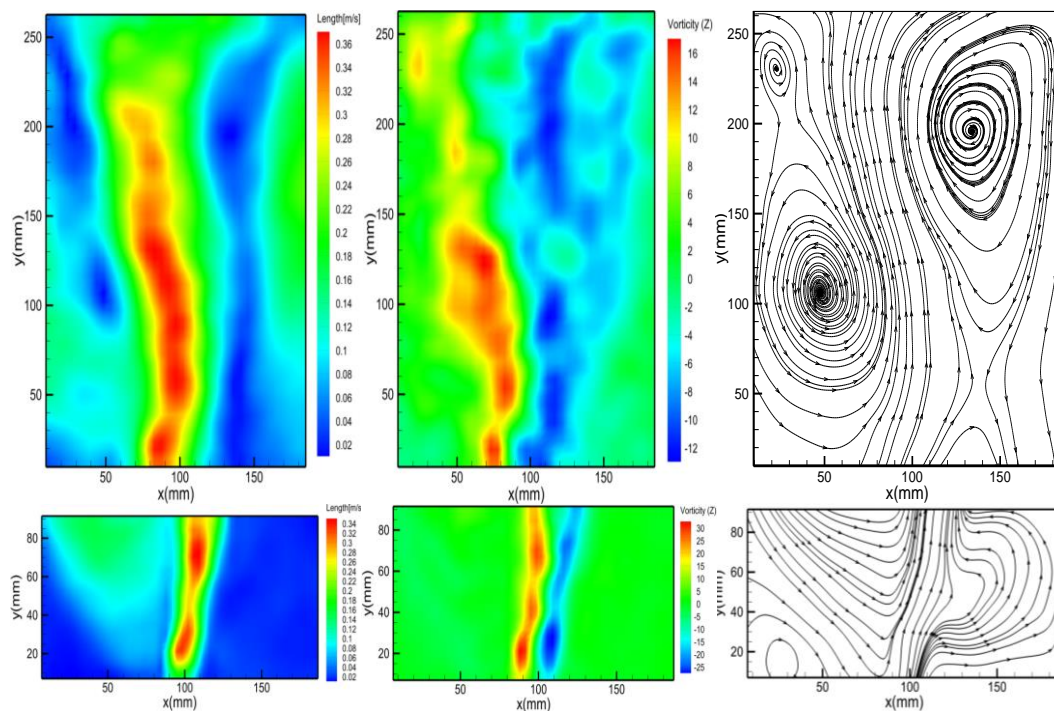


Figure 21 Time-averaged (a) resultant liquid velocity profiles, (b) vorticity profiles, (c) streamline profiles for flow 200 L/h for 3.5 mm needle diameter.

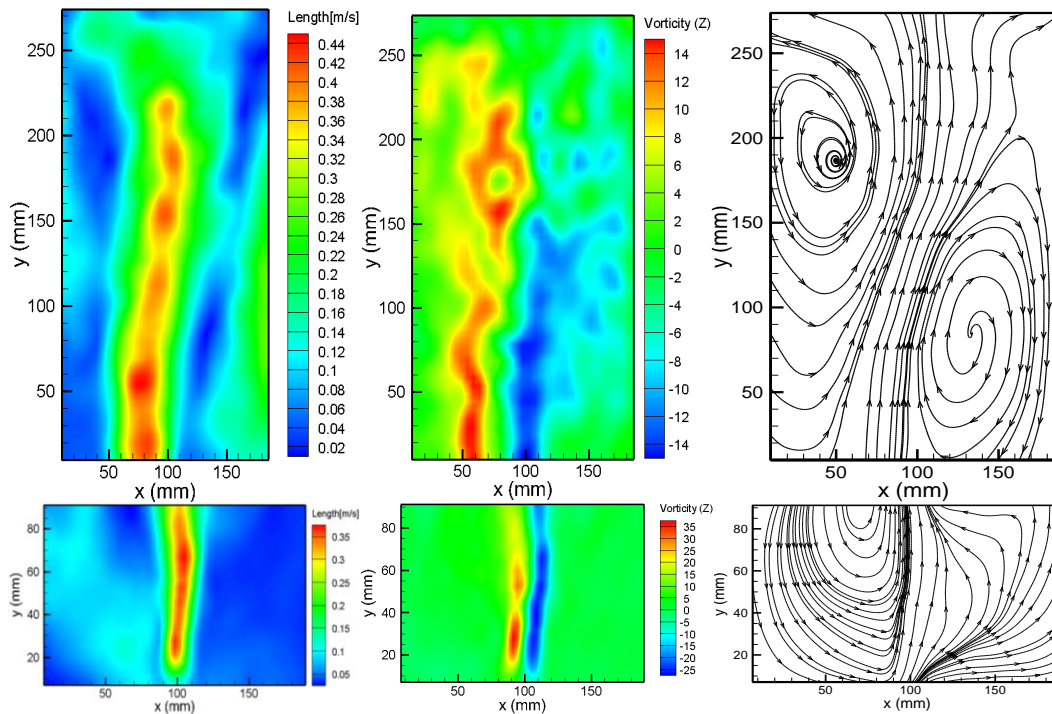


Figure 22 Time-averaged (a) resultant liquid velocity profiles, (b) vorticity profiles, (c) streamline profiles for flow 300 L/h for 3.5 mm needle diameter.

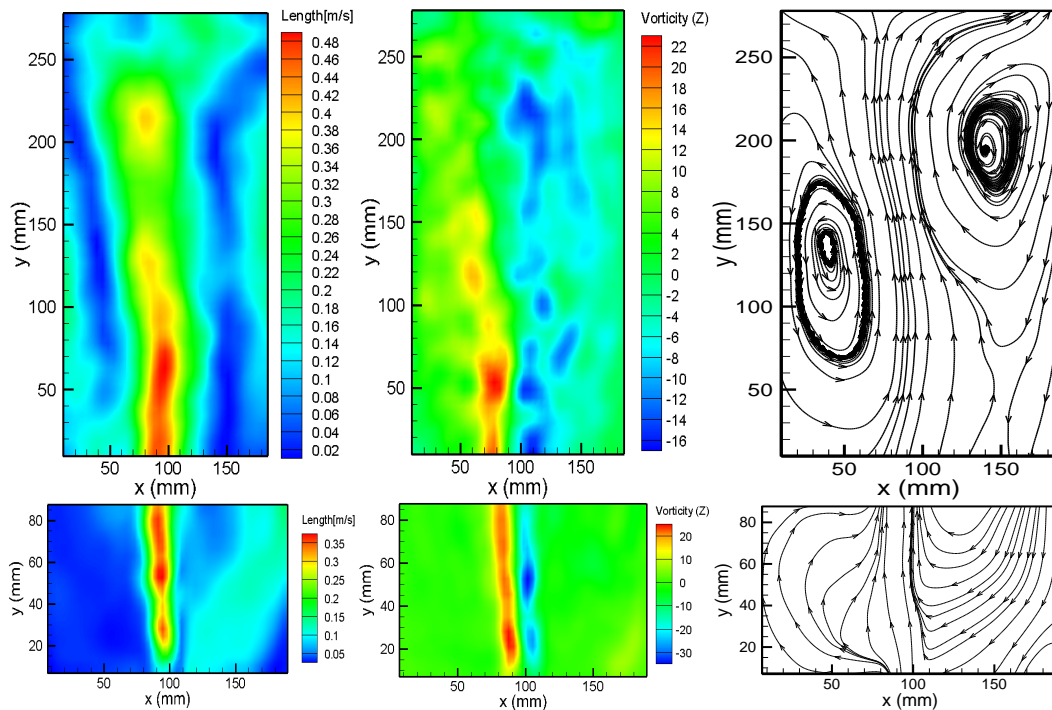


Figure 23 Time-averaged (a) resultant liquid velocity profiles, (b) vorticity profiles, (c) streamline profiles for flow 400 L/h for 3.5 mm needle diameter.

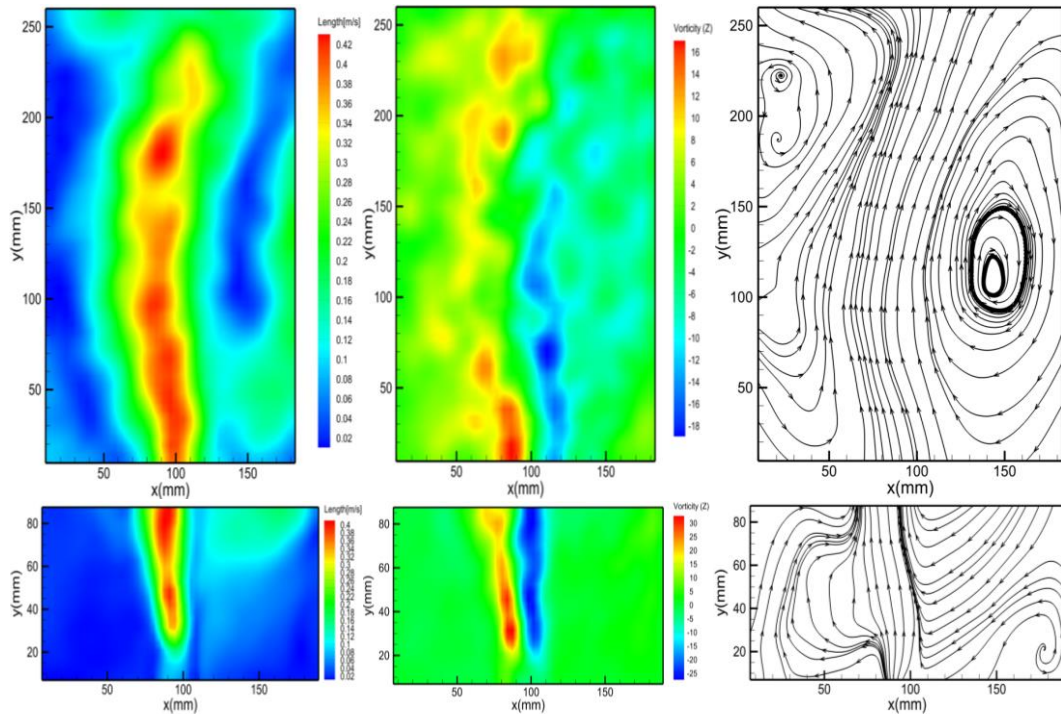


Figure 24 Time-averaged (a) resultant liquid velocity profiles, (b) vorticity profiles, (c) streamline profiles for flow 500 L/h for 3.5 mm needle diameter.

2) For single nozzle source (0.5mm,0.7mm,0.9mm diameter) bubble dynamics

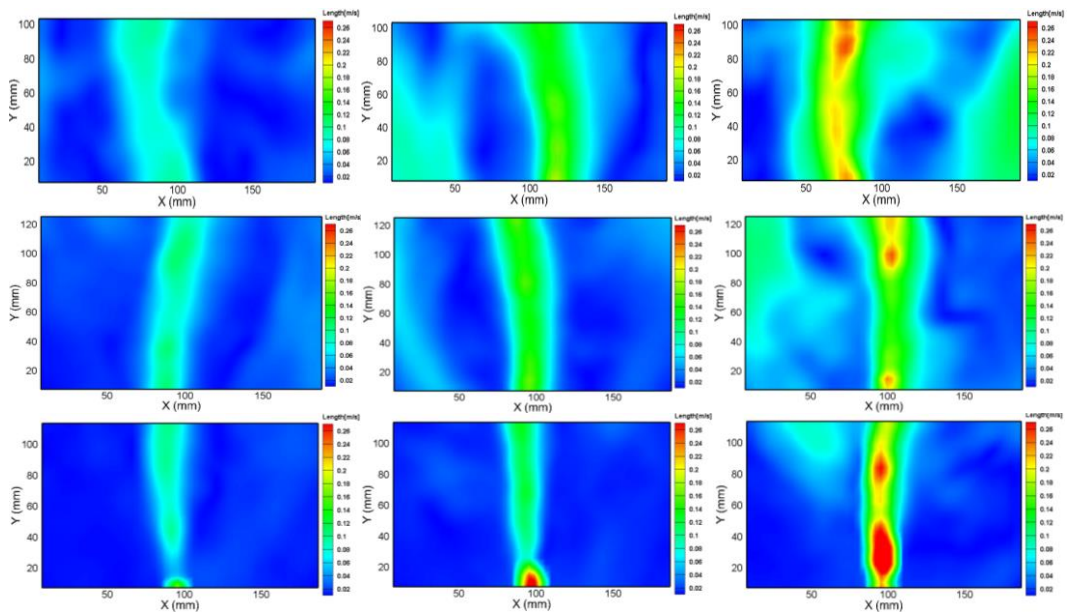


Figure 25 Time-averaged resultant liquid velocity profiles for (a) 10 L/h, (b) 20 L/h and (c) 30 L/h and for 0.5 mm nozzle diameter w/o MIBC.

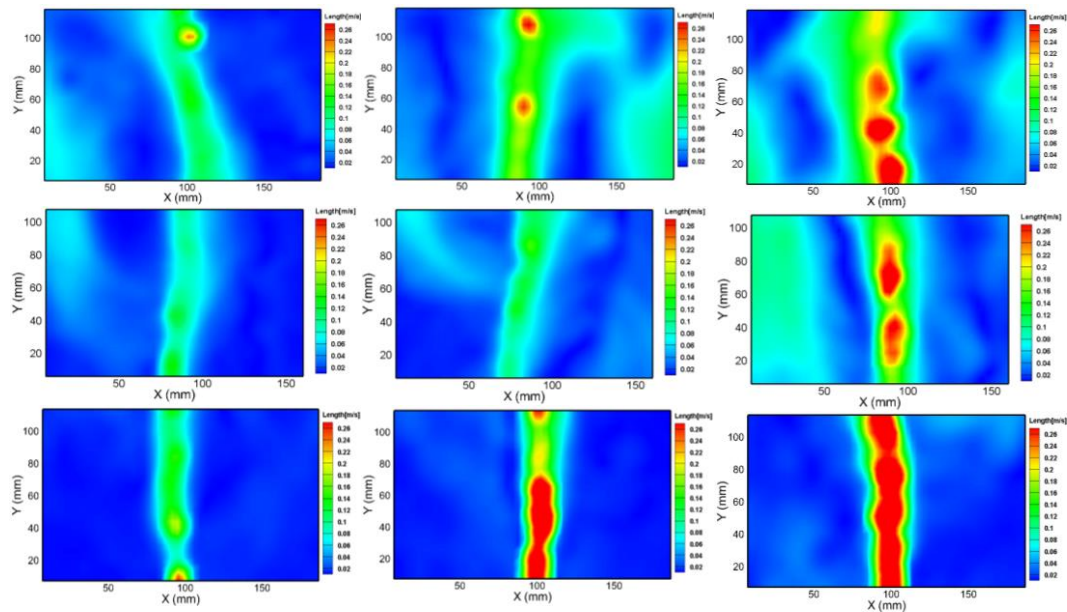


Figure 26 Time-averaged resultant liquid velocity profiles for (a) 10 L/h, (b) 20 L/h and (c) 30 L/h and for 0.5 mm nozzle diameter with 0.5 ml MIBC.

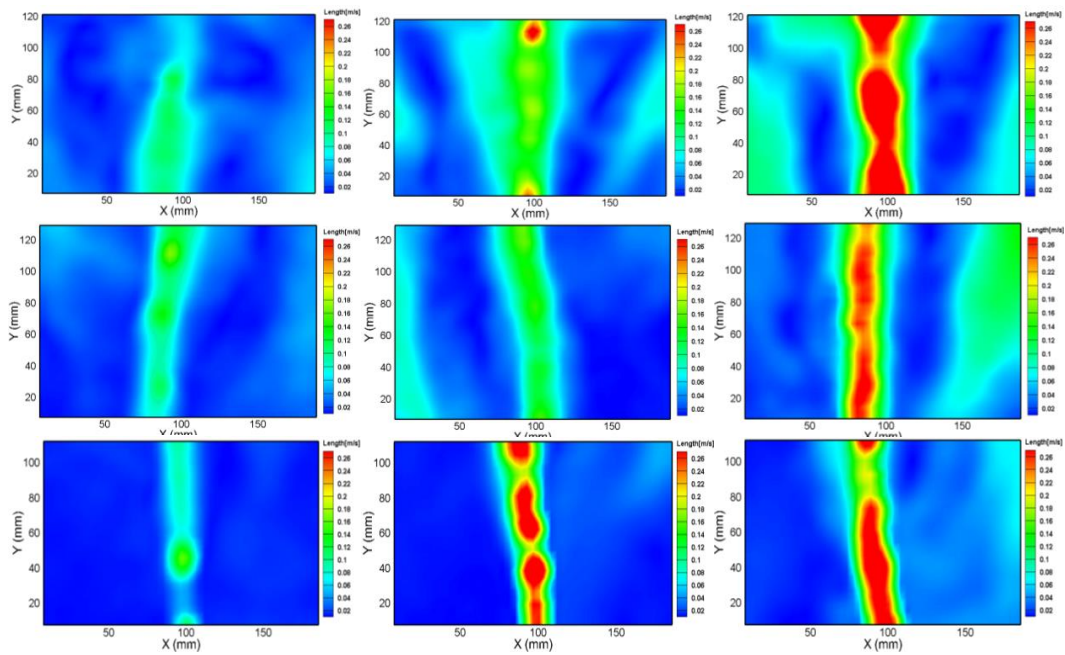


Figure 27 Time-averaged resultant liquid velocity profiles for (a) 10 L/h, (b) 20 L/h and (c) 30 L/h and for 0.5 mm nozzle diameter with 1.5 ml MIBC.

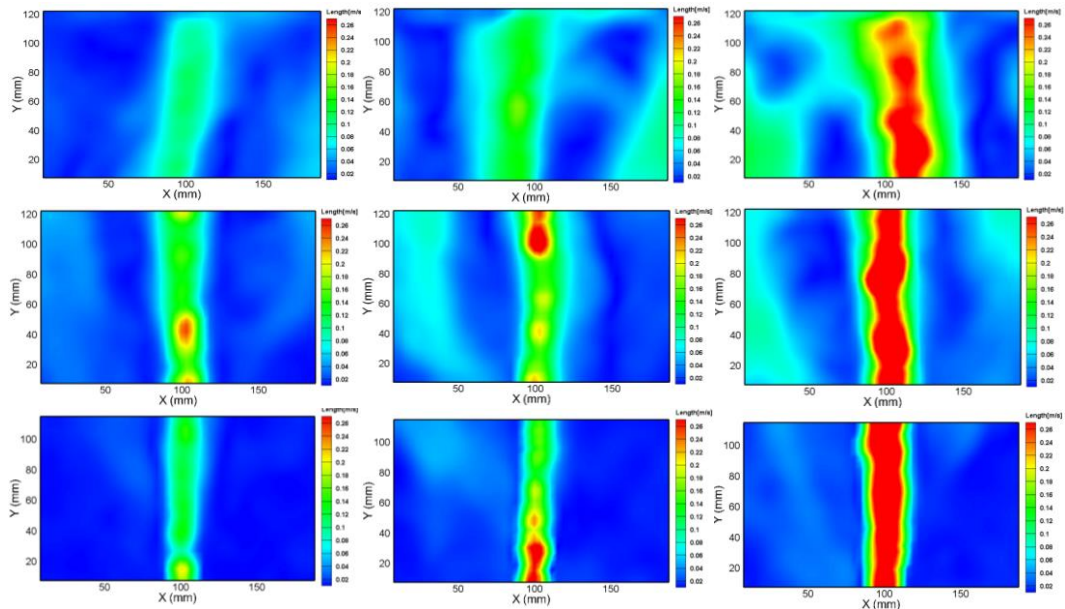


Figure 28 Time-averaged resultant liquid velocity profiles for (a) 10 L/h, (b) 20 L/h and (c) 30 L/h and for 0.5 mm nozzle diameter with 3 ml MIBC.

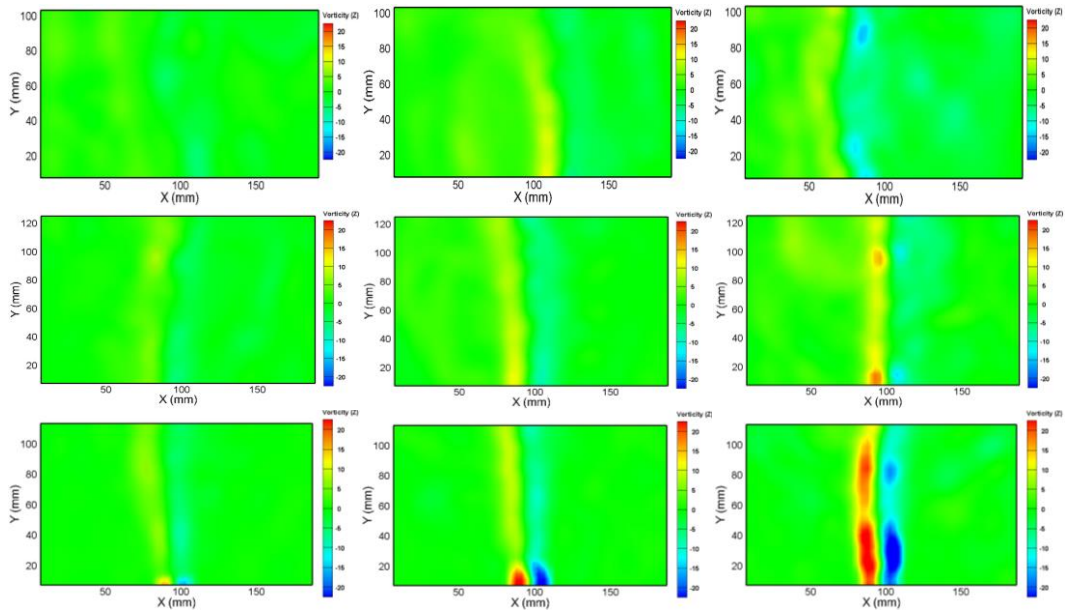


Figure 29 Time-averaged vorticity profiles for (a) 10 L/h, (b) 20 L/h and (c) 30 L/h and for 0.5 mm nozzle diameter w/o MIBC.

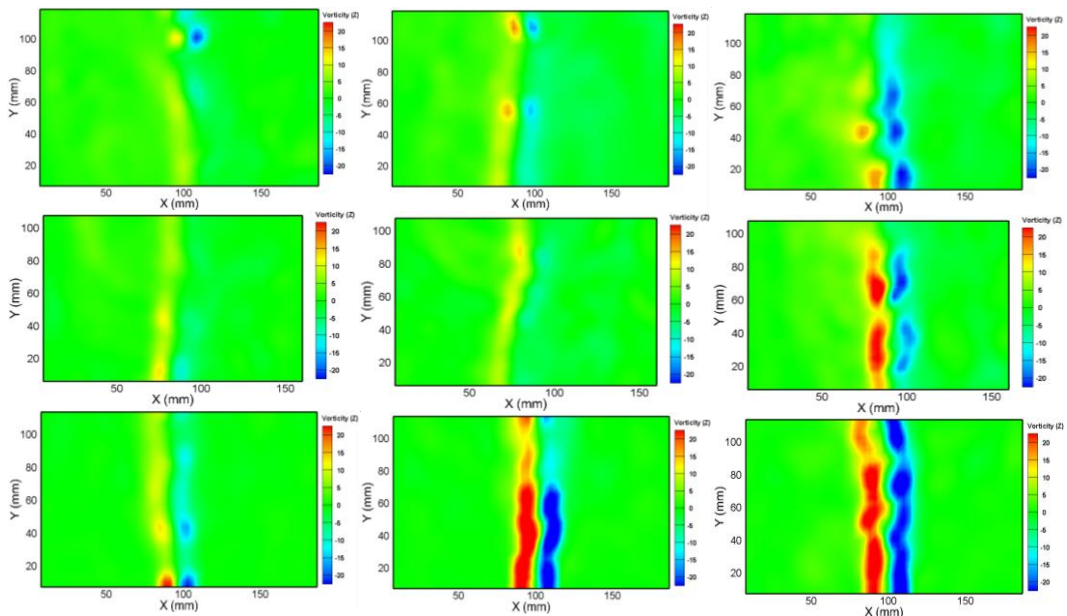


Figure 30 Time-averaged vorticity profiles for (a) 10 L/h, (b) 20 L/h and (c) 30 L/h and for 0.5 mm nozzle diameter with 0.5 ml MIBC.

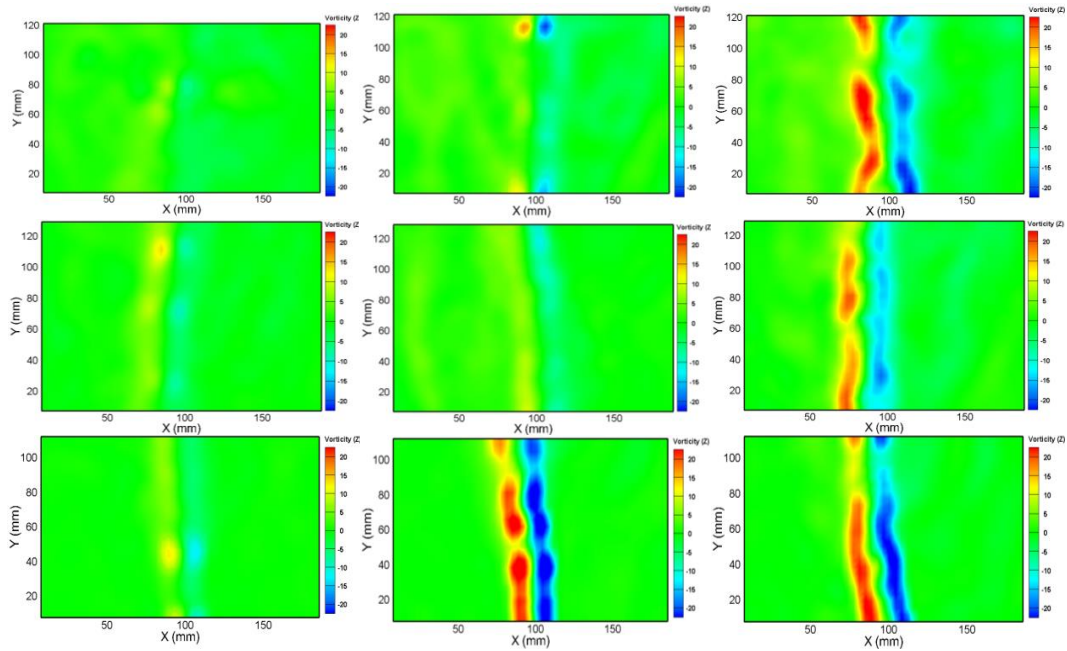


Figure 31 Time-averaged vorticity profiles for (a) 10 L/h, (b) 20 L/h and (c) 30 L/h and for 0.5 mm nozzle diameter with 1.5 ml MIBC.

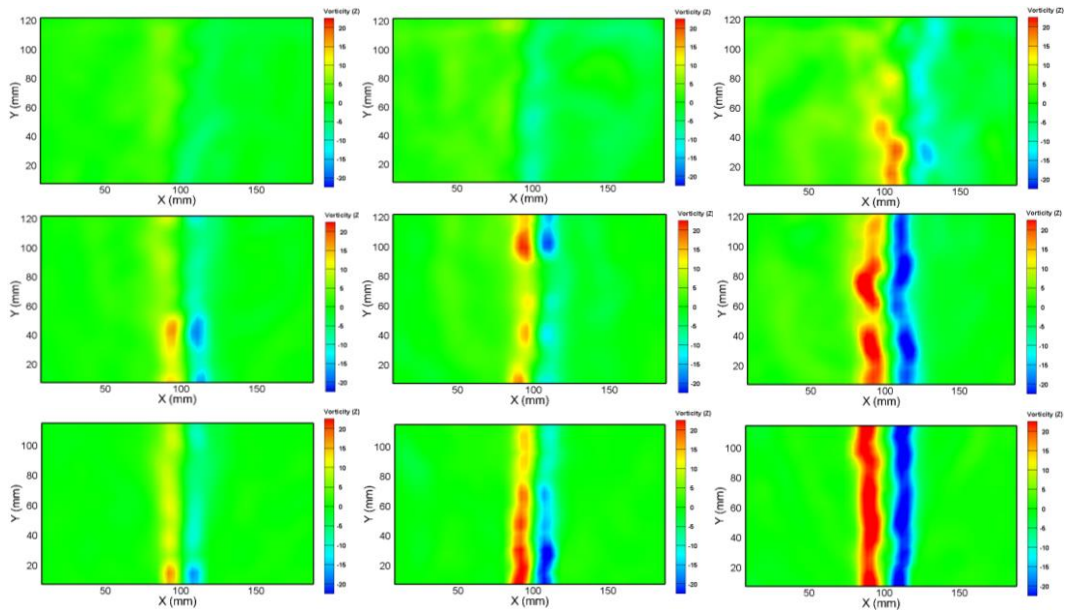


Figure 32 Time-averaged vorticity profiles for (a) 10 L/h, (b) 20 L/h and (c) 30 L/h and for 0.5 mm nozzle diameter with 3 ml MIBC.

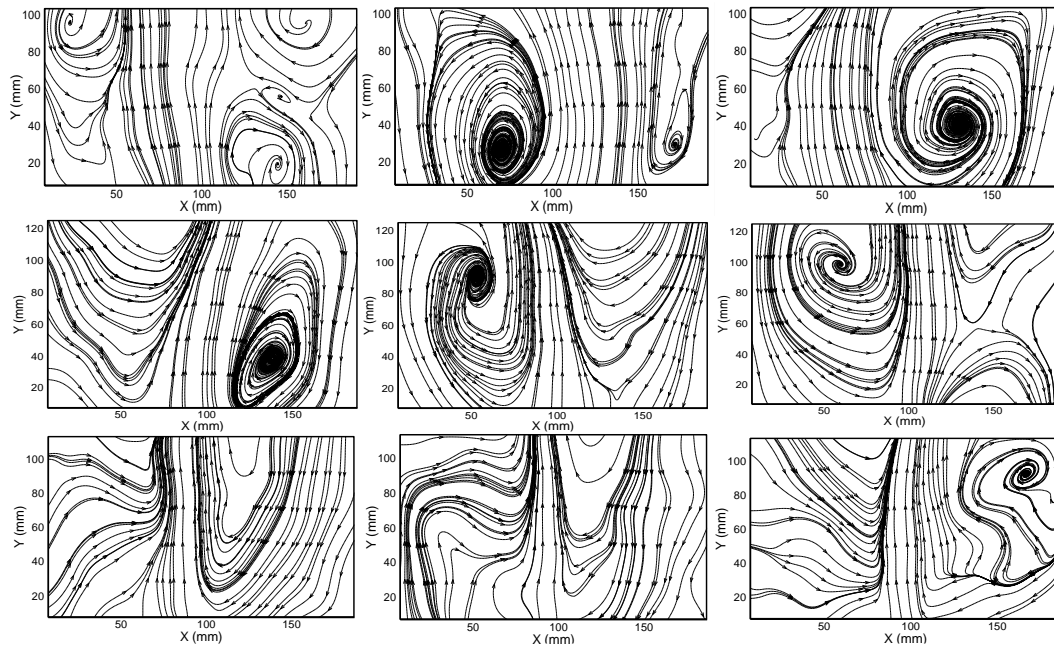


Figure 33 Time-averaged streamline profiles for (a) 10 L/h, (b) 20 L/h and (c) 30 L/h and for 0.5 mm nozzle diameter w/o MIBC.

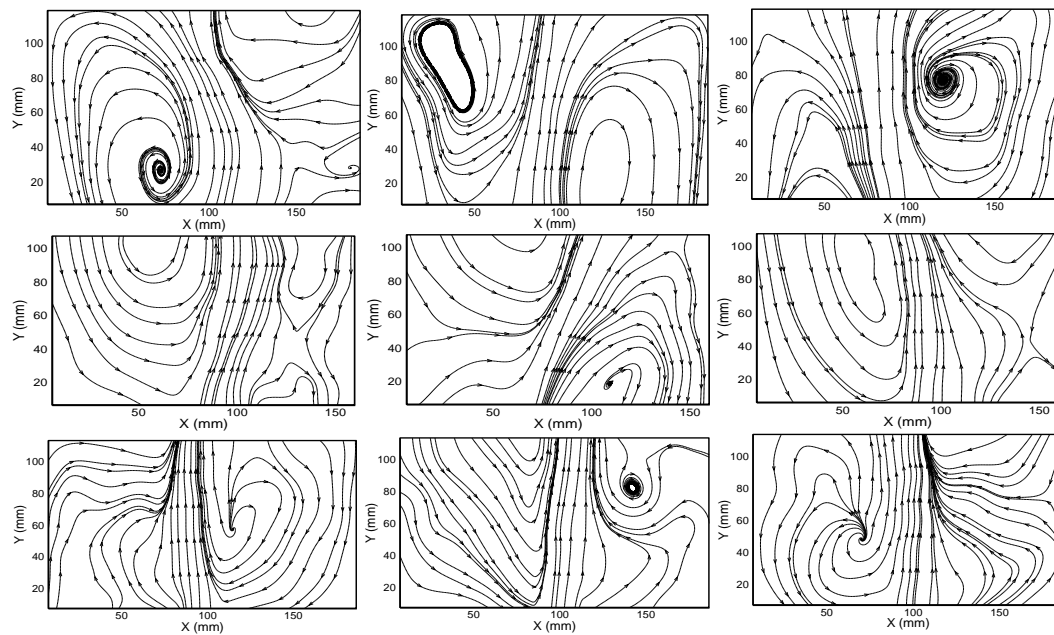


Figure 34 Time-averaged streamline profiles for (a) 10 L/h, (b) 20 L/h and (c) 30 L/h and for 0.5 mm nozzle diameter with 0.5 ml MIBC.

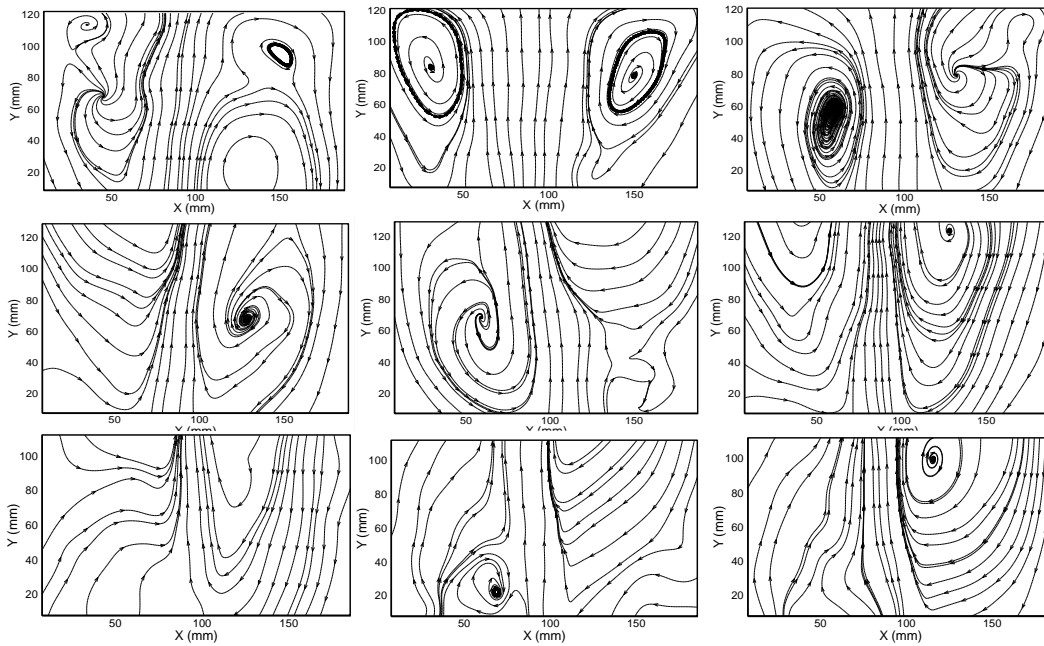


Figure 35 Time-averaged streamline profiles for (a) 10 L/h, (b) 20 L/h and (c) 30 L/h and for 0.5 mm nozzle diameter with 1.5 ml MIBC.

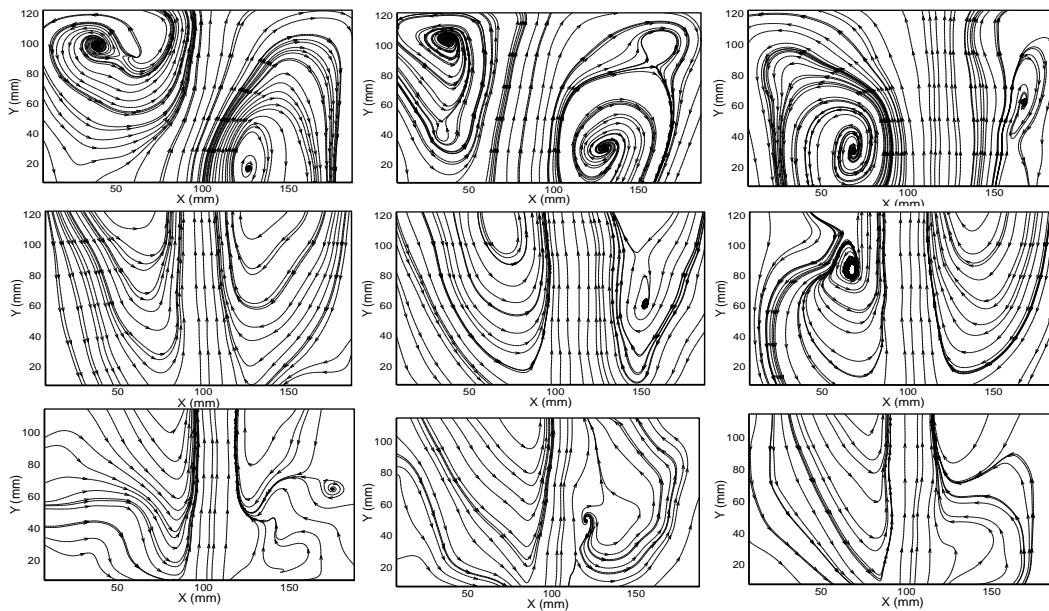


Figure 36 Time-averaged streamline profiles for (a) 10 L/h, (b) 20 L/h and (c) 30 L/h and for 0.5 mm nozzle diameter with 3 ml MIBC.

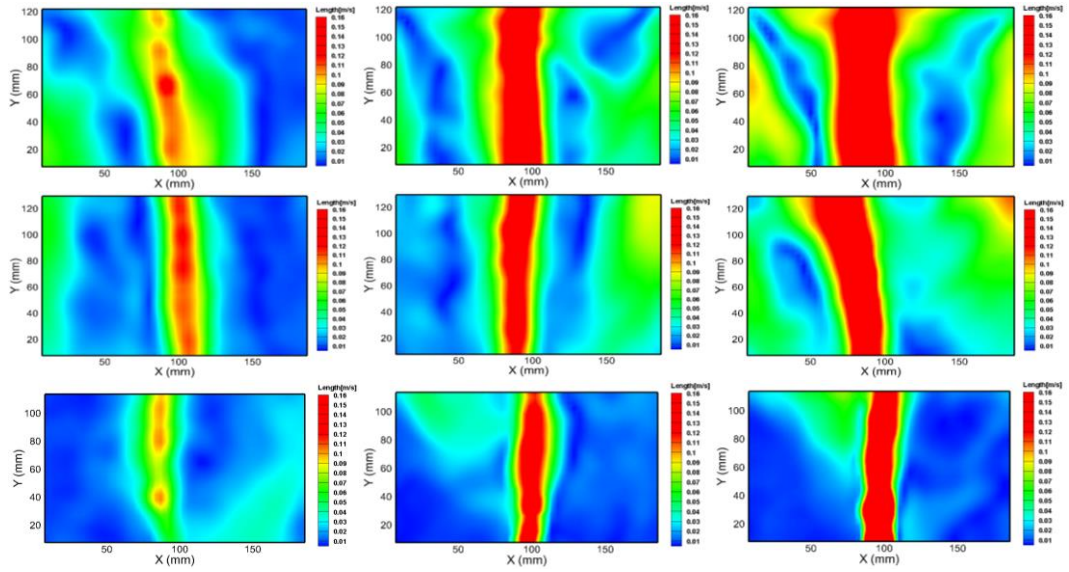


Figure 37 Time-averaged resultant liquid velocity profiles for (a) 10 L/h, (b) 20 L/h and (c) 30 L/h and for 0.7 mm nozzle diameter w/o MIBC.

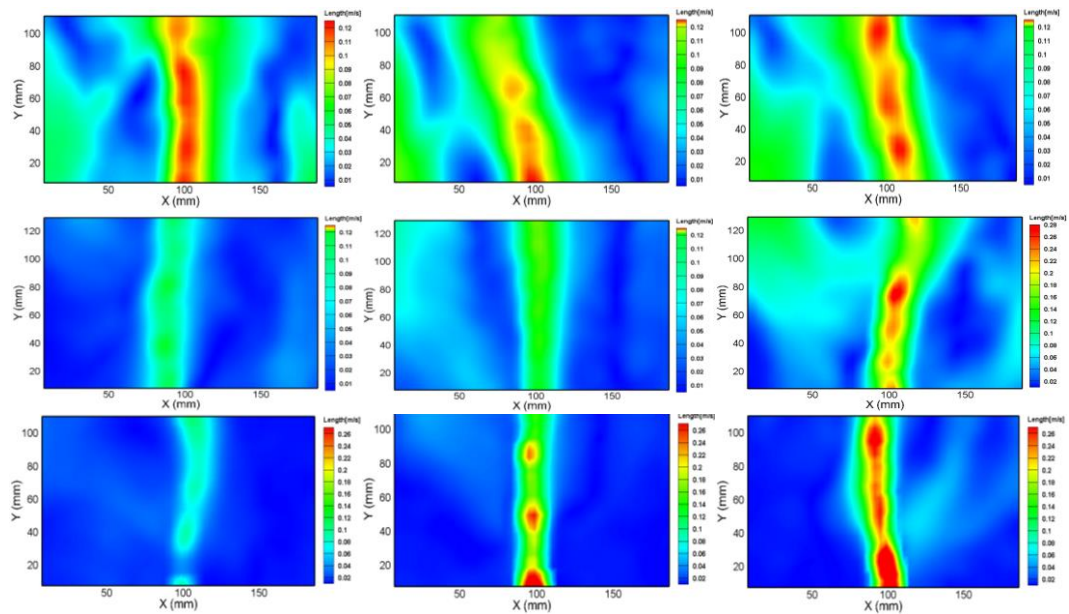


Figure 38 Time-averaged resultant liquid velocity profiles for (a) 10 L/h, (b) 20 L/h and (c) 30 L/h and for 0.7 mm nozzle diameter with 0.5 ml MIBC.

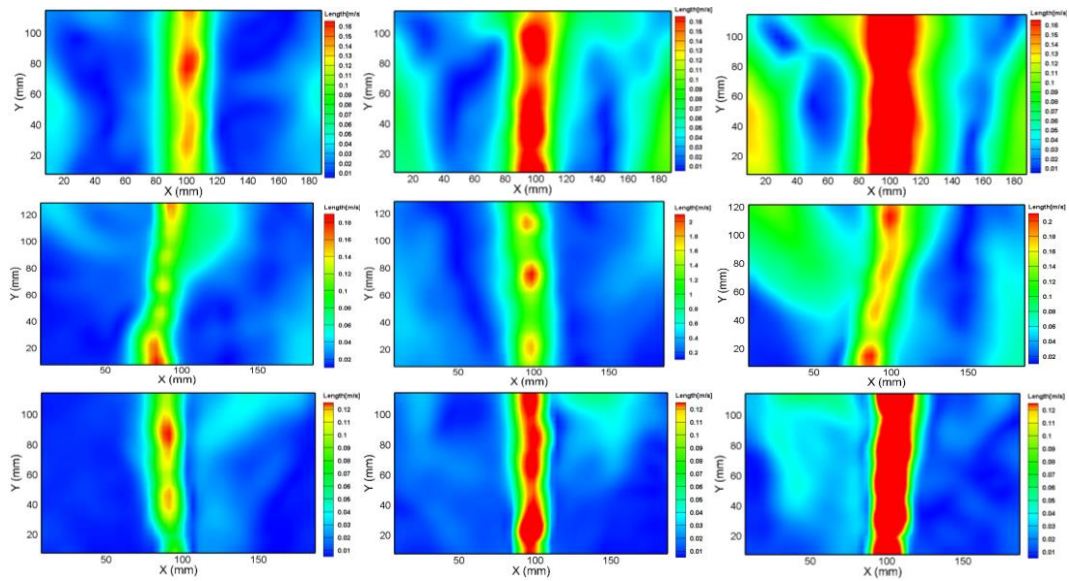


Figure 39 Time-averaged resultant liquid velocity profiles for (a) 10 L/h, (b) 20 L/h and (c) 30 L/h and for 0.7 mm nozzle diameter with 1.5 ml MIBC.

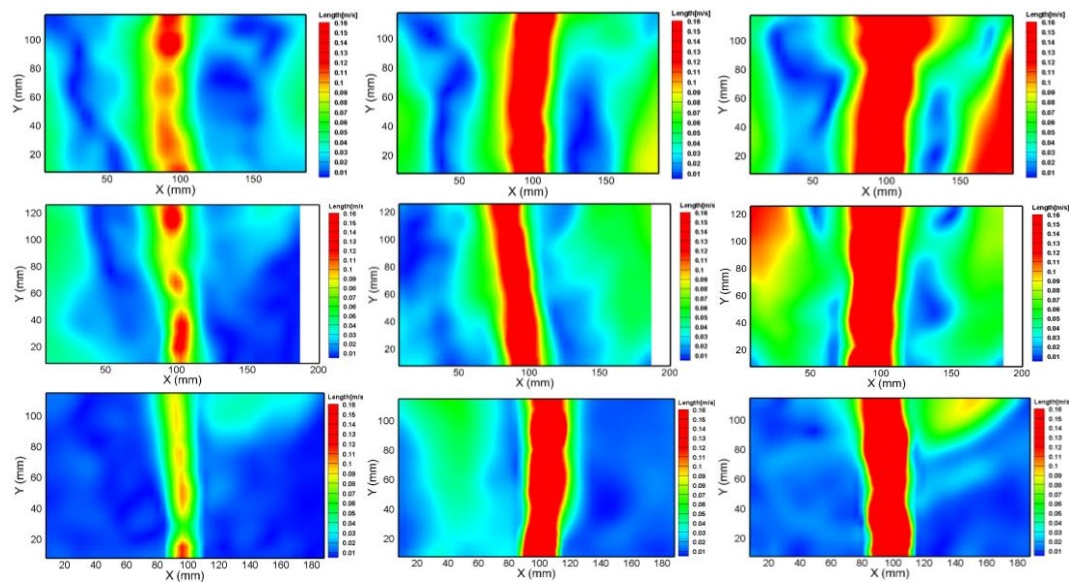


Figure 40 Time-averaged resultant liquid velocity profiles for (a) 10 L/h, (b) 20 L/h and (c) 30 L/h and for 0.7 mm nozzle diameter with 3 ml MIBC.

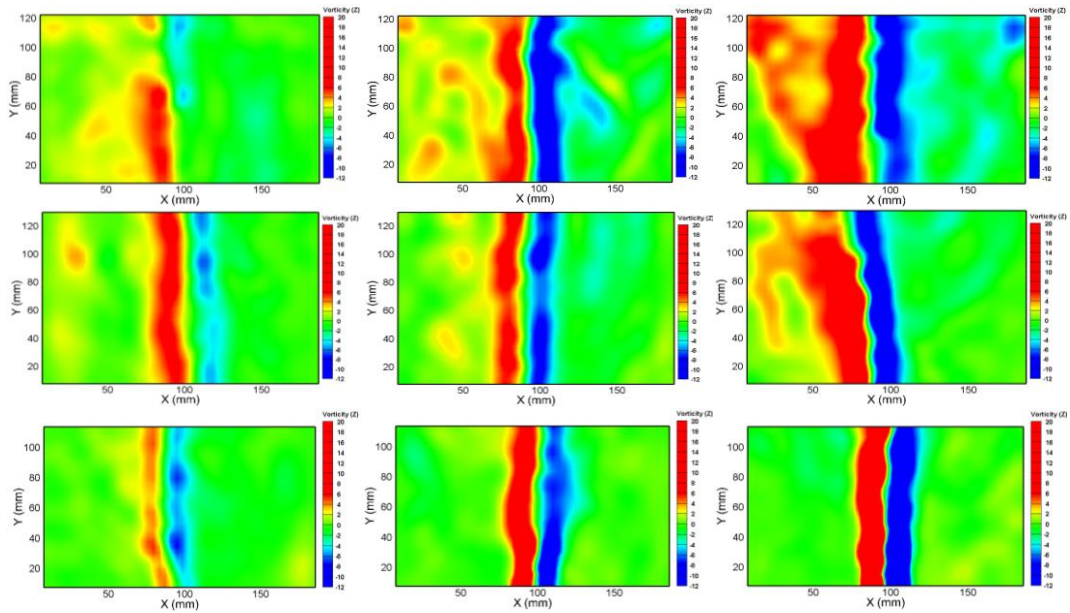


Figure 41 Time-averaged vorticity profiles for (a) 10 L/h, (b) 20 L/h and (c) 30 L/h and for 0.7 mm nozzle diameter w/o ml MIBC.

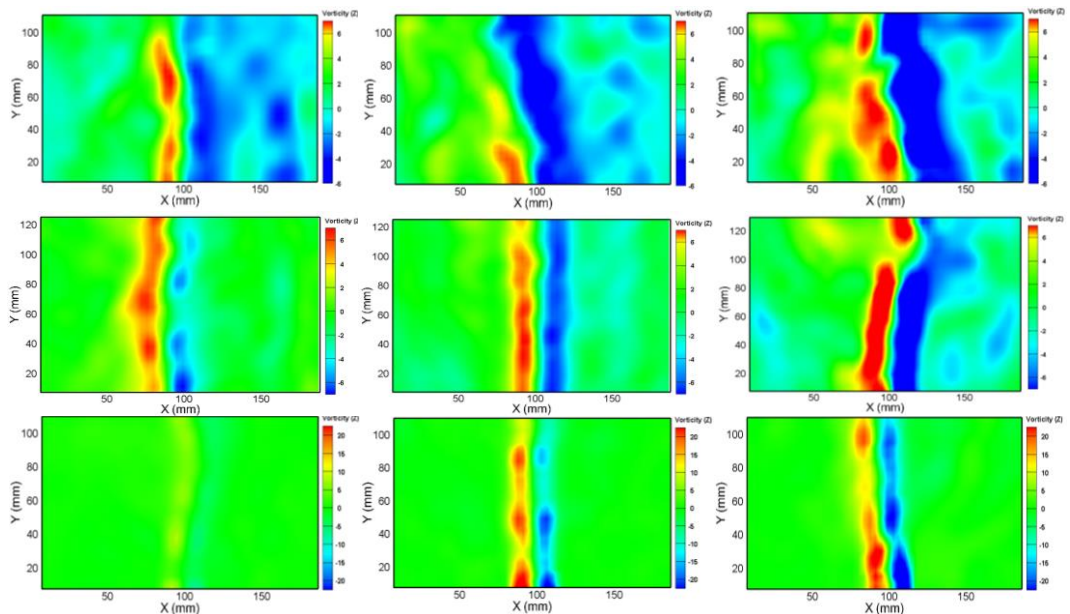


Figure 42 Time-averaged vorticity profiles for (a) 10 L/h, (b) 20 L/h and (c) 30 L/h and for 0.7 mm nozzle diameter with 0.5 ml MIBC.

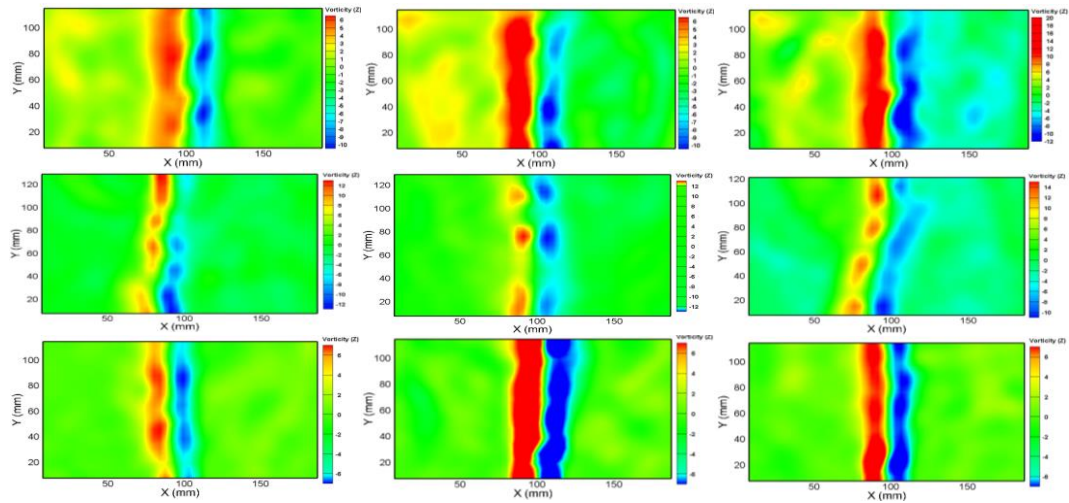


Figure 43 Time-averaged vorticity profiles for (a) 10 L/h, (b) 20 L/h and (c) 30 L/h and for 0.7 mm nozzle diameter with 1.5 ml MIBC.

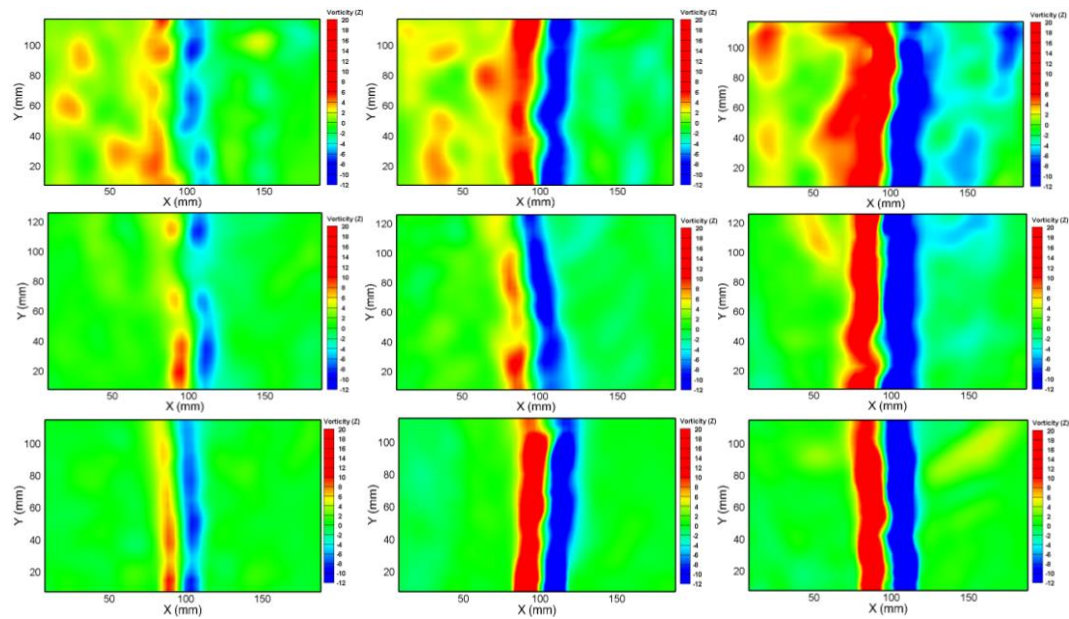


Figure 44 Time-averaged vorticity profiles for (a) 10 L/h, (b) 20 L/h and (c) 30 L/h and for 0.7 mm nozzle diameter with 3 ml MIBC.

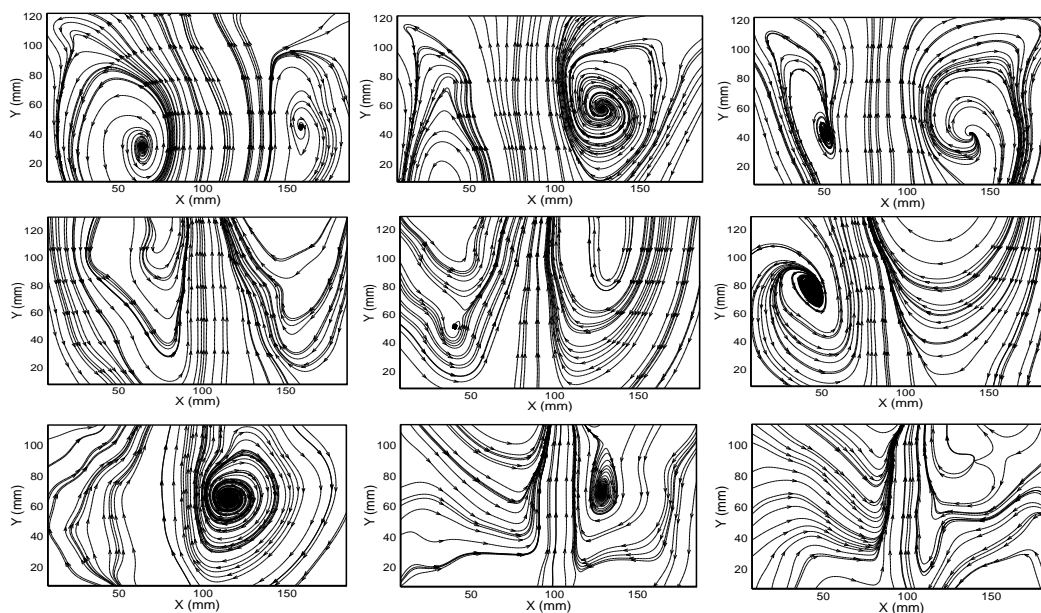


Figure 45 Time-averaged streamline profiles for (a) 10 L/h, (b) 20 L/h and (c) 30 L/h and for 0.7 mm nozzle diameter w/o MIBC.

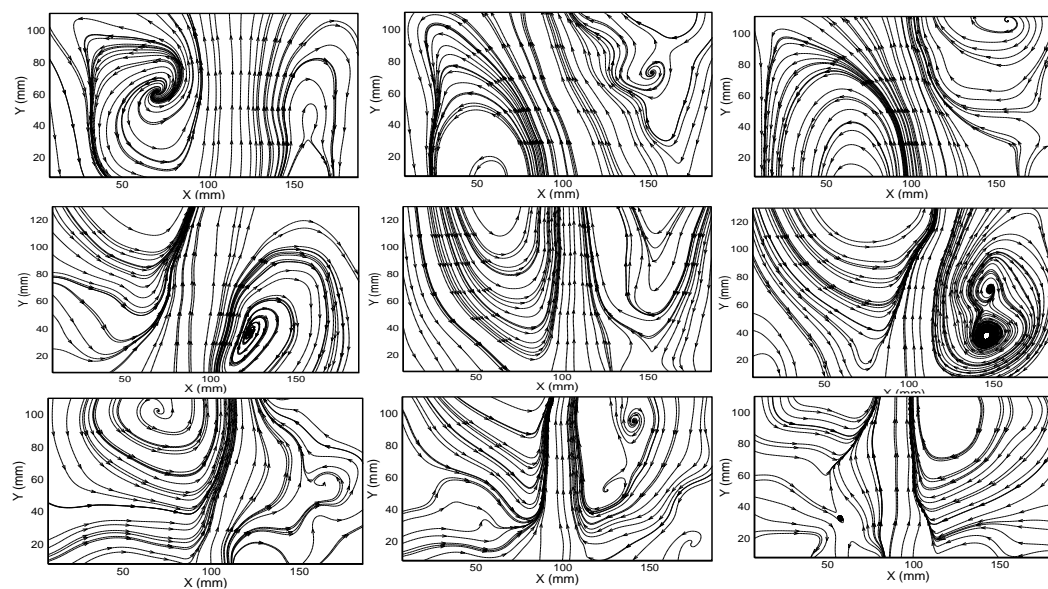


Figure 46 Time-averaged streamline profiles for (a) 10 L/h, (b) 20 L/h and (c) 30 L/h and for 0.7 mm nozzle diameter with 0.5 ml MIBC.

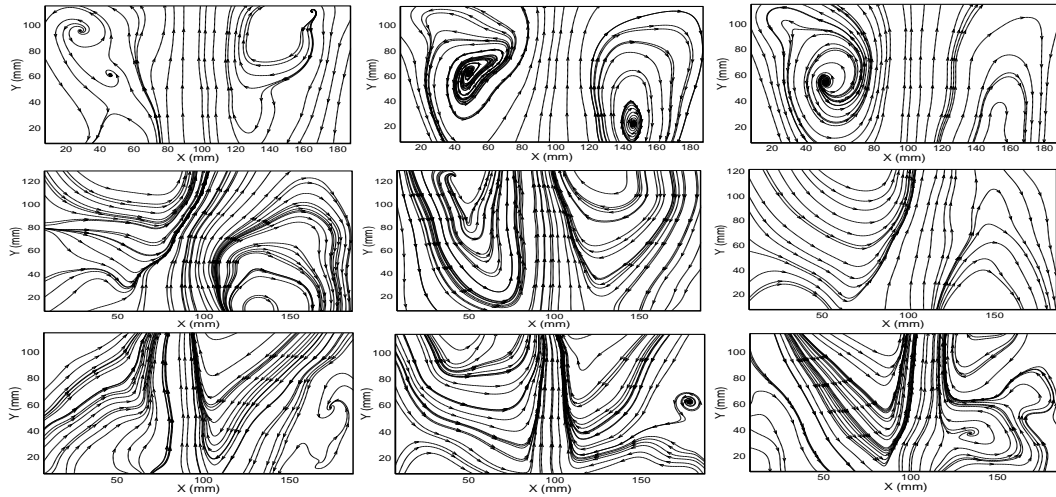


Figure 47 Time-averaged streamline profiles for (a) 10 L/h, (b) 20 L/h and (c) 30 L/h and for 0.7 mm nozzle diameter with 1.5 ml MIBC.

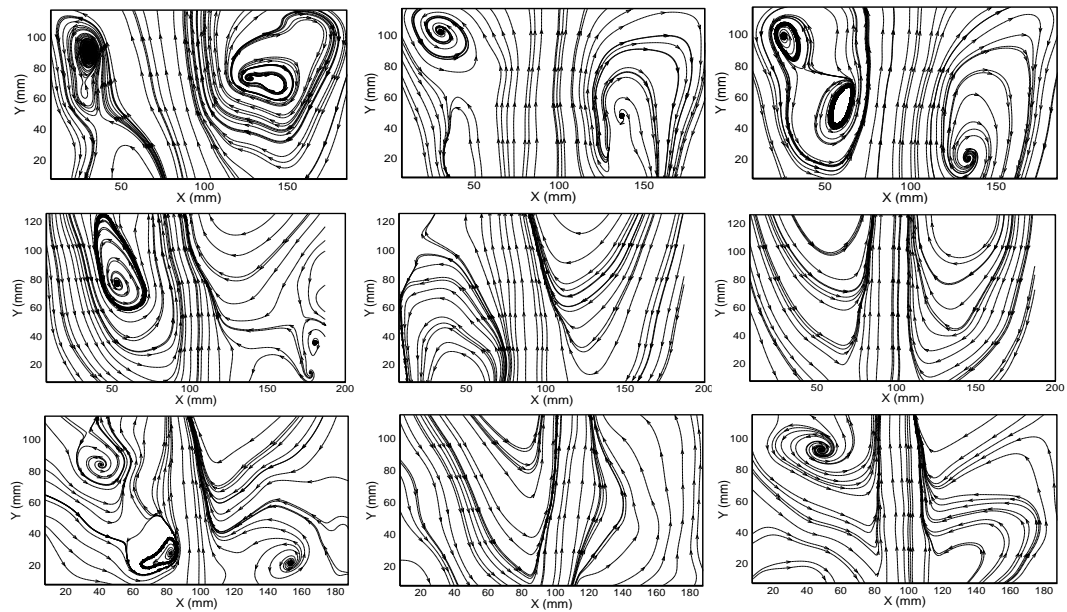


Figure 48 Time-averaged streamline profiles for (a) 10 L/h, (b) 20 L/h and (c) 30 L/h and for 0.7 mm nozzle diameter with 3 ml MIBC.

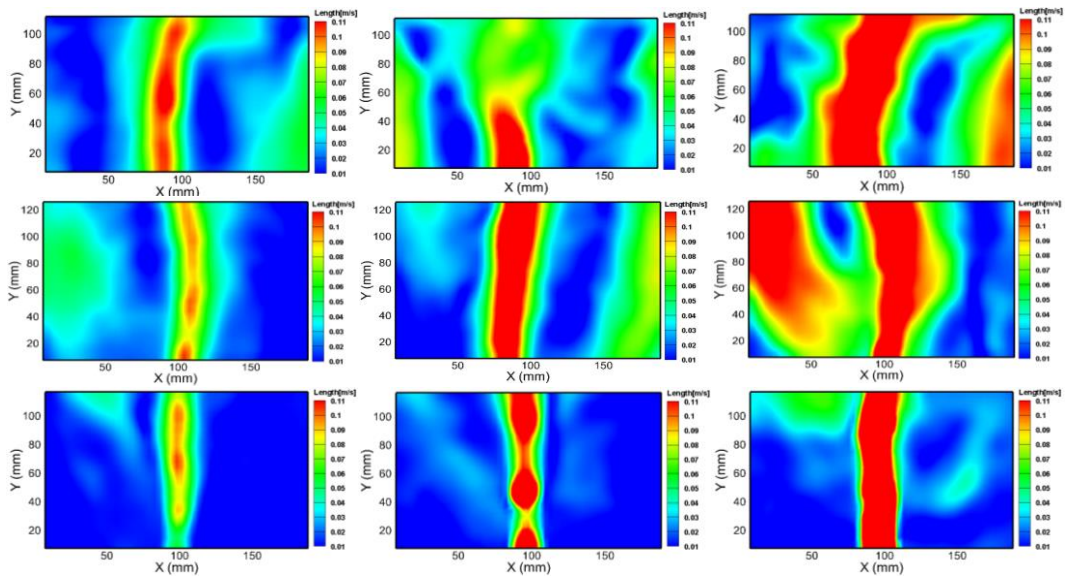


Figure 49 Time-averaged resultant liquid velocity profiles for (a) 10 L/h, (b) 20 L/h and (c) 30 L/h and for 0.9 mm nozzle diameter w/o MIBC.

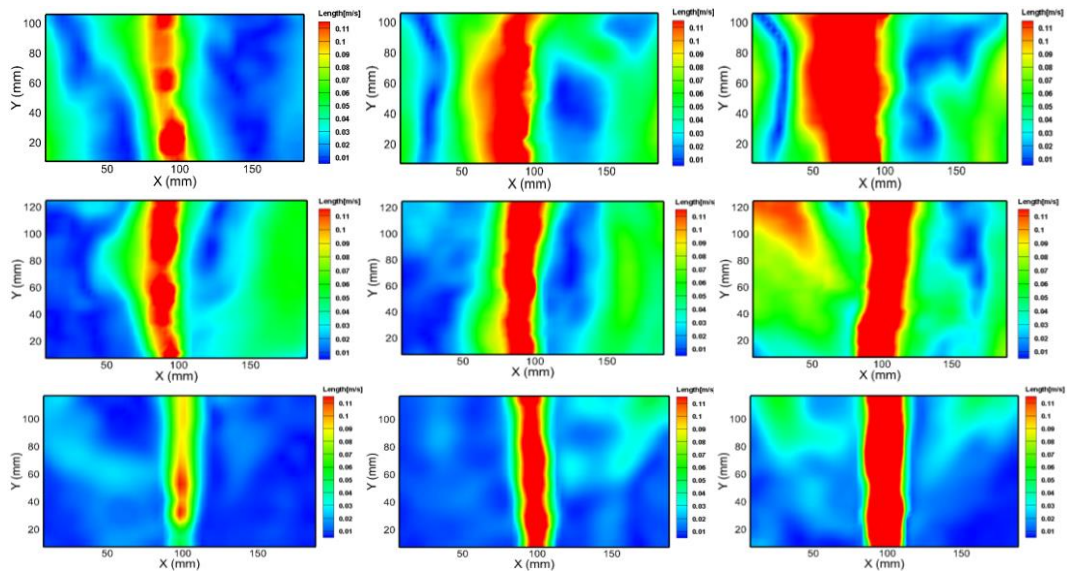


Figure 50 Time-averaged resultant liquid velocity profiles for (a) 10 L/h, (b) 20 L/h and (c) 30 L/h and for 0.9 mm nozzle diameter with 0.5 ml MIBC.

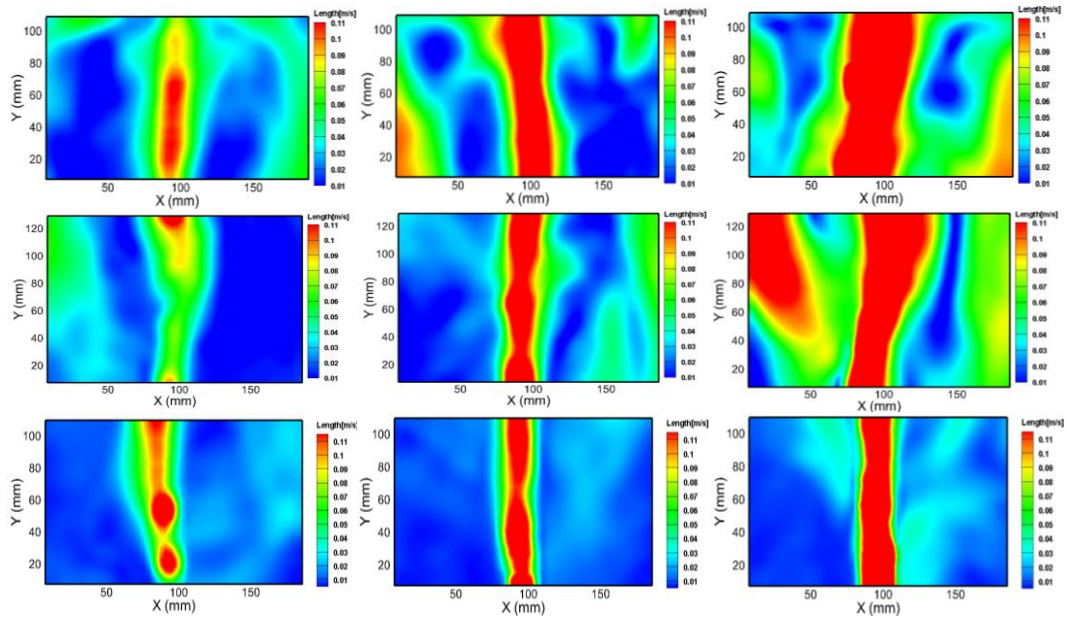


Figure 51 Time-averaged resultant liquid velocity profiles for (a) 10 L/h, (b) 20 L/h and (c) 30 L/h and for 0.9 mm nozzle diameter with 1.5 ml MIBC.

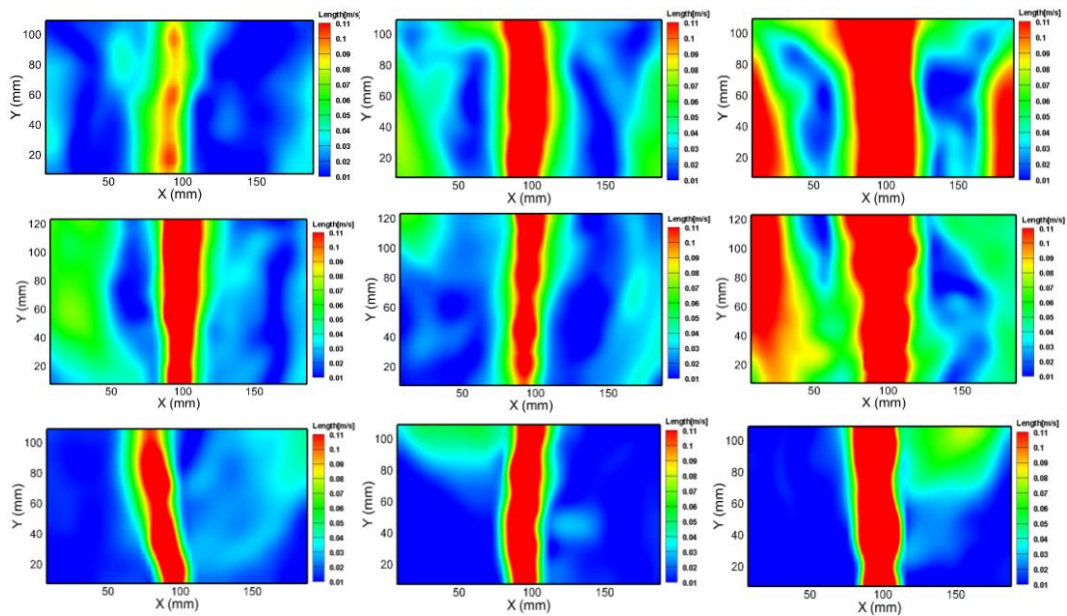


Figure 52 Time-averaged resultant liquid velocity profiles for (a) 10 L/h, (b) 20 L/h and (c) 30 L/h and for 0.9 mm nozzle diameter with 1.5 ml MIBC.

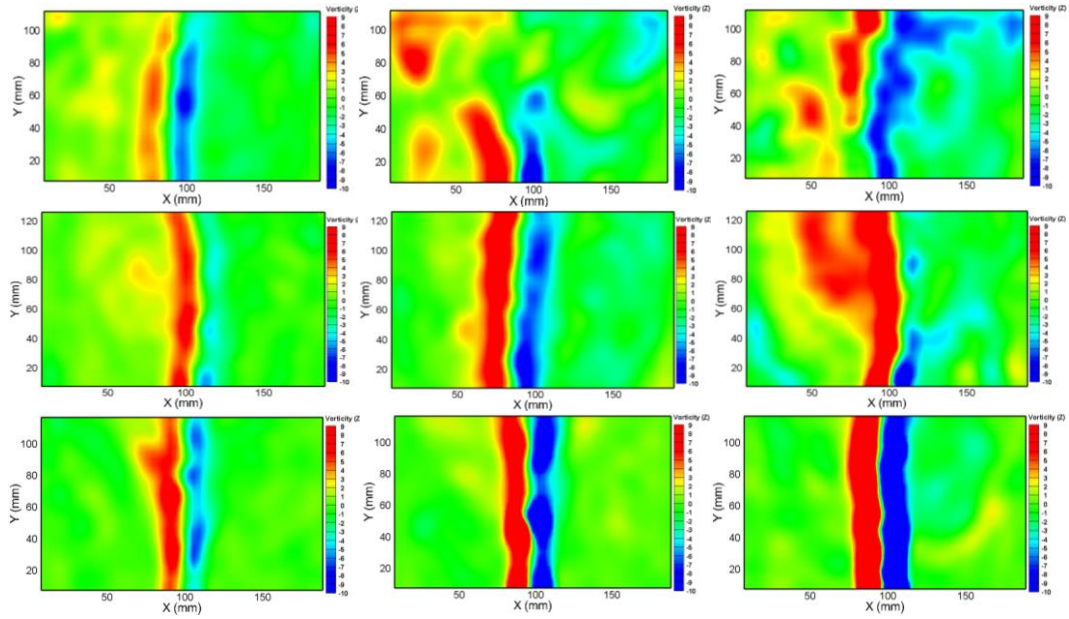


Figure 53 Time-averaged vorticity profiles for (a) 10 L/h, (b) 20 L/h and (c) 30 L/h and for 0.9 mm nozzle diameter w/o MIBC.

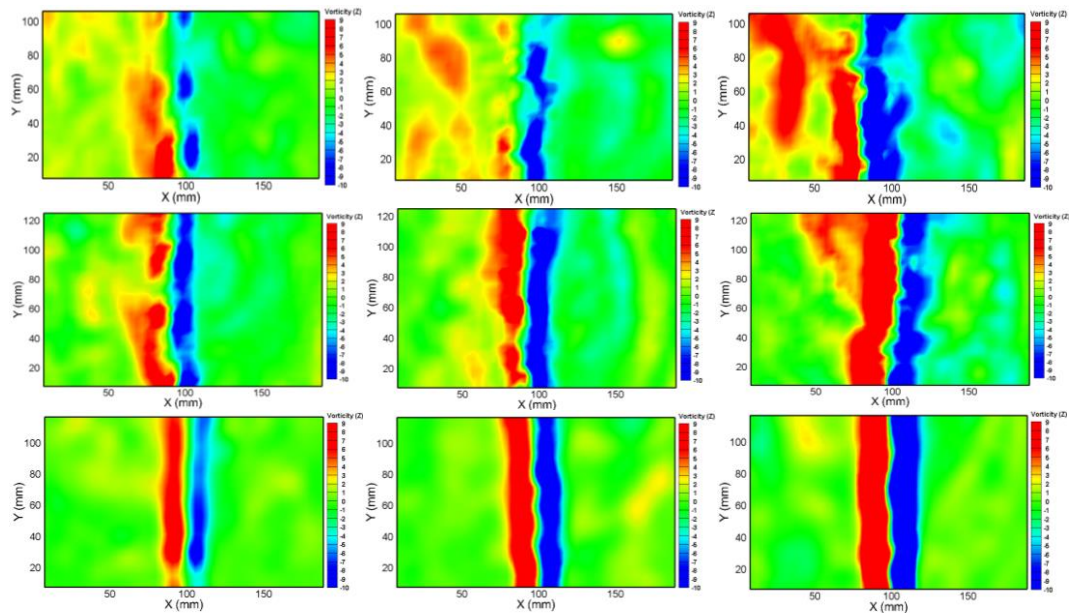


Figure 54 Time-averaged vorticity profiles for (a) 10 L/h, (b) 20 L/h and (c) 30 L/h and for 0.9 mm nozzle diameter with 0.5 ml MIBC.

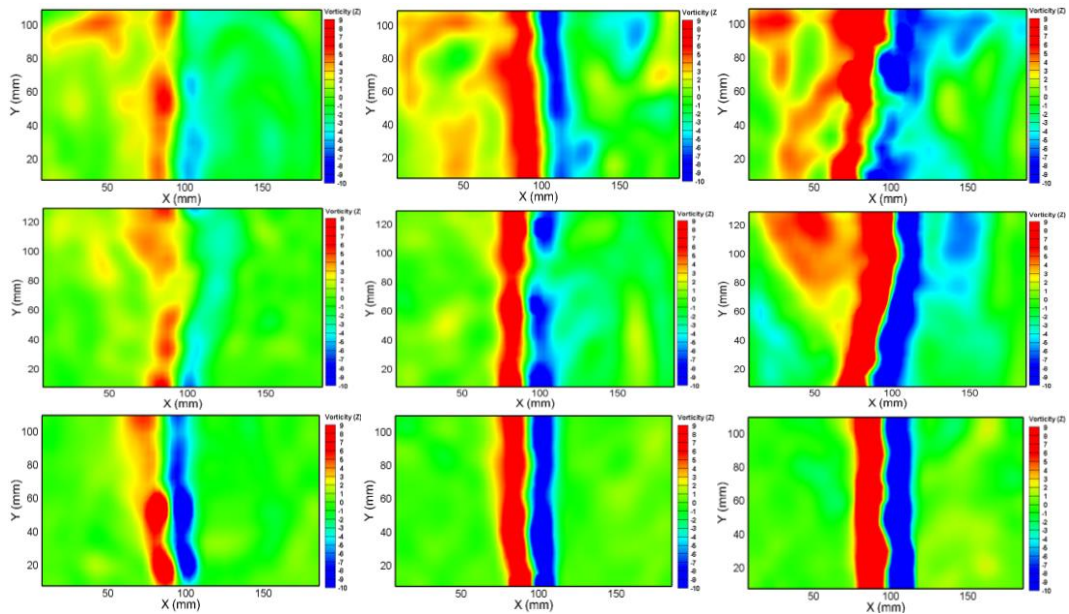


Figure 55 Time-averaged vorticity profiles for (a) 10 L/h, (b) 20 L/h and (c) 30 L/h and for 0.9 mm nozzle diameter with 1.5 ml MIBC.

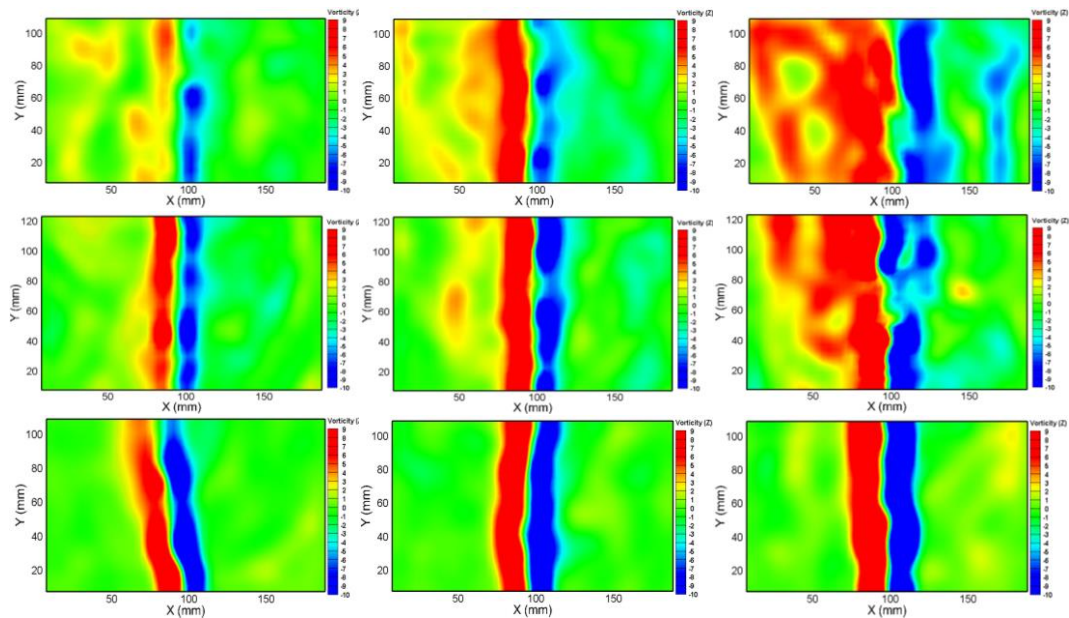


Figure 56 Time-averaged vorticity profiles for (a) 10 L/h, (b) 20 L/h and (c) 30 L/h and for 0.9 mm nozzle diameter with 3 ml MIBC.

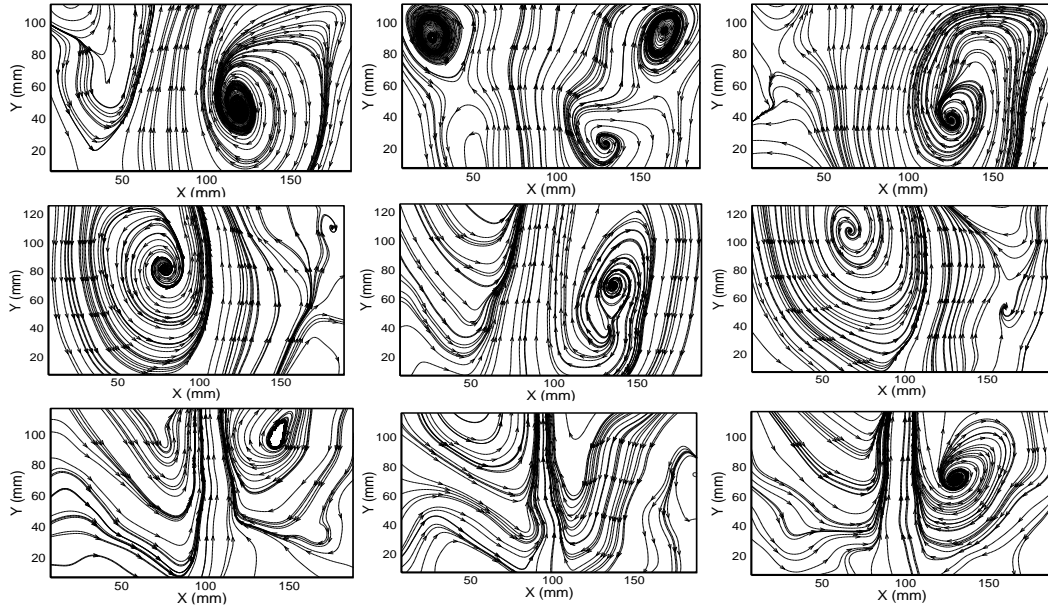


Figure 57 Time-averaged streamline profiles for (a) 10 L/h, (b) 20 L/h and (c) 30 L/h and for 0.9 mm nozzle diameter w/o MIBC.

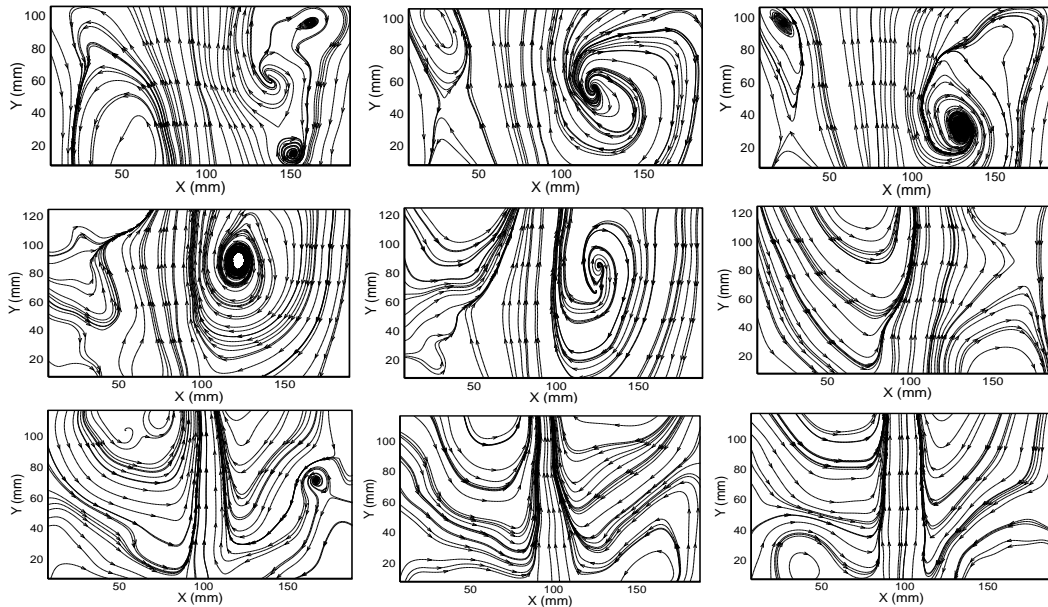


Figure 58 Time-averaged streamline profiles for (a) 10 L/h, (b) 20 L/h and (c) 30 L/h and for 0.9 mm nozzle diameter with 0.5 ml MIBC.

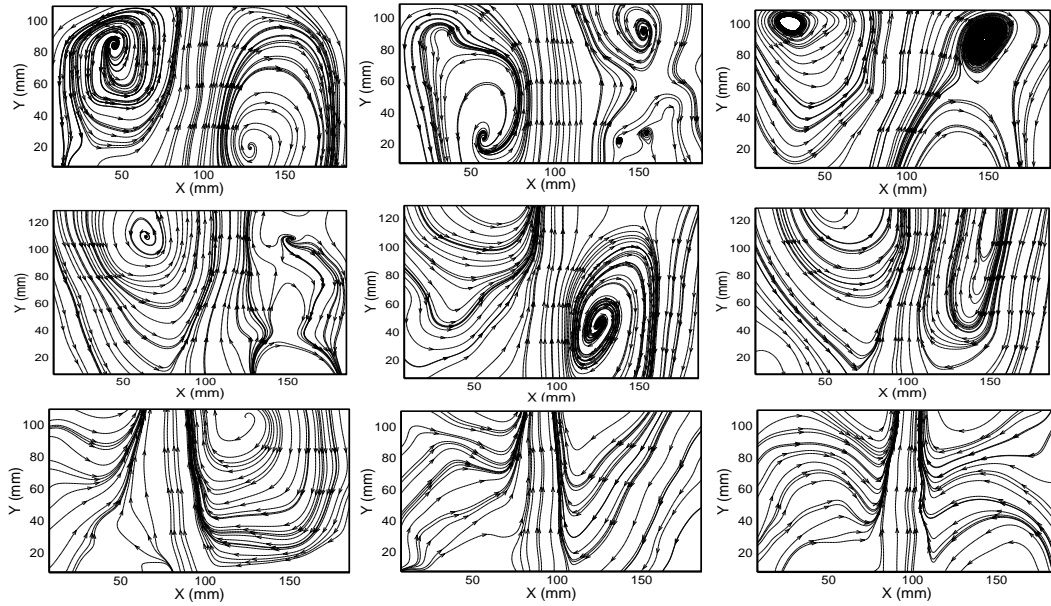


Figure 59 Time-averaged streamline profiles for (a) 10 L/h, (b) 20 L/h and (c) 30 L/h and for 0.9 mm nozzle diameter with 1.5 ml MIBC.

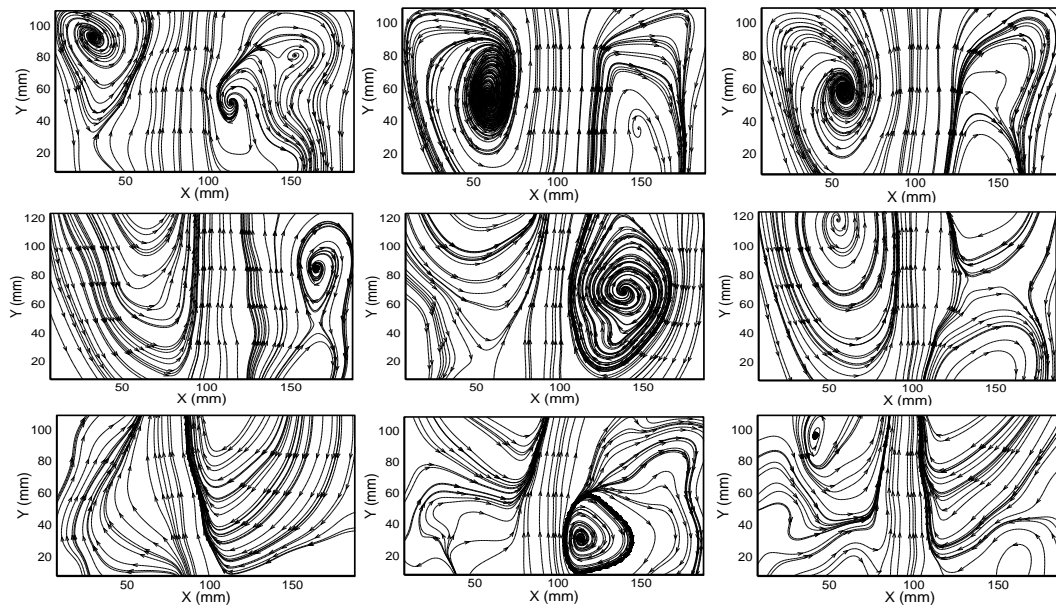


Figure 60 Time-averaged streamline profiles for (a) 10 L/h, (b) 20 L/h and (c) 30 L/h and for 0.9 mm nozzle diameter with 3 ml MIBC.

3) Multiple nozzle source (0.5mm,0.7mm,0.9mm diameter)bubble dynamics

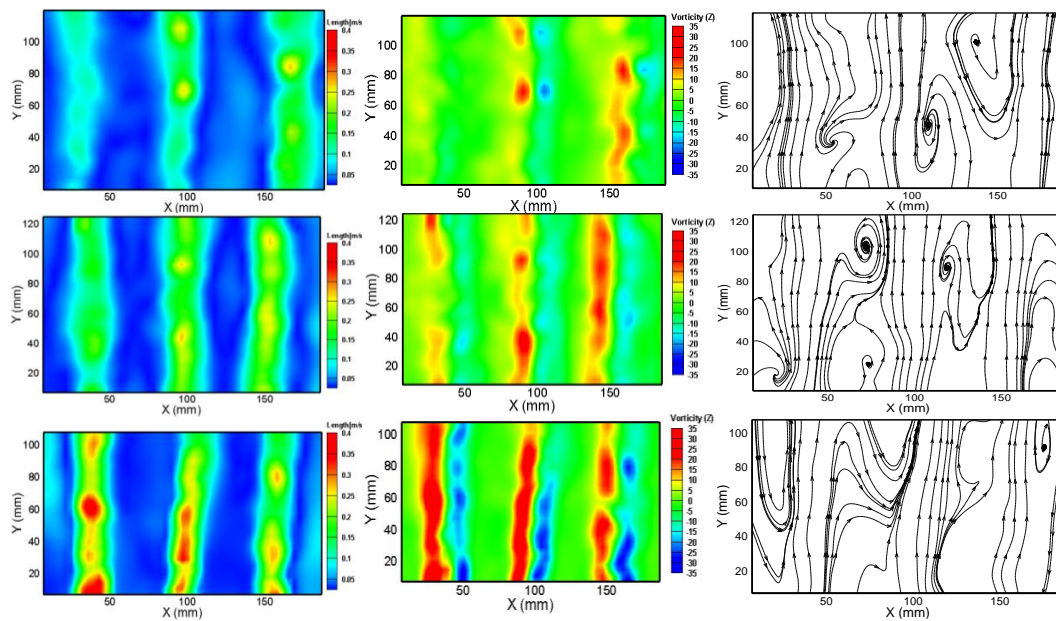


Figure 61 Time-averaged (a) resultant liquid velocity profiles, (b) vorticity profiles, (c) streamline profiles for flow 60 L/h for 0.5 mm nozzle diameter w/o MIBC

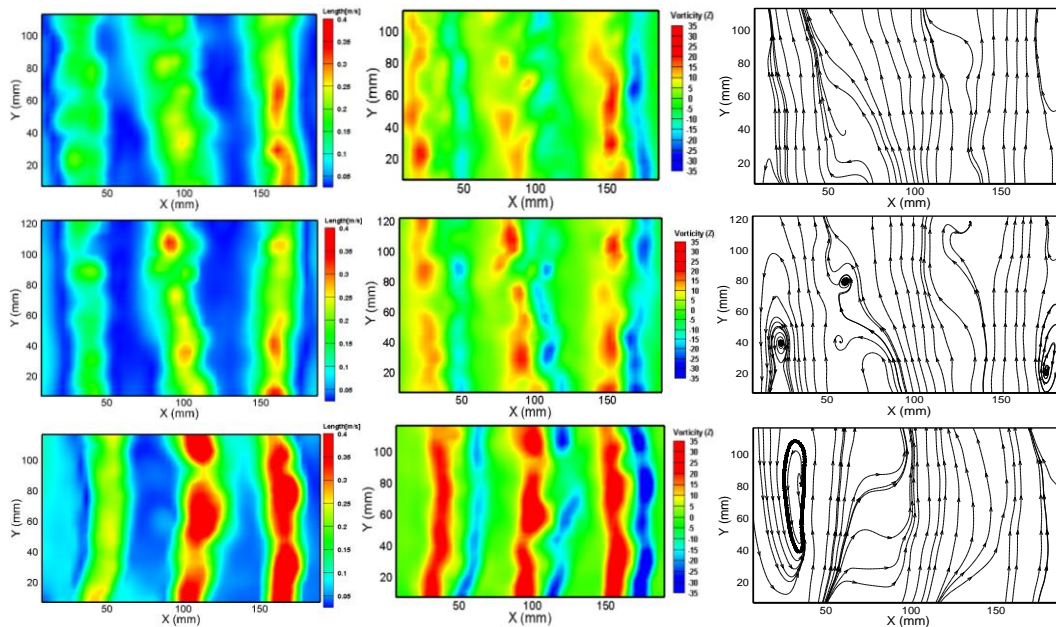


Figure 62 Time-averaged (a) resultant liquid velocity profiles, (b) vorticity profiles, (c) streamline profiles for flow 60 L/h for 0.5 mm nozzle diameter with 0.5 ml MIBC

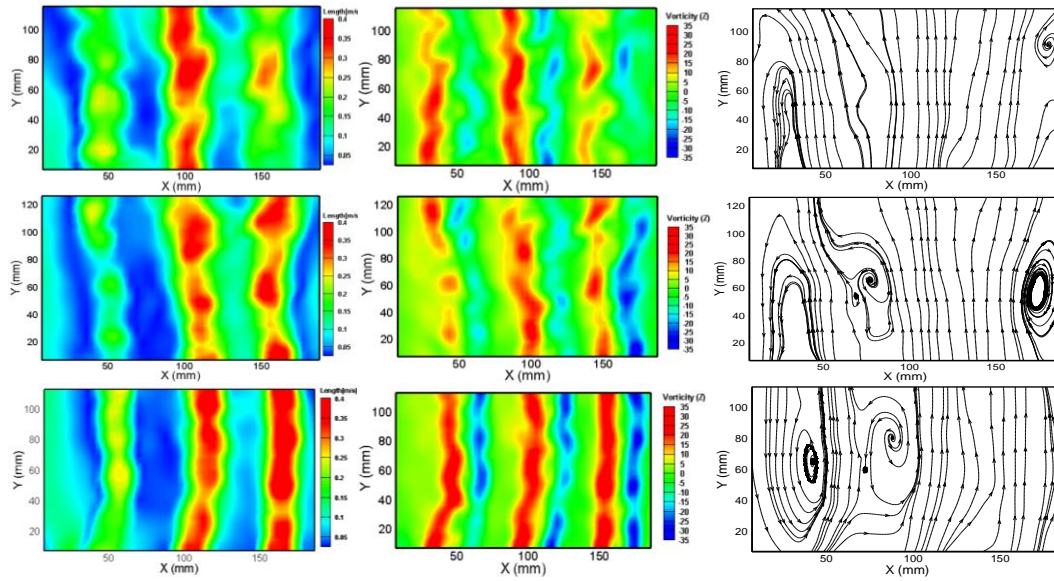


Figure 63 Time-averaged (a) resultant liquid velocity profiles, (b) vorticity profiles, (c) streamline profiles for flow 60 L/h for 0.5 mm nozzle diameter with 1.5 ml MIBC

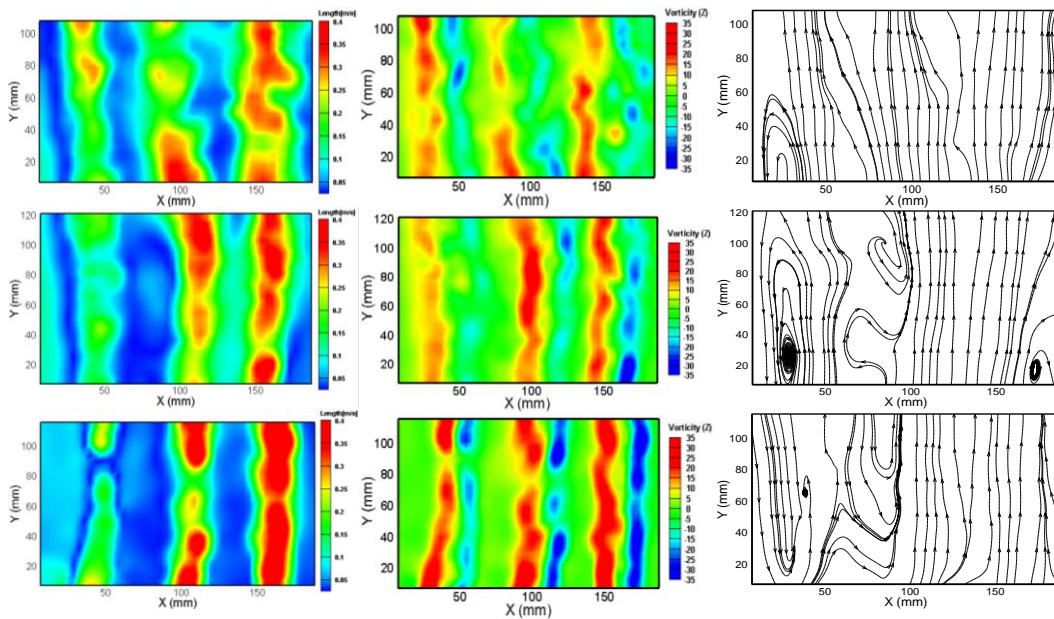


Figure 64 Time-averaged (a) resultant liquid velocity profiles, (b) vorticity profiles, (c) streamline profiles for flow 60 L/h for 0.5 mm nozzle diameter with 3 ml MIBC

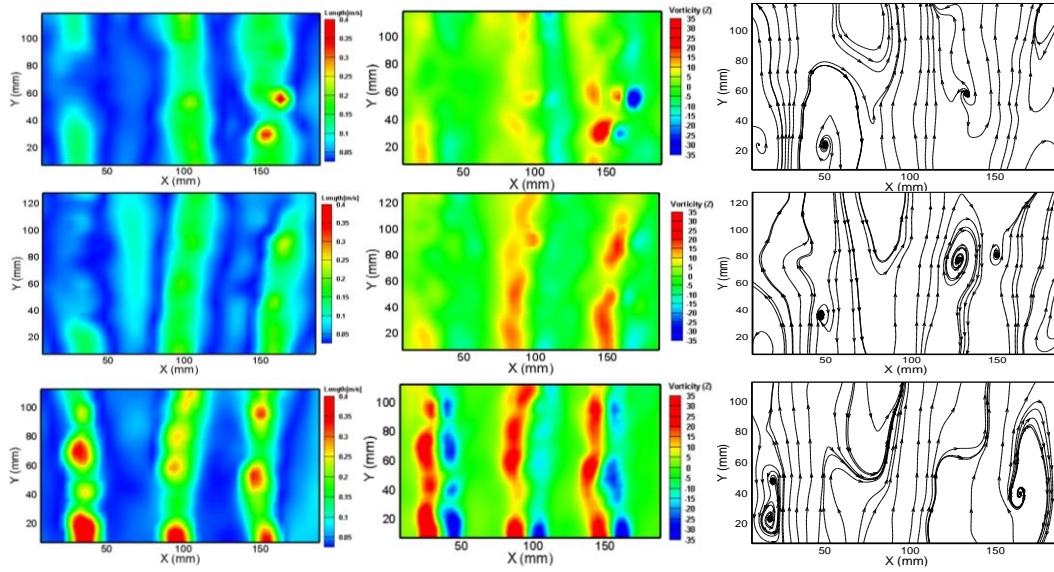


Figure 65 Time-averaged (a) resultant liquid velocity profiles, (b) vorticity profiles, (c) streamline profiles for flow 60 L/h for 0.7 mm nozzle diameter w/o MIBC

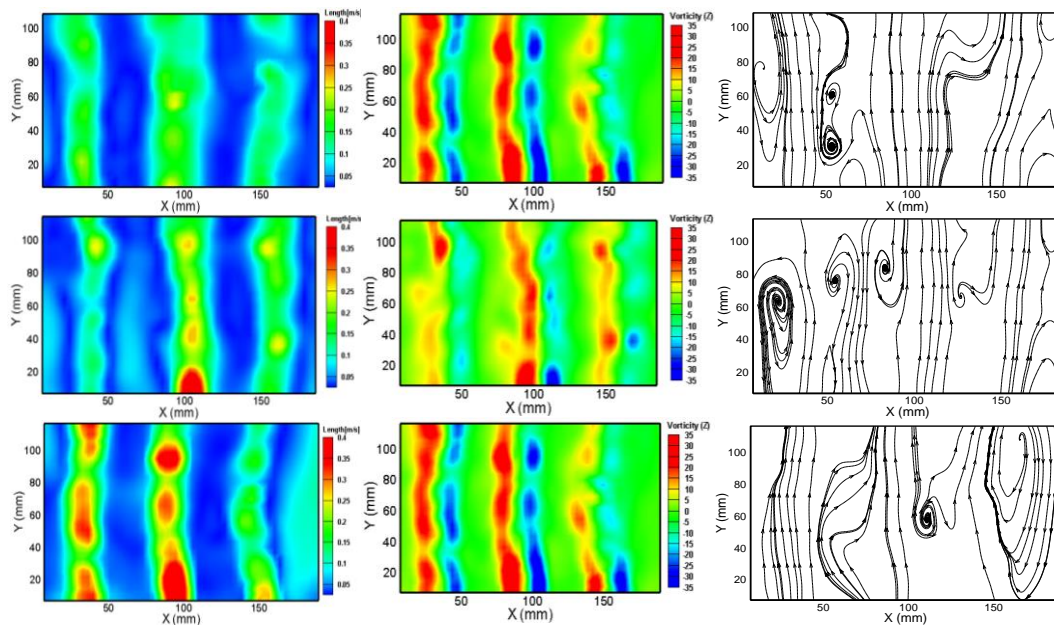


Figure 66 Time-averaged (a) resultant liquid velocity profiles, (b) vorticity profiles, (c) streamline profiles for flow 60 L/h for 0.7 mm nozzle diameter with 0.5 ml MIBC

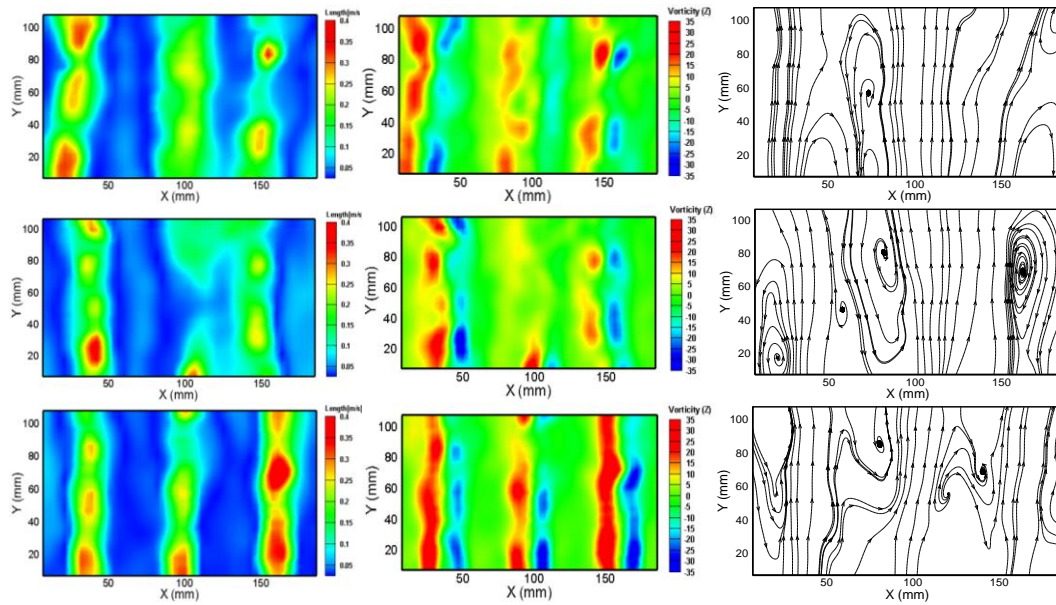


Figure 67 Time-averaged (a) resultant liquid velocity profiles, (b) vorticity profiles, (c) streamline profiles for flow 60 L/h for 0.7 mm nozzle diameter with 1.5 ml MIBC

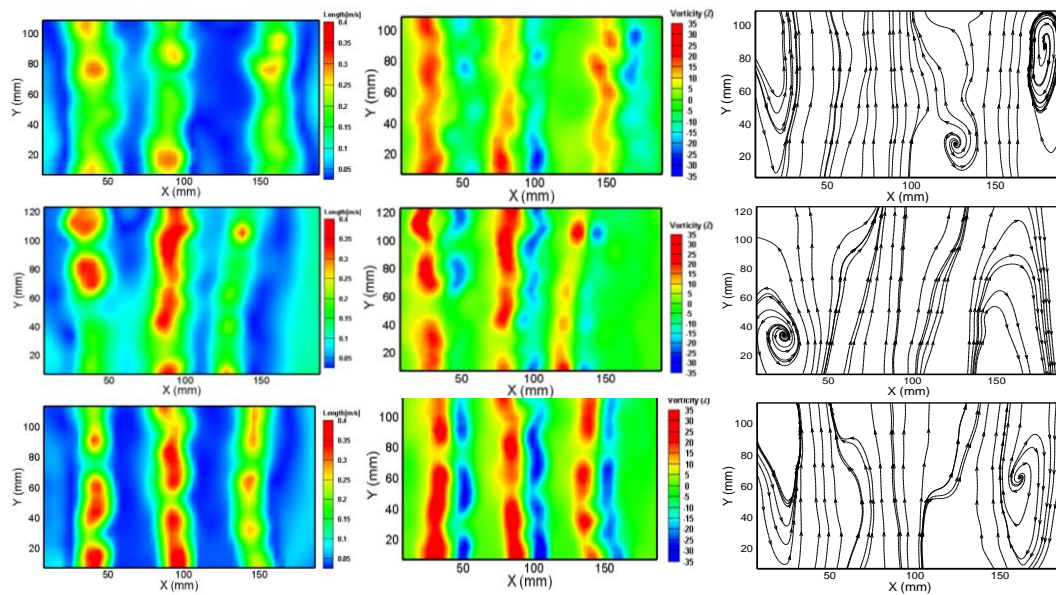


Figure 68 Time-averaged (a) resultant liquid velocity profiles, (b) vorticity profiles, (c) streamline profiles for flow 60 L/h for 0.7 mm nozzle diameter with 3 ml MIBC

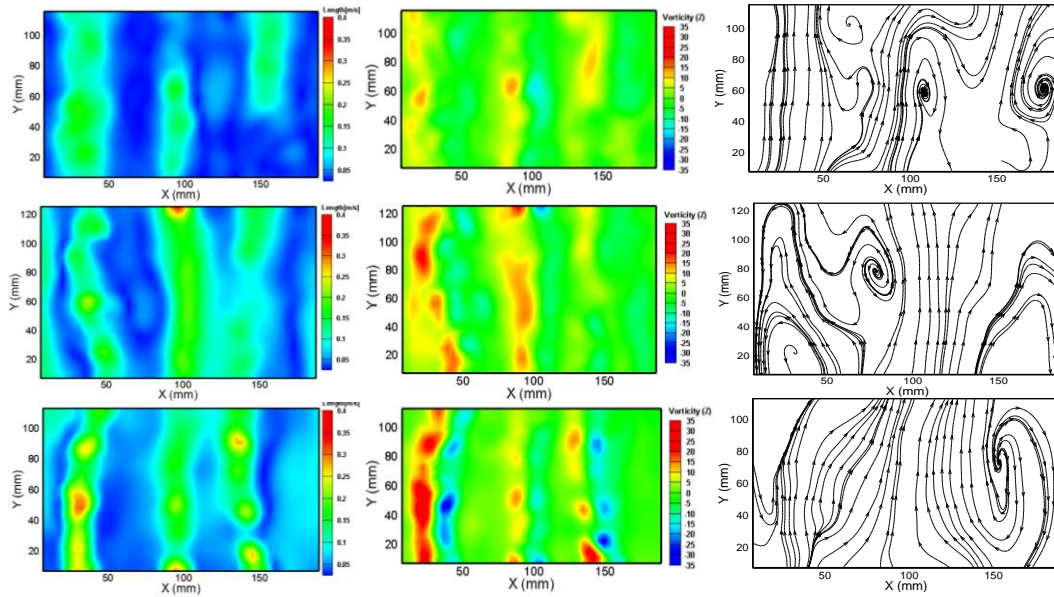


Figure 69 Time-averaged (a) resultant liquid velocity profiles, (b) vorticity profiles, (c) streamline profiles for flow 60 L/h for 0.9 mm nozzle diameter w/o MIBC

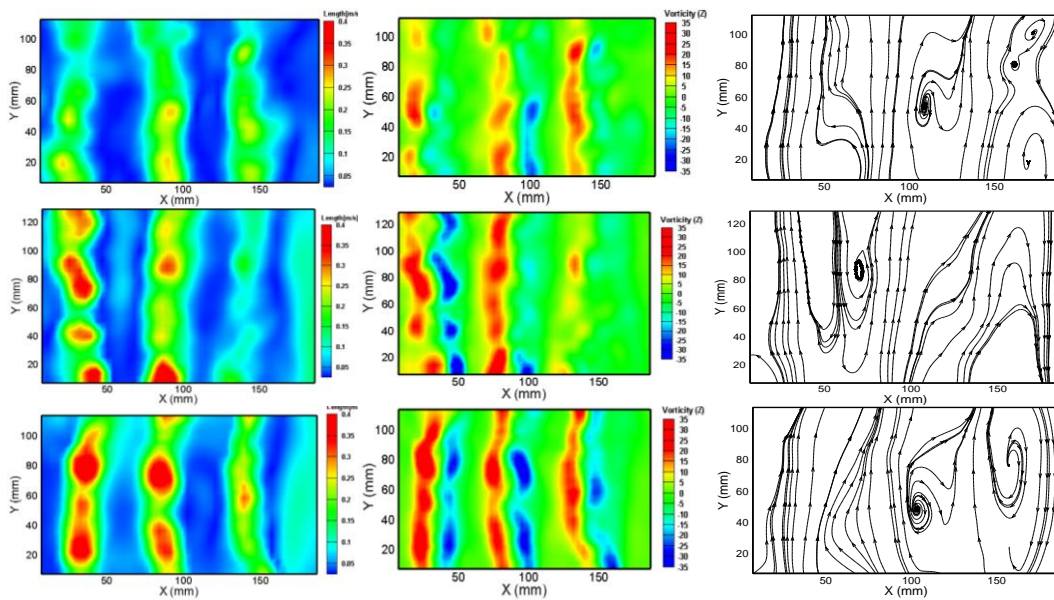


Figure 70 Time-averaged (a) resultant liquid velocity profiles, (b) vorticity profiles, (c) streamline profiles for flow 60 L/h for 0.9 mm nozzle diameter with 0.5 ml MIBC

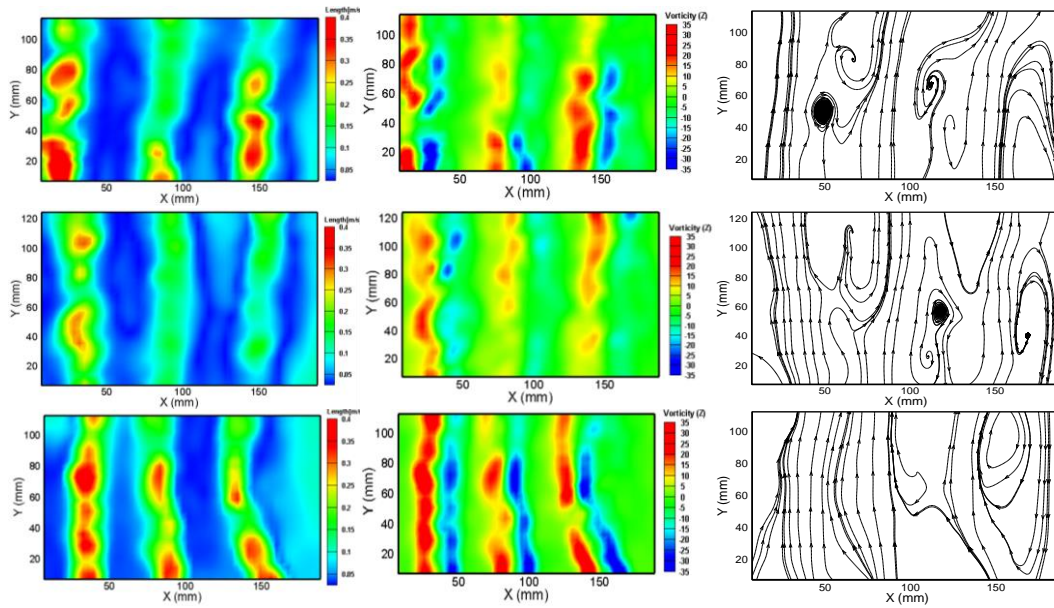


Figure 71 Time-averaged (a) resultant liquid velocity profiles, (b) vorticity profiles, (c) streamline profiles for flow 60 L/h for 0.9 mm nozzle diameter with 1.5 ml MIBC

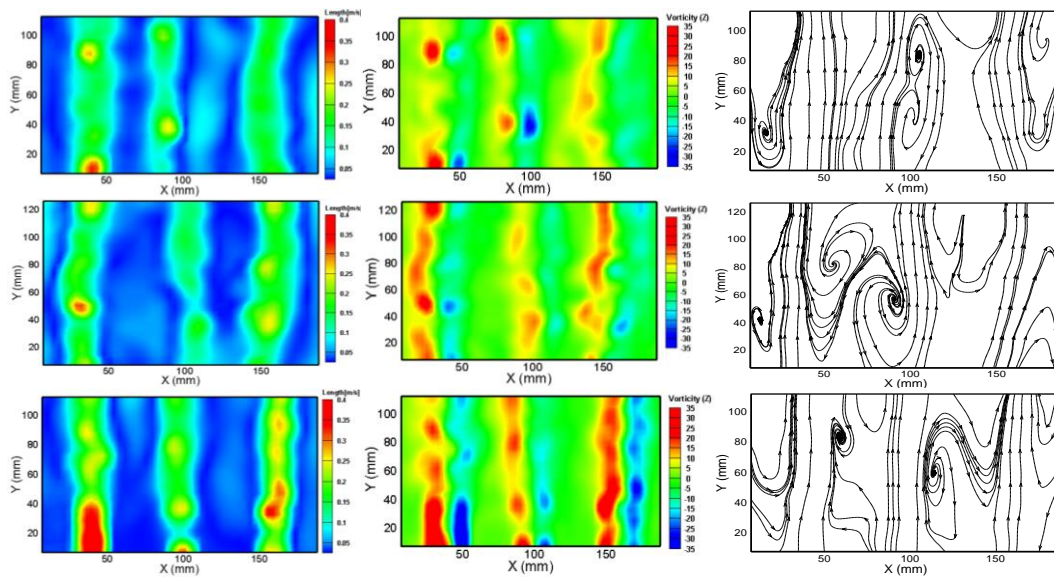


Figure 72 Time-averaged (a) resultant liquid velocity profiles, (b) vorticity profiles, (c) streamline profiles for flow 60 L/h for 0.9 mm nozzle diameter with 3 ml MIBC

Appendix C

BSD and gas holdup as bar diagrams for 3.5 mm needle source

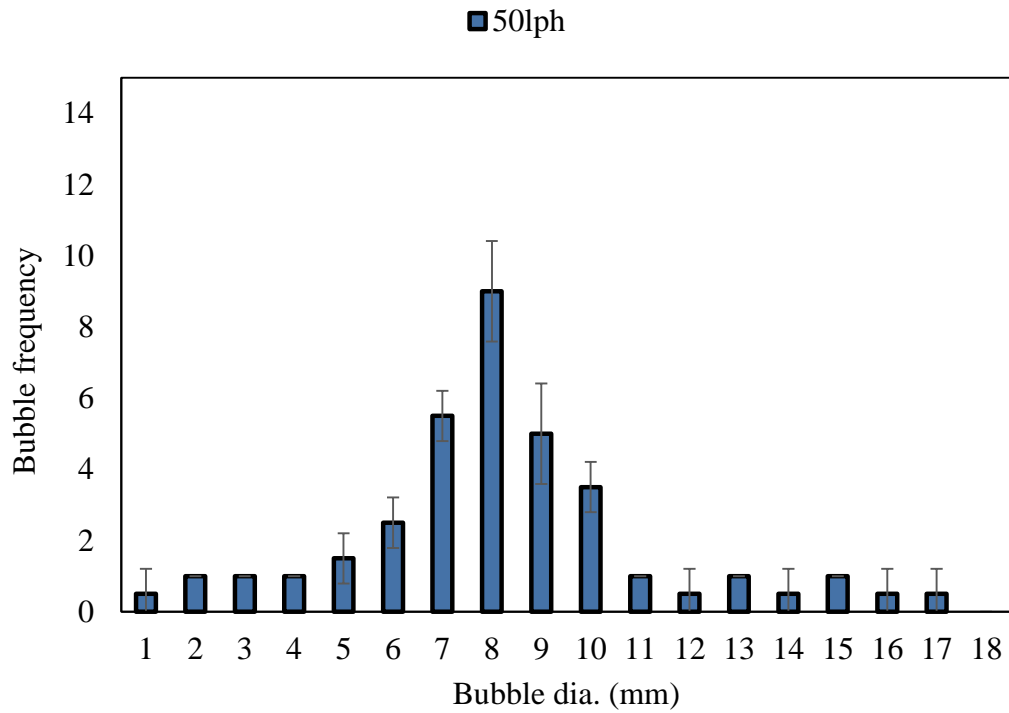


Figure 73 BSD as bar diagram for 50 L/h gas flow rate and 3.5 mm diameter needle

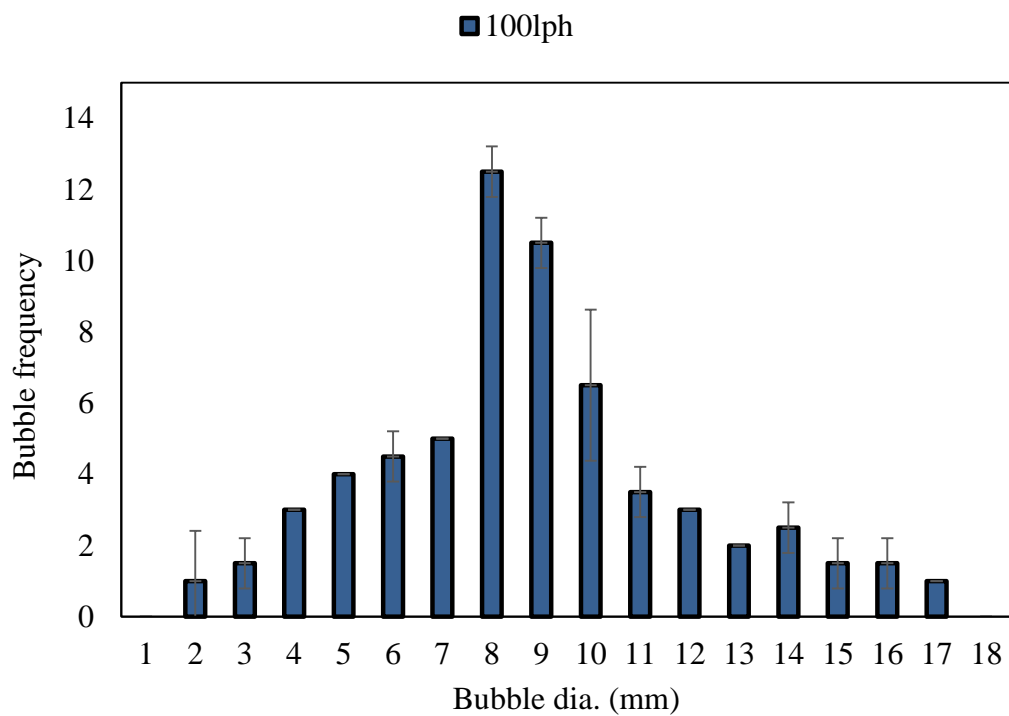


Figure 74 BSD as bar diagram for 100 L/h gas flow rate and 3.5 mm diameter needle

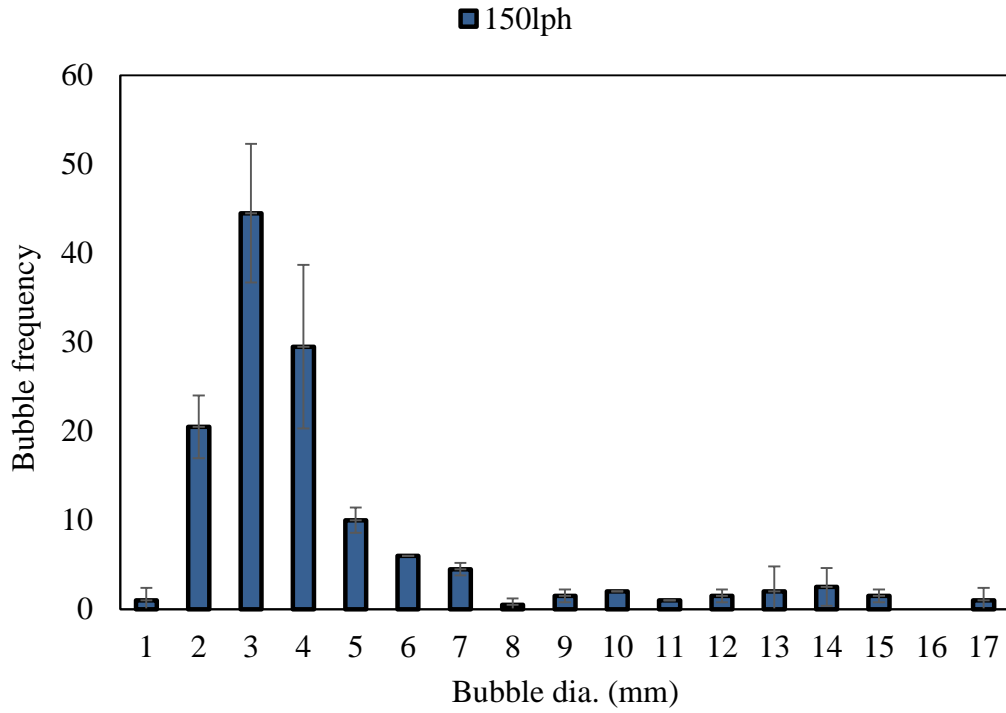


Figure 75 BSD as bar diagram for 150 L/h gas flow rate and 3.5 mm diameter needle

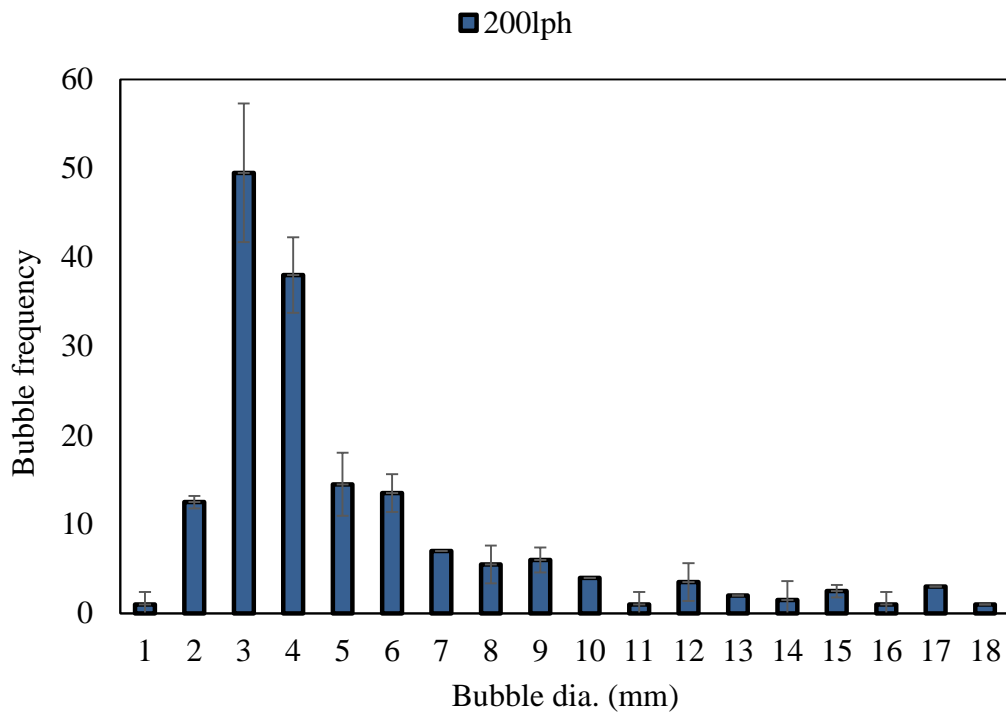


Figure 76 BSD as bar diagram for 200 L/h gas flow rate and 3.5 mm diameter needle

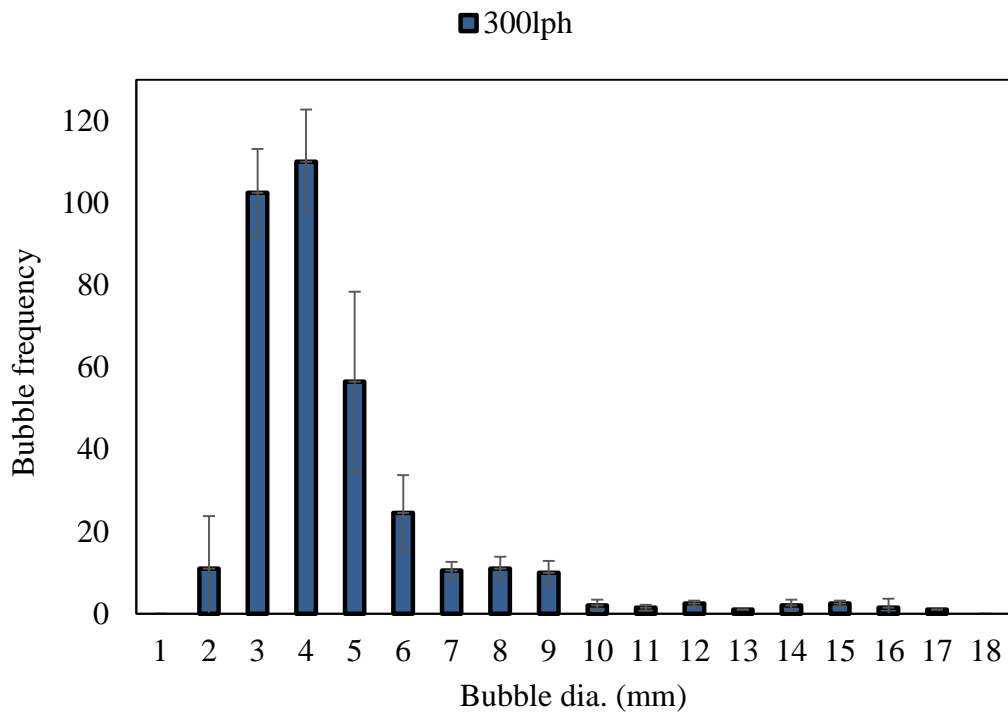


Figure 77 BSD as bar diagram for 300 L/h gas flow rate and 3.5 mm diameter needle

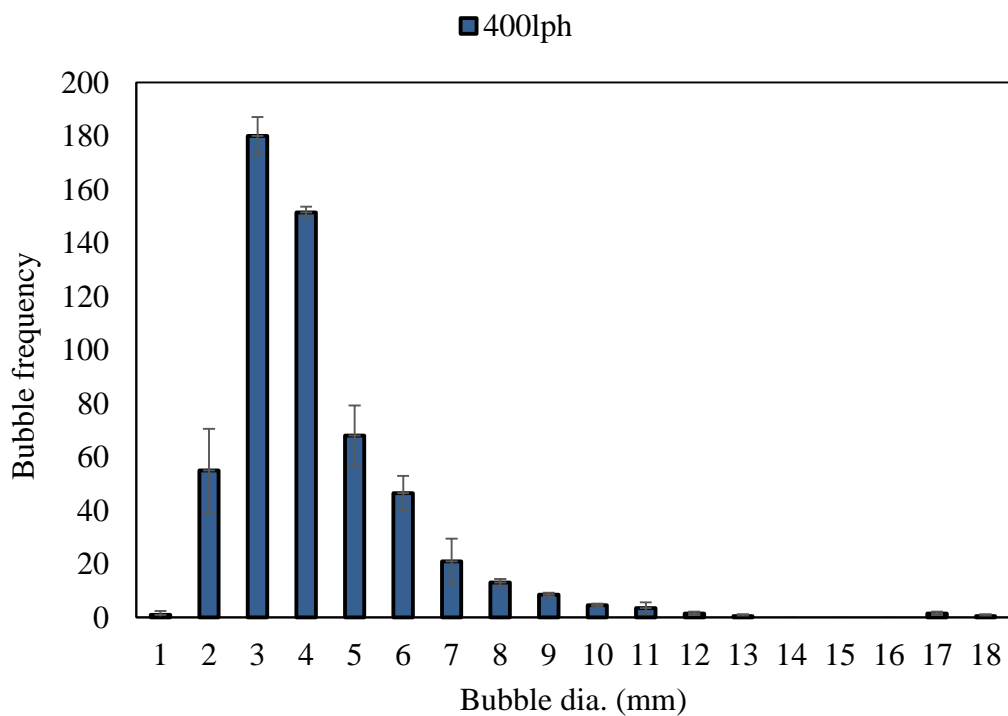


Figure 78 BSD as bar diagram for 400 L/h gas flow rate and 3.5 mm diameter needle

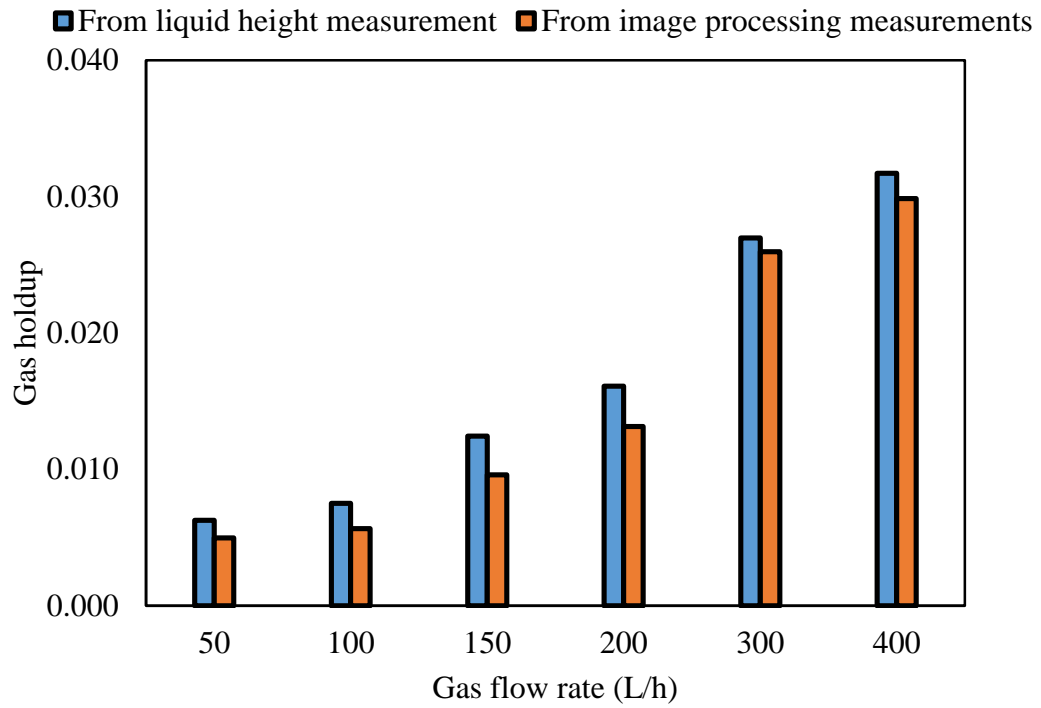


Figure 79 Gas holdup as bar diagram for 3.5 mm diameter needle

Appendix D

Bubble track plots for single nozzle source (0.5mm, 0.7mm, 0.9mm diameter)

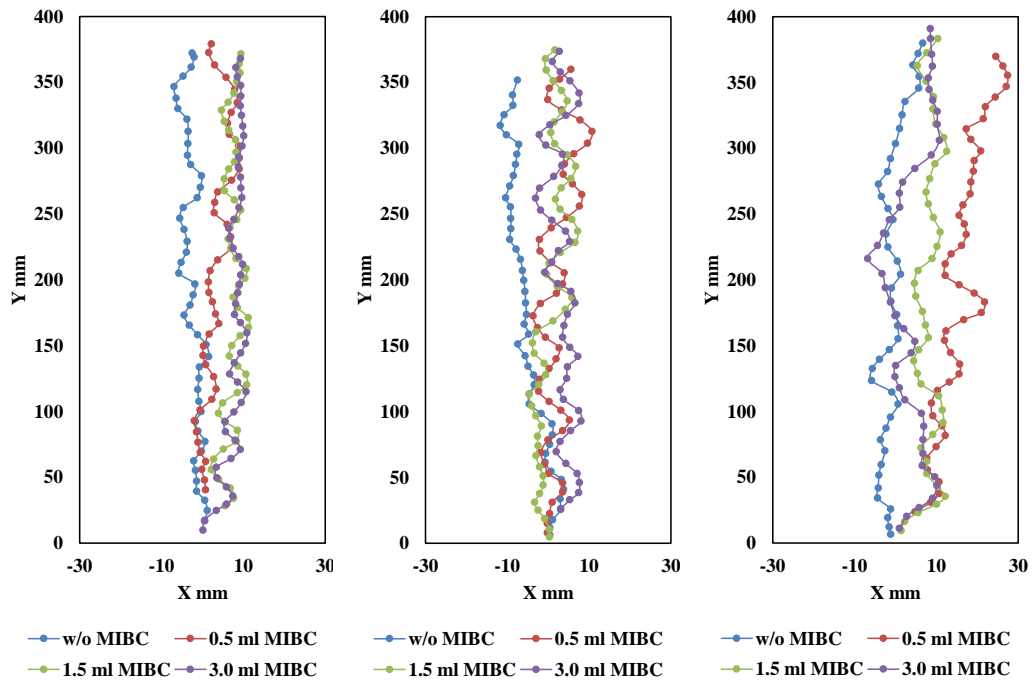


Figure 80 Bubble track plots of 10 L/h flow for (a) 0.5 mm dia., (b) 0.7 mm dia., and (c) 0.9 mm dia. nozzle

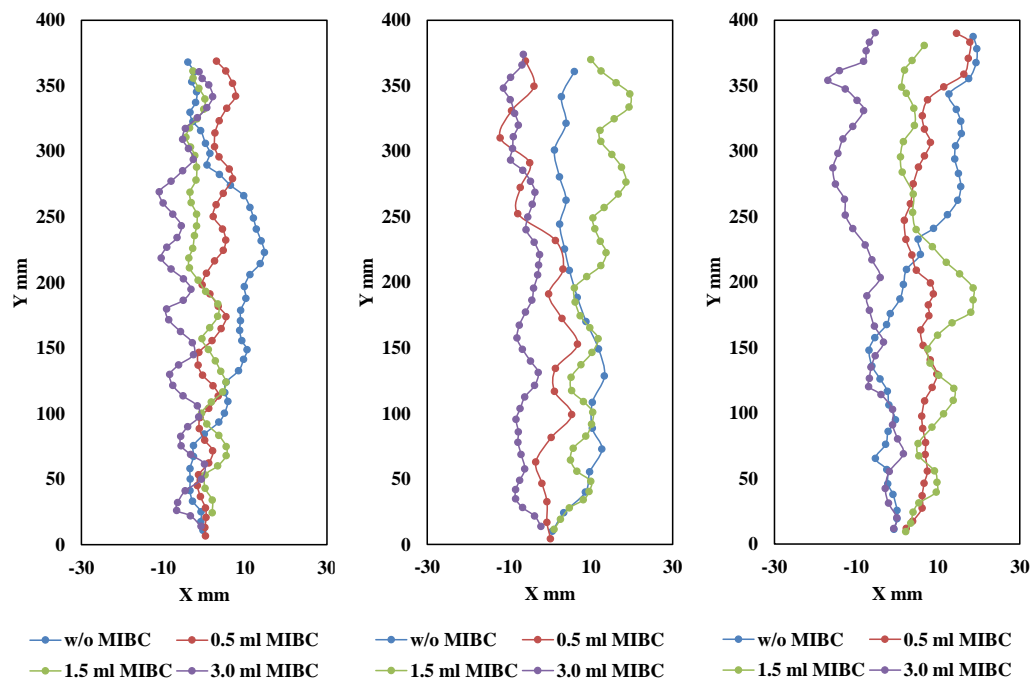


Figure 81 Bubble track plots of 20 L/h flow for (a) 0.5 mm dia., (b) 0.7 mm dia., and (c) 0.9 mm dia. nozzle

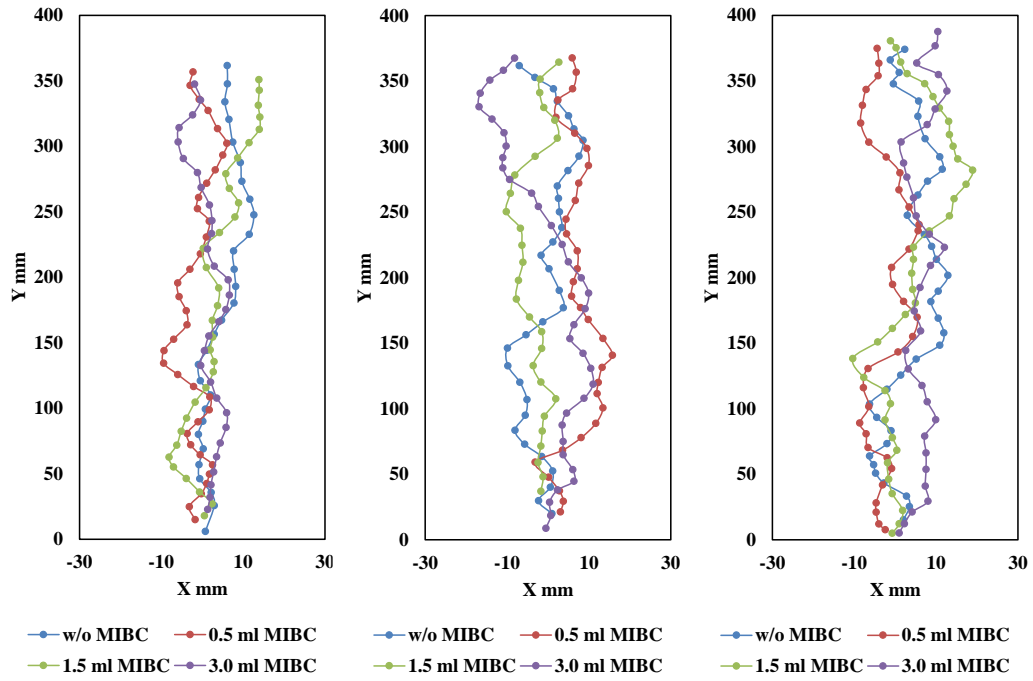


Figure 82 Bubble track plots of 30 L/h flow for (a) 0.5 mm dia., (b) 0.7 mm dia., and (c) 0.9 mm dia. nozzle

Appendix E

Tables for time-averaged liquid velocity plots at five positions above the needle for single needle source (3.5 mm diameter) bubble dynamic

Table 1 For 50 L/h gas flow and 20 mm above the needle

x [mm]	y [mm]	U[m/s]	V[m/s]	Length[m/s]
11.3296332	20.51650807	-0.007552573	0.00863169	0.011673103
14.84577655	20.50695968	-0.013708362	0.00898912	0.01642635
18.3619199	20.4974113	-0.016812893	0.009453255	0.019309492
21.87806325	20.48786292	-0.018914229	0.009868788	0.021357342
25.39420661	20.47831454	-0.021128701	0.010156797	0.023469554
28.91034996	20.46876616	-0.023827445	0.010394063	0.026016807
32.42649331	20.45921778	-0.026550856	0.010781935	0.028670822
35.94263667	20.4496694	-0.028720429	0.011104807	0.030802259
39.45878002	20.44012102	-0.029965656	0.011167195	0.031986877
42.97492337	20.43057264	-0.030539651	0.010819086	0.0324087
46.49106672	20.42102426	-0.031125145	0.010264215	0.032780409
50.00721008	20.41147588	-0.031620426	0.009901451	0.03314176
53.52335343	20.4019275	-0.032205258	0.00943345	0.03356394
57.03949678	20.39237912	-0.032250863	0.009136811	0.033525515
60.55564013	20.38283074	-0.032399081	0.008974965	0.033625039
64.07178349	20.37328236	-0.033148595	0.009156833	0.034395115
67.58792684	20.36373398	-0.033806817	0.009969158	0.035253161
71.10407019	20.35418559	-0.033896363	0.012060859	0.0360301
74.62021355	20.34463721	-0.034464814	0.01924431	0.039638187
78.1363569	20.33508883	-0.040892482	0.037732378	0.055939152
81.65250025	20.32554045	-0.054194871	0.077255919	0.094573461
85.1686436	20.31599207	-0.071074013	0.134310149	0.152085212
88.68478696	20.30644369	-0.07950514	0.183039097	0.199618048
92.20093031	20.29689531	-0.079381217	0.204338465	0.219268432
95.71707366	20.28734693	-0.069456982	0.188486773	0.200929322
99.23321701	20.27779855	-0.057105207	0.145200741	0.156191035
102.7493604	20.26825017	-0.047832418	0.074463405	0.090243111
106.2655037	20.25870179	-0.050574883	0.013125568	0.055330257
109.7816471	20.24915341	-0.058368569	-0.024394554	0.06327398
113.2977904	20.23960503	-0.064647113	-0.029333757	0.070992094
116.8139338	20.23005665	-0.063424455	-0.028992778	0.069737694
120.3300771	20.22050827	-0.061635787	-0.028526535	0.067917625
123.8462205	20.21095988	-0.05911362	-0.028074331	0.065443353
127.3623638	20.2014115	-0.056095502	-0.028151509	0.062767603
130.8785072	20.19186312	-0.052807957	-0.028671247	0.060095297
134.3946505	20.18231474	-0.0496207	-0.029338259	0.057651564
137.9107939	20.17276636	-0.046200655	-0.029668735	0.054910778
141.4269372	20.16321798	-0.042669448	-0.029378214	0.051809492
144.9430806	20.1536696	-0.038959338	-0.028897699	0.048510881

148.459224	20.14412122	-0.035414047	-0.028341248	0.045363789
151.9753673	20.13457284	-0.031943334	-0.027681061	0.042270655
155.4915107	20.12502446	-0.028685547	-0.026123265	0.038798724
159.007654	20.11547608	-0.025402278	-0.023768409	0.034788398
162.5237974	20.1059277	-0.022133303	-0.020881945	0.030429486
166.0399407	20.09637932	-0.01929283	-0.017813733	0.026261372
169.5560841	20.08683094	-0.017137914	-0.014540535	0.022484237
173.0722274	20.07728256	-0.015431701	-0.011085112	0.019015569
176.5883708	20.06773417	-0.013768975	-0.007739119	0.015818357
180.1045141	20.05818579	-0.011678075	-0.004208636	0.012472636
183.6206575	20.04863741	-0.009837715	-0.000762184	0.009897587

Table 2 For 50 L/h gas flow and 50 mm above the needle

x [mm]	y [mm]	U[m/s]	V[m/s]	Length[m/s]
10.86586193	50.69416514	-0.005718772	0.022020179	0.022773314
14.41039945	50.69416514	-0.009049066	0.022303108	0.024081879
17.95493696	50.69416514	-0.011602327	0.023299254	0.026036217
21.49947447	50.69416514	-0.013604704	0.024622692	0.028137921
25.04401198	50.69416514	-0.015571005	0.025871101	0.030200426
28.58854949	50.69416514	-0.016745684	0.02601404	0.030942429
32.133087	50.69416514	-0.017321829	0.02540534	0.03075543
35.67762452	50.69416514	-0.017779417	0.024500522	0.030281132
39.22216203	50.69416514	-0.01808398	0.023605927	0.029750374
42.76669954	50.69416514	-0.018789979	0.023305106	0.0299549
46.31123705	50.69416514	-0.019598237	0.023334756	0.030494095
49.85577456	50.69416514	-0.020729258	0.024465428	0.03208973
53.40031207	50.69416514	-0.021464695	0.026709516	0.034301899
56.94484959	50.69416514	-0.021166978	0.030170366	0.036916968
60.4893871	50.69416514	-0.020458744	0.035375988	0.040940354
64.03392461	50.69416514	-0.020273255	0.044728883	0.049256335
67.57846212	50.69416514	-0.019309731	0.063485807	0.066430512
71.12299963	50.69416514	-0.022706528	0.097747288	0.100371145
74.66753714	50.69416514	-0.030523094	0.144356927	0.147558536
78.21207466	50.69416514	-0.041701905	0.187985723	0.192577256
81.75661217	50.69416514	-0.049757951	0.205929865	0.211904633
85.30114968	50.69416514	-0.053997589	0.183843887	0.191794849
88.84568719	50.69416514	-0.057324191	0.131298781	0.143865966
92.3902247	50.69416514	-0.059963517	0.074985589	0.0971785
95.93476221	50.69416514	-0.061813321	0.03411804	0.071665729
99.47929973	50.69416514	-0.06392262	0.00947602	0.06510686
103.0238372	50.69416514	-0.066644493	-0.005619941	0.067043328
106.5683747	50.69416514	-0.069827307	-0.014451449	0.071321781
110.1129123	50.69416514	-0.071989855	-0.017806094	0.074163738
113.6574498	50.69416514	-0.073304018	-0.020069211	0.076008066

117.2019873	50.69416514	-0.073896209	-0.022759983	0.077334472
120.7465248	50.69416514	-0.073659169	-0.025954038	0.078113527
124.2910623	50.69416514	-0.072573603	-0.029028623	0.078178487
127.8355998	50.69416514	-0.070844221	-0.031549229	0.077563813
131.3801373	50.69416514	-0.0686591	-0.033507181	0.076411761
134.9246748	50.69416514	-0.066503173	-0.035458154	0.075379827
138.4692124	50.69416514	-0.064143815	-0.037300306	0.074213226
142.0137499	50.69416514	-0.061647136	-0.038831968	0.072868971
145.5582874	50.69416514	-0.05886371	-0.040160412	0.071272934
149.1028249	50.69416514	-0.055511569	-0.041452307	0.069300222
152.6473624	50.69416514	-0.051570041	-0.042636848	0.066938569
156.1918999	50.69416514	-0.047107217	-0.043263577	0.06397966
159.7364374	50.69416514	-0.042769595	-0.043040633	0.060691385
163.2809749	50.69416514	-0.038624297	-0.042321715	0.05731477
166.8255124	50.69416514	-0.034452088	-0.041158445	0.053691251
170.37005	50.69416514	-0.030371982	-0.039114095	0.049538176
173.9145875	50.69416514	-0.026391275	-0.036116867	0.04474555
177.459125	50.69416514	-0.022584116	-0.032350148	0.039465284
181.0036625	50.69416514	-0.018733894	-0.027797801	0.033528554
184.5482	50.69416514	-0.015650954	-0.023655303	0.028368804

Table 3 For 50 L/h gas flow and 100 mm above the needle

x [mm]	y [mm]	U[m/s]	V[m/s]	Length[m/s]
12.10165285	25.32530002	0.018601058	-0.005718617	0.019580703
15.57462422	25.33219745	0.020282522	-0.009433004	0.022569747
19.04759559	25.33909487	0.023111541	-0.014904076	0.02756807
22.52056696	25.3459923	0.028147088	-0.020808358	0.035053414
25.99353833	25.35288972	0.034067798	-0.026871529	0.043422162
29.46650971	25.35978715	0.040516604	-0.033197875	0.052396621
32.93948108	25.36668457	0.046680413	-0.039004217	0.060841968
36.41245245	25.373582	0.051939343	-0.044012948	0.068086674
39.88542382	25.38047942	0.056052782	-0.048031825	0.073820256
43.35839519	25.38737685	0.057506438	-0.049379734	0.075800702
46.83136657	25.39427427	0.05815021	-0.049689991	0.076491593
50.30433794	25.4011717	0.058285175	-0.049249451	0.076310575
53.77730931	25.40806912	0.057956269	-0.047785767	0.075122303
57.25028068	25.41496655	0.057840709	-0.045241313	0.07345378
60.72325206	25.42186397	0.057197948	-0.040773074	0.07030432
64.19622343	25.4287614	0.056056667	-0.034016586	0.065705841
67.6691948	25.43565882	0.055254092	-0.019362999	0.059149031
71.14216617	25.44255625	0.055036262	0.002333925	0.057967291
74.61513754	25.44945367	0.055597911	0.03241916	0.066475125
78.08810892	25.4563511	0.058446246	0.079012004	0.099867593
81.56108029	25.46324852	0.059885392	0.131689924	0.145704748

85.03405166	25.47014595	0.060189293	0.182598369	0.192511632
88.50702303	25.47704337	0.058843658	0.22868198	0.236172171
91.97999441	25.4839408	0.053459489	0.246269497	0.252129048
95.45296578	25.49083822	0.046015479	0.243732491	0.248083651
98.92593715	25.49773565	0.036911879	0.222359004	0.225416078
102.3989085	25.50463307	0.027813329	0.184600457	0.186709365
105.8718799	25.5115305	0.017926495	0.142750195	0.14391579
109.3448513	25.51842792	0.008805694	0.103646057	0.104070477
112.8178226	25.52532535	0.001426281	0.073429287	0.073491019
116.290794	25.53222277	-0.004384063	0.052673289	0.053135862
119.7637654	25.5391202	-0.008603967	0.036535179	0.037812813
123.2367368	25.54601762	-0.011274435	0.02423861	0.026910974
126.7097081	25.55291505	-0.012254199	0.014735387	0.019862979
130.1826795	25.55981247	-0.012783817	0.006765293	0.015230013
133.6556509	25.5667099	-0.013119594	0.000292608	0.013403361
137.1286222	25.57360732	-0.013831034	-0.004841742	0.014915033
140.6015936	25.58050475	-0.014300544	-0.009287099	0.017231863
144.074565	25.58740217	-0.01510185	-0.013633101	0.020397267
147.5475364	25.5942996	-0.016588209	-0.018184576	0.024614468
151.0205077	25.60119702	-0.01799907	-0.023017967	0.029248424
154.4934791	25.60809445	-0.019446483	-0.028002253	0.034119349
157.9664505	25.61499187	-0.020940982	-0.033193024	0.039276886
161.4394219	25.6218893	-0.021862498	-0.038813169	0.044567405
164.9123932	25.62878672	-0.022047971	-0.045015092	0.050180369
168.3853646	25.63568415	-0.021887842	-0.050990103	0.055534087
171.858336	25.64258157	-0.021459704	-0.056027295	0.060014113
175.3313073	25.649479	-0.020430422	-0.058626152	0.062106577
178.8042787	25.65637642	-0.018930072	-0.059116894	0.062097966
182.2772501	25.66327385	-0.017002363	-0.057569217	0.060040488

Table 4 For 50 L/h gas flow and 200 mm above the needle

x [mm]	y[mm]	U[m/s]	V[m/s]	Length[m/s]
10.21081288	115.9022856	0.032019565	-0.192962028	0.195615618
13.78025567	115.8953882	0.033810403	-0.189128348	0.192143095
17.34969847	115.8884908	0.036400448	-0.182099098	0.185737936
20.91914127	115.8815933	0.038039577	-0.173319519	0.17746562
24.48858407	115.8746959	0.037515314	-0.163287063	0.167560347
28.05802687	115.8677985	0.036209257	-0.150220123	0.154548627
31.62746967	115.8609011	0.034762012	-0.135459775	0.139891208
35.19691247	115.8540036	0.033481839	-0.119273208	0.123943782
38.76635527	115.8471062	0.033225434	-0.102167024	0.107489424
42.33579807	115.8402088	0.032445615	-0.086480983	0.092447019

45.90524087	115.8333114	0.031570213	-0.071900747	0.078633853
49.47468367	115.8264139	0.030733347	-0.058069272	0.065771741
53.04412647	115.8195165	0.029880891	-0.04346863	0.052898015
56.61356927	115.8126191	0.029567402	-0.027906054	0.041446081
60.18301206	115.8057217	0.029301665	-0.011785244	0.032989507
63.75245486	115.7988242	0.02870717	0.004677451	0.029418193
67.32189766	115.7919268	0.027524333	0.02144703	0.036336573
70.89134046	115.7850294	0.026363599	0.038692233	0.04742956
74.46078326	115.778132	0.0254646	0.056991476	0.06258238
78.03022606	115.7712345	0.025445507	0.078435273	0.082582393
81.59966886	115.7643371	0.025275005	0.103085338	0.106269749
85.16911166	115.7574397	0.024315924	0.129408996	0.131763733
88.73855446	115.7505423	0.022316273	0.156853332	0.158464452
92.30799726	115.7436448	0.018491639	0.182444365	0.183439986
95.87744006	115.7367474	0.014383488	0.202333376	0.202893919
99.44688286	115.72985	0.010100196	0.216352558	0.21661741
103.0163257	115.7229526	0.005705662	0.223019804	0.223110927
106.5857685	115.7160551	0.00165218	0.218532736	0.21856534
110.1552113	115.7091577	-0.001458578	0.2083927	0.208410974
113.7246541	115.7022603	-0.003459649	0.193412301	0.193448417
117.2940969	115.6953629	-0.003938513	0.173966817	0.174014064
120.8635397	115.6884654	-0.003710655	0.152146243	0.152192475
124.4329825	115.681568	-0.003624107	0.129954343	0.13000684
128.0024252	115.6746706	-0.003966297	0.108083404	0.108156573
131.571868	115.6677732	-0.004231257	0.088804994	0.088908273
135.1413108	115.6608757	-0.003829633	0.071813054	0.071916259
138.7107536	115.6539783	-0.002758143	0.056484747	0.056560121
142.2801964	115.6470809	-0.000916265	0.042362011	0.042382697
145.8496392	115.6401835	0.001365952	0.026565146	0.026695125
149.419082	115.633286	0.003611726	0.010014761	0.014594029
152.9885248	115.6263886	0.005587226	-0.006761949	0.009161844
156.5579676	115.6194912	0.006369848	-0.021769812	0.022917803
160.1274104	115.6125938	0.005456873	-0.033753116	0.034282125
163.6968532	115.6056963	0.003325278	-0.043508647	0.043704062
167.266296	115.5987989	7.51E-05	-0.051188573	0.051195006
170.8357388	115.5919015	-0.003906919	-0.056820552	0.057001823
174.4051816	115.5850041	-0.00706842	-0.06157758	0.062000337
177.9746244	115.5781066	-0.009209168	-0.065409695	0.066055336
181.5440672	115.5712092	-0.009724472	-0.068014598	0.068708135
185.11351	115.5643118	-0.009575777	-0.06942437	0.070084754

Table 5 For 50 L/h gas flow and 300 mm above the needle

x [mm]	y [mm]	U[m/s]	V[m/s]	Length[m/s]
10.52595287	216.2805122	0.003169278	-0.09050782	0.090573682

14.10825853	216.2736148	0.000760112	-0.083878035	0.08388828
17.69056418	216.2667173	-0.004290577	-0.072645552	0.072890587
21.27286984	216.2598199	-0.009837967	-0.06229151	0.063238028
24.8551755	216.2529225	-0.01537678	-0.054007527	0.056242834
28.43748115	216.2460251	-0.021210298	-0.04614145	0.050983291
32.01978681	216.2391276	-0.027255441	-0.037829686	0.047124636
35.60209246	216.2322302	-0.033002198	-0.028491685	0.044153571
39.18439812	216.2253328	-0.038100165	-0.017602022	0.042060147
42.76670378	216.2184354	-0.04120984	-0.007121017	0.042410421
46.34900943	216.2115379	-0.042061986	0.003378662	0.042812013
49.93131509	216.2046405	-0.041103042	0.014212653	0.043874478
53.51362074	216.1977431	-0.0388796	0.025991824	0.047085521
57.0959264	216.1908457	-0.03717132	0.041661482	0.056476016
60.67823206	216.1839482	-0.036729447	0.06113821	0.07165875
64.26053771	216.1770508	-0.037722202	0.084936853	0.092989584
67.84284337	216.1701534	-0.039405373	0.116876678	0.123469229
71.42514903	216.1632559	-0.040736334	0.147508181	0.153119504
75.00745468	216.1563585	-0.041395245	0.175601267	0.180456893
78.58976034	216.1494611	-0.041037419	0.199822565	0.20401791
82.17206599	216.1425637	-0.038763962	0.205717827	0.20937118
85.75437165	216.1356662	-0.034294668	0.202531634	0.205446546
89.33667731	216.1287688	-0.027940588	0.191762843	0.193809967
92.91898296	216.1218714	-0.020302837	0.174127735	0.175334091
96.50128862	216.114974	-0.011836287	0.153246386	0.153768426
100.0835943	216.1080765	-0.004493396	0.132198826	0.132325351
103.6658999	216.1011791	0.001224963	0.111176436	0.111192109
107.2482056	216.0942817	0.004155944	0.087897729	0.088019837
110.8305112	216.0873843	0.004268081	0.066914493	0.067050909
114.4128169	216.0804868	0.00239081	0.048653656	0.048750873
117.9951226	216.0735894	-0.001190061	0.034033085	0.034059235
121.5774282	216.066692	-0.005027994	0.026010784	0.026692341
125.1597339	216.0597946	-0.009137287	0.021055557	0.023239032
128.7420395	216.0528971	-0.013298964	0.018892139	0.023148655
132.3243452	216.0459997	-0.016791499	0.019071805	0.025451267
135.9066508	216.0391023	-0.018341171	0.019554026	0.026812572
139.4889565	216.0322049	-0.018242666	0.02010918	0.027169922
143.0712621	216.0253074	-0.016511317	0.02036404	0.026236514
146.6535678	216.01841	-0.013422481	0.01868264	0.02302155
150.2358735	216.0115126	-0.010632677	0.016069846	0.019296456
153.8181791	216.0046152	-0.007990507	0.01239875	0.014826403
157.4004848	215.9977177	-0.005614081	0.007620798	0.009590927
160.9827904	215.9908203	-0.004290578	0.001618745	0.005780348
164.5650961	215.9839229	-0.00333544	-0.005534281	0.007756646
168.1474017	215.9770255	-0.002791122	-0.013947523	0.014387323

171.7297074	215.970128	-0.002437011	-0.02400369	0.024206849
175.3120131	215.9632306	-0.001460967	-0.033740134	0.033818731
178.8943187	215.9563332	-0.00025751	-0.043204195	0.043226319
182.4766244	215.9494358	0.001122499	-0.051700931	0.051716111
186.05893	215.9425383	0.002305601	-0.055470489	0.05552058

Table 6 For 200 L/h gas flow and 20 mm above the needle

x [mm]	y[mm]	U[m/s]	V[m/s]	Length[m/s]
12.2787987	19.62079628	0.002489247	0.007036471	0.007538568
15.81714242	19.62650771	0.001202613	0.006072904	0.006200902
19.35548614	19.63221914	0.001865677	0.004737122	0.005186084
22.89382986	19.63793056	0.003209961	0.002804939	0.004460192
26.43217358	19.64364199	0.004289615	-0.00030416	0.004688479
29.9705173	19.64935341	0.004989727	-0.004631254	0.007045488
33.50886102	19.65506484	0.005380381	-0.009215929	0.010794688
37.04720473	19.66077627	0.006719863	-0.012996127	0.01475799
40.58554845	19.66648769	0.009893423	-0.015966032	0.018944235
44.12389217	19.67219912	0.014812432	-0.019583801	0.024671358
47.66223589	19.67791055	0.020662862	-0.024501624	0.032110409
51.20057961	19.68362197	0.025322936	-0.030843227	0.039936699
54.73892333	19.68933334	0.02815642	-0.037807902	0.047159832
58.27726705	19.69504483	0.03014684	-0.044284256	0.053581588
61.81561077	19.70075625	0.032428083	-0.048884693	0.058662803
65.35395449	19.70646768	0.035251318	-0.049890265	0.061105955
68.89229821	19.71217911	0.037785367	-0.048347202	0.061387054
72.43064193	19.71789053	0.0395174	-0.045266279	0.06013134
75.96898565	19.72360196	0.040828057	-0.042774169	0.059160573
79.50732937	19.72931338	0.042491762	-0.039569671	0.058121678
83.04567309	19.73502481	0.041006558	-0.02538086	0.048856356
86.58401681	19.74073624	0.031919538	0.051736275	0.077234078
90.12236053	19.74644766	0.0216777	0.169576255	0.171485973
93.66070425	19.75215909	0.020261413	0.274585773	0.275338303
97.19904797	19.75787052	0.030023461	0.311730224	0.313240592
100.7373917	19.76358194	0.045300344	0.287396437	0.291136138
104.2757354	19.76929337	0.055906171	0.227045574	0.234104596
107.8140791	19.7750048	0.055343934	0.140421076	0.15153693
111.3524228	19.78071622	0.042859247	0.062447855	0.076632044
114.8907666	19.78642765	0.02980837	0.01735907	0.035783837
118.4291103	19.79213908	0.025543047	0.000632696	0.025945777
121.967454	19.7978505	0.027403851	-0.003713796	0.027672221
125.5057977	19.80356193	0.028119853	-0.003421057	0.028334199
129.0441414	19.80927335	0.026475351	-0.002055675	0.026562576
132.5824852	19.81498478	0.023875918	-0.000351938	0.02390112
136.1208289	19.82069621	0.021295488	0.001624669	0.021395187
139.6591726	19.82640763	0.019669229	0.003393339	0.019990963
143.1975163	19.83211906	0.01874778	0.004406177	0.019270087

146.73586	19.83783049	0.018305902	0.004622378	0.01888397
150.2742038	19.84354191	0.017346312	0.004393032	0.017896876
153.8125475	19.84925334	0.015832153	0.00367939	0.016258654
157.3508912	19.85496477	0.014069765	0.003053689	0.014404156
160.8892349	19.86067619	0.012752094	0.002717155	0.013049501
164.4275786	19.86638762	0.012130779	0.002454466	0.012390838
167.9659224	19.87209905	0.01180905	0.002188518	0.012026453
171.5042661	19.87781047	0.011665517	0.002130358	0.011875573
175.0426098	19.8835219	0.010919886	0.002824348	0.011313504
178.5809535	19.88923333	0.009656083	0.00450672	0.010737007
182.1192972	19.89494475	0.007786779	0.007011766	0.010646468
185.657641	19.90065618	0.006596934	0.008849851	0.011142904

Table 7 For 200 L/h gas flow and 50 mm above the needle

x [mm]	y [mm]	U[m/s]	V[m/s]	Length[m/s]
10.71682715	50.40538479	0.016421582	-0.000971158	0.016614316
14.27642218	50.41109621	0.020901508	-0.006550951	0.022030808
17.83601721	50.41680764	0.026025323	-0.014383488	0.029803684
21.39561225	50.42251907	0.031950335	-0.023382703	0.039615602
24.95520728	50.42823049	0.038075847	-0.031353871	0.049332281
28.51480231	50.43394192	0.045169734	-0.038512565	0.059363852
32.07439735	50.43965335	0.051108082	-0.044116974	0.067517347
35.63399238	50.44536477	0.056725267	-0.04850353	0.07463519
39.19358741	50.4510762	0.06008224	-0.05230938	0.079664189
42.75318244	50.45678762	0.062633062	-0.055892044	0.083950839
46.31277748	50.46249905	0.064605706	-0.059817102	0.088054057
49.87237251	50.46821048	0.066892542	-0.062685407	0.091687076
53.43196754	50.4739219	0.069962509	-0.064312418	0.095048519
56.99156258	50.47963333	0.072138615	-0.06319953	0.095920371
60.55115761	50.48534476	0.073019932	-0.060643517	0.09493229
64.11075264	50.49105618	0.073319707	-0.056556483	0.092617658
67.67034768	50.49676761	0.074088122	-0.051588469	0.090309279
71.22994271	50.50247904	0.075168854	-0.046383441	0.088347547
74.78953774	50.50819046	0.074529765	-0.042118522	0.085608664
78.34913278	50.51390189	0.071998364	-0.039693124	0.082216939
81.90872781	50.51961332	0.068979373	-0.034461261	0.07722648
85.46832284	50.52532474	0.063789284	-0.017230226	0.067141794
89.02791788	50.53103617	0.056116395	0.018744756	0.063247928
92.58751291	50.5367476	0.054063018	0.078140346	0.096314274
96.14710794	50.54245902	0.061245783	0.153949227	0.165882604
99.70670298	50.54817045	0.07689623	0.223113085	0.236008711
103.266298	50.55388187	0.094417555	0.254460687	0.271432452

106.825893	50.5595933	0.096021789	0.238994058	0.257594537
110.3854881	50.56530473	0.080039021	0.185447992	0.201987081
113.9450831	50.57101615	0.050989587	0.120797751	0.131165362
117.5046781	50.57672758	0.024641875	0.065135283	0.069726131
121.0642732	50.58243901	0.008586972	0.031711286	0.033521739
124.6238682	50.58815043	-0.00102655	0.016781934	0.017281635
128.1834632	50.59386186	-0.002698437	0.010640361	0.011460874
131.7430583	50.59957329	-0.002347979	0.008229217	0.009004159
135.3026533	50.60528471	-0.000504877	0.008171892	0.008609812
138.8622483	50.61099614	0.001803791	0.008742994	0.009235825
142.4218434	50.61670757	0.004126192	0.009589948	0.01063495
145.9814384	50.62241899	0.005720578	0.010675736	0.01225322
149.5410334	50.62813042	0.00633396	0.011933066	0.013627095
153.1006285	50.63384184	0.006527632	0.013440845	0.015021612
156.6602235	50.63955327	0.00662889	0.015019968	0.016459124
160.2198185	50.6452647	0.006782217	0.016322994	0.01769188
163.7794136	50.65097612	0.006764743	0.016784471	0.018102599
167.3390086	50.65668755	0.006308871	0.016258336	0.017442981
170.8986036	50.66239898	0.00540451	0.014916099	0.015868801
174.4581987	50.6681104	0.004406727	0.013534956	0.014238072
178.0177937	50.67382183	0.003767274	0.012924006	0.013464358
181.5773887	50.67953326	0.003645456	0.013450308	0.013937653
185.1369838	50.68524468	0.003621744	0.014375298	0.014827153

Table 8 For 200 L/h gas flow and 100 mm above the needle

x [mm]	y [mm]	U[m/s]	V[m/s]	Length[m/s]
13.81896631	20.33934657	0.044664072	-0.035111881	0.056956438
17.25052998	20.33934657	0.048747771	-0.036831015	0.061220268
20.68209365	20.33934657	0.054439701	-0.037936903	0.06644708
24.11365732	20.33934657	0.061844283	-0.038326055	0.072825117
27.545221	20.33934657	0.069075416	-0.037806585	0.078847374
30.97678467	20.33934657	0.075463786	-0.038088977	0.084552341
34.40834834	20.33934657	0.080877903	-0.039241013	0.089905395
37.83991201	20.33934657	0.085291999	-0.039690746	0.094091478
41.27147568	20.33934657	0.086185093	-0.038183093	0.094275754
44.70303936	20.33934657	0.086068619	-0.034693068	0.092868404
48.13460303	20.33934657	0.085934338	-0.027586561	0.090302574
51.5661667	20.33934657	0.086735924	-0.014245354	0.088477685
54.99773037	20.33934657	0.089374489	0.003325335	0.09049197
58.42929404	20.33934657	0.093943093	0.02538297	0.097564923
61.86085772	20.33934657	0.092750339	0.052754521	0.108212238
65.29242139	20.33934657	0.090269814	0.084365205	0.125074538

68.72398506	20.33934657	0.086764331	0.123768562	0.151986595
72.15554873	20.33934657	0.083436667	0.184070787	0.203033477
75.58711241	20.33934657	0.085216783	0.244693609	0.259434637
79.01867608	20.33934657	0.08948198	0.300177065	0.313259477
82.45023975	20.33934657	0.095810306	0.346533803	0.359543074
85.88180342	20.33934657	0.099977858	0.350688481	0.364667997
89.31336709	20.33934657	0.104989085	0.340653237	0.356561473
92.74493077	20.33934657	0.110354977	0.318496801	0.33709585
96.17649444	20.33934657	0.112806074	0.29299019	0.314029104
99.60805811	20.33934657	0.110985344	0.261381669	0.284080895
103.0396218	20.33934657	0.105418026	0.228281913	0.25146911
106.4711855	20.33934657	0.093873079	0.198553568	0.219659238
109.9027491	20.33934657	0.078446373	0.162294116	0.180295415
113.3343128	20.33934657	0.065359706	0.129888765	0.145432676
116.7658765	20.33934657	0.055382399	0.104448217	0.118226889
120.1974401	20.33934657	0.047348822	0.084980808	0.097301013
123.6290038	20.33934657	0.04040919	0.06417381	0.075974226
127.0605675	20.33934657	0.033943951	0.044235403	0.055946137
130.4921312	20.33934657	0.026294033	0.025517467	0.036813822
133.9236948	20.33934657	0.019593022	0.007758544	0.023415148
137.3552585	20.33934657	0.014478401	-0.007114595	0.017515011
140.7868222	20.33934657	0.011420726	-0.018274107	0.021720281
144.2183858	20.33934657	0.01091657	-0.026477411	0.028745662
147.6499495	20.33934657	0.010315934	-0.034655367	0.036218239
151.0815132	20.33934657	0.009589659	-0.042746912	0.043813009
154.5130769	20.33934657	0.009031471	-0.047350601	0.048211815
157.9446405	20.33934657	0.008859971	-0.050977882	0.051743609
161.3762042	20.33934657	0.009165319	-0.053929721	0.054704035
164.8077679	20.33934657	0.010189403	-0.056393167	0.057307162
168.2393316	20.33934657	0.012178317	-0.060416453	0.061638083
171.6708952	20.33934657	0.013936585	-0.064947468	0.066426224
175.1024589	20.33934657	0.015114909	-0.069944774	0.071559688
178.5340226	20.33934657	0.015233814	-0.075018572	0.076552861
181.9655862	20.33934657	0.014900959	-0.077684818	0.079104205

Table 9 For 200 L/h gas flow and 200 mm above the needle

x [mm]	y [mm]	U[m/s]	V[m/s]	Length[m/s]
10.32803302	115.4032282	-0.011782157	-0.132212956	0.132744935
13.866462	115.4032282	-0.012474217	-0.12555556	0.126188352
17.40489098	115.4032282	-0.014018412	-0.113124272	0.11404445
20.94331995	115.4032282	-0.014015339	-0.102551464	0.103568157
24.48174893	115.4032282	-0.012403925	-0.09554212	0.096422934
28.02017791	115.4032282	-0.012426722	-0.08908544	0.090037837
31.55860688	115.4032282	-0.012400501	-0.081655396	0.08267433

35.09703586	115.4032282	-0.013199236	-0.071561363	0.072885703
38.63546484	115.4032282	-0.015990509	-0.056302927	0.058681912
42.17389381	115.4032282	-0.020168952	-0.033851838	0.040868705
45.71232279	115.4032282	-0.024646126	-0.007684877	0.032533019
49.25075177	115.4032282	-0.029667655	0.021107641	0.037561251
52.78918074	115.4032282	-0.034348899	0.050791332	0.06186788
56.32760972	115.4032282	-0.036544515	0.079566618	0.087976515
59.8660387	115.4032282	-0.038099423	0.109036909	0.115809216
63.40446767	115.4032282	-0.039619762	0.140851032	0.146480328
66.94289665	115.4032282	-0.039548029	0.180750575	0.185171983
70.48132563	115.4032282	-0.041604964	0.221352095	0.225367045
74.0197546	115.4032282	-0.04519422	0.261444464	0.265433262
77.55818358	115.4032282	-0.049026535	0.298671964	0.302744645
81.09661256	115.4032282	-0.056445091	0.325659602	0.330594994
84.63504153	115.4032282	-0.062665963	0.347185111	0.352843635
88.17347051	115.4032282	-0.06686103	0.360829355	0.367005227
91.71189949	115.4032282	-0.067714416	0.360392533	0.366725057
95.25032846	115.4032282	-0.06377248	0.349840934	0.355622151
98.78875744	115.4032282	-0.057723242	0.332859152	0.33784535
102.3271864	115.4032282	-0.049868623	0.310049142	0.314046431
105.8656154	115.4032282	-0.041338179	0.284173482	0.287189019
109.4040444	115.4032282	-0.034429757	0.254876064	0.257238516
112.9424733	115.4032282	-0.029561268	0.222841981	0.224870034
116.4809023	115.4032282	-0.027235555	0.189992571	0.192046433
120.0193313	115.4032282	-0.028749336	0.160104709	0.162869179
123.5577603	115.4032282	-0.032643731	0.133209494	0.137402507
127.0961893	115.4032282	-0.037656054	0.109739895	0.116191211
130.6346182	115.4032282	-0.041902715	0.088343301	0.097996839
134.1730472	115.4032282	-0.045414896	0.066778668	0.081376809
137.7114762	115.4032282	-0.048035894	0.043926864	0.066386937
141.2499052	115.4032282	-0.049508414	0.019392327	0.053678707
144.7883341	115.4032282	-0.047768213	-0.004696992	0.050026185
148.3267631	115.4032282	-0.046284992	-0.028550481	0.056315213
151.8651921	115.4032282	-0.044509937	-0.052156216	0.06917691
155.4036211	115.4032282	-0.041946733	-0.075213329	0.0862182
158.94205	115.4032282	-0.040903416	-0.096762901	0.10523765
162.480479	115.4032282	-0.039687688	-0.116685976	0.123351963
166.018908	115.4032282	-0.037907806	-0.134398661	0.139672201
169.557337	115.4032282	-0.034837161	-0.147378957	0.151471715
173.095766	115.4032282	-0.032406757	-0.156669429	0.160014683
176.6341949	115.4032282	-0.029337296	-0.162832144	0.165479957
180.1726239	115.4032282	-0.025518307	-0.166317826	0.168268898
183.7110529	115.4032282	-0.024030544	-0.168065016	0.169783739

Table 10 For 200 L/h gas flow and 300 mm above the needle

x [mm]	y [mm]	U[m/s]	V[m/s]	Length[m/s]
10.03712191	215.6149735	0.019171773	-0.073549475	0.07602211
13.56367697	215.5939618	0.021598643	-0.067938759	0.071322926
17.09023202	215.5729501	0.023946754	-0.053761295	0.059199646
20.61678708	215.5519384	0.02479049	-0.032741073	0.04300676
24.14334213	215.5309267	0.023005115	-0.005023798	0.023933204
27.66989718	215.509915	0.017386426	0.02434861	0.034500304
31.19645224	215.4889033	0.009804056	0.051666003	0.053398377
34.72300729	215.4678916	0.000837492	0.077989528	0.078104792
38.24956235	215.4468799	-0.00860359	0.105068262	0.105529697
41.7761174	215.4258683	-0.017810105	0.135260893	0.136534116
45.30267245	215.4048566	-0.02449315	0.167743842	0.169577353
48.82922751	215.3838449	-0.028183744	0.202236907	0.204233611
52.35578256	215.3628332	-0.02882802	0.232129534	0.233940206
55.88233762	215.3418215	-0.026554289	0.253776931	0.255212074
59.40889267	215.3208098	-0.022470104	0.268420304	0.269411067
62.93544772	215.2997981	-0.017777137	0.275541137	0.276145603
66.46200278	215.2787864	-0.014090997	0.273657281	0.27407968
69.98855783	215.2577748	-0.00915827	0.27116914	0.271459762
73.51511289	215.2367631	-0.004476024	0.268683414	0.268863683
77.04166794	215.2157514	-0.002154155	0.264984157	0.265140047
80.56822299	215.1947397	0.000996841	0.261880411	0.262047614
84.09477805	215.173728	0.003216338	0.258644703	0.25881606
87.6213331	215.1527163	0.004640678	0.253960168	0.254119084
91.14788816	215.1317046	0.007408632	0.245520528	0.245715284
94.67444321	215.1106929	0.011769255	0.236194813	0.236590198
98.20099827	215.0896812	0.018090788	0.223503767	0.22438075
101.7275533	215.0686696	0.026013233	0.205393394	0.207094722
105.2541084	215.0476579	0.033860076	0.183514728	0.186781186
108.7806634	215.0266462	0.039309562	0.158022181	0.163049133
112.3072185	215.0056345	0.042457082	0.129725903	0.136681207
115.8337735	214.9846228	0.044439115	0.099534211	0.109195797
119.3603286	214.9636111	0.045577363	0.072748398	0.086426683
122.8868836	214.9425994	0.047029387	0.049329889	0.06901553
126.4134387	214.9215877	0.049403093	0.029587353	0.057611259
129.9399938	214.9005761	0.04848525	0.017604681	0.051971702
133.4665488	214.8795644	0.046344736	0.00619355	0.047330671
136.9931039	214.8585527	0.043336769	-0.004868912	0.043995053
140.5196589	214.837541	0.039762975	-0.016638123	0.043486778
144.046214	214.8165293	0.034853622	-0.025574298	0.043890861
147.572769	214.7955176	0.030644693	-0.034298713	0.046374714
151.0993241	214.7745059	0.02712771	-0.043469178	0.051412898
154.6258791	214.7534942	0.021936628	-0.054555302	0.059203293

158.1524342	214.7324825	0.016770492	-0.072461624	0.074709718
161.6789892	214.7114709	0.011051787	-0.093169373	0.093966796
165.2055443	214.6904592	0.004306909	-0.114513072	0.114610735
168.7320993	214.6694475	-0.001604402	-0.134955746	0.135017647
172.2586544	214.6484358	-0.005439221	-0.150208522	0.150313078
175.7852095	214.6274241	-0.007632398	-0.161621468	0.16180207
179.3117645	214.6064124	-0.009119281	-0.172119491	0.172361654
182.8383196	214.5854007	-0.008855245	-0.17691644	0.177138911

Table 11 For 500 L/h gas flow and 20 mm above the needle

x [mm]	y [mm]	U[m/s]	V[m/s]	Length[m/s]
9.961393377	34.37599237	0.007604837	0.022173136	0.023448378
13.62625094	34.37066974	0.005606754	0.021620129	0.022345353
17.2911085	34.36534712	0.004479709	0.019163814	0.019681623
20.95596606	34.36002449	0.00357604	0.016141619	0.016540045
24.62082362	34.35470187	0.002471961	0.012249745	0.012515788
28.28568118	34.34937924	0.000985385	0.009426348	0.00953414
31.95053875	34.34405662	-0.000687688	0.006891545	0.007035801
35.61539631	34.338734	-0.001832273	0.005340095	0.005738448
39.28025387	34.33341137	-0.002179138	0.00504982	0.005563879
42.94511143	34.32808875	-0.00219011	0.00602891	0.0064671
46.60996899	34.32276612	-0.002314727	0.007687373	0.008083341
50.27482655	34.3174435	-0.002994303	0.008841817	0.009402224
53.93968412	34.31212087	-0.003670221	0.009345635	0.010124866
57.60454168	34.30679825	-0.00403901	0.008915284	0.009899366
61.26939924	34.30147562	-0.003933655	0.007712037	0.008821971
64.9342568	34.296153	-0.003825009	0.006920087	0.008185756
68.59911436	34.29083038	-0.004459737	0.00742147	0.00911403
72.26397192	34.28550775	-0.007507847	0.011668966	0.014405327
75.92882949	34.28018513	-0.016031416	0.022728786	0.028218387
79.59368705	34.2748625	-0.03522525	0.053990385	0.064787217
83.25854461	34.26953988	-0.053451484	0.132873139	0.14383071
86.92340217	34.26421725	-0.063472558	0.237779958	0.246265305
90.58825973	34.25889463	-0.054471638	0.324172545	0.328859208
94.25311729	34.253572	-0.034421601	0.340786724	0.342594217
97.91797486	34.24824938	-0.013303902	0.280272242	0.280667527
101.5828324	34.24292676	-0.001812645	0.182466806	0.182570951
105.24769	34.23760413	-0.0134917	0.078944968	0.080803996
108.9125475	34.23228151	-0.033211831	0.016289428	0.038493656
112.5774051	34.22695888	-0.052681136	-0.015378432	0.054973593
116.2422627	34.22163626	-0.062752116	-0.027027513	0.068328882
119.9071202	34.21631363	-0.06613411	-0.029833232	0.072555453
123.5719778	34.21099101	-0.065443456	-0.030800168	0.07233611
127.2368353	34.20566838	-0.062540518	-0.031151505	0.069873478
130.9016929	34.20034576	-0.058353582	-0.030109029	0.065664809
134.5665505	34.19502314	-0.053920465	-0.028319864	0.060908168
138.231408	34.18970051	-0.049840058	-0.027100327	0.056742367
141.8962656	34.18437789	-0.046834314	-0.027721709	0.054455717
145.5611232	34.17905526	-0.044435579	-0.029484303	0.053360734

149.2259807	34.17373264	-0.042115759	-0.030787495	0.052196187
152.8908383	34.16841001	-0.039700545	-0.030158716	0.049877755
156.5556958	34.16308739	-0.037670147	-0.027758408	0.046826323
160.2205534	34.15776476	-0.036092907	-0.024741751	0.043809396
163.885411	34.15244214	-0.034824618	-0.020687024	0.040587241
167.5502685	34.14711952	-0.032273364	-0.015904154	0.036054472
171.2151261	34.14179689	-0.027305744	-0.009059175	0.028848856
174.8799836	34.13647427	-0.02065875	-0.001444888	0.020782705
178.5448412	34.13115164	-0.013849196	0.007651844	0.0159625
182.2096988	34.12582902	-0.009303549	0.015617663	0.01823139
185.8745563	34.12050639	-0.005765446	0.021289106	0.022071048

Table 12 For 500 L/h gas flow and 50 mm above the needle

x [mm]	y [mm]	U[m/s]	V[m/s]	Length[m/s]
11.82092909	50.80693403	0.006848384	0.024808235	0.025741139
15.37193753	50.80693403	0.006351532	0.023745673	0.024583134
18.92294596	50.80693403	0.006387228	0.021775075	0.022696109
22.4739544	50.80693403	0.006481604	0.01992778	0.020956636
26.02496284	50.80693403	0.006113844	0.01820535	0.019204707
29.57597127	50.80693403	0.005006359	0.016645864	0.017391274
33.12697971	50.80693403	0.003072892	0.014953199	0.015299009
36.67798815	50.80693403	0.000912251	0.013309291	0.013398742
40.22899658	50.80693403	-0.00063336	0.012564583	0.012640959
43.78000502	50.80693403	-0.001117122	0.013596974	0.013712657
47.33101345	50.80693403	-0.000321198	0.015385716	0.015489085
50.88202189	50.80693403	0.000786256	0.016993203	0.017098223
54.43303033	50.80693403	0.001423338	0.017859014	0.017991602
57.98403876	50.80693403	0.001325204	0.018229494	0.018324617
61.5350472	50.80693403	0.000518569	0.019480888	0.019506411
65.08605563	50.80693403	-0.001579927	0.022910083	0.023010421
68.63706407	50.80693403	-0.004247182	0.031017	0.031359586
72.18807251	50.80693403	-0.008666999	0.048651436	0.049486065
75.73908094	50.80693403	-0.012146509	0.081199051	0.082143143
79.29008938	50.80693403	-0.024229021	0.14235283	0.144428283
82.84109782	50.80693403	-0.044345091	0.232561659	0.236758142
86.39210625	50.80693403	-0.064845585	0.320288901	0.326795681
89.94311469	50.80693403	-0.072377643	0.358476347	0.365728757
93.49412312	50.80693403	-0.063971589	0.332200019	0.338349517
97.04513156	50.80693403	-0.051571034	0.24882709	0.254241296
100.59614	50.80693403	-0.046728606	0.15322245	0.160692377
104.1471484	50.80693403	-0.056053348	0.064071375	0.089363432
107.6981569	50.80693403	-0.068156119	0.011199036	0.071525151
111.2491653	50.80693403	-0.07559161	-0.017880355	0.078377183
114.8001737	50.80693403	-0.07505538	-0.030641212	0.081167772

118.3511822	50.80693403	-0.075153181	-0.036155171	0.083413937
121.9021906	50.80693403	-0.073422515	-0.038482551	0.082904287
125.453199	50.80693403	-0.070151531	-0.039860805	0.080693158
129.0042075	50.80693403	-0.066259735	-0.040595437	0.077712824
132.5552159	50.80693403	-0.063338091	-0.041391781	0.075667828
136.1062244	50.80693403	-0.061693127	-0.042372746	0.07484536
139.6572328	50.80693403	-0.059809632	-0.043671027	0.074060112
143.2082412	50.80693403	-0.057305319	-0.044957321	0.072840469
146.7592497	50.80693403	-0.053659397	-0.044984963	0.070024942
150.3102581	50.80693403	-0.050621741	-0.043753053	0.066911455
153.8612665	50.80693403	-0.04827343	-0.04051727	0.063031963
157.412275	50.80693403	-0.046579488	-0.036510138	0.059200065
160.9632834	50.80693403	-0.046104834	-0.03140362	0.055809962
164.5142918	50.80693403	-0.045424122	-0.026372464	0.052546711
168.0653003	50.80693403	-0.045153683	-0.021167528	0.049885633
171.6163087	50.80693403	-0.044001265	-0.017048389	0.047205674
175.1673172	50.80693403	-0.041750106	-0.011798211	0.043402419
178.7183256	50.80693403	-0.037367811	-0.003191401	0.037543488
182.269334	50.80693403	-0.030562223	0.006946193	0.031434748
185.8203425	50.80693403	-0.022987301	0.017310787	0.028822932

Table 13 For 500 L/h gas flow and 100 mm above the needle

x [mm]	y [mm]	U[m/s]	V[m/s]	Length[m/s]
12.51163986	31.29126676	0.036461223	-0.058262119	0.068745738
15.94674021	31.25668877	0.03625323	-0.056449604	0.067105735
19.38184057	31.22211078	0.035092122	-0.053932839	0.064380882
22.81694092	31.18753279	0.036125003	-0.049600254	0.061420375
26.25204128	31.1529548	0.036009449	-0.043773708	0.056759571
29.68714163	31.11837681	0.034588809	-0.036019672	0.05004956
33.12224199	31.08379882	0.031066234	-0.024900587	0.039898582
36.55734234	31.04922083	0.026817522	-0.012632576	0.03032914
39.9924427	31.01464284	0.023163305	0.000983816	0.02545288
43.42754305	30.98006485	0.020404698	0.016065709	0.026547249
46.86264341	30.94548686	0.015978417	0.032921171	0.03780313
50.29774377	30.91090887	0.011099891	0.049782325	0.051783521
53.73284412	30.87633088	0.00499569	0.067349931	0.068078939
57.16794448	30.8417529	-0.004461259	0.087208998	0.087655567
60.60304483	30.80717491	-0.012445892	0.1102345	0.111156976
64.03814519	30.77259692	-0.017864812	0.134635618	0.13596271
67.47324554	30.73801893	-0.020261805	0.158981824	0.16037934
70.9083459	30.70344094	-0.023173381	0.177233938	0.178835487
74.34344625	30.66886295	-0.028161449	0.194649231	0.196766307
77.77854661	30.63428496	-0.03613361	0.213847735	0.216976296
81.21364696	30.59970697	-0.04906334	0.240348695	0.245378211

84.64874732	30.56512898	-0.06608403	0.280409221	0.288166709
88.08384767	30.53055099	-0.081021412	0.320406371	0.330534596
91.51894803	30.495973	-0.092318624	0.358659502	0.370408335
94.95404838	30.46139501	-0.107750826	0.384305746	0.399193901
98.38914874	30.42681702	-0.113242715	0.395461458	0.411401619
101.8242491	30.39223903	-0.112443473	0.395185426	0.410906171
105.2593494	30.35766104	-0.110826829	0.382869385	0.398600845
108.6944498	30.32308305	-0.101874196	0.354964786	0.369304419
112.1295502	30.28850506	-0.093363313	0.316524163	0.330071962
115.5646505	30.25392707	-0.087570723	0.269839999	0.283723446
118.9997509	30.21934908	-0.081089093	0.213322998	0.228403654
122.4348512	30.18477109	-0.078574103	0.160117999	0.179223249
125.8699516	30.1501931	-0.079108413	0.111942889	0.138298905
129.3050519	30.11561511	-0.084456872	0.071837137	0.111848812
132.7401523	30.08103712	-0.092851667	0.043343115	0.104197812
136.1752526	30.04645913	-0.099592572	0.020381948	0.102443326
139.610353	30.01188115	-0.104109953	0.001539696	0.104139506
143.0454534	29.97730316	-0.107657856	-0.017928284	0.109798484
146.4805537	29.94272517	-0.109991195	-0.037227975	0.11674843
149.9156541	29.90814718	-0.111749075	-0.056883186	0.125681874
153.3507544	29.87356919	-0.113339202	-0.078343074	0.138077371
156.7858548	29.8389912	-0.11005581	-0.093985096	0.145046519
160.2209551	29.80441321	-0.104357128	-0.106510128	0.149307762
163.6560555	29.76983522	-0.096890405	-0.116138921	0.151250135
167.0911558	29.73525723	-0.087528396	-0.118115129	0.14711566
170.5262562	29.70067924	-0.07814981	-0.117289952	0.141008848
173.9613566	29.66610125	-0.068302889	-0.112689814	0.131784132
177.3964569	29.63152326	-0.05745459	-0.101038689	0.116248767
180.8315573	29.59694527	-0.050713641	-0.093196366	0.106107525

Table 14 For 500 L/h gas flow and 200 mm above the needle

x [mm]	y [mm]	U[m/s]	V[m/s]	Length[m/s]
13.14561318	115.3296126	0.009837175	0.008875711	0.013383252
16.58718265	115.3296126	0.00577547	0.011971417	0.013958625
20.02875212	115.3296126	0.001652647	0.016703517	0.016815714
23.47032159	115.3296126	0.000186493	0.02445458	0.024468737
26.91189106	115.3296126	0.001454036	0.037040913	0.037081151
30.35346054	115.3296126	0.005022393	0.052008534	0.052313789
33.79503001	115.3296126	0.01074069	0.068818866	0.069652163
37.23659948	115.3296126	0.014389558	0.085868061	0.087067051
40.67816895	115.3296126	0.017018783	0.10219312	0.103601825
44.11973842	115.3296126	0.019764135	0.119231633	0.12086103
47.56130789	115.3296126	0.024558579	0.139846538	0.141989174
51.00287736	115.3296126	0.030789008	0.167187627	0.170002435

54.44444683	115.3296126	0.037125254	0.19790113	0.201353809
57.8860163	115.3296126	0.043170825	0.23104662	0.235045454
61.32758577	115.3296126	0.048317958	0.259506104	0.263966193
64.76915524	115.3296126	0.051247514	0.28098797	0.285625221
68.21072471	115.3296126	0.053630912	0.297541679	0.302338464
71.65229418	115.3296126	0.058004666	0.310435172	0.315809803
75.09386365	115.3296126	0.060366823	0.323514896	0.329099796
78.53543313	115.3296126	0.064049516	0.33824678	0.344262606
81.9770026	115.3296126	0.06936899	0.354620749	0.361349866
85.41857207	115.3296126	0.070098427	0.365877608	0.372539403
88.86014154	115.3296126	0.067586652	0.369052297	0.375217074
92.30171101	115.3296126	0.061915269	0.362405727	0.367714562
95.74328048	115.3296126	0.051582486	0.339302891	0.343236884
99.18484995	115.3296126	0.038992147	0.31199505	0.314517551
102.6264194	115.3296126	0.026701264	0.281022828	0.282380192
106.0679889	115.3296126	0.015331392	0.246794651	0.247294581
109.5095584	115.3296126	0.008850117	0.217547972	0.217758394
112.9511278	115.3296126	0.004104111	0.186634074	0.186699986
116.3926973	115.3296126	0.000696715	0.15776469	0.157770396
119.8342668	115.3296126	-0.001098136	0.136942181	0.136948644
123.2758362	115.3296126	-0.00252476	0.121509846	0.121541656
126.7174057	115.3296126	-0.002665346	0.107314554	0.107349944
130.1589752	115.3296126	-0.001179267	0.093124935	0.093138039
133.6005447	115.3296126	0.002590031	0.072390348	0.072479197
137.0421141	115.3296126	0.005863702	0.047871971	0.048471979
140.4836836	115.3296126	0.008592674	0.021806011	0.026344696
143.9252531	115.3296126	0.010451719	-0.003353848	0.014248573
147.3668225	115.3296126	0.00816194	-0.023101728	0.025760609
150.808392	115.3296126	0.003770392	-0.040854278	0.041310994
154.2499615	115.3296126	-0.002176211	-0.057473002	0.057536211
157.691531	115.3296126	-0.006522361	-0.076963773	0.077266995
161.1331004	115.3296126	-0.010102068	-0.098133602	0.098661251
164.5746699	115.3296126	-0.012651902	-0.119839005	0.120510198
168.0162394	115.3296126	-0.013456437	-0.14027936	0.140929187
171.4578088	115.3296126	-0.014003015	-0.156904977	0.157532141
174.8993783	115.3296126	-0.014265496	-0.171554127	0.172149796
178.3409478	115.3296126	-0.014159501	-0.184060963	0.18460705
181.7825172	115.3296126	-0.013245883	-0.189555218	0.190022291

Table 15 For 500 L/h gas flow and 300 mm above the needle

x [mm]	y [mm]	U[m/s]	V[m/s]	Length[m/s]
12.51163986	214.9557162	0.004115167	-0.01921055	0.019700089
15.96614756	214.9557162	0.005702517	-0.014129813	0.015587275
19.42065526	214.9557162	0.007652502	-0.007422622	0.010981851

22.87516296	214.9557162	0.00830859	0.00117981	0.009779718
26.32967067	214.9557162	0.007939927	0.009439018	0.013061138
29.78417837	214.9557162	0.006770279	0.017519987	0.018954012
33.23868607	214.9557162	0.004572039	0.025762879	0.026217876
36.69319377	214.9557162	0.002584888	0.034483217	0.034630658
40.14770147	214.9557162	-0.000134932	0.04340588	0.043473718
43.60220917	214.9557162	-0.003789519	0.052742573	0.052897098
47.05671688	214.9557162	-0.004504005	0.064498998	0.064690206
50.51122458	214.9557162	-0.004472803	0.075420696	0.075617233
53.96573228	214.9557162	-0.002717261	0.086128917	0.086345943
57.42023998	214.9557162	0.001974643	0.097497192	0.09766806
60.87474768	214.9557162	0.010151284	0.110767808	0.111454204
64.32925539	214.9557162	0.019408473	0.122660402	0.124554205
67.78376309	214.9557162	0.029158351	0.133422323	0.136865545
71.23827079	214.9557162	0.042715478	0.146256149	0.152572174
74.69277849	214.9557162	0.055149577	0.160825506	0.170191391
78.14728619	214.9557162	0.066605062	0.178161085	0.190290181
81.60179389	214.9557162	0.07805004	0.199927995	0.214638238
85.0563016	214.9557162	0.087563807	0.226799348	0.243122979
88.5108093	214.9557162	0.09211952	0.248332587	0.264890079
91.965317	214.9557162	0.093519686	0.26411348	0.280189995
95.4198247	214.9557162	0.093864002	0.274421156	0.290035605
98.8743324	214.9557162	0.091740322	0.283878775	0.298361206
102.3288401	214.9557162	0.090047802	0.295403123	0.308834342
105.7833478	214.9557162	0.090402735	0.311003942	0.323877982
109.2378555	214.9557162	0.092697822	0.324641891	0.337620513
112.6923632	214.9557162	0.095213354	0.329622506	0.34311435
116.1468709	214.9557162	0.09912195	0.32471935	0.339568102
119.6013786	214.9557162	0.105637311	0.306768338	0.324520264
123.0558863	214.9557162	0.110027893	0.282497268	0.303310286
126.510394	214.9557162	0.113835016	0.254971717	0.279410987
129.9649017	214.9557162	0.116530583	0.225953258	0.254253882
133.4194094	214.9557162	0.116768141	0.201322852	0.232867023
136.8739171	214.9557162	0.116823121	0.17766306	0.212867722
140.3284248	214.9557162	0.115124493	0.1550927	0.193258864
143.7829325	214.9557162	0.108209818	0.13422336	0.172502692
147.2374402	214.9557162	0.100478535	0.113390051	0.151668425
150.6919479	214.9557162	0.091970697	0.091824512	0.130274209
154.1464556	214.9557162	0.083262408	0.06905339	0.108300593
157.6009633	214.9557162	0.077979689	0.045172491	0.090673929
161.055471	214.9557162	0.071616121	0.023506056	0.076426113
164.5099787	214.9557162	0.06500703	0.004852304	0.065482006
167.9644864	214.9557162	0.058568758	-0.006804892	0.059179566
171.4189941	214.9557162	0.052178202	-0.017881878	0.055795384

174.8735018	214.9557162	0.046141206	-0.030328475	0.056065974
178.3280095	214.9557162	0.040196366	-0.04318012	0.059084241
181.7825172	214.9557162	0.036507794	-0.053443171	0.064957817

Appendix F

MATLAB Code for BSD calculation

1) Load and image-

```
warning off all % to stop warnings about images being too big to display
close all % close existing figures
fname=uigetfile('*.*','Select input file'); % read image data file
[X, map] = imread(fname);
scrsz = get(0,'ScreenSize');
f = figure('Visible','on','Name','Bubble Size Measurement', ...
'Position',[1 1 scrsz(3)-100 scrsz(4)-100]);
himage=imshow(X);
hold on
zoom(1);
n=0; % no of bubbles measured; reset for each new image loaded
button = questdlg('Calibrate image using reference line?','Image Calibration');
if button=='Yes'
    Calibrate
end
%%
```

2) Calibration-

```
msgbox('Use the mouse to select a line of known length', ...
'Image Calibration','help','modal')
h=imline(gca,[]); % use mouse to define reference line for calibraion
api=iptgetapi(h);
pos=api.getPosition(); % get position of the centre of the
image
x1=pos(1,1);
y1=pos(1,2);
x2=pos(2,1);
y2=pos(2,2);
Lmm=inputdlg('Enter the line length in mm','Image Calibration');
pix=sqrt((x2-x1)^2+(y2-y1)^2);
L=cell2mat(Lmm);
L=str2num(L);
CF=pix/L;
Measure
```

3) Ellipse point selection-

```
function h=ellipse(ra,rb,ang,x0,y0,C,Nb)
% Ellipse adds ellipses to the current plot
%
% ELLIPSE(ra,rb,ang,x0,y0) adds an ellipse with semimajor axis of ra,
% a semimajor axis of radius rb, a semimajor axis of ang, centered at
% the point x0,y0.
%
% The length of ra, rb, and ang should be the same.
% If ra is a vector of length L and x0,y0 scalars, L ellipses
% are added at point x0,y0.
% If ra is a scalar and x0,y0 vectors of length M, M ellipse are with the same
% radii are added at the points x0,y0.
```

```

% If ra, x0, y0 are vectors of the same length L=M, M ellipses are added.
% If ra is a vector of length L and x0, y0 are vectors of length
% M~=L, L*M ellipses are added, at each point x0,y0, L ellipses of radius ra.
%
% ELLIPSE(ra,rb,ang,x0,y0,C)
% adds ellipses of color C. C may be a string ('r','b',...) or the RGB value.
% If no color is specified, it makes automatic use of the colors specified by
% the axes ColorOrder property. For several circles C may be a vector.
%
% ELLIPSE(ra,rb,ang,x0,y0,C,Nb), Nb specifies the number of points
% used to draw the ellipse. The default value is 300. Nb may be used
% for each ellipse individually.
%
% h=ELLIPSE(...) returns the handles to the ellipses.
%
% as a sample of how ellipse works, the following produces a red ellipse
% tipped up at a 45 deg axis from the x axis
% ellipse(1,2,pi/8,1,1,'r')
%
% note that if ra=rb, ELLIPSE plots a circle
%
% written by D.G. Long, Brigham Young University, based on the
% CIRCLES.m original
% written by Peter Blattner, Institute of Microtechnology, University of
% Neuchatel, Switzerland, blattner@imt.unine.ch
% Check the number of input arguments
if nargin<1,
ra=[];
end;
if nargin<2,
rb=[];
end;
if nargin<3,
ang=[];
end;
%if nargin==1,

% error('Not enough arguments');
%end;
if nargin<5,
x0=[];
y0=[];
end;
if nargin<6,
C=[];
end
if nargin<7,
Nb=[];
end
% set up the default values
if isempty(ra),ra=1;end;
if isempty(rb),rb=1;end;
if isempty(ang),ang=0;end;
if isempty(x0),x0=0;end;
if isempty(y0),y0=0;end;
if isempty(Nb),Nb=300;end;
if isempty(C),C=get(gca,'colororder');end;
% work on the variable sizes
x0=x0(:);
y0=y0(:);

```

```

ra=ra(:);
rb=rb(:);
ang=ang(:);
Nb=Nb(:);
if isstr(C),C=C(:);end;
if length(ra)~=length(rb),
error('length(ra)~=length(rb)');
end;
if length(x0)~=length(y0),
error('length(x0)~=length(y0)');
end;
% how many inscribed ellipses are plotted
if length(ra)~=length(x0)
maxk=length(ra)*length(x0);
else
maxk=length(ra);
end;
% drawing loop
for k=1:maxk
if length(x0)==1
xpos=x0;
ypos=y0;
radm=ra(k);
radn=rb(k);
if length(ang)==1
an=ang;
else
an=ang(k);
end;
elseif length(ra)==1
xpos=x0(k);
ypos=y0(k);
radm=ra;
radn=rb;
an=ang;
elseif length(x0)==length(ra)
xpos=x0(k);
ypos=y0(k);
radm=ra(k);
radn=rb(k);
an=ang(k);
else
rada=ra(fix((k-1)/size(x0,1))+1);
radb=rb(fix((k-1)/size(x0,1))+1);
an=ang(fix((k-1)/size(x0,1))+1);
xpos=x0(rem(k-1,size(x0,1))+1);
ypos=y0(rem(k-1,size(y0,1))+1);
end;
co=cos(an);
si=sin(an);
the=linspace(0,2*pi,Nb(rem(k-1,size(Nb,1))+1,:)+1);
% x=radm*cos(the)*co-si*radn*sin(the)+xpos;
% y=radm*cos(the)*si+co*radn*sin(the)+ypos;
h(k)=line(radm*cos(the)*co-si*radn*sin(the)+xpos,radm*cos(the)*si+co*radn*sin(the)+ypos);
set(h(k),'color',C(rem(k-1,size(C,1))+1,:),'linewidth',2);
end;

```

4) Ellipse fitting-

```
function [varargout]=ellipsefit(x,y)
% ELLIPSEFIT Stable Direct Least Squares Ellipse Fit to Data.
% [Xc,Yc,A,B,Phi,P]=ELLIPSEFIT(X,Y) finds the least squares ellipse that
% best fits the data in X and Y. X and Y must have at least 5 data points.
% Xc and Yc are the x- and y-axis center of the ellipse respectively.
% A and B are the major and minor axis of the ellipse respectively.
% Phi is the radian angle of the major axis with respect to the x-axis.
% P is a vector containing the general conic parameters of the ellipse.
% The conic representation of the ellipse is given by:
%
%  $P(1)*x^2 + P(2)*x*y + P(3)*y^2 + P(4)*x + P(5)*y + P(6) = 0$ 
%
% S=ELLIPSEFIT(X,Y) returns the output data in a structure with field names
% equal to the variable names given above, e.g., S.Xc, S.Yc, S.A, S.B,
% S.Phi and S.P
%
% Reference: R. Halif and J. Flusser, "Numerically Stable Direct Least
% Squares Fitting of Ellipses," Department of Software Engineering, Charles
% University, Czech Republic, 2000.
% Conversion from conic to conventional ellipse equation inspired by
% fit_ellipse.m on MATLAB Central
% D.C. Hanselman, University of Maine, Orono, ME 04469
% Mastering MATLAB 7
% 2005-02-28
% Rotation angle fixed 2005-08-09
%-----

x=x(:); % convert data to column vectors
y=y(:);
if numel(x)~=numel(y) || numel(x)<5
error('X and Y Must be the Same Length and Contain at Least 5 Values.')
end
D1=[x.*x x.*y y.*y]; % quadratic terms
D2=[x y ones(size(x))]; % linear terms
S1=D1*D1;
S2=D1*D2;
[Q2,R2]=qr(D2,0);
if condest(R2)>1.0e10
warning('ellipsefit','Data is Poorly Conditioned and May Not Represent an Ellipse.')
end
T=-R2\((R2\S2)'); % -inv(S3) * S2'
M=S1+S2*T;
CinvM=[M(3,:)/2; -M(2,:); M(1,:)/2];
[V,na]=eig(CinvM);
c=4*V(1,:).*V(3,:)-V(2,:).^2;
A1=V(:,c>0);
P=[A1; T*A1];
% correct signs if needed
P=sign(P(1))*P;
Phi=atan(P(2)/(P(3)-P(1)))/2;
c=cos(Phi);
s=sin(Phi);
% rotate the ellipse parallel to x-axis
Pr=zeros(6,1);
Pr(1)=P(1)*c*c - P(2)*c*s + P(3)*s*s;
Pr(2)=2*(P(1)-P(3))*c*s + (c^2-s^2)*P(2);
Pr(3)=P(1)*s*s + P(2)*s*c + P(3)*c*c;
Pr(4)=P(4)*c - P(5)*s;
```

```

Pr(5)=P(4)*s + P(5)*c;
Pr(6)=P(6);
% extract other data
XcYc=[c s;-s c]*[-Pr(4)/(2*Pr(1));-Pr(5)/(2*Pr(3))];
Xc=XcYc(1);
Yc=XcYc(2);
F=-Pr(6) + Pr(4)^2/(4*Pr(1)) + Pr(5)^2/(4*Pr(3));
AB=sqrt(F./Pr(1:2:3));
A=AB(1);
B=AB(2);
Phi=-Phi;
if A<B % x-axis not major axis, so rotate it pi/2
Phi=Phi-sign(Phi)*pi/2;
A=AB(2);
B=AB(1);
end
S.Xc=Xc;
S.Yc=Yc;
S.A=A;
S.B=B;
S.Phi=Phi;
S.P=P;
if nargout==1
varargout{1}=S;
else
outcell=struct2cell(S);
varargout=outcell(1:nargout);
end

```

5) Diameter and volume information from fitted ellipse-

```

button = questdlg({'Start measuring bubble sizes?', ...
'Use left mouse button to select sets of 6 points',...
'Any other button will finish measurement'},'Measure sizes');
if strcmp(button,'No')
return
end
button=1;
while button == 1
clear x;
clear y;
for j=1:6 % collect sets of 6 points
[x(j),y(j),button] = ginput(1);
if button ==2
[x(j),y(j),button] = ginput(1);
end
if button ==3
return
end
end
n=n+1;
[Xc(n),Yc(n),A(n),B(n),Phi(n),P]=ellipsefit(x,y);
hold on
ellipse(A(n),B(n),Phi(n),Xc(n),Yc(n));
A(n)=A(n)/CF;
B(n)=B(n)/CF;
Xc(n)=Xc(n)/CF;
Yc(n)=Yc(n)/CF;

```



```
volume(n)=4*pi*A(n)^2*B(n)/3
Equi_Dia(n)=2*(A(n)^2*B(n))^(1/3)
AREA(n)=pi*Equi_Dia(n)^2

end
```

References

- [1] Abrahamson, J. 1975. "Collision Rates of Small Particles in a Vigorously Turbulent Fluid." *Chemical Engineering Science* 30(11): 1371–79.
- [2] Adrian, R. J. 2005. "Twenty Years of Particle Image Velocimetry." *Experiments in Fluids* 39(2): 159–69.
- [3] Anabtawi, M. Z A, S. I. Abu-Eishah, N. Hilal, and M. B W Nabhan. 2003. "Hydrodynamic Studies in Both Bi-Dimensional and Three-Dimensional Bubble Columns with a Single Sparger." *Chemical Engineering and Processing: Process Intensification* 42(5): 403–8.
- [4] Asari, Maedeh, and Faramarz Hormozi. 2013. "Effects of Surfactant on Bubble Size Distribution and Gas Hold-up in a Bubble Column." *American Journal of Chemical Engineering* 1(2):50.
<http://www.sciencepublishinggroup.com/journal/paperinfo.aspx?journalid=224&doi=10.11648/j.ajche.20130102.14>.
- [5] Becker, S, A Sokolichin, and G Eigenberger. 1995. "Flow in Bubble Columns and Loop." 49(248).
- [6] Becker, S., H. De Bie, and J. Sweeney. 1999. "Dynamic Flow Behaviour in Bubble Columns." *Chemical Engineering Science* 54(November 1999): 4929–35.
- [7] Besbes, S. et al. 2015. "PIV Measurements and Eulerian-Lagrangian Simulations of the Unsteady Gas-Liquid Flow in a Needle Sparger Rectangular Bubble Column." *Chemical Engineering Science* 126(April): 560–72.
- [8] Bhole, Manish R., Swarnendu Roy, and Jyeshtharaj B. Joshi. 2006. "Laser Doppler Anemometer Measurements in Bubble Column: Effect of Sparger." *Industrial and Engineering Chemistry Research* 45(26): 9201–7.
- [9] Borchers, O, C Busch, a Sokolichin, and G Eigenberger. 1999. "Applicability of the Standard K– ϵ Turbulence Model to the Dynamic Simulation of Bubble Columns. Part II:" *Chemical Engineering Science* 54(24): 5927–35.
- [10] Bouaifi, M., G. Hebrard, D. Bastoul, and M. Roustan. 2001. "A Comparative Study of Gas Hold-Up, Bubble Size, Interfacial Area and Mass Transfer Coefficients in Stirred Gas-Liquid Reactors and Bubble Columns." *Chemical Engineering and Processing* 40(2): 97–111.
- [11] Brady, Michael R., Demetri P. Telionis, Pavlos P. Vlachos, and Roe Hoan Yoon. 2006. "Evaluation of Multiphase Flotation Models in Grid Turbulence via Particle Image

- Velocimetry.” *International Journal of Mineral Processing* 80(2-4): 133–43.
- [12] Bröder, Dirk, and Martin Sommerfeld. 2003. “Combined PIV/PTV-Measurements for the Analysis of Bubble Interactions and Coalescence in a Turbulent Flow.” *The Canadian Journal of Chemical Engineering* 81(3-4): 756–63. <http://dx.doi.org/10.1002/cjce.5450810356>.
- [13] Bryanston-Cross, P. et al. 2000. “Intelligent Diagnostic Optics for Flow Visualization.” *Optics and Laser Technology* 32(7-8): 641–54.
- [14] Buwa, Vivek V, and Vivek V Ranade. 2002. “Dynamics of Gas – Liquid Flow in a Rectangular Bubble Column : Experiments and Single Multi-Group CFD Simulations.” *Chemical Engineering Science* 57:4715–36. <http://linkinghub.elsevier.com/retrieve/pii/S0009250902002749>.
- [15] “Mixing in Bubble Column Reactors: Role of Unsteady Flow Structures.” 81(August):2003 402–11.
- [16] Buwa, Vivek V., and Vivek V. Ranade. 2004. “Characterization of Dynamics of Gas-Liquid Flows in Rectangular Bubble Columns.” *AIChE Journal* 50(10): 2394–2407.
- [17] Chen, J. J. J., M. Jamialahmadi, and S.M. Li. 1989. “Effect of Liquid Depth on Circulation in Bubble Columns: A Visual Study.” *Chemical Engineering Research and Design* 67: 203–7.
- [18] Chen, R. C., and L. S. Fan. 1992. “Particle Image Velocimetry for Characterizing the Flow Structure in Three-Dimensional Gas-Liquid-Solid Fluidized Beds.” *Chemical Engineering Science* 47(13-14): 3615–22.
- [19] Chen, R. C., J. Reese, and L.-S. Fan. 1994. “Flow Structure in a Three-Dimensional Bubble Column and Three-Phase Fluidized Bed.” *AIChE Journal* 40(7): 1093–1104.
- [20] Delnoij, E, J A M Kuipers, W P M van Swaij, and J Westerweel. 2000. “Measurement of Gas–liquid Two-Phase Flow in Bubble Columns Using Ensemble Correlation {PIV}.” *Chemical Engineering Science* 55(17): 3385–95. <http://www.sciencedirect.com/science/article/pii/S0009250999005953>.
- [21] Delnoij, E., J.a.M. Kuipers, and W.P.M. van Swaij. 1997. “Dynamic Simulation of Gas-Liquid Two-Phase Flow: Effect of Column Aspect Ratio on the Flow Structure.” *Chemical Engineering Science* 52(21-22): 3759–72. <http://linkinghub.elsevier.com/retrieve/pii/S0009250997002224>.
- [22] Drahoš, J. et al. 1991. “Effect of Operating Conditions on the Characteristics of Pressure Fluctuations in a Bubble Column.” *Chemical Engineering and Processing: Process Intensification* 29(2):107–15.

<http://www.sciencedirect.com/science/article/pii/025527019187019Y>.

- [23] Elena Díaz, M., Francisco J. Montes, and Miguel A. Galán. 2006. "Influence of Aspect Ratio and Superficial Gas Velocity on the Evolution of Unsteady Flow Structures and Flow Transitions in a Rectangular Two-Dimensional Bubble Column." *Industrial and Engineering Chemistry Research* 45(21): 7301–12.
- [24] Finch, James A., Jan E. Nisset, and Claudio Acuña. 2008. "Role of Frother on Bubble Production and Behaviour in Flotation." *Minerals Engineering* 21(12-14): 949–57.
- [25] Fransolet, E., M. Crine, P. Marchot, and D. Toye. 2005. "Analysis of Gas Holdup in Bubble Columns with Non-Newtonian Fluid Using Electrical Resistance Tomography and Dynamic Gas Disengagement Technique." *Chemical Engineering Science* 60(22): 6118–23.
- [26] Grau, R. A., and K. Heiskanen. 2002. "Visual Technique for Measuring Bubble Size in Flotation Machines." *Minerals Engineering* 15(7): 507–13.
- [27] Hal, Radim, and Jan Flusser. 1998. "Numerically Stable Direct Least Squares Fitting of Ellipses." *Proc. 6th International Conference in Central Europe on Computer Graphics and Visualization 98(WSCG)*:125–32.
<http://citeseerx.ist.psu.edu/viewdoc/download?doi=10.1.1.1.7559&rep=rep1&type=pdf>.
- [28] Hikita, H. et al. 1980. "Gas Hold-up in Bubble Columns." *The Chemical Engineering Journal* 20(1): 59–67.
- [29] Homayouni, S.-S. et al. 2008. "Bubble Size Distribution in Oil-Based Bubble Columns." *Chemical Engineering & Technology* 31(11): 1668–75.
<http://doi.wiley.com/10.1002/ceat.200800117>.
- [30] Hyndman, Caroline L., Faiçal Larachi, and Christophe Guy. 1997. "Understanding Gas-Phase Hydrodynamics in Bubble Columns: A Convective Model Based on Kinetic Theory." *Chemical Engineering Science* 52(1): 63–77.
- [31] Jambunathan, K, X Y Ju, B N Dobbins, and S Ashforth-Frost. 1995. "An Improved Cross Correlation Technique for Particle Image Velocimetry." *Measurement Science and Technology* 6(5): 507–14.
- [32] Jensen, K D. 2004. "Flow Measurements Techniques." *Most* XXVI(4): 2–3.
http://www.scielo.br/scielo.php?script=sci_arttext&pid=S1678-58782004000400006&lng=en&nrm=iso&tlng=en.
- [33] Jin, Haibo, Suohe Yang, Mi Wang, and R. A. Williams. 2007. "Measurement of Gas Holdup Profiles in a Gas Liquid Cocurrent Bubble Column Using Electrical Resistance

- Tomography.” *Flow Measurement and Instrumentation* 18(5-6): 191–96.
- [34] Kantarci, Nigar, Fahir Borak, and Kutlu O. Ulgen. 2005. “Bubble Column Reactors.” *Process Biochemistry* 40(7): 2263–83.
- [35] Krishna, Rajamani et al. 1997. “Gas Holdup in Slurry Bubble Columns: Effect of Column Diameter and Slurry Concentrations.” *AIChE Journal* 43(2): 311–16.
- [36] Krishna, Rajamani, and Jürg Ellenberger. 1996. “Gas Holdup in Bubble Column Reactors Operating in the Churn-Turbulent Flow Regime.” *AIChE Journal* 42(9): 2627–34. <http://doi.wiley.com/10.1002/aic.690420923>.
- [37] Kulkarni, A.V., and J.B. Joshi. 2006. “Estimation of Hydrodynamic and Heat Transfer Characteristics of Bubble Column by Analysis of Wall Pressure Measurements and CFD Simulations.” *Chemical Engineering Research and Design* 84(7): 601–9. <http://www.sciencedirect.com/science/article/pii/S0263876206729379>.
- [38] Kumar, S., R. A. Kumar, P. Munshi, and A. Khanna. 2012. “Gas Hold-up in Three Phase Co-Current Bubble Columns.” *Procedia Engineering* 42(August): 782–94. <http://dx.doi.org/10.1016/j.proeng.2012.07.470>.
- [39] Laakkonen, Marko, Pasi Moilanen, Ville Alopaeus, and Juhani Aittamaa. 2007. “Modelling Local Bubble Size Distributions in Agitated Vessels.” *Chemical Engineering Science* 62(3): 721–40.
- [40] Lage, P. L C, and R. O. Esp??sito. 1999. “Experimental Determination of Bubble Size Distributions in Bubble Columns: Prediction of Mean Bubble Diameter and Gas Hold up.” *Powder Technology* 101(2): 142–50.
- [41] Lee, D. J., X. Luo, and L. S. Fan. 1999. “Gas Disengagement Technique in a Slurry Bubble Column Operated in the Coalesced Bubble Regime.” *Chemical Engineering Science* 54(13-14): 2227–36.
- [42] Letzel, H.M., J.C. Schouten, R. Krishna, and C.M. van den Bleek. 1997. “Characterization of Regimes and Regime Transitions in Bubble Columns by Chaos Analysis of Pressure Signals.” *Chemical Engineering Science* 52(24): 4447–59. <http://www.sciencedirect.com/science/article/pii/S000925099700290X>.
- [43] “Gas Holdup and Mass Transfer in Bubble Column Reactors Operated at Elevated Pressure.” *Chemical Engineering Science* 54(13-14):1999 2237–46.
- [44] Li, Xiangyang, Chao Yang, Shifang Yang, and Guozheng Li. 2012. “Fiber-Optical Sensors: Basics and Applications in Multiphase Reactors.” *Sensors (Switzerland)* 12(9): 12519–44.
- [45] Lin, T J, K Tsuchiya, and L S Fan. 1998. “Bubble Flow Characteristics in Bubble

- Columns at Elevated Pressure and Temperature.” *AICHE Journal* 44(3): 545–60.
- [46] Lin, T.-J., J. Reese, T. Hong, and L.-S. Fan. 1996. “Quantitative Analysis and Computation of Two-Dimensional Bubble Columns.” *AICHE Journal* 42(2): 301–18. <http://doi.wiley.com/10.1002/aic.690420202>.
- [47] Liu, Zhengliang, and Ying Zheng. 2006. “PIV Study of Bubble Rising Behavior.” *Powder Technology* 168(1): 10–20.
- [48] Liu, Zhengliang, Ying Zheng, Lufei Jia, and Qikai Zhang. 2005. “Study of Bubble Induced Flow Structure Using PIV.” *Chemical Engineering Science* 60(13): 3537–52.
- [49] Luo, Xukun et al. 1999. “Maximum Stable Bubble Size and Gas Holdup in High-Pressure Slurry Bubble Columns.” *AICHE Journal* 45(4): 665–80. <http://doi.wiley.com/10.1002/aic.690450402>.
- [50] Marks, G H. 2014. “Measurements of the Terminal Velocity of Bubbles Rising in a Chain.” : 7–12.
- [51] Meernik, P R. 2016. “An Optical Method for Determining Bubble Size Distributions — Part I: Theory.”
- [52] Melling, a. 1997. “Tracer Particles and Seeding for Particle Image Velocimetry.” *Measurement Science and Technology* 8(12): 1406–16. <http://stacks.iop.org/0957-0233/8/i=12/a=005?key=crossref.828d3477f9cf4538526e17cfeed03203>.
- [53] Moshtari, Behnoosh, Ensieh Ganji Babakhani, and Jafar Sadegh Moghaddas. 2009. “Experimental Study of Gas Hold-Up and Bubble Behavior in Gas – Liquid Bubble Column.” *Petroleum and Coal* 51(1): 27–32. http://www.vurup.sk/pc/vol51_2009/issue1/pdf/pc_1_2009_moshtari.pdf.
- [54] Mudde, R. F., D. J. Lee, J. Reese, and L.-S. Fan. 1997. “Role of Coherent Structures on Reynolds Stresses in a 2-D Bubble Column.” *AICHE Journal* 43(4): 913–26. <http://doi.wiley.com/10.1002/aic.690430407>.
- [55] Mudde, R.F., J.S. Groen, and H.E.a. Van Den Akker. 1997. “Liquid Velocity Field in a Bubble Column: LDA Experiments.” *Chemical Engineering Science* 52(97): 4217–24.
- [56] Olmos, E., C. Gentric, S. Poncin, and N. Midoux. 2003. “Description of Flow Regime Transitions in Bubble Columns via Laser Doppler Anemometry Signals Processing.” *Chemical Engineering Science* 58(9): 1731–42.
- [57] Pandit, A. B., J. Varley, R. B. Thorpe, and J. F. Davidson. 1992. “Measurement of Bubble Size Distribution: An Acoustic Technique.” *Chemical Engineering Science* 47(5): 1079–89.

- [58] Prasser, H.-M., D. Scholz, and C. Zippe. 2001. "Bubble Size Measurement Using Wire-Mesh Sensors." *Flow Measurement and Instrumentation* 12(4): 299–312.
- [59] Rafael C. Gonzalez, Richard E. Woods, and Steven L Eddins. 2009. "Digital Image Processing Using MATLAB." : 609.
- [60] Raffel, Markus, C E Willert, S T Wereley, and Jürgen Kompenhans. 2007. 79 *Current Science Particle Image Velocimetry*.
<http://scholar.google.com/scholar?hl=en&btnG=Search&q=intitle:No+Title#0>
http://books.google.com/books?hl=en&lr=&id=jbDl2-yHbooC&oi=fnd&pg=PR7&dq=Particle+Image+Velocimetry&ots=T1sqOsf5mU&sig=gEvGBErY1oPK-uQr_BQgYjnsSpM
<http://books.google.com/books?hl=>
- [61] Rensen, J., and V. Roig. 2001. "Experimental Study of the Unsteady Structure of a Confined Bubble Plume." *International Journal of Multiphase Flow* 27(8): 1431–49.
- [62] Rodrigo, A., and D. Sanchez. 2015. "Comparison Between Fluorescent Classic 2D Piv and Fluorescent Stereo- Piv Measurements of the Liquid Phase Velocity in a Bubble Column Fluorescent Stereo-Piv Measurements of the Liquid Phase." (November).
- [63] Sadr-Kazemi, N, and J.J Cilliers. 1997. "An Image Processing Algorithm for Measurement of Flotation Froth Bubble Size and Shape Distributions." *Minerals Engineering* 10(10): 1075–83.
- [64] Saffman, P.G., and J.S. Turner. 1956. "On the Collision of Drops in Turbulent Clouds." *Journal of Fluid Mechanis* 1(November 1955): 16–30.
- [65] Sarrafi, Amir. 1999. "Gas Holdup in Homogeneous and Heterogeneous Gas—liquid Bubble Column Reactors." *Can. J. Chem. Eng.* 77: 11–21.
- [66] Le Sauze, N. et al. 1992. "The Residence Time Distribution of the Liquid Phase in a Bubble Column and Its Effect on Ozone Transfer." *Ozone: Science & Engineering* 14(3): 245–62.
- [67] Schafer, R., C. Merten, and G. Eigenberger. 2002. "Bubble Size Distributions in a Bubble Column Reactor under Industrial Conditions." *Experimental Thermal and Fluid Science* 26(6-7): 595–604.
- [68] Schubert, Heinrich. 1999. "On the Turbulence-Controlled Microprocesses in Flotation Machines." *International Journal of Mineral Processing* 56(1-4): 257–76.
- [69] Shah, Y T, B Godbole Kelkar, S P Godbole, and W-D Deckwer. 1982. "Design Parameters Estimations for Bubble Column Reactors." *AIChE Journal* 28(3): 353–79.
- [70] Sharifi, Mohadeseh, and Brent Young. 2013. "Electrical Resistance Tomography (Ert) Applications to Chemical Engineering." *Chemical Engineering Research and Design*

- 91(9): 1625–45. <http://dx.doi.org/10.1016/j.cherd.2013.05.026>.
- [71] Talaia, Mário a R. 2007. “Terminal Velocity of a Bubble Rise in a Liquid Column.” *Engineering and Technology* 22(5):264–68.
<http://citeseerx.ist.psu.edu/viewdoc/download?doi=10.1.1.192.9665&rep=rep1&type=pdf>.
- [72] Tokuhiro, A. et al. 1998. “Turbulent Flow Past a Bubble and an Ellipsoid Using Shadow-Image and PIV Techniques.” *International Journal of Multiphase Flow* 24(8): 1383–1406.
- [73] Tomiyama, a. 2002. “Transverse Migration of Single Bubble in Simple Shear Flows.” *Chem. Eng. Sci.* 57: 1849–58.
- [74] Tzeng, J.-W., R. C. Chen, and L.-S. Fan. 1993. “Visualization of Flow Characteristics in a 2-D Bubble Column and Three-Phase Fluidized Bed.” *AIChE Journal* 39(5): 733–44. <http://doi.wiley.com/10.1002/aic.690390502>.
- [75] Urseanu, M.I. 2000. “Scaling up Bubble Column Reactors.”
- [76] Veera, U. Parasu, K. L. Kataria, and J. B. Joshi. 2004. “Effects of Superficial Gas Velocity on Gas Hold-up Profiles in Foaming Liquids in Bubble Column Reactors.” *Chemical Engineering Journal* 99(1): 53–58.
- [77] De Vries, A. W. G. 2001. “Path and Wake of a Rising Bubble.”
- [78] Westerweel, Jerry. 1993. “Analysis of PIV Interrogation with Low-Pixel Resolution.” In , 624–35. <http://dx.doi.org/10.1117/12.163745>.
- [79] Wilkinson, Peter M., and Laurent L. v. Dierendonck. 1990. “Pressure and Gas Density Effects on Bubble Break-up and Gas Hold-up in Bubble Columns.” *Chemical Engineering Science* 45(8): 2309–15.
- [80] Willert, C. E., and M. Gharib. 1991. “Digital Particle Image Velocimetry.” *Experiments in Fluids* 10(4): 181–93.
- [81] Wu, Xiong Jun, and Georges L. Chahine. 2010. “Development of an Acoustic Instrument for Bubble Size Distribution Measurement.” *Journal of Hydrodynamics* 22(5 SUPPL. 1): 325–31.
- [82] Xia, Wencheng, Jianguo Yang, and Yuling Wang. 2011. “Reliability of Gas Holdup Measurements Using the Differential Pressure Method in a Cyclone-Static Micro-Bubble Flotation Column.” *Mining Science and Technology* 21(6): 797–801. <http://dx.doi.org/10.1016/j.mstc.2011.06.026>.
- [83] Zhang, Yi, and Hui Sun. 2012. “Measurement of Bubble Size Distribution in Liquids by Optical and Acoustical Methods.” 2012 International Conference on

Communication Systems and Network Technologies: 671–74.
<http://ieeexplore.ieee.org/lpdocs/epic03/wrapper.htm?arnumber=6200698>.